UNIVERSITY OF ICELAND

Holographic Models of Emergent Spacetime

Vyshnav Mohan

2026

FACULTY OF PHYSICAL SCIENCES

Holographic Models of Emergent Spacetime

Vyshnav Mohan

Dissertation submitted in partial fulfillment of a
Philosophiae Doctor degree in Physics

Supervisor
Lárus Thorlacius

Doctoral Committee
David A. Lowe
Friðrik Freyr Gautason
Valentina Giangreco M. Puletti
Watse Sybesma

Opponents
Johanna Erdmenger,
Institute for Theoretical Physics and Astrophysics,
Julius-Maximilians-Universität Würzburg

Vijay Balasubramanian,
David Rittenhouse Laboratories, University of Pennsylvania

Faculty of Physical Sciences
School of Engineering and Natural Sciences
University of Iceland
Reykjavik, May 2026

Holographic Models of Emergent Spacetime
(Holographic Models of Emergent Spacetime)

Dissertation submitted in partial fulfillment of a *Philosophiae Doctor* degree in Physics

Faculty of Physical Sciences
School of Engineering and Natural Sciences
University of Iceland
Tæknigarður, Dunhagi 5
107 Reykjavik
Iceland

Telephone: 525-4000

Bibliographic information:
Vyshnav Mohan (2026) *Holographic Models of Emergent Spacetime*, PhD dissertation, Faculty of Physical Sciences, University of Iceland, 162 pp.

Author ORCID: 0000-0002-4782-5136
ISBN 978-9935-585-02-8

Printing: Háskólaprent
Reykjavik, Iceland, May 2026

Abstract

Black holes are exceptional laboratories where the apparent incompatibility between gravity and quantum mechanics can be sharpened. In this thesis, quantum features of black holes are probed using the holographic principle, with tools from quantum information and algebraic quantum field theory.

Operator algebras provide a natural framework for studying gravity as an emergent phenomenon, and we identify sufficient conditions for the emergence of gravitational dynamics. Going in the opposite direction, quantum gravity effects in an eternal black hole can be modelled by adding certain non-perturbative quantum corrections to its semiclassical operator algebra. This leads to an approximate type I von Neumann algebra whose dimension is equal to the exponential of the Bekenstein-Hawking entropy with logarithmic corrections.

Non-perturbative corrections also lead to the late-time saturation of holographic complexity, defined as the volume of a codimension-one extremal surface passing through the black hole interior. A second law associated with this complexity is used to establish a black hole singularity theorem.

Non-perturbative corrections may become important during gravitational collapse. Black shells, which have been proposed as an alternative endpoint of collapse in string theory, are studied from a thermodynamic perspective and shown to be thermodynamically favoured over black holes for a range of temperatures.

Ágrip

Svarthol eru fræðilegar rannsóknarstofur sem veita einstaka innsýn í ósamræmið sem virðist vera milli þyngdarfræði og skammtafræði. Í ritgerðinni eru skammtafræðilegir eiginleikar svarthola kannaðir með vísun til þyngdarfræðilegrar heilmyndunar og aðferðum skammtaupplýsingafræði og algebrulegrar skammtasviðsfræði.

Virkjaalgebrur eru ákjósanlegur fræðilegur vettvangur til að útskýra tímarúm og þyngdaráhrif sem tilkomin úr gangverki undirliggjandi skammtakerfis. Í ritgerðinni eru sett fram nauðsynleg skilyrði sem slíkt skammtakerfi þarf að uppfylla. Einnig er sýnt hvernig lýsa megi áhrifum þyngdarskammtafræði á tímarúm sístæðs svarthols með því að innleiða tilteknar skammtaleiðréttingar í hálfskammtaða virkjaalgebru kerfisins. Niðurstöðuna má nálga með von Neumann algebru af gerð I sem hefur vídd í samræmi við Bekenstein-Hawking óreiðu svartholsins með lograleiðréttingum.

Sambærilegar skammtaleiðréttingar leiða einnig til mettunar skammtafræðilegs flækjustigs svarthols með tíma þegar flækjustigið er skilgreint útfrá rúmmáli ákveðins sniðs í gegnum tímarúm svartholsins. Hliðstæða við annað lögmál varmafræðinnar, sem gildir um flækjustigið, er notuð til að leiða út nýja sérgildissetningu fyrir svarthol.

Skammtaleiðréttingar gegna mögulega lykilhlutverki í fræðilegri lýsingu á þyngdarhruni. Í því samhengi gæti svonefnd svartskel, sem kemur úr strengjafræði, verið endastöð þyngdarhruns í stað svarthols. Í ritgerðinni er borin saman varmafræði svartskelja og svarthola og sýnt að í kórsafni eru svartskeljar ráðandi á ákveðnu hitastigsbili.

To the two most important women in my life, Amma and Athi.

Contents

Abstract iii

Ágrip v

Dedication vii

Contents ix

List of Figures xi

List of Tables xiii

List of Original Publications xiii

Abbreviations xv

Acknowledgments xvii

1 Introduction 1

2 Holographic Complexity 5
2.1 Krylov Complexity 5
2.2 Complexity=Volume 7
2.3 Quantum Complexity in JT gravity 10

3 Black Hole Singularities and Quantum Complexity 13
3.1 Penrose's Singularity Theorem 13
3.2 Generalized Entropy and Inclusion of Quantum Corrections . . 16
3.3 Second Law of Complexity and Black Hole Singularities 17

4 Late-time Behaviour of Holographic Complexity 19

5 Black Hole Mimickers 21
5.1 Black Shells 21
5.2 Thermodynamics of Black Shells 23

6 Operator Algebras and Quantum Gravity 27
6.1 A Primer on von Neumann algebras and Classification of Factors 27
6.2 Large N Holography and von Neumann Algebras 29

6.3 Emergence of Horizons from Operator Algebras 30
6.4 Perturbative $1/N^2$ Corrections and Crossed Product Algebras . 32
6.5 Emergence of Spacetime and the Construction of a Type I factor 34

7 Conclusions **41**

References **41**

Paper I **51**

Paper II **71**

Paper III **105**

Paper IV **121**

List of Figures

2.1 The Penrose diagram of a $(d+1)$-dimensional AdS-Schwarzschild black hole. The codimension-one extremal volume surface is shown in blue. The turning point of the surface, located at $r = r_{\min}$, lies in the interior of the black hole. The extremal surface is anchored at a cutoff surface located at $r = r_{\text{UV}}$, with anchoring times $t_R = -t_L = \tau/2$. The accumulation surface, located at $r = r_a$, is indicated by the black dashed curve. 8

2.2 The plot of the effective potential for a $(d+1)$-dimensional eternal AdS-Schwarzschild black hole. The extremal volume surface can be thought of as a particle with fixed energy p^2 scattering off this potential. 9

2.3 The log-log plot of the average length $\overline{\ell(\tau)}$ as a function of τ for $\beta \gg \phi_b$. 11

3.1 Extremal volume surfae anchored to a null sheet $N = \partial I^+(p)$. The point p lies in the interior of the black hole. 17

6.1 Blind Physicists and a Quantum Elephant. Physicists blinded by the semiclassical limit will see a smooth horizon or a wormhole when probing different regimes, while a physicist studying the full quantum black hole will instead see a finite-dimensional quantum mechanical system. (Adapted from Sketchplanations). 38

List of Original Publications

Paper I: **V. Mohan**, Black hole singularities from holographic complexity, JHEP 07 (2025) 275, arXiv:2504.10194 [hep-th].

Paper II: F.F. Gautason, **V. Mohan** and L. Thorlacius, Late-time saturation of black hole complexity, JHEP 08 (2025) 056, arXiv:2502.17179 [hep-th]

Paper III: U. Danielsson, **V. Mohan** and L. Thorlacius, Black shell thermodynamics, JHEP 09 (2025) 167, arXiv:2506.02117 [hep-th]

Paper IV: **V. Mohan** and L. Thorlacius, Spacetime from Operator Algebras, arXiv:2606.10924 [hep-th]

Publications not included in the thesis:

Paper V: **V. Mohan** and L. Thorlacius, Non-Perturbative Corrections to Charged Black Hole Evaporation, JHEP 04 (2025) 069, arXiv:2411.13454 [hep-th]

Paper VI: **V. Mohan**, Krylov complexity of open quantum systems: from hard spheres to black holes, JHEP 11 (2023) 222, arXiv:2308.10945 [hep-th]

Paper VII: C. Krishnan, and **V. Mohan**, State-independent black hole interiors from the crossed product, JHEP 05 (2024) 278, arXiv:2310.05912 [hep-th]

Paper VIII: **V. Mohan**, and W. Sybesma, de sitter complexity grows linearly in the static patch, Phys. Rev. D 113 (Jun, 2026) L121902, arXiv:2508.10093[hep-th]

Abbreviations

AdS Anti-de Sitter

CFT Conformal Theory

K-Complexity Krylov Complexity

CV Complexity=Volume

CA Complexity=Action

JT Jackiw-Teitelboim

RMT Random Matrix Theory

NEC Null Energy Condition

GSL Generalized Second Law

SLC Second Law of Complexity

SYM Super-Yang-Mills

GFF Generalized Free Field

GNS Gelfand-Naimark-Segal

SFF Spectral Form Factor

Acknowledgments

I would like to express my sincere gratitude to my advisor, Lárus Thorlacius, for all the support and guidance during my PhD at the University of Iceland, and also for translating the thesis abstract into Icelandic. I have learnt so much from him, not only about physics and academic writing, but also about life more broadly. I am grateful to him for hiring me as his PhD student and for patiently entertaining my often overly enthusiastic and sometimes chaotic ideas whenever I walked into his office.

I would also like to thank my local doctoral committee members Friðrik Freyr Gautason, Valentina Giangreco M. Puletti, and Watse Sybesma, as well as Matthew Roberts, for many helpful discussions. The warm environment they provided, even during the cold Icelandic winters, gave me a solid academic home in which I could grow roots and explore my ideas with confidence. The journal clubs and paper lunches have always been a delight, and I learnt so much about topics that I would not have otherwise explored. I would also like to thank my external doctoral committee member David Lowe for taking the time to be on my committee. I am also very grateful to have collaborated with Ulf Danielsson during my six-month stay at Uppsala University, and I thank the department for giving me office space and welcoming me as one of their own.

I could not be happier to have Alexia Nix, Evangelos Tsolakidis, Matthias Harksen, and Rahul Poddar as my fellow PhD students. I believe their mere presence in the group made my PhD journey much better. I would also like to thank the people I met in Iceland along the way: Diego Hidalgo, Victoria Martin, Davide Astesiano, Agnese Caruso, Tako Meshveliani, Bobby Scully, Álfheiður Edda Sigurðardóttir, Sixten Nordegren, Breki Pálsson, Rögnvaldur Konráð Helgason, Sigurður Jens Albertsson, Sébastien Matlosz, Juan Ouyang, and Ivan Makarov.

I am very grateful to my Master's supervisor Chethan Krishnan, who constantly supported and motivated me to do physics at the highest level. His enthusiasm and inclination towards deep and fundamental questions in physics shaped my research trajectory significantly.

I am fortunate to have a loving and supportive family: my Amma, Achan, brother, and grandparents. I am deeply grateful for their efforts and for always believing in me. The savings they devoted to my studies and travel are invaluable to me, and I am very lucky to have them in my life.

Finally, I would like to thank my wife, Athi. Her presence in my life has grounded me as a person, and I have learnt so much from her. Her constant love and encouragement helped me finish this journey. Thank you for being a part of my life.

My doctoral studies have been supported by the Icelandic Research Fund under Grant No. 228952-053, as well as by a doctoral grant from The University of Iceland Science Park.

1 Introduction

In 1916, Einstein proposed the theory of general relativity, geometrizing gravity as the curvature of spacetime [1]. Over the following century, the extraordinary predictions of the theory, ranging from solar system phenomena such as the precession of Mercury's perihelion to the large-scale structure of the universe, have been tested extensively and found to agree with observations across an enormous range of length scales [2]. Almost in parallel, the 1920s witnessed the foundations of quantum mechanics being laid. What began as a framework for explaining the spectral properties of atoms gradually evolved into a systematic procedure for quantizing fields. Quantum electrodynamics, and later the full Standard Model of particle physics, demonstrated the remarkable success of this framework, producing predictions that agree with experiment to astonishing precision.

The obvious next step was to apply the same quantization procedure to gravity and thereby arrive at a theory of quantum gravity. This programme, however, encounters severe difficulties. Canonically quantizing the gravitational field in the same spirit as the other field theories leads to a non-renormalizable theory. Ultraviolet divergences proliferate at every loop order and cannot be absorbed into a finite set of counterterms (see, for example, [3]). General relativity and quantum mechanics, each individually extraordinarily successful in their own domain, appear fundamentally incompatible when combined.

These tensions become particularly sharp in the study of black holes. Black holes are highly compact classical solutions of Einstein's field equations formed at the end of gravitational collapse. When quantum effects are incorporated, black holes radiate, evaporate, and *apparently* destroy information, leading to the black hole information paradox [4]. Black holes, therefore, provide a natural laboratory for probing the incompatibility between general relativity and quantum mechanics. What was missing, however, was a systematic framework for incorporating quantum gravitational corrections in a fully controlled manner.

A major breakthrough came in 1996, when Maldacena discovered the AdS/CFT correspondence [5, 6, 7]. Often referred to as the *holographic principle*, the duality posits that a theory of quantum gravity in an asymptotically anti-de Sitter (AdS) spacetime is equivalent to a conformal field theory (CFT) living on its boundary. Since the boundary CFT is an ordinary quantum field theory without gravity, the correspondence provides a fully non-perturbative and ultraviolet-complete definition of bulk quantum gravity, something that had previously been unavailable. This framework forms the backdrop of this thesis.

A central question in holography is identifying the appropriate tools in the boundary theory that probe geometric and dynamical features of the bulk spacetime. Following the discovery of AdS/CFT, it was realized that quantum information-theoretic quantities such as entanglement entropy admit elegant geometric dual descriptions in the bulk [8], despite the subtleties involved in defining these quantities precisely in quantum field theory [9]. It was also understood that the encoding of bulk gravitational information in the boundary theory is closely related to quantum error correction [10]. These developments established quantum information theory as a powerful framework for studying holography.

In the first part of this thesis, we study one such quantity called *complexity*. In **Section 2**, we review a notion of complexity in quantum systems and discuss its holographic realisation in the bulk. In particular, we review the Complexity=Volume (CV) prescription, in which the complexity of a black hole is defined as the volume of a codimension-one extremal surface passing through its interior. As an application, in **Section 3**, we show that a second law associated with this holographic complexity can be used to arrive at a black hole singularity theorem, demonstrating that black hole singularities are unavoidable under generic physical conditions.

The complexity of a chaotic quantum system is expected to exhibit a characteristic late-time behaviour. Since black holes are also expected to be maximally chaotic systems [11], one may ask whether holographic complexity reproduces this behaviour. However, the standard CV prescription fails to capture the expected late-time behaviour. In **Section 4**, we show that for a large class of black hole solutions, the expected behaviour can in fact be recovered once certain non-perturbative quantum gravitational corrections arising from an emergent random matrix theory description are included.

Another regime where non-perturbative quantum gravity effects may become important is at the endpoint of gravitational collapse. If the collapse results in the formation of a horizonless ultracompact object rather than a black hole, then the information loss paradox may be avoided altogether. In **Section 5**, we review one such proposal known as *black shells*. These objects admit constructions in string theory and therefore provide a possible alternative endpoint to gravitational collapse. Since no detailed dynamical mechanism for their formation is currently known, we instead study their thermodynamics. We show that for certain temperature ranges, black shells are thermodynamically favoured over black holes, modifying the standard Hawking-Page phase transition [12].

In 1995, Jacobson showed that Einstein's field equations can be derived as a thermodynamic equation of state [13]. This observation suggests that gravity may itself be an emergent phenomenon, potentially explaining why attempts at a direct canonical quantization of gravity fail. In **Section 6**, we argue that the language of algebraic quantum field theory, and in particular operator algebras, provides a natural framework for understanding this emergence. We identify specific structures in the operator algebra of the matter sector, in an appropriate semiclassical limit, whose existence is *sufficient* for an emergent gravitational description to exist. A remarkable feature of this characterization is that it is independent of both the dimensionality and asymptotic structure of the spacetime.

In **Section 6**, we further show that one can systematically encode quantum gravitational corrections within the language of operator algebras starting from a semiclassical low-energy effective field theory description. In the case of an eternal black hole, we show that the resulting non-perturbatively corrected algebra is approximately equal to a type I von Neumann algebra that acts on a finite-dimensional Hilbert space whose dimension is given by the exponential of the Bekenstein-Hawking entropy, together with the logarithmic correction in the horizon area.

In **Section 7**, we conclude the thesis by outlining a few possible future directions.

This thesis is based on the four publications:

1. V. Mohan, Black hole singularities from holographic complexity, *JHEP* **07** (2025) 275.

2. F.F. Gautason, V. Mohan and L. Thorlacius, Late-time saturation of black hole complexity, *JHEP* **08** (2025) 056.

3. U. Danielsson, V. Mohan and L. Thorlacius, Black shell thermodynamics, *JHEP* **09** (2025) 167.

4. V. Mohan and L. Thorlacius, Spacetime from Operator Algebras, arXiv:2606.10924 [hep-th].

2 Holographic Complexity

In our universe, the grandest forms often arise from the simplest beginnings. It is natural to ask what drives the growth of this *complexity* and whether there exist fundamental bounds on its rate of growth. In physics, such questions are particularly important when studying the dynamics of quantum systems. In the next subsection, we introduce and review the notion of *Krylov complexity*, which quantifies the growth of operators under Hamiltonian evolution in quantum systems.

2.1 Krylov Complexity

In theoretical computer science, one introduces a notion of computational complexity to quantify how complicated a string of bits is. More precisely, complexity may be defined as the minimal number of universal gates required to obtain a given output string from some fixed reference string. This notion naturally extends to quantum systems, where it gives rise to what is referred to as *circuit complexity*. Consider a state $|\Psi\rangle$ in the Hilbert space of the theory. We then ask what is the minimal number of unitary gates required to reconstruct $|\Psi\rangle$ from some reference state $|\Psi\rangle_{\text{ref}}$ [14]. This notion of complexity appears in the theory of quantum computation and provides an example of *state complexity*. In this thesis, however, we will not work with this notion, but instead focus on the concept of operator complexity.[1]

Developments in the study of quantum chaos and scrambling of information in many-body quantum systems [16, 17] have led to the notion of *Krylov complexity* (or K-complexity) [18]. We now define K-complexity and refer [19, 20, 21] for recent detailed reviews. Interestingly, many of the mathematical tools underlying this construction can be traced back to the work of Krylov [22] and Lanczos [23] several decades earlier (see [24] for a detailed historical discussion).

Consider a quantum mechanical system with a time-independent Hamiltonian H. The time evolution of an operator $\mathcal{O}$ is given by

$$\mathcal{O}(t) = e^{-iHt}\mathcal{O}e^{iHt}\,, \tag{1}$$

[1]There is also an operational reason for shifting away from circuit complexity. To obtain a finite circuit complexity, one must introduce a tolerance parameter [15]. In the quantum field theories we are ultimately interested in studying, this parameter cannot be naturally identified with the UV cutoff, obscuring its physical relevance in the situations of interest.

where we have denoted $\mathcal{O}(0)$ by $\mathcal{O}$. Introducing the Liouvillian super-operator

$$\mathcal{L} = [H, \cdot]\,, \tag{2}$$

we may formally expand the operator evolution as

$$\mathcal{O}(t) = \sum_{n=0}^{\infty} \frac{(it)^n}{n!} \mathcal{L}^n \mathcal{O}\,. \tag{3}$$

The space of linear operators acting on a Hilbert space $\mathcal{H}$ also forms a Hilbert space, which we denote by $\hat{\mathcal{H}}$. We therefore associate to every operator $\mathcal{O}$ a state

$$|\mathcal{O}) \in \hat{\mathcal{H}}\,. \tag{4}$$

In this space, we can then introduce an inner product. A convenient choice is to use the inner product inherited from $\mathcal{H}$, or alternatively a physically relevant inner product such as the thermal inner product (see [25] or [21] for further details).

Now consider the vector space generated by repeated action of the Liouvillian:

$$\mathcal{K} = \{|\mathcal{O}),\ \mathcal{L}|\mathcal{O}),\ \mathcal{L}^2|\mathcal{O}),\ \cdots\}\,, \tag{5}$$

This space is referred to as *Krylov subspace*. We now construct an orthonormal basis $|\mathcal{O}_n)$ for the Krylov subspace using the Gram-Schmidt orthogonalization procedure. We begin with

$$|\mathcal{O}_0) = |\mathcal{O})\,, \qquad |\mathcal{O}_1) = b_1^{-1}\mathcal{L}|\mathcal{O})\,, \tag{6}$$

where $b_1 = (\mathcal{O}\mathcal{L}|\mathcal{L}\mathcal{O})^{1/2}$. The remaining basis elements are generated iteratively through

$$|A_n) = \mathcal{L}|\mathcal{O}_{n-1}) - b_{n-1}|\mathcal{O}_{n-2})\,, \tag{7}$$

followed by normalization,

$$|\mathcal{O}_n) = b_n^{-1}|A_n), \quad b_n = (A_n|A_n)^{1/2}\,. \tag{8}$$

The resulting states $|\mathcal{O}_n)$ form an orthonormal basis of the Krylov subspace.

The time-evolved operator can then be expanded in this basis as follows:

$$|\mathcal{O}(t)) = \sum_n i^n \varphi_n(t)|\mathcal{O}_n)\,, \tag{9}$$

where the wavefunctions $\varphi_n(t)$ satisfy the discrete Schrödinger equation

$$\partial_t \varphi_n(t) = b_n \varphi_{n-1}(t) - b_{n+1}\varphi_{n+1}(t)\,. \tag{10}$$

This equation admits a simple physical interpretation as that of a particle hopping on a semi-infinite chain labelled by the index n. Krylov complexity is then defined as the average position of the particle on this chain:

$$C_K(t) = \sum_n n|\varphi_n(t)|^2\,. \tag{11}$$

Therefore, Krylov complexity provides a reformulation of the time evolution of an operator as a one-dimensional quantum mechanical problem.[2]

In a chaotic system, complexity is expected to display universal features that are largely independent of microscopic details [27]. As a function of time, it first grows exponentially, then transitions to a linear regime, with a rate proportional to the number of degrees of freedom. This linear growth continues up to times exponential order in the entropy of the system, after which the complexity saturates to a constant. This exponential growth-ramp-plateau structure is expected to be universal across chaotic systems.

2.2 Complexity=Volume

The study of Krylov complexity has attracted significant attention in recent years, see for example its applications in conformal field theories [28, 29] and open quantum systems [30, 31, 32]. Since Krylov complexity can be defined in field theories with gravitational duals, it is natural to ask whether there exists a corresponding bulk notion of complexity. Motivated by the growth of codimension-two extremal surfaces studied by Hartman and Maldacena [33], Susskind and Stanford conjectured that the complexity of a black hole is given by the volume of boundary anchored extremal volumes passing through the interior of the black hole [34, 35]. We now review this proposal.

Consider a static $(d+1)$-dimensional black hole with metric

$$\mathrm{d}s^2 = -f(r)\mathrm{d}t^2 + \frac{\mathrm{d}r^2}{f(r)} + r^2 \mathrm{d}\Omega_{d-1}^2\,, \tag{12}$$

where $f(r)$ denotes the blackening factor. Depending on the solution, the spacetime may be asymptotically flat, AdS, or dS. The solution could even be charged. The event horizon is located at $r = r_h$. It is convenient to introduce Eddington-Finkelstein coordinates,

$$v = t + r^*\,, \qquad u = t - r^*\,, \qquad \text{where} \quad \frac{\mathrm{d}r^*}{\mathrm{d}r} = \frac{1}{f(r)}\,. \tag{13}$$

Now consider a codimension-one surface passing through the black hole interior (see Figure 2.1). Its volume is given by

$$\mathcal{V} = \Omega_{d-1} \int \mathrm{d}\lambda\; r^{d-1} \sqrt{-f(r)\dot{v}^2 + 2\dot{v}\dot{r}}\,, \tag{14}$$

where the surface is parametrized by λ through the embedding functions $(v(\lambda), r(\lambda))$. Here, Ω_{d-1} denotes the volume of the unit $(d-1)$-sphere. We anchor the surface to a cutoff surface located in the asymptotic region at $r = r_{\mathrm{UV}}$, with boundary times chosen as

$$t_R = -t_L = \frac{\tau}{2}\,. \tag{15}$$

[2] As an aside, one can also define a notion of state complexity on the Krylov subspace, known as *spread complexity* [26].

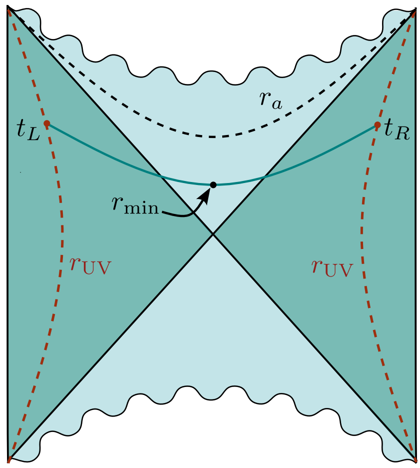

Figure 2.1. The Penrose diagram of a $(d+1)$-dimensional AdS-Schwarzschild black hole. The codimension-one extremal volume surface is shown in blue. The turning point of the surface, located at $r = r_{\min}$, lies in the interior of the black hole. The extremal surface is anchored at a cutoff surface located at $r = r_{\mathrm{UV}}$, with anchoring times $t_R = -t_L = \tau/2$. The accumulation surface, located at $r = r_a$, is indicated by the black dashed curve.

We also denote the location of the turning point of the surface by $r = r_{\min}$.

We now extremize the volume functional to obtain the extremal surfaces. Choosing the parametrization

$$r^{d-1}\sqrt{-f\dot{v}^2 + 2\dot{v}\dot{r}} = 1\,, \tag{16}$$

the equations of motion become

$$\begin{aligned} p &= r^{2(d-1)}\left(f(r)\dot{v} - \dot{r}\right)\,, \\ r^{2(d-1)}\dot{r}^2 &= f(r) + r^{-2(d-1)}p^2\,. \end{aligned} \tag{17}$$

Here, p is a conserved quantity associated with translations in v. The turning point $r_{\min}$ is determined by setting $\dot{r} = 0$:

$$r_{\min}^{2d-2} f(r_{\min}) + p^2 = 0\,. \tag{18}$$

The holographic complexity, defined through Complexity=Volume (CV) proposal, is then given by the volume of this extremal surface V_{ext}:

$$C_V = \frac{V_{\mathrm{ext}}}{G_N \ell_0}\,. \tag{19}$$

Here, ℓ_0 is a reference length scale. For an AdS-Schwarzschild black hole, ℓ_0 is typically chosen to be the AdS radius, while for asymptotically flat Schwarzschild black holes, it is usually taken to be the horizon radius r_h. In charged black holes, ℓ_0 is identified with the outer horizon radius.

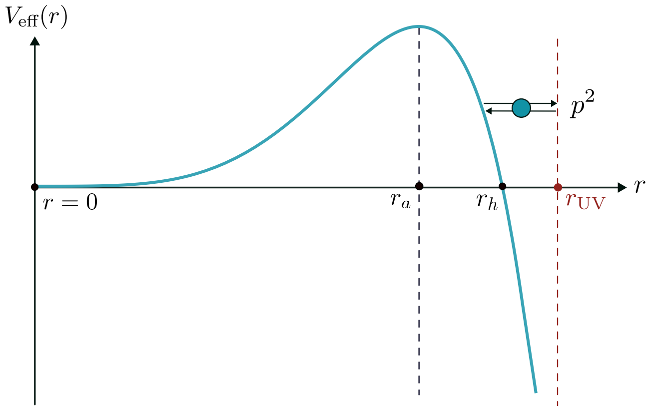

Figure 2.2. The plot of the effective potential for a $(d+1)$-dimensional eternal AdS-Schwarzschild black hole. The extremal volume surface can be thought of as a particle with fixed energy p^2 scattering off this potential.

The appearance of this additional length scale, whose definition depends on the particular black hole solution under consideration, was one of the original motivations for alternative proposals such as Complexity=Action (CA), where no such scale appears explicitly [36]. Nevertheless, it was argued in [37] that a universal prescription for ℓ_0 may still exist.

Now, let us compute the growth rate of the holographic complexity. Using the equations of motion (17), one can express the boundary time τ as an integral over the radial coordinate:

$$\frac{\tau}{2} + r_{\text{UV}} - r^*_{\text{min}} = \int_{r_{\text{min}}}^{r_{\text{UV}}} \mathrm{d}r \left[\frac{p}{f(r)\sqrt{f(r)r^{2(d-1)} + p^2}} + \frac{1}{f(r)} \right] . \tag{20}$$

Then, we can then arrive at the following expression [38]

$$\frac{\mathrm{d}C_V}{\mathrm{d}\tau} = \frac{\Omega_{d-1}}{G_N \ell_0} \sqrt{f(r_{\text{min}})} r^{d-1}_{\text{min}} . \tag{21}$$

We now study the late-time behaviour of these extremal surfaces. There is a useful reformulation of the equations of motion in terms of a particle scattering problem. Performing the change of variables

$$\frac{\mathrm{d}\tilde{r}}{\mathrm{d}r} = r^{2d-2} , \tag{22}$$

the equation of motion can be rewritten as

$$\dot{\tilde{r}}^2 + V_{\text{eff}} = p^2 , \qquad V_{\text{eff}} = -r^{2d-2} f(r) . \tag{23}$$

In this picture, the conserved quantity p^2 plays the role of the energy of the particle.

An interesting feature is that, for essentially all static black hole solutions, including charged black holes, the effective potential exhibits the same qualitative structure (see Figure 2.2). The potential vanishes at $r = 0$ and develops a maximum at some radius $r = r_a$ located inside the event horizon. We refer to the hypersurface at $r = r_a$ as the *accumulation surface*.

Let us now study how the extremal surface evolves as the boundary anchoring time τ is increased. When $\tau = 0$, the equations of motion imply that $p = 0$. As τ increases, the conserved quantity p increases monotonically. In the scattering picture, this means that, at early times, the particle is scattering off the bottom of the potential. As τ increases, the turning point of the particle approaches the top of the potential. Consequently, in the $\tau \to \infty$ limit, the turning point $r_{\min}$ can be very well approximated by the location of the accumulation surface at $r = r_a$.[3]

As a result, the late-time growth rate of holographic complexity is given by

$$\frac{\mathrm{d}C_V}{\mathrm{d}\tau} \simeq \frac{\Omega_{d-1}}{G_N \ell_0} \sqrt{-f(r_a)}\, r_a^{d-1} \,. \tag{24}$$

Using the definitions of the black hole entropy S and temperature T, one can further show that

$$\frac{\mathrm{d}C_V}{\mathrm{d}\tau} \propto ST \,. \tag{25}$$

Thus, holographic complexity grows linearly at late times, with a growth rate proportional to the number of degrees of freedom associated with the horizon entropy. This reproduces the expected behaviour of a finite-dimensional chaotic quantum system, sans the complexity plateau. The plateau does not appear here because we have only performed a classical computation. As we will see in the next subsection, the inclusion of quantum corrections restores the plateau as well.

2.3 Quantum Complexity in JT gravity

In certain two-dimensional models of dilaton gravity, holographic complexity can in fact be defined non-perturbatively using their matrix model duals. An example is Jackiw-Teitelboim (JT) gravity [39, 40], whose action is given by

$$S = S_0 \chi(\mathcal{M}) + \frac{1}{2}\int_{\mathcal{M}} \mathrm{d}^2x \sqrt{-g}\,(R+2)\,\phi + \frac{1}{2}\int_{\partial\mathcal{M}} \mathrm{d}t \sqrt{-h}\,(K-1)\,, \tag{26}$$

Here, $\chi(\mathcal{M})$ denotes the Euler character of the manifold $\mathcal{M}$, and we have set the AdS_2 radius to unity. This theory can be obtained through the spherical reduction of Einstein-Maxwell theory near the horizon of a four-dimensional near-extremal black hole [41, 42]. In that context, the parameter S_0 corresponds

[3] This accumulating behaviour is the reason we refer to the late-time limiting surface as the accumulation surface.

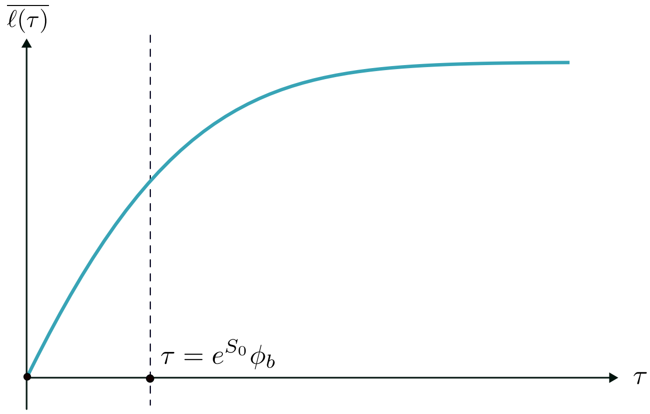

Figure 2.3. The log-log plot of the average length $\overline{\ell(\tau)}$ as a function of τ for $\beta \gg \phi_b$.

to the extremal entropy of the higher-dimensional black hole. However, when JT gravity is viewed as a standalone two-dimensional theory, we simply treat S_0 as a constant parameter.

JT gravity is argued to be dual to a one-cut Hermitian matrix model whose leading disk density of states is [43]

$$\rho_0 = \mathrm{e}^{S_0} \sinh(2\pi\sqrt{E})\,. \tag{27}$$

This matrix model completion allows us to probe non-perturbative quantum gravity effects.

Since we are working in two dimensions, the holographic complexity, defined through the CV prescription, is given by the length of a boundary anchored spacelike geodesic [44]:

$$C_V = S_0 \ell \tag{28}$$

The bulk gravitational theory is dual to a boundary Schwarzian theory, and the average length of the spacelike geodesic admits a non-perturbative definition in terms of matrix elements of an operator $\mathcal{O}_\Delta$ with scaling dimension Δ [45]:

$$\overline{\ell(\tau)} = \int_0^\infty \mathrm{d}E_1 \mathrm{d}E_2\, \overline{\rho(E)\rho(E')}\; e^{-\frac{\beta}{2}(E_1+E_2)} e^{-i\tau(E_1-E_2)} \mathcal{M}_\Delta\left(E_1, E_2\right)\,. \tag{29}$$

The quantity $\mathcal{M}_\Delta(E_1, E_2)$ is related to the matrix elements of the operator $\mathcal{O}_\Delta$ through

$$\mathcal{M}_\Delta(E_1, E_2) = -\lim_{\Delta\to 0} \frac{\partial}{\partial\Delta} \left|\langle E_1|\mathcal{O}_\Delta|E_2\rangle\right|^2\,. \tag{30}$$

The connected two-point function of the density of states is given by

$$\overline{\rho(E)\rho(E')} = \rho_0(E)\rho_0(E') - \frac{\sin^2\left(\pi\rho_0(\bar{E})\left(E-E'\right)\right)}{\left(\pi\left(E-E'\right)\right)^2} + \rho_0(\bar{E})\delta\left(E-E'\right)\,, \tag{31}$$

where $\bar{E} = (E + E')/2$ is the average energy. The second term is usually referred to as the *sine-kernel* in literature. This term encodes the level repulsion of the random matrix theory (RMT), and it will play an important role both in the present discussion and in later sections.

In Figure 2.3, the length $\overline{\ell(\tau)}$ is plotted as a function of τ. It is useful to obtain closed-form expressions for the length in the early-time and late-time limits. Substituting the explicit expressions into (29), one finds that the averaged geodesic length behaves as [45]

$$\overline{\ell(\tau)} \approx \begin{cases} C_1 \tau + \dots & \tau \ll e^{S_0} \phi_b \\ C_0 - \dots & \tau \gg e^{S_0} \phi_b \end{cases} , \tag{32}$$

where

$$\begin{aligned} C_0 &= \frac{e^{S_0} \phi_b}{6\pi^2} \left[e^{6\pi^2 \phi_b/\beta} \left(1 + \frac{16\pi^2 \phi_b}{\beta} \right) - e^{-2\pi^2 \phi_b/\beta} \right] , \\ C_1 &= 2e^{-2\pi^2 \phi_b/\beta} \sqrt{\frac{\phi_b}{\pi\beta/2}} + \frac{\operatorname{erf}\left(\sqrt{\frac{2\pi^2 \phi_b}{\beta}} \right)}{\pi} \left(1 + \frac{4\pi^2 \phi_b}{\beta} \right) . \end{aligned} \tag{33}$$

Here, ϕ_b denotes the boundary value of the dilaton and sets the scale for the breaking of the boundary time reparametrization symmetry [46]. Using the definition (28), we obtain the holographic complexity. In the regime where the inverse temperature β is much smaller than ϕ_b, the early-time growth reproduces the same linear behaviour as in (25). At times of order $e^{S_0} \phi_b$, the complexity saturates, precisely as expected from general arguments.

It is important to emphasize that this saturation relies crucially on the sine-kernel and Dirac delta contributions in the density-density correlator (31). If one retained only the disconnected contribution $\rho_0(E)\rho_0(E')$, then the complexity would continue to grow linearly forever, reproducing the semiclassical behaviour discussed earlier [47]. The non-perturbative corrections encoded in the sine kernel are therefore directly responsible for the saturation of complexity.

The fact that bulk extremal volumes reproduce the behaviour of boundary Krylov complexity strongly suggests that the two quantities are holographically dual to one another. Indeed, in two-dimensional models such as JT gravity [48, 49] and sine-dilaton gravity [50], one can explicitly demonstrate that the complexity computed through the CV proposal equals the Krylov complexity of the dual boundary theory, described in terms of double-scaled or triple-scaled variants of the Sachdev-Ye-Kitaev model. This provides another entry in the holographic dictionary and opens new avenues for probing quantum gravity in the bulk through boundary dynamics.

3 Black Hole Singularities and Quantum Complexity

Before 1965, there were already hints of catastrophic infinities appearing in general relativity. A classic example is the singularity in the past of the Friedmann closed universe [51]. Oppenheimer and Snyder later studied the time-reversed situation and constructed an explicit solution to Einstein's field equations describing the gravitational collapse of a massive star that had exhausted its thermonuclear fuel [52].

At the time, however, these observations were either dismissed [53] or largely forgotten by the community [54], owing to the highly symmetric nature of the Schwarzschild solution and the belief that such situations were physically unattainable in our universe.

In 1965, Penrose published his singularity theorem [55], which immediately triggered a wave of activity in the community [56, 57, 58]. Penrose's proof not only established the inevitability of singularities in classical general relativity under broad physically relevant assumptions, but also introduced powerful new mathematical tools into the field.[4]

3.1 Penrose's Singularity Theorem

Characterizing singularities in general relativity is a difficult problem. If one uses the divergence of curvature tensors, or invariants constructed out of them, as the definition of a singularity, then one immediately encounters several difficulties ([60] contains many examples). A way around this problem is to instead use *geodesic incompleteness* as a *sufficient* condition for the existence of a singularity. A critical limitation of this approach, however, is that geodesic incompleteness does not necessarily imply the existence of a singularity. We will return to this point at the end of this section.

Let us begin with some definitions. We will mostly follow the notation and conventions of Hawking and Ellis [61]. Consider a point p on a manifold M. We define its *chronological future* $I^+(p)$ as the set of all points on the manifold that can be reached from p by a future-directed timelike curve. Similarly, one defines the *chronological past* $I^-(p)$ by replacing 'future' with 'past' and '+' with '−'.

We define the *causal future* of p, denoted by $J^+(p)$, as the set of all points

[4] See [59] for a letter from Chandrasekhar to Hawking inquiring about a syllabus to learn the mathematics behind the singularity theorems.

that can be reached from p by a non-spacelike curve. From the definition, it follows that $\partial I^+(p) = \partial J^+(p)$.

A spacetime is said to be *globally hyperbolic* iff there are no closed timelike curves and, for any two points p and q, the set, $J^+(p) \cap J^-(q)$ is compact.

We now introduce the notion of a *closed trapped surface*. One of the central ingredients in Penrose's theorem is the existence of such surfaces. In [55], a closed trapped surface is defined as a closed spacelike two-dimensional surface for which the two families of orthogonal future-directed null rays initially converge. Denoting the tangent vector fields of the two null congruences by k_1^μ and k_2^μ, we require their corresponding expansions

$$\theta_{1,2} = \nabla_\mu k^\mu_{1,2} \tag{34}$$

to satisfy

$$\theta_{1,2} < 0 \tag{35}$$

at the trapped surface.

Using these definitions, we can now state Penrose's theorem:

Theorem: A manifold M cannot be null geodesically complete if

- $R_{\mu\nu} k^\mu k^\nu \geq 0$ for all null vectors k^μ
- there is a closed trapped surface $\mathcal{T}$
- the manifold is globally hyperbolic.

The complete proof of this theorem can be found in several standard references. Here, we will only sketch the proof following [61], emphasizing the aspects that will be relevant for later discussions.

Proof: Since the manifold is globally hyperbolic, the boundary of the causal future $\partial J^+(\mathcal{T})$ is generated by null geodesics emerging orthogonally from $\mathcal{T}$. The expansion θ of these null geodesics, with tangent vector k^μ, obeys the Raychaudhuri equation[5]

$$\frac{\mathrm{d}\theta}{\mathrm{d}s} = -R_{\mu\nu} k^\mu k^\nu - 2\sigma^2 - \frac{1}{2}\theta^2 \,, \tag{36}$$

where $\sigma^2 \equiv \sigma_{\mu\nu}\sigma^{\mu\nu} \geq 0$ is the squared shear of the congruence. Since $R_{\mu\nu} k^\mu k^\nu \geq 0$, the first two terms on the right-hand side are non-positive. Dropping them gives the inequality

$$\frac{\mathrm{d}\theta}{\mathrm{d}s} \leq -\frac{\theta^2}{2} \,. \tag{37}$$

Integrating the above expression, we get

$$\theta(s) \leq \frac{2}{s - (2\theta_0)^{-1}} \,, \tag{38}$$

[5] For a timelike congruence, the factor in front of the square of the expansion will be -1/3.

where θ_0 is the expansion at $\mathcal{T}$. Since $\mathcal{T}$ is a trapped surface, we have $\theta_0 < 0$ for both orthogonal null congruences. It then follows that there exists a finite value of the affine parameter s at which the expansion diverges to $-\infty$. The corresponding point is referred to as a conjugate point.

Geometrically, the divergence of the expansion indicates that neighboring geodesics intersect at the conjugate point. More importantly for our purposes, any continuation of the null geodesic beyond the conjugate point necessarily lies *inside* $I^+(\mathcal{T})$, rather than on its boundary (see Proposition 4.5.14 of [61]). Therefore, every null curve generating $\partial J^+(\mathcal{T})$ would have an endpoint at or before the conjugate point to $\mathcal{T}$.

Now suppose, for contradiction, that the spacetime is future null geodesically complete. Then every null generator can be extended to an arbitrary affine parameter. In particular, the conjugate point along each generator also lies within the spacetime. As a result, $\partial J^+(\mathcal{T})$ is closed.

Now consider the continuous map

$$\beta : \mathcal{T} \times [0, b] \times \{1, 2\} \to M \tag{39}$$

defined by flowing a point $p \in \mathcal{T}$ along one of its two orthogonal future-directed null geodesics, labelled by 1 or 2, for an affine distance $v \in [0, b]$. If $b = b_0$ is chosen sufficiently large so that both orthogonal null geodesics reach their conjugate points before the affine parameter b_0, then every point of $\partial J^+(\mathcal{T})$ lies in the image of β. Since $\mathcal{T} \times [0, b_0] \times Q$ is compact and β is continuous, the image of β is compact. As $\partial J^+(\mathcal{T})$ is a closed subset in this compact set, it follows that $J^+(\mathcal{T})$ is compact.

However, this is incompatible with the global hyperbolicity of the spacetime. To see this, consider a non-compact Cauchy surface Σ, whose existence is guaranteed by global hyperbolicity. Since $J^+(\mathcal{T})$ is achronal, we can always find a smooth timelike vector field that intersects both the Cauchy surface Σ and $J^+(\mathcal{T})$ once. The integral curve of this field then defines a one-to-one correspondence between points of $J^+(\mathcal{T})$ and points on Σ. Since Σ is non-compact, $J^+(\mathcal{T})$ cannot be compact. This contradiction shows that the assumption of future null geodesic completeness is false. ■

It is worth emphasizing that Penrose's theorem only establishes null geodesic incompleteness of the spacetime. In general, this does not necessarily mean that the spacetime terminates at a singularity. In many situations, it instead indicates the presence of a Cauchy horizon beyond which the spacetime may admit a regular extension.

It is interesting to note that Penrose's theorem, as well as many later singularity theorems, share the same three basic ingredients [62]:

1. an energy condition,
2. an initial condition,
3. a causality condition.

Using Einstein's equations, the condition

$$R_{\mu\nu} k^\mu k^\nu \geq 0 \tag{40}$$

may be rewritten as the null energy condition (NEC),

$$T_{\mu\nu}k^{\mu}k^{\nu} \geq 0, . \tag{41}$$

Similarly, global hyperbolicity guarantees an appropriate notion of causal simplicity [61]. One may therefore think of the singularity theorem as the statement that, under suitable causality and energy conditions, the existence of certain initial conditions necessarily leads to null geodesic incompleteness.

3.2 Generalized Entropy and Inclusion of Quantum Corrections

Penrose's theorem is a result of *classical* general relativity: The null energy condition (NEC) is satisfied by all classical matter fields but is known to be violated by quantum systems [63, 64, 65, 66]. It is therefore natural to ask whether one can prove a singularity theorem when quantum corrections are included.

To answer this question, consider the generalized entropy associated with a codimension-two surface:

$$S_{\text{gen}} = \frac{A}{4G_N} + S_{\text{out}}\,, \tag{42}$$

where A is the area of the entangling surface and S_{out} is the von Neumann entropy of the quantum fields outside the surface. The motivation for this combination goes back to Bekenstein [67], who observed that identifying the Bekenstein-Hawking area term alone with thermodynamic entropy leads to apparent violations of the second law in processes such as black hole evaporation. In semiclassical gravity, one can show that the generalized entropy associated with a causal horizon is monotonically non-decreasing as the surface is evolved toward the future along the horizon [68, 69, 70]. This statement is the *generalized second law* (GSL). The key point to note here is that GSL holds even when the classical NEC is violated.

With these ingredients in place, Wall [71] established a remarkable singularity theorem. The first step is to replace the classical notion of a trapped surface with a *quantum trapped surface*: a codimension-two surface on which the functional derivative of the generalized entropy with respect to deformations along both future-directed null normals is everywhere negative,

$$\left.\frac{\delta S_{\text{gen}}}{\delta\lambda_{(A)}}\right|_{\mathcal{S}} < 0\,, \qquad A = 1, 2\,. \tag{43}$$

This replaces the classical condition $\theta_{(A)} < 0$ on both null expansions. The GSL then plays the role of the 'energy condition', ensuring that quantum trapped surfaces cannot escape to future null infinity. Together with global hyperbolicity, the 'causality condition', Wall showed that the existence of a quantum trapped surface implies future null geodesic incompleteness [71].

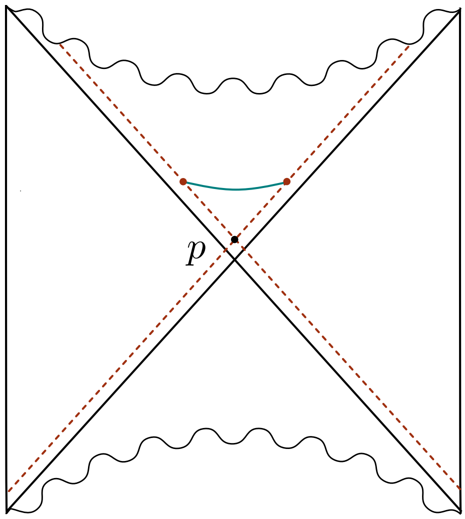

Figure 3.1. Extremal volume surfae anchored to a null sheet $N = \partial I^+(p)$. The point p lies in the interior of the black hole.

Holographic complexity has also been proposed to satisfy a second law [72, 73]. This raises a natural question: if the GSL is sufficient to arrive at a singularity theorem, can an analogous result be derived using complexity and its second law as the guiding principle? This question is the central motivation of [74], which we briefly review in the following subsection.

3.3 Second Law of Complexity and Black Hole Singularities

We start by defining a notion of a *causal horizon*, following Jacobson and Parentani [75]. Consider a timelike worldline W that is future-infinite, meaning that the proper time runs all the way to infinity. We then define the future causal horizon associated with W as the boundary of its chronological past,

$$H_{\text{fut}} = \partial I^-(W)\,. \tag{44}$$

This definition includes standard black hole horizons as well as observer-dependent horizons such as Rindler and de Sitter horizons.

Using this notion of a causal horizon, we state the second law of complexity (SLC) as follows:

Second Law of Complexity: The volume of extremal surfaces anchored to a causal horizon H_{fut} always increases as the anchor point is moved toward the future along the horizon.

Unlike the generalized second law, we currently do not have a proof of the SLC. Instead, its validity is motivated by several explicit computations in different gravitational settings that consistently exhibit this behaviour. In this section, we therefore assume the validity of the SLC. At face value, the law provides a constraint on the growth of extremal volumes in spacetime and therefore plays the role of an effective energy condition.

If the SLC provides the analogue of the energy condition, then the next step is to identify the appropriate 'initial condition' that leads to geodesic incompleteness. To motivate this, consider the eternal black hole discussed in the CV review of Section 2.2. There, extremal volume surfaces were anchored to a cutoff surface near the asymptotic boundary. Instead, let us now anchor the extremal surfaces on an infalling null sheet

$$N \equiv \partial I^+(p)\,, \tag{45}$$

where p is a point in the interior of the black hole (see Figure 3.1). We can then ask the same question as before: how does the extremal volume change as the anchor point is moved toward the future along N?

Two qualitatively distinct behaviours emerge. First, if the anchor points lie outside the accumulation surface, then one reproduces the standard behaviour discussed earlier: the extremal volume increases as the anchor point approaches the accumulation surface.

However, once the anchor points cross the accumulation surface, the behaviour changes dramatically. The extremal volumes now begin to decrease as the anchor point is moved further toward the future. We refer to such surfaces as *trapped extremal surfaces*: extremal surfaces whose volumes decrease under future evolution of their anchor points. These surfaces play the role of trapped surfaces in Penrose's theorem. Since they occur only inside the accumulation surface, the accumulation surface itself acts as a *trapping* surface.[6]

Let us now briefly explain how the existence of trapped extremal surfaces together with the SLC leads to null geodesic incompleteness. Consider the null sheet $N = \partial I^+(p)$ on which the trapped extremal surface is anchored. The null sheet is generated by null geodesics. The affine parameter along these curves cannot extend to infinity. Indeed, if the curves were future complete, then N would itself define a causal horizon. But the SLC states that *any* extremal volumes anchored on a causal horizon must increase toward the future. But by definition, trapped extremal surfaces have decreasing volume. This contradiction implies that the null curves generating N must have a future endpoint.

The remainder of the argument then follows Penrose's proof. If the spacetime were null geodesically complete, then N would contain its future endpoints, making it closed. One can then define the same map β used in the Penrose theorem and show that N is compact. However, the existence of such a compact null hypersurface is incompatible with global hyperbolicity. We therefore conclude that the spacetime is null geodesically incomplete.

[6] It is interesting to compare this behaviour with the standard trapped surface analysis, where such objects can occur anywhere inside the black hole horizon. In contrast, trapped extremal surfaces appear only behind the accumulation surface, which lies deeper in the black hole interior.

4 Late-time Behaviour of Holographic Complexity

The principle of black hole complementarity puts forward the proposition that, when viewed from afar, a black hole behaves as a quantum mechanical system with a finite number of degrees of freedom accounting for the Bekenstein-Hawking entropy [76]. The dynamics of such a quantum mechanical system is expected to be chaotic in order to scramble information as efficiently as possible [11]. As a result, the complexity of a quantum black hole should display the standard behaviour of a generic finite-dimensional chaotic quantum system: an initial scrambling regime followed by a ramp and eventually a late-time plateau.

However, we have seen that if one studies holographic complexity through the Complexity=Volume (CV) proposal, one never observes such a late-time plateau in a higher-dimensional black hole. In the case of JT gravity, the complexity plateau arose from non-perturbative corrections that encode information about the energy spectrum of the theory (see the discussion in Section 2.3). From this perspective, it is not surprising that a classical gravitational computation fails to capture these genuinely non-perturbative quantum effects.

A natural question is then whether there exists a systematic way to recover such corrections starting from the classical computation itself. In [77], we showed that this is indeed possible for a large class of static black hole solutions. We now review the main ideas and results of this construction.

The central observation is that, at late times, the growth rate of extremal volumes is dominated by the contribution from a region near the accumulation surface. This follows from two related facts. First, the late-time growth rate (21) depends only on the turning point of the extremal surface and not on the location of the UV cutoff surface at $r = r_{\text{UV}}$. The only requirement for obtaining the same growth rate is that the volume computation includes a small neighborhood around the turning point. This suggests that the dominant contribution to the growth originates from this region.

Second, in the effective scattering picture discussed earlier, we saw that the turning point approaches the accumulation surface at late times. Combining these observations, we conclude that the late-time growth of extremal volumes comes almost exclusively from a small region around the accumulation surface.

Since the accumulation surface lies at a fixed radial coordinate r, its transverse area remains constant. The volume computation in a neighborhood of this surface may therefore be approximated by a geodesic length computation in an auxiliary two-dimensional geometry. Remarkably, one can show quite generally that this auxiliary geometry is AdS_2 for all static black hole solutions. This result is independent of both the spacetime dimension and the asymptotic structure of the geometry; the black hole may even carry charge.

Furthermore, if one dimensionally reduces the Einstein-Hilbert action around the accumulation surface and expand upto linear order, the resulting effective theory is precisely JT gravity, with an extremal entropy S_0 determined by the area of the accumulation surface.

The upshot is therefore that, at late times, the extremal volume computation in a $(d+1)$-dimensional static black hole can be rewritten as a geodesic length computation in an auxiliary AdS_2 spacetime governed by an emergent JT gravity description.

In Section 2.3, we saw that geodesic lengths in JT gravity admit a non-perturbative completion through the dual matrix model description. Performing this completion and translating the result back into the variables of the higher-dimensional theory, one finds that the holographic complexity saturates at times of order $e^{O(S)}$, where S is the Bekenstein-Hawking entropy of the higher-dimensional black hole. This reproduces the expected behaviour from black hole complementarity.

Since the parameters of the emergent JT gravity theory depend on the higher-dimensional black hole solution, different black holes exhibit different saturation timescales (see [77] for a table of results). An interesting consistency check arises for near-extremal Reissner-Nordström black holes, where the saturation timescale agrees precisely with that of the near-horizon JT gravity description.

Finally, it is worth emphasizing that the non-perturbative corrections arising from the matrix model description of the emergent JT gravity kick in when the extremal volume surfaces reach the vicinity of the accumulation surface. This suggests the possibility that the classical volume computations break down *behind* the accumulation surface as well, since we are only getting closer to the black hole singularity. In [74], we showed that trapped extremal surfaces appear precisely behind this surface. It is therefore natural to expect that these pathological trapped extremal surfaces also receive non-perturbative corrections. This raises the intriguing possibility that these effects may ultimately be related to the resolution of black hole singularities.

A curious observation we make in [77] is that the average graph distance traveled by a random walker from the origin of a high-dimensional hypercube reproduces the expected behaviour of the complexity of a chaotic system. The saturation of the complexity admits a neat geometric interpretation. Once the random walker gets lost in the 'bulk' of the hypercube, the next step is equally likely to increase or decrease the distance from the origin. This toy model acts as a discretization of Nielsen's complexity geometry [78] and can also be seen to be related to Krylov complexity [79].

5 Black Hole Mimickers

In the previous section, we saw that non-perturbative quantum gravity corrections are necessary to obtain the late-time saturation of black hole complexity. Another regime where such non-perturbative effects may be expected to play an important role is at the endpoint of gravitational collapse. The production of a black hole with a horizon leads to information loss, and one proposed resolution is that black holes do not form in a UV-complete theory like string theory. Instead, horizonless ultra-compact objects, collectively referred to as black hole mimickers, replace them and avoid the information paradox altogether. In this section, we review *black shells* constructed in [80] and check their thermodynamic favourability when pitted against black holes (see [81] for further examples of such objects).

5.1 Black Shells

In 2001, Mazur and Mottola proposed an alternative endpoint for gravitational collapse called a *gravastar*, short for gravitational vacuum condensate star [82]. These are non-singular, horizonless compact objects consisting of a de Sitter interior and an exterior Schwarzschild geometry. The two regions are separated by a layer of stiff matter, with pressure p equal to the energy density ρ, confined between two thin shells.

Visser and Wiltshire later replaced the two-shell construction with a single thin shell and constructed a thin-shell gravastar [83]. They showed that these configurations are stable under perturbations for certain physically reasonable equations of state for the matter living on the shell.

In [80], Danielsson, Dibitetto, and Giri constructed *black shells*, in which the de Sitter interior of a thin-shell gravastar is replaced by an AdS vacuum. This modification is important because it allows a top-down construction in string theory, as many examples of AdS vacuum solutions are known, whereas the existence of controlled de Sitter vacua remains unclear. We now review this construction in more detail.

Consider a spherical shell of radius r_0 with an AdS_4 interior and a Schwarzschild exterior. The metric of the spacetime is then given by

$$\begin{aligned}
\mathrm{d}s_-^2 &= -\left(\frac{r^2}{\ell^2}+1\right)\mathrm{d}t_-^2 + \frac{\mathrm{d}r^2}{\left(\frac{r^2}{\ell^2}+1\right)} + r^2\mathrm{d}\Omega_2^2 \qquad && \text{if } r < r_0 \\
\mathrm{d}s_+^2 &= -\left(1-\frac{2M}{r}\right)\mathrm{d}t_+^2 + \frac{\mathrm{d}r^2}{\left(1-\frac{2M}{r}\right)} + r^2\mathrm{d}\Omega_2^2 \qquad && \text{if } r > r_0
\end{aligned} \tag{46}$$

We set Newton's constant to one. The time coordinates in the exterior and interior regions are denoted by t_+ and t_- respectively. The stress-energy tensor of the matter on the shell is taken to be that of a perfect fluid at rest,

$$S_{ij} = (\rho + p)u_i u_j + p h_{ij}\,, \tag{47}$$

where p is the pressure, ρ is the energy density, and u^i is the three-velocity of the fluid. Imposing the standard junction conditions [84, 85, 86] across the interface then gives

$$\rho = \frac{1}{4\pi r_0}\left(\sqrt{\frac{r_0^2}{\ell^2}+1} - \sqrt{1-\frac{2M}{r_0}}\right)\,, \tag{48}$$

$$p = \frac{1}{8\pi r_0}\left(\frac{1-\frac{M}{r_0}}{\sqrt{1-\frac{2M}{r_0}}} - \frac{1+\frac{2r_0^2}{\ell^2}}{\sqrt{\frac{r_0^2}{\ell^2}+1}}\right)\,. \tag{49}$$

The first junction condition (48) can be rewritten as an energy conservation equation:

$$4\pi r^2\rho - r\left(\sqrt{1+\frac{r_0^2}{\ell^2}} - 1\right) = E\,. \tag{50}$$

The terms on the left can be understood as the sum of the energy of the shell and the negative energy of AdS, while the energy on the right, defined as

$$E = r_0\left(1-\sqrt{1-\frac{2M}{r_0}}\right)\,, \tag{51}$$

corresponds to the energy of the exterior Schwarzschild geometry.

For a black shell configuration of energy E, the energy density is then given by

$$\rho_b \equiv \frac{E}{4\pi r_0^2} = \frac{1}{4\pi r_0}\left(1-\sqrt{1-\frac{2M}{r_0}}\right)\,. \tag{52}$$

Since we allow the black shell to be dynamical, its surface energy density $\rho_b(r)$ and surface pressure $p_b(r)$ satisfy the stress-energy conservation equation

$$p_b = -\rho_b - \frac{r}{2}\frac{d\rho_b}{dr}\bigg|_{r=r_0}\,. \tag{53}$$

Substituting the expression (52) for ρ_b, we can then solve for the surface pressure:

$$p_b = \frac{1}{8\pi r_0}\left(\frac{\frac{2r_0^2}{L^2}+1-\frac{M}{r_0}}{\sqrt{\frac{r_0^2}{L^2}+1-\frac{2M}{r_0}}} - \frac{1+\frac{2r_0^2}{L^2}}{\sqrt{1+\frac{r_0^2}{L^2}}}\right). \tag{54}$$

The key observation in [80] is that the matter content appearing in the junction conditions (48) and (49) can be realized explicitly in string theory. First, we replace the thin shell with a spherical brane. Then consider D0-branes in four dimensions. These D0-branes polarize and dissolve into the spherical brane. The dissolved D0 branes in turn support a gas of open strings stretching between them. As a result, the stress-energy tensor on the brane receives contributions from three sources:

1. the tension of the brane,
2. dissolved D0-branes behaving as stiff matter with equation of state $p_s = \rho_s$,
3. a gas of open strings with equation of state $p_g = \rho_g/2$.

These contributions uniquely solve the junction conditions provided the black shell satisfies the radiation equation of state [80]

$$p_b = \frac{1}{2}\rho_b\,. \tag{55}$$

Plugging in the expressions for the black shell surface energy density ρ_b and surface pressure p_b, we can immediately see that the radius of the shell gets fixed at the Buchdahl radius

$$r_0 = \frac{9M}{4}\,. \tag{56}$$

It can also be shown that this black shell configuration is stable against small radial perturbations, since various components are able to exchange energy and stabilize the system.

5.2 Thermodynamics of Black Shells

The existence of black shells as solutions to Einstein's equations, albeit with matter content motivated by string theory, raises the possibility that such objects could replace black holes as the endpoint of gravitational collapse. However, to establish such a statement, one must show that the nucleation of black shells is dynamically favoured over the formation of black holes.

An argument in favour of this process can be made by analogy with fuzzballs [87]. The nucleation of a shell may be viewed as a tunneling process whose amplitude is very small. However, black shells have a very large entropy, exceeding that of black holes at the same energy. As a result, the suppression from the small tunneling amplitude can be compensated by the large number of available states, resulting in a total amplitude that is not exponentially small and may even be favoured over black hole production.

Since a detailed dynamical computation of this process is currently unavailable, one may instead study the problem thermodynamically. This analysis was carried out in [88], whose main results we now summarize.

To obtain a well-defined canonical ensemble, we consider an exterior AdS-Schwarzschild geometry rather than the asymptotically flat Schwarzschild geometry discussed in the previous section. Operationally, this amounts to introducing an AdS length scale L in the exterior region:

$$\begin{aligned} \mathrm{d}s_-^2 &= -\left(\frac{r^2}{\ell^2}+1\right)\mathrm{d}t_-^2 + \frac{\mathrm{d}r^2}{\left(\frac{r^2}{\ell^2}+1\right)} + r^2\mathrm{d}\Omega_2^2 && \text{if } r<r_0 \\ \mathrm{d}s_+^2 &= -\left(\frac{r^2}{L^2}+1-\frac{2M}{r}\right)\mathrm{d}t_+^2 + \frac{\mathrm{d}r^2}{\left(\frac{r^2}{L^2}+1-\frac{2M}{r}\right)} + r^2\mathrm{d}\Omega_2^2 && \text{if } r>r_0 \end{aligned} \tag{57}$$

One can then repeat the same analysis as before. Imposing the radiation equation of state for the shell (55) gives a relation between the shell radius and the mass,

$$M = \frac{4r_0}{9}\left(\frac{1+\frac{3r_0^2}{2L^2}}{1+\frac{r_0^2}{L^2}}\right) \tag{58}$$

When we take $L \to \infty$, we obtain the Buchdahl radius of the previous subsection.

The temperature of the shell is determined by assuming that the open string gas thermalizes to the Unruh temperature at the shell surface, giving

$$T_S = \frac{1}{2\pi r_0^2}\left(M + \frac{r_0^3}{L^2}\right). \tag{59}$$

The entropy can be obtained via the first law of thermodynamics,

$$\frac{\mathrm{d}S}{\mathrm{d}M} = \frac{1}{T}, \tag{60}$$

and we find

$$S = \frac{2}{3}\pi L^2\left(3\log\left(L^2+r_0^2\right) - 2\log\left(L^3 + \frac{3Lr_0^2}{4}\right)\right). \tag{61}$$

The free energy of the shell F is then given by

$$\begin{aligned} F &= M - T_S S\,, \\ &= \frac{2r\left(2L^2+3r_0^2\right)}{9\left(L^2+r_0^2\right)} \\ &\quad - \frac{15L^2r_0^2+4L^4+9r_0^4}{27r^3+27L^2r_0}\left[3\log\left(L^2+r_0^2\right) - 2\log\left(L^3+\frac{3Lr_0^2}{4}\right)\right]. \end{aligned} \tag{62}$$

Now we can compare this free energy with that of AdS-Schwarzschild black holes and thermal AdS. To get a better understanding of the new phase transitions, let us first recall the standard Hawking-Page transition:

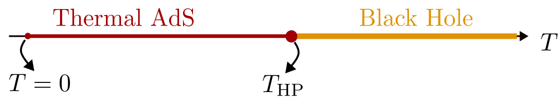

For temperatures in the range $0 < T < T_{\mathrm{HP}}$, where T_{HP} is the Hawking-Page temperature, empty AdS has lower free energy and is therefore thermodynamically preferred. When $T > T_{\mathrm{HP}}$, AdS black holes dominate the canonical ensemble.

Now let us introduce black shells into this mix. This gives us the phase diagram:

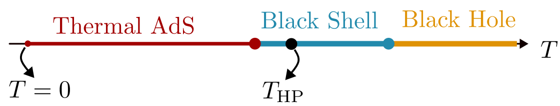

The black shell introduces more phase transitions. At low temperatures, empty AdS remains the thermodynamically preferred phase. At a temperature slightly lower than the Hawking-Page temperature, the black shell phase takes over. Then at a temperature higher than T_{HP}, black holes once again become thermodynamically favoured.

These phase transitions have interesting implications for AdS/CFT. In the temperature range where black shells dominate, the bulk dual of a thermal state in the boundary theory would correspond to a black shell rather than a black hole. Since most studies of the duality are performed in the planar limit, where AdS black holes dominate, this observation does not immediately require substantial modifications to the standard picture.

It is also straightforward to include charge in the analysis. Doing so leads to a much richer phase structure, with additional transitions between different phases depending on the value of the charge [88].

It is important to emphasize that this analysis only compares the thermodynamic favourability of the various solutions through their free energies. To determine whether black shells are genuinely preferred as the endpoint of gravitational collapse, one would need a dynamical understanding of the collapse process itself and of the mechanism selecting black shells over black holes. Exploring this question further would be very interesting.

6 Operator Algebras and Quantum Gravity

The study of von Neumann algebras and the algebraic formulation of quantum field theory has seen a revival of interest in recent years, driven in part by its applications to quantum gravity. In this chapter, we introduce von Neumann algebras and review some of the recent developments. We then turn to the results of [89], where we argue that the language of operator algebras provides a natural framework for addressing important questions in quantum gravity.

6.1 A Primer on von Neumann algebras and Classification of Factors

Let us briefly review some basic facts about von Neumann algebras and their classification. More detailed discussions can be found in the classic textbook of Haag [90].

Consider a Hilbert space $\mathcal{H}$. We can then define a norm on the space of operators acting on $\mathcal{H}$ using the norm on the Hilbert space

$$||a|| = \sup_{||\Psi||=1} ||a\Psi|| \,, \tag{63}$$

where $|\Psi\rangle \in \mathcal{H}$. The space of linear operators with finite operator norm is denoted by $\mathcal{B}(\mathcal{H})$.

A $*$-*algebra* S is a subset of $\mathcal{B}(\mathcal{H})$ that satisfies the following conditions:

1. $\forall a, b \in S$ and $\alpha, \beta \in \mathbb{C}$, $\alpha a + \beta b \in S$ and $ab \in S$,
2. If $a \in S$, then its adjoint $a^* \in S$.

On the space of bounded operators $\mathcal{B}(\mathcal{H})$, one may introduce the *weak operator topology.* In this topology, a sequence of operators $a_n \in \mathcal{B}(\mathcal{H})$ converges weakly to an operator $a \in \mathcal{B}(\mathcal{H})$ when

$$\langle\Psi|a_n|\Phi\rangle \to \langle\Psi|a|\Phi\rangle \,, \quad \forall|\Psi\rangle, |\Phi\rangle \in \mathcal{H}. \tag{64}$$

A *von Neumann algebra* is then defined as a weakly closed $*$-algebra containing the identity operator. These objects will play an important role in our later discussions. There is also an alternative characterization of von Neumann algebras that makes their physical relevance more transparent.

The *commutant* of an algebra $S \subset \mathcal{B}(\mathcal{H})$, denoted by S', is defined as the set of all operators in $\mathcal{B}(\mathcal{H})$ that commute with every element of S. In terms of the commutant, a von Neumann algebra may equivalently be defined as a self-adjoint subset of $\mathcal{B}(\mathcal{H})$ satisfying the bicommutant condition

$$S = S'' \,. \tag{65}$$

As an example, consider a massive free scalar field on D-dimensional Minkowski spacetime. Given a bounded open region on the $t = 0$ Cauchy slice, one can associate with it an algebra of (smeared) field operators. However, this algebra is in general not a von Neumann algebra as it does not satisfy the bicommutant condition. If one instead works with operators in a causal diamond, the resulting algebra is a von Neumann algebra. The fact that von Neumann algebras arise precisely from causally complete regions reflects how the causal structure of spacetime is encoded algebraically, making them the natural mathematical language for local quantum field theory.

One could have, in principle, defined a *uniform topology* on $\mathcal{B}(\mathcal{H})$ by introducing ϵ-neighborhoods around an operator a through the condition

$$||a - b|| < \epsilon, \tag{66}$$

and study the $*$-algebras closed under this topology. The resulting algebra is called a C*-algebra. Crucially, C*-algebras miss some important properties of von Neumann algebras. In particular, sequences of spectral projectors converge weakly, but not uniformly (see [90] for more details). As a result, taking the closure in the uniform topology excludes certain physically relevant operators.

A von Neumann algebra $\mathcal{M}$ is called a *factor* if its center $\mathcal{C}$ is trivial:

$$\mathcal{C} \equiv \mathcal{M} \cap \mathcal{M}' = \mathbb{C} I \,, \tag{67}$$

where I is the identity operator. For von Neumann factors $\mathcal{M}$, Murray and von Neumann proposed a classification scheme, which we will discuss below.

A projector P is an operator in $\mathcal{B}(\mathcal{H})$ satisfying the condition $P^2 = P$. We say that two projectors $P_{1,2}$ in $\mathcal{M}$ are equivalent $P_1 \sim P_2$ when there exists an operator $V \in \mathcal{M}$ such that

$$P_1 = V^* V; \quad P_2 = V V^*. \tag{68}$$

We say that $P_1 > P_2$ or $P_2 < P_1$ when there exists a subspace in $P_1 \mathcal{H}$ whose projector $P_{11} \sim P_2$. We call P_2 a subprojector of P_1 if the inequality $P_2 < P_1$ holds. Then we can show any two projectors $P_{1,2}$ in $\mathcal{M}$ will satisfy precisely only one of the following conditions [90]:

$$P_1 < P_2 \,, \qquad P_1 \sim P_2 \,, \qquad P_1 > P_2 \,. \tag{69}$$

A projector P is called *finite* if every subprojector $P_1 < P$ is inequivalent to P. A non-zero projector P is called *minimal* if there exists no subprojector $P_1 < P$ in $\mathcal{M}$. These definitions then allow us to classify von Neumann factors as follows:

- **Type I** : Contains a minimal projector.
- **Type II** : Contains non-zero finite projectors but no minimal projectors.
- **Type III** : Contains no non-zero finite projectors.

Let us end this section with a brief review of Tomita-Takesaki. A vector $|\omega\rangle \in \mathcal{H}$ is *cyclic* if for all $a \in \mathcal{M}$, $a|\omega\rangle$ is dense in the Hilbert space. The vector is *separating* if $a|\omega\rangle = 0$ iff $a = 0$. If $|\omega\rangle$ is cyclic and separating, then Tomita-Takesaki theory can be used to construct two operators Δ and J [91]. The operators Δ and J are called *modular operator* and *modular conjugation* respectively.

The modular operator generates a one-parameter family of evolutions in the von Neumann algebra:

$$\Delta^{it}\mathcal{M}\Delta^{-it} = \mathcal{M}\,, \qquad \forall t \in \mathbb{R}\,. \tag{70}$$

We can also define a modular Hamiltonian $\hat{h}$ from the modular operator,

$$\Delta = e^{-\hat{h}}\,. \tag{71}$$

The modular conjugation maps the algebra to its commutant:

$$J\mathcal{M}J = \mathcal{M}'. \tag{72}$$

6.2 Large N Holography and von Neumann Algebras

In AdS/CFT duality, a quantum gravity theory in AdS_{d+1} spacetime is dual to a CFT_d living on the boundary $\mathbb{R} \times S_{d-1}$ [5, 6, 7]. The boundary theory is characterized by a parameter N, which can then be identified with the bulk Newton's constant through the relation $N^2 \sim 1/G_N$.

The duality can also be formulated elegantly in the language of von Neumann algebras [92, 93, 94]. We now briefly review this perspective using the canonical example of Type IIB string theory on $\mathrm{AdS}_5 \times S^5$, dual to $\mathcal{N} = 4$ Super-Yang-Mills (SYM) theory on $\mathbb{R} \times S_3$ with gauge group $SU(N)$.

Let us first consider the boundary theory. We assume that the system is prepared in a thermofield double (TFD) state built from two copies of the CFT, denoted by $\mathrm{CFT}_{L,R}$. We denote their corresponding Hamiltonians by $H_{L,R}$. With a choice of normalization, the action of the theory can be written as $N\mathrm{Tr}(L)$, where L is a gauge-invariant polynomial composed of the fields and their derivative. Note that L does not contain any explicit factors of N. With this normalization, the expectation value of a single-trace operator $\mathcal{W}$ scales as N, the connected two-point function scales as $O(N^0)$, while connected k-point functions scale as N^{2-k} [95].

Now consider the $N \to \infty$ limit. To obtain a well-defined large N algebra, we introduce subtracted single-trace operators $\widetilde{\mathcal{W}} = \mathcal{W} - \langle W \rangle$. Then we can see that, in the $N \to \infty$ limit, all higher connected correlators vanish, while the two-point functions remain finite. The resulting theory therefore behaves as a generalized free field (GFF) theory. Using bounded functions of these generalized free fields, one can construct a von Neumann algebra, which we denote by $\mathcal{A}_{R,0}$. Similarly, one obtains an emergent GFF von Neumann algebra in the left CFT, denoted by $\mathcal{A}_{L,0}$.

In [92, 93], Leutheusser and Liu argued that the algebras $\mathcal{A}_{R,0}$ and $\mathcal{A}_{L,0}$ are both of type III. There are two ways to understand this result. Consider the Wightman function of the GFFs in the thermofield double state. Its Fourier transform takes the form

$$G_+(\omega, \vec{q}) = \frac{1}{1 - e^{-\beta\omega}} \rho(\omega, \vec{q}) \,, \tag{73}$$

where $(\omega, \vec{q})$ are the Fourier variables conjugate to the boundary coordinates $(t, \vec{x})$, and $\rho(\omega, \vec{q})$ is the spectral function.

Below the Hawking-Page temperature, it can be shown that this spectral function has support only at discrete points on the real ω-axis. When the temperature is higher than the Hawking-Page temperature, then the spectral function is supported on the full real ω-axis and has a *complete spectrum*. It can then be shown that when generalized free fields acting on the thermofield double state have a continuous spectrum, the corresponding von Neumann algebra is of type III [96, 97].

There is an alternative way to understand the type of the emergent GFF algebras [98]. Above the Hawking-Page temperature, the two-point functions of the GFFs decay forever. This beahviour, called clustering in time, can also be shown to be a diagnostic of a type III nature of the algebra.

Now let us bulk description. The $N \to \infty$ limit corresponds to the $G_N \to 0$ limit of the bulk string theory. In this limit, the theory reduces to a massive scalar field living on a fixed eternal black hole background. Let us denote $\mathcal{A}_{l,0}$ and $\mathcal{A}_{r,0}$ by the algebra of operators of this effective field theory description in the left and right exterior wedges of the spacetime. Then we can write the AdS/CFT duality in the language of operator algebras as

$$\mathcal{A}_{R,0} = \mathcal{A}_{r,0}, \quad \mathcal{A}_{L,0} = \mathcal{A}_{\ell,0}. \tag{74}$$

6.3 Emergence of Horizons from Operator Algebras

The emergence of a type III algebra in the large N limit has several interesting consequences. Consider a type III von Neumann algebra $\mathcal{M}$ with a cyclic and separating vector $|\Omega\rangle$. Tomita-Takesaki theory then allows us to construct the associated modular operator $\Delta_{\mathcal{M}}$. Now suppose there exists a von Neumann subalgebra $\mathcal{N} \subset \mathcal{M}$ satisfying the following inclusion properties:

- $|\Omega\rangle$ is cyclic for all operators in $\mathcal{N}$,

- The subalgebra $\mathcal{N}$ is preserved under the half-sided modular flow:

$$\Delta_{\mathcal{M}}^{-it}\mathcal{N}\Delta_{\mathcal{M}}^{it} \subset \mathcal{N}, \quad t \leq 0 \tag{75}$$

Then there exists a unitary operator $U(s)$ called *half-sided modular translations*, satisfying the properties [99, 100, 101]

1. $U(s) = e^{-iGs}$, with $G \geq 0$ and $s \in \mathbb{R}$,
2. $U(s)|\Omega\rangle = |\Omega\rangle$,
3. $U^\dagger(s)\mathcal{M}U(s) \subseteq \mathcal{M}, \quad s \leq 0$
4. $\mathcal{N} = U^\dagger(-1)\mathcal{M}U(1)$.

The positive operator G can be constructed from the modular Hamiltonians of $\mathcal{M}$ and $\mathcal{N}$ as follows:

$$\hat{h}_{\mathcal{M}} - \hat{h}_{\mathcal{N}} = 2\pi G\,. \tag{76}$$

These half-sided modular translations have played an important role in the proof of the CPT theorem [99] and the construction of Poincaré group from wedge algebras [102]. The crucial point for us is that, once we have a type III algebra with an appropriate inclusion structure, an emergent "time evolution" naturally arises in the system. As we will see, this evolution maps operators from the exterior to the interior of Killing horizons and therefore encodes information about the location of the horizon.

Traditionally, the operator $U(s)$ is constructed by first specifying a subalgebra $\mathcal{N}$ satisfying the half-sided modular inclusion property. In [92, 93], Leutheusser and Liu showed that for generalized free fields one can derive an explicit expression for $U(s)$ without specifying either $\mathcal{N}$ or $\Delta_{\mathcal{M}}$. We will not review the explicit construction here, since only its physical consequences will be relevant for us.

Let us look at the Poincaré patch of AdS_3 with the metric

$$\mathrm{d}s^2 = \frac{1}{z^2}\left(-\mathrm{d}x^+\mathrm{d}x^- + \mathrm{d}z^2\right)\,. \tag{77}$$

This spacetime can be divided into four regions $\mathcal{R}, \mathcal{L}, \mathcal{F}$ and $\mathcal{P}$ corresponding respectively to the sign choices $(x^+, x^-) = (+,-), (-,+), (+,+)$ and $(-,-)$. The conformal boundary lies at $z = 0$, and bulk operators are related to boundary operators through the standard extrapolate dictionary.

Now consider a free massive scalar field supported only in the right Rindler wedge $\mathcal{R}$. We denote this field by $\phi_R(X)$, where $X = (x^+, x^-, z)$ is a bulk point in $\mathcal{R}$. The algebra generated by these operators forms a type III von Neumann algebra, and one can construct the corresponding half-sided modular translations. One then finds that there exists a threshold value s_1 such that [92, 93]

$$U^\dagger(s)\,\phi_R(X)\,U(s) = \begin{cases} \phi_R(X_s), & s < s_1, \\ \phi_F(X_s), & s > s_1, \end{cases} \tag{78}$$

where

$$X_s = (x^+, x^- + s, z)\,, \tag{79}$$

and $\phi_F(X_s)$ denotes the scalar field evaulated at some point X_s in the future Rindler wedge $\mathcal{F}$. Therefore, when the modular translation parameter exceeds a critical value, the evolved operator crosses the AdS-Rindler horizon. Since the same evolution operator can be reconstructed in the dual boundary description through (74), the same threshold also appears in the boundary theory. In this sense, half-sided modular translations provide a precise boundary signature of the bulk Killing horizon.

It is worth emphasizing that only type III algebras admit half-sided modular translations. Since these operators encode the existence of horizons, this suggests that bulk causal structure becomes sharply defined only in the strict large N limit of the boundary theory.

6.4 Perturbative $1/N^2$ Corrections and Crossed Product Algebras

In the previous subsections, we studied the strict $N \to \infty$ limit of the boundary theory and saw that there was an emergent type III algebra. These algebras are pathological in the sense that we cannot define traces, density matrices and entanglement entropy. In [95], Witten showed that these difficulties are resolved once perturbative $1/N^2$ corrections are included.

To understand this construction, consider the subtracted right CFT Hamiltonian

$$H'_R \equiv H_R - \langle H_R \rangle\ . \tag{80}$$

The operator H'_R/N has a well-defined large N limit [95]. In particular, for any element $a \in \mathcal{A}_{R,0}$, we have

$$[H'_R/N, a] = -(i/N)\partial_t a\,. \tag{81}$$

In the strict $N \to \infty$ limit, the right side vanishes, so including H'_R/N does not introduce any additional dynamics. Away from the strict large N limit, however, this commutator is non-zero and the operator must be incorporated into the algebra. The resulting enlarged algebra, which we denote by $\mathcal{A}_R$, is therefore generated by $\mathcal{A}_{R,0}$ together with the additional operator H'_R/N.

This enlarged algebra $\mathcal{A}_R$ is isomporphic to what is known as a *crossed product algebra*. To see this structure, let us note that we can formally decompose the right CFT Hamiltonian as follows

$$\frac{H'_R}{N} = U + \frac{\hat{h}}{\beta N}\,, \qquad \text{where } U = \frac{H'_L}{N}\,. \tag{82}$$

H'_L is the subtracted left CFT Hamiltonian and $\hat{h}$ is the modular Hamiltonian assocaited to the TFD state. Note that the operator U commutes with every element of the right CFT algebra. As a result, the extended Hilbert space on which $\mathcal{A}_R$ acts factorizes as

$$\mathcal{H} \cong \mathcal{H}_{\text{TFD}} \otimes L^2(\mathbb{R})\,, \tag{83}$$

where $\mathcal{H}_{\text{TFD}}$ is the Gelfand-Naimark-Segal (GNS) Hilbert space formed by the action of the GFFs on the TFD state and $L^2(\mathbb{R})$ is the Hilbert space where U acts as a position operator. The crossed product algebra, denoted by

$$\mathcal{A}_R = \mathcal{A}_{R,0} \rtimes \mathbb{R}\,, \tag{84}$$

is defined by the span of operators of the form

$$a \otimes 1\,, \qquad \text{and} \qquad e^{i\hat{h}s} \otimes e^{iXs}\,. \tag{85}$$

Here, $a \in \mathcal{A}_{R,0}$ and the operator X is defined as follows

$$X = \beta N U\,. \tag{86}$$

As a result, a general element of the crossed product algebra $\hat{a}$ is given by

$$\hat{a} = \int \mathrm{d}s\; a(s) e^{i\hat{h}s} \otimes e^{iXs}\,, \qquad \text{with } a(s) \in \mathcal{A}_{R,0}\,. \tag{87}$$

Similarly, a general state in the extended Hilbert space can be written as

$$|\hat{\Phi}\rangle = \int \mathrm{d}x\; g(x) |\Phi\rangle \otimes |x\rangle\,, \qquad \text{where } |\Phi\rangle \in \mathcal{H}_{\text{TFD}}\,. \tag{88}$$

where $|x\rangle$ are eigenstates of the operator X, and $g(x)$ is a square-integrable wavefunction.

The crucial point is that the crossed product algebra $\mathcal{A}_R$ is of type II_∞. As a result, density matrices and von Neumann entropies can now be defined for states in the enlarged Hilbert space.

An especially important class of states is the *semiclassical states*, for which the wavefunction $g(x)$ in equation (88) varies slowly with x. Such states may be interpreted as states evolved by the boundary Hamiltonian for only a short time. From our earlier discussion of operator complexity, we saw that long-time evolution probes the discreteness of the spectrum. To remain semiclassical, the state must therefore remain sharply localized around small boundary times. For such states, one can show that the von Neumann entropy reproduces the generalized entropy [103, 104]

$$S_{\text{vN}}(\hat{\Phi}) = \frac{A}{4G_N} + S_{\text{out}}(\Phi) + c = S_{\text{gen}} + c\,, \tag{89}$$

where A is the area of the black hole horizon, $S_{\text{out}}(\Phi)$ is the von Neumann entropy of the state $|\Phi\rangle$ in the GNS Hilbert space, and c is a state-independent constant.

6.5 Emergence of Spacetime and the Construction of a Type I factor

Einstein's theory of general relativity achieved the remarkable feat of rewriting gravity as the curvature of spacetime. Two ideas lie at the core of the framework. The equivalence principle states that freely falling observers follow geodesics, while Einstein's field equations determine what those geodesics are.

The equivalence principle can trace its roots back to simple thought experiments involving falling elevators, while the field equations, on the other hand, were wrested from the mathematics by searching for the *simplest* set of equations that reduce to Newtonian gravity in the weak-field limit. This search was a formidable task, with several incorrect candidate equations being proposed before arriving at the correct formulation [105].

It is natural to ask whether the field equations follow from a deeper principle. A major breakthrough came in 1995, when Jacobson showed that Einstein's field equations can be understood as a thermodynamic equation of state [13]. Let us now look at the details of this computation. Around a point $\mathcal{P}$ on the manifold, we can find a locally flat patch $\mathcal{U}$. Consider an accelerating observer in this patch, whose local Rindler horizons partition the region into four wedges. Focusing on one of these horizons, Jacobson showed that Einstein's equations follow from a local equilibrium condition via a Clausius relation

$$\delta Q = T \mathrm{d}S \,, \tag{90}$$

where T is the temperature of the horizon, δQ is the heat flux of the matter fields through the horizon, and $\mathrm{d}S$ is the corresponding change in the area of the horizon.

To see this, let the stress-energy tensor of the matter fields be $T_{\mu\nu}$. Consider the past Rindler horizon $\mathcal{H}_P$ associated with the point $\mathcal{P}$. We denote the approximate local boost Killing vector generating the horizon by χ^μ. Then the heat flux through the horizon is given by

$$\delta Q = \int_{\mathcal{H}_P} T_{\mu\nu} \chi^\mu \mathrm{d}\Sigma^\nu \,. \tag{91}$$

Let us parametrize the past horizon by an affine parameter λ that vanishes at $\mathcal{P}$ and is negative to the past of $\mathcal{P}$. If k^μ is the tangent vector to the horizon, then we can rewrite

$$\chi^\mu = -\kappa \lambda k^\mu \,, \tag{92}$$

where κ is the surface gravity. We also have

$$\mathrm{d}\Sigma^\nu = k^\nu \mathrm{d}\lambda \mathrm{d}\mathcal{A} \,, \tag{93}$$

where $\mathrm{d}\mathcal{A}$ is the area element on the cross-section of the local Rindler horizon. This gives us

$$\delta Q = -\kappa \int_{\mathcal{H}_P} \lambda T_{\mu\nu} k^\mu k^\nu \mathrm{d}\lambda \mathrm{d}\mathcal{A} \,. \tag{94}$$

Now let us look at the right-hand side of the equilibrium condition (90). Using the definition of the expansion parameter θ for the null generators of the horizon, we have

$$\delta\mathcal{A} = \int_{\mathcal{H}_P} \theta \mathrm{d}\lambda \mathrm{d}\mathcal{A} \,. \tag{95}$$

We can rewrite the expansion in terms of the Ricci tensor using the Raychaudhuri equation (36). Near $\mathcal{P}$, the shear and quadratic expansion terms in (36) are subleading and therefore do not contribute at leading order. Neglecting these terms and integrating, we obtain

$$\theta = -\lambda R_{\mu\nu} k^{\mu} k^{\nu} \,. \tag{96}$$

The temperature of the horizon is given by $T = \kappa/2\pi$. Note that we have set $\hbar$ to one. If we assume the Bekenstein-Hawking area law $S = A/4G_N$, then the equilibrium condition (90) gives us

$$8\pi G_N \int_{\mathcal{H}_P} \lambda T_{\mu\nu} k^{\mu} k^{\nu} \mathrm{d}\lambda \mathrm{d}\mathcal{A} = \int_{\mathcal{H}_P} \lambda R_{\mu\nu} k^{\mu} k^{\nu} \mathrm{d}\lambda \mathrm{d}\mathcal{A} \,. \tag{97}$$

This implies that

$$8\pi G_N T_{\mu\nu} = R_{\mu\nu} + f g_{\mu\nu} \,, \tag{98}$$

for some function f. Imposing conservation of the stress-energy tensor fixes f, giving us the familiar Einstein field equations

$$R_{\mu\nu} - \frac{1}{2} R g_{\mu\nu} + \Lambda g_{\mu\nu} = 8\pi G_N T_{\mu\nu} \,. \tag{99}$$

Jacobson's derivation of Einstein's equations follows from the Clausius relation (90) and the existence of an underlying Lorentzian manifold. The derivation carries an important implication. The derivation hints that gravity may be an *emergent* phenomenon, much like thermodynamics. This perspective is particularly appealing because it bypasses many of the difficulties associated with canonical quantization of gravity. Instead, one is led to search for theories in which gravity emerges only in an appropriate semiclassical limit. AdS/CFT correspondence provides an explicit realization of such an emergent description.

This raises an interesting follow-up question: what is the appropriate language for understanding the emergence of gravity? In [89], we argued that operator algebras provide a natural framework for addressing this question. This proposal is motivated by two observations. First, a foundational result in noncommutative geometry is Connes' reconstruction theorem, which shows that a Riemannian spin manifold can be reconstructed from the algebra of commutative functions defined on it [106]. Since operator algebras of quantum fields provide a generalized notion of functions on spacetime, they offer a natural starting point for an emergence program. Second, as we saw in Section 6.3, the large N von Neumann algebra already contains enough structure to detect the emergence of Killing horizons in the bulk spacetime.

In [89], we push this idea further by studying a free massive scalar field propagating on a fixed $(d+1)$-dimensional spacetime. We show that the metric and curvature tensors of the manifold can be reconstructed from the triple

$$(\mathcal{A}, \mathcal{H}, |\omega\rangle), \tag{100}$$

where $\mathcal{A}$ is the operator algebra of the quantized scalar field, $\mathcal{H}$ is the Hilbert space on which the operators act, and $|\omega\rangle$ is some preferred state in this Hilbert space, under the following assumptions:

1. The state $|\omega\rangle$ is Hadamard.
2. The algebra $\mathcal{A}$ contains a class of subalgebras $\mathcal{W}_j$, which we refer to as *local Rindler algebras.*
3. The correlation functions of the quantized matter fields in $|\omega\rangle$ have a well-defined large mass limit.

Before proceeding further, let us briefly explain the defining properties of local Rindler algebras. Consider a locally flat patch on the manifold. As before, one can define a local Rindler horizon that partitions the patch into four regions. The local Rindler algebras $\mathcal{W}_j$ are obtained by restricting the full algebra $\mathcal{A}$ to one of these wedges, for different choices of local Rindler horizons within the same patch. We then require the correlation functions of $\mathcal{W}_j$ in the state ω to be well approximated by the vacuum correlation functions of a global Rindler wedge algebra in an auxiliary Minkowski spacetime.

With this definition in hand, we can see that the first two assumptions (1)-(2) together implement the equivalence principle in the language of operator algebras. The equivalence principle is not merely the statement that every manifold admits locally flat coordinate patches, since this is true for any smooth manifold. Rather, it is the requirement that matter dynamics in these patches reduce locally to their flat-space counterparts, up to tidal corrections. The Hadamard condition implements a part of this requirement by forcing the short-distance structure of correlation functions to match that of flat spacetime. The existence of the local Rindler algebras $\mathcal{W}_j$ further ensures that the operator algebraic structure, and in particular its correlation functions, can be approximated by those of some globally flat Rindler wedge algebras.

Although the conditions (1)-(3) were identified by studying a scalar field on a curved spacetime, the final conditions themselves are formulated entirely in the language of operator algebras and Hilbert spaces, without any direct geometric input. This allows us to reverse the logic. Starting from some quantum theory, one can identify a semiclassical regime in which the operator algebra and Hilbert space of the matter sector develop precisely these properties. Whenever this happens, a spacetime geometry can be reconstructed directly from the algebraic data. The conditions (1)-(3) are therefore not merely diagnostic as they also provide *sufficient* conditions for the emergence of spacetime.

What remains unclear, however, is whether this emergent geometry satisfies Einstein's equations. In [89], we show that if, for every local Rindler algebra

$\mathcal{W}_j$, there exists a state ω_j that is stationary under affine dilations along the corresponding local Rindler horizon, then the emergent geometry satisfies the full non-linear Einstein equations sourced by the scalar field. We refer to such states as *locally stationary states*. The existence of these locally stationary states plays the role of Jacobson's Clausius relation (90) in the language of operator algebras.

The conditions (1)-(3), together with the existence of locally stationary states, thus characterize the emergence of Einstein gravity from an underlying quantum theory in purely operator-algebraic terms, independent of the spacetime dimension and asymptotic structure.

In practice, however, one often does not have access to the full microscopic quantum theory. A more useful question is whether one can instead begin with a low-energy effective field theory and systematically modify it so as to model features expected from a full quantum theory of gravity. In [89], we argue that operator algebras provide a natural framework for addressing this question as well.

As we have already seen, the strict large N limit of the boundary theory produces type III von Neumann algebras. Incorporating perturbative corrections enlarges these to type II algebras. Although type II algebras are less pathological, they still lack certain structures needed to address important questions such as the counting of their microstates. To perform such computations, one requires a type I factor. However, there is no canonical procedure for constructing a type I algebra from a type II algebra. This is to be expected, since the large N limit leads to a loss of information about the underlying quantum theory, and one should not generally expect such information to be recoverable within perturbation theory alone.

In [89], we show that, nevertheless, there is a way to construct an approximate type I factor from the type II algebra. We obtain this type I factor by first spectrally decomposing the right CFT Hamiltonian as follows:

$$H_R = \int \mathrm{d}E \rho_0(E) e^{iEs} |E\rangle\langle E| \,, \tag{101}$$

where $\rho_0(E)$ is the large N continuous density of states of the CFT. We then replace $\rho_0(E)$ with the density of states of a random matrix ensemble satisfying

$$\overline{\rho(E)} = \rho_0(E) \,. \tag{102}$$

The higher moments of the density of states are fixed by choosing a Gaussian Unitary Ensemble (GUE) completion. In particular, the averaged two-point function of the density of states contains the sine-kernel term, as in (31).

The introduction of level repulsion through the sine-kernel term emulates the level spacing of the theory that was lost in the large N limit. We then construct projectors whose support in the energy space precisely corresponds to that prescribed by the level repulsion. When ensemble-averaged, these projectors look like the minimal projectors of a single eigenstate of the theory.

For eternal black holes, we show that the dimension of the resulting type I factor is equal to the exponential of the Bekenstein-Hawking entropy, including

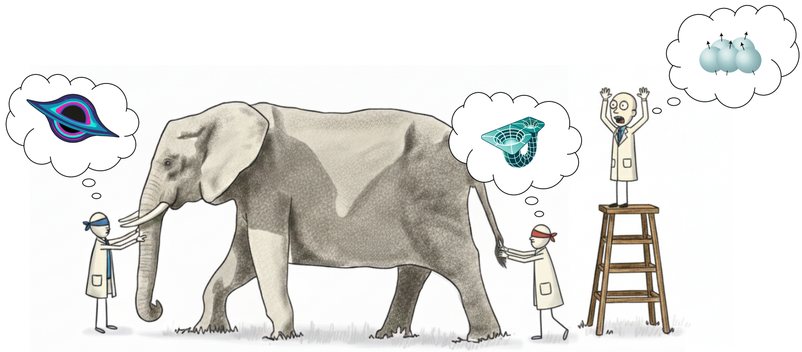

Figure 6.1. Blind Physicists and a Quantum Elephant. Physicists blinded by the semiclassical limit will see a smooth horizon or a wormhole when probing different regimes, while a physicist studying the full quantum black hole will instead see a finite-dimensional quantum mechanical system. (Adapted from Sketchplanations).

the logarithmic correction in the horizon area. The existence of such a type I factor has already appeared in earlier work, for example, in [107]. The goal of our work is to fill in the missing algebraic steps by explicitly constructing the minimal projectors of the factor.

When studying the corresponding black hole microstates, the breakdown of the low-energy effective field theory can be related directly to the spectral form factor (SFF) of the random matrix theory. More precisely, we find that the onset of the ramp and plateau in the SFF coincides with the breakdown of the low-energy effective field theory description. A natural way to reinterpret these observations is through the notion of complexity. We have already seen that the sine-kernel, which is responsible for the ramp and plateau in the SFF, also governs the saturation of complexity [45]. From this perspective, when spacetime is probed by operators whose complexity is of the exponential order in the Bekenstein-Hawking entropy, the low-energy effective field theory description breaks down completely (see [108, 109, 110] for related discussions).

This 'observer' dependence of the geometry, through the complexity of the probe operator, lies at the heart of black hole complementarity [76]. When a quantum black hole is probed with a "simple operator", the resulting spacetime looks like the classical geometry with a smooth event horizon. However, when the black hole is probed with a "complex operator", the effective field theory description breaks down and one may encounter a wormhole or a baby universe emission. The crucial point is that these different observable-dependent descriptions are complementary. Each measurement probes a different operational regime.

This feature is nicely captured by a retelling of an old parable (see Figure 6.1). A group of blind physicists, each probing only one part of a quantum elephant, would naturally arrive at different conclusions. However, as long as each physicist remains within their own regime of validity, these seemingly contrasting descriptions are all equally valid accounts of the same underlying quantum elephant that, in reality, *might* be describable in terms of a collection of qubits.

7 Conclusions

In this thesis, we studied quantum aspects of black holes using tools from quantum information theory and algebraic quantum field theory. Let us conclude by briefly discussing some possible future directions.

An important open question concerns the geometric interpretation of the non-perturbative corrections responsible for the saturation of holographic complexity in black holes. We saw that the saturation is ultimately driven by the sine-kernel contribution in the two-point function of the density of states. In JT gravity, the sine-kernel can be obtained from the insertion of D-branes [43, 111, 112]. It would therefore be interesting to understand whether the effects of the sine-kernel can be modeled directly as geometric corrections to the black hole spacetime. Furthermore, the sine-kernel contribution to the spectral form factor and matter correlation functions has been shown to admit a description in terms of an infinite sum over *constrained instantons* [113]. A natural direction is to investigate whether the saturation of holographic volume complexity can similarly be reproduced through the inclusion of such constrained instantons. It would also be interesting to relate these effects, if such a construction exists, to the thin-shell microstates studied in [114], where a similar saturation of volume complexity was argued to occur.

Although we studied the thermodynamic favourability of black shells relative to black holes, it remains unclear whether black shells are dynamically favoured as endpoints of gravitational collapse. In particular, it would be valuable to make more precise the heuristic arguments often invoked in the black shell literature, namely that the exponential suppression of the tunneling amplitude may be compensated by the exponentially large number of available microstates. Establishing such a mechanism explicitly, even within a simplified toy model, would significantly strengthen the viability of black shells as alternatives to black holes.

Another interesting direction is to further develop the emergence of gravity programme using more realistic matter theories. In this thesis, we primarily focused on scalar fields. It would be important to understand whether the inclusion of fermions and gauge fields leads to qualitatively new structures or whether the same algebraic mechanisms continue to govern the emergence of gravitational dynamics.

References

[1] A. Einstein, *Die grundlage der allgemeinen relativitätstheorie*, *Annalen der Physik* **354** (1916) 769–822, https://onlinelibrary.wiley.com/doi/pdf/10.1002/andp.19163540702.

[2] C. M. Will, *The Confrontation between General Relativity and Experiment*, *Living Rev. Rel.* **17** (2014) 4, arXiv:1403.7377 [gr-qc].

[3] G. 't Hooft and M. J. G. Veltman, *One-loop divergencies in the theory of gravitation*, *Ann. Inst. H. Poincare Phys. Theor. A* **20** (1974) 69–94.

[4] S. W. Hawking, *Breakdown of predictability in gravitational collapse*, *Phys. Rev. D* **14** (Nov, 1976) 2460–2473.

[5] J. M. Maldacena, *The Large N limit of superconformal field theories and supergravity*, *Adv. Theor. Math. Phys.* **2** (1998) 231–252, arXiv:hep-th/9711200.

[6] E. Witten, *Anti-de Sitter space and holography*, *Adv. Theor. Math. Phys.* **2** (1998) 253–291, arXiv:hep-th/9802150.

[7] S. S. Gubser, I. R. Klebanov, and A. M. Polyakov, *Gauge theory correlators from noncritical string theory*, *Phys. Lett. B* **428** (1998) 105–114, arXiv:hep-th/9802109.

[8] S. Ryu and T. Takayanagi, *Holographic derivation of entanglement entropy from AdS/CFT*, *Phys. Rev. Lett.* **96** (2006) 181602, arXiv:hep-th/0603001.

[9] E. Witten, *APS Medal for Exceptional Achievement in Research: Invited article on entanglement properties of quantum field theory*, *Rev. Mod. Phys.* **90** (2018) 045003, arXiv:1803.04993 [hep-th].

[10] A. Almheiri, X. Dong, and D. Harlow, *Bulk Locality and Quantum Error Correction in AdS/CFT*, *JHEP* **04** (2015) 163, arXiv:1411.7041 [hep-th].

[11] Y. Sekino and L. Susskind, *Fast Scramblers*, *JHEP* **10** (2008) 065, arXiv:0808.2096 [hep-th].

[12] S. W. Hawking and D. N. Page, *Thermodynamics of Black Holes in anti-De Sitter Space*, *Commun. Math. Phys.* **87** (1983) 577.

[13] T. Jacobson, *Thermodynamics of space-time: The Einstein equation of state*, *Phys. Rev. Lett.* **75** (1995) 1260–1263, arXiv:gr-qc/9504004.

[14] M. A. Nielsen and I. L. Chuang, *Quantum Computation and Quantum Information.* Cambridge University Press, 6, 2012.

[15] L. Susskind, *Three Lectures on Complexity and Black Holes,* SpringerBriefs in Physics. Springer, 10, 2018. arXiv:1810.11563 [hep-th].

[16] D. A. Roberts, D. Stanford, and L. Susskind, *Localized shocks, JHEP* **03** (2015) 051, arXiv:1409.8180 [hep-th].

[17] D. A. Roberts, D. Stanford, and A. Streicher, *Operator growth in the SYK model, JHEP* **06** (2018) 122, arXiv:1802.02633 [hep-th].

[18] D. E. Parker, X. Cao, A. Avdoshkin, T. Scaffidi, and E. Altman, *A Universal Operator Growth Hypothesis, Phys. Rev. X* **9** (2019) 041017, arXiv:1812.08657 [cond-mat.stat-mech].

[19] P. Nandy, A. S. Matsoukas-Roubeas, P. Martínez-Azcona, A. Dymarsky, and A. del Campo, *Quantum dynamics in Krylov space: Methods and applications, Phys. Rept.* **1125-1128** (2025) 1–82, arXiv:2405.09628 [quant-ph].

[20] S. Baiguera, V. Balasubramanian, P. Caputa, S. Chapman, J. Haferkamp, M. P. Heller, and N. Y. Halpern, *Quantum complexity in gravity, quantum field theory, and quantum information science, Phys. Rept.* **1159** (2026) 1–77, arXiv:2503.10753 [hep-th].

[21] E. Rabinovici, A. Sánchez-Garrido, R. Shir, and J. Sonner, *Krylov Complexity,* arXiv:2507.06286 [hep-th].

[22] A. N. Krylov, *On the numerical solution of the equation by which, in technical matters, frequencies of small oscillations of material systems are determined, Izvestiya Akademii Nauk SSSR* **7** (1931) 491–539. In Russian. Zentralblatt MATH: 2561215. JFM: 57.1454.02.

[23] C. Lanczos, *An iteration method for the solution of the eigenvalue problem of linear differential and integral operators, J. Res. Natl. Bur. Stand. B* **45** (1950) 255–282.

[24] A. Sánchez-Garrido, *On Krylov Complexity.* PhD thesis, Southampton U., U. Geneva (main), 2024. arXiv:2407.03866 [hep-th].

[25] V. Viswanath and G. Mueller, *The recursion method. Application to many-body dynamics*, vol. 23. Springer., Jan., 2025.

[26] V. Balasubramanian, P. Caputa, J. M. Magan, and Q. Wu, *Quantum chaos and the complexity of spread of states, Phys. Rev. D* **106** (2022) 046007, arXiv:2202.06957 [hep-th].

[27] J. L. F. Barbón, E. Rabinovici, R. Shir, and R. Sinha, *On The Evolution Of Operator Complexity Beyond Scrambling, JHEP* **10** (2019) 264, arXiv:1907.05393 [hep-th].

[28] A. Dymarsky and M. Smolkin, *Krylov complexity in conformal field theory, Phys. Rev. D* **104** (2021) L081702, arXiv:2104.09514 [hep-th].

[29] A. Kundu, V. Malvimat, and R. Sinha, *State dependence of Krylov complexity in 2d CFTs, JHEP* **09** (2023) 011, arXiv:2303.03426 [hep-th].

[30] A. Bhattacharya, P. Nandy, P. P. Nath, and H. Sahu, *Operator growth and Krylov construction in dissipative open quantum systems*, *JHEP* **12** (2022) 081, arXiv:2207.05347 [quant-ph].

[31] B. Bhattacharjee, X. Cao, P. Nandy, and T. Pathak, *Operator growth in open quantum systems: lessons from the dissipative SYK*, *JHEP* **03** (2023) 054, arXiv:2212.06180 [quant-ph].

[32] V. Mohan, *Krylov complexity of open quantum systems: from hard spheres to black holes*, *JHEP* **11** (2023) 222, arXiv:2308.10945 [hep-th].

[33] T. Hartman and J. Maldacena, *Time Evolution of Entanglement Entropy from Black Hole Interiors*, *JHEP* **05** (2013) 014, arXiv:1303.1080 [hep-th].

[34] L. Susskind, *Computational Complexity and Black Hole Horizons*, *Fortsch. Phys.* **64** (2016) 24–43, arXiv:1403.5695 [hep-th]. [Addendum: Fortsch.Phys. 64, 44–48 (2016)].

[35] D. Stanford and L. Susskind, *Complexity and Shock Wave Geometries*, *Phys. Rev. D* **90** (2014) 126007, arXiv:1406.2678 [hep-th].

[36] A. R. Brown, D. A. Roberts, L. Susskind, B. Swingle, and Y. Zhao, *Holographic Complexity Equals Bulk Action?*, *Phys. Rev. Lett.* **116** (2016) 191301, arXiv:1509.07876 [hep-th].

[37] J. Couch, S. Eccles, T. Jacobson, and P. Nguyen, *Holographic Complexity and Volume*, *JHEP* **11** (2018) 044, arXiv:1807.02186 [hep-th].

[38] D. Carmi, S. Chapman, H. Marrochio, R. C. Myers, and S. Sugishita, *On the Time Dependence of Holographic Complexity*, *JHEP* **11** (2017) 188, arXiv:1709.10184 [hep-th].

[39] R. Jackiw, *Lower Dimensional Gravity*, *Nucl. Phys. B* **252** (1985) 343–356.

[40] C. Teitelboim, *Gravitation and Hamiltonian Structure in Two Space-Time Dimensions*, *Phys. Lett. B* **126** (1983) 41–45.

[41] J. Navarro-Salas and P. Navarro, *AdS(2) / CFT(1) correspondence and near extremal black hole entropy*, *Nucl. Phys. B* **579** (2000) 250–266, arXiv:hep-th/9910076.

[42] P. Nayak, A. Shukla, R. M. Soni, S. P. Trivedi, and V. Vishal, *On the Dynamics of Near-Extremal Black Holes*, *JHEP* **09** (2018) 048, arXiv:1802.09547 [hep-th].

[43] P. Saad, S. H. Shenker, and D. Stanford, *JT gravity as a matrix integral*, arXiv:1903.11115 [hep-th].

[44] A. R. Brown, H. Gharibyan, H. W. Lin, L. Susskind, L. Thorlacius, and Y. Zhao, *Complexity of Jackiw-Teitelboim gravity*, *Phys. Rev. D* **99** (2019) 046016, arXiv:1810.08741 [hep-th].

[45] L. V. Iliesiu, M. Mezei, and G. Sárosi, *The volume of the black hole interior at late times*, *JHEP* **07** (2022) 073, arXiv:2107.06286 [hep-th].

[46] J. Maldacena, D. Stanford, and Z. Yang, *Conformal symmetry and its breaking in two dimensional Nearly Anti-de-Sitter space, PTEP* **2016** (2016) 12C104, arXiv:1606.01857 [hep-th].

[47] Z. Yang, *The Quantum Gravity Dynamics of Near Extremal Black Holes, JHEP* **05** (2019) 205, arXiv:1809.08647 [hep-th].

[48] S.-K. Jian, B. Swingle, and Z.-Y. Xian, *Complexity growth of operators in the SYK model and in JT gravity, JHEP* **03** (2021) 014, arXiv:2008.12274 [hep-th].

[49] E. Rabinovici, A. Sánchez-Garrido, R. Shir, and J. Sonner, *A bulk manifestation of Krylov complexity, JHEP* **08** (2023) 213, arXiv:2305.04355 [hep-th].

[50] M. P. Heller, J. Papalini, and T. Schuhmann, *Krylov Spread Complexity as Holographic Complexity beyond Jackiw-Teitelboim Gravity, Phys. Rev. Lett.* **135** (2025) 151602, arXiv:2412.17785 [hep-th].

[51] A. Friedman, *On the Curvature of space, Z. Phys.* **10** (1922) 377–386.

[52] J. R. Oppenheimer and H. Snyder, *On Continued gravitational contraction, Phys. Rev.* **56** (1939) 455–459.

[53] A. Einstein, *On a stationary system with spherical symmetry consisting of many gravitating masses, Annals Math.* **40** (1939) 922–936.

[54] W. Israel, *Black hole 2000: The astrophysical era1, Publications of the Astronomical Society of the Pacific* **112** (May, 2000) 583.

[55] R. Penrose, *Gravitational collapse and space-time singularities, Phys. Rev. Lett.* **14** (1965) 57–59.

[56] S. Hawking, *Occurrence of singularities in open universes, Phys. Rev. Lett.* **15** (1965) 689–690.

[57] S. Hawking and G. F. R. Ellis, *Singularities in homogeneous world models, Phys. Lett.* **17** (1965) 246–247.

[58] R. P. Geroch, *Singularities in closed universes, Phys. Rev. Lett.* **17** (1966) 445–447.

[59] S. Chandrasekhar, "Letter to Stephen Hawking." May 22. Subrahmanyan Chandrasekhar Papers, Box 25, Folder 11, Special Collections Research Center, University of Chicago Library, 1980.

[60] J. M. M. Senovilla and D. Garfinkle, *The 1965 Penrose singularity theorem, Class. Quant. Grav.* **32** (2015) 124008, arXiv:1410.5226 [gr-qc].

[61] S. W. Hawking and G. F. R. Ellis, *The Large Scale Structure of Space-Time.* Cambridge Monographs on Mathematical Physics. Cambridge University Press, 2, 2023.

[62] J. M. M. Senovilla, *Singularity Theorems and Their Consequences, Gen. Rel. Grav.* **30** (1998) 701, arXiv:1801.04912 [gr-qc].

[63] H. Epstein, V. Glaser, and A. Jaffe, *Nonpositivity of energy density in Quantized field theories, Nuovo Cim.* **36** (1965) 1016.

[64] P. C. W. Davies and S. A. Fulling, *Radiation from a moving mirror in two-dimensional space-time conformal anomaly*, *Proc. Roy. Soc. Lond. A* **348** (1976) 393–414.

[65] M. S. Morris, K. S. Thorne, and U. Yurtsever, *Wormholes, Time Machines, and the Weak Energy Condition*, *Phys. Rev. Lett.* **61** (1988) 1446–1449.

[66] L. S. Brown and G. J. Maclay, *Vacuum stress between conducting plates: An Image solution*, *Phys. Rev.* **184** (1969) 1272–1279.

[67] J. D. Bekenstein, *Generalized second law of thermodynamics in black hole physics*, *Phys. Rev. D* **9** (1974) 3292–3300.

[68] A. C. Wall, *Ten Proofs of the Generalized Second Law*, *JHEP* **06** (2009) 021, arXiv:0901.3865 [gr-qc].

[69] A. C. Wall, *A Proof of the generalized second law for rapidly-evolving Rindler horizons*, *Phys. Rev. D* **82** (2010) 124019, arXiv:1007.1493 [gr-qc].

[70] A. C. Wall, *A proof of the generalized second law for rapidly changing fields and arbitrary horizon slices*, *Phys. Rev. D* **85** (2012) 104049, arXiv:1105.3445 [gr-qc]. [Erratum: Phys.Rev.D 87, 069904 (2013)].

[71] A. C. Wall, *The Generalized Second Law implies a Quantum Singularity Theorem*, *Class. Quant. Grav.* **30** (2013) 165003, arXiv:1010.5513 [gr-qc]. [Erratum: Class.Quant.Grav. 30, 199501 (2013)].

[72] A. R. Brown, L. Susskind, and Y. Zhao, *Quantum Complexity and Negative Curvature*, *Phys. Rev. D* **95** (2017) 045010, arXiv:1608.02612 [hep-th].

[73] A. R. Brown and L. Susskind, *Second law of quantum complexity*, *Phys. Rev. D* **97** (2018) 086015, arXiv:1701.01107 [hep-th].

[74] V. Mohan, *Black hole singularities from holographic complexity*, *JHEP* **07** (2025) 275, arXiv:2504.10194 [hep-th].

[75] T. Jacobson and R. Parentani, *Horizon entropy*, *Found. Phys.* **33** (2003) 323–348, arXiv:gr-qc/0302099.

[76] L. Susskind, L. Thorlacius, and J. Uglum, *The Stretched horizon and black hole complementarity*, *Phys. Rev. D* **48** (1993) 3743–3761, arXiv:hep-th/9306069.

[77] F. F. Gautason, V. Mohan, and L. Thorlacius, *Late-time saturation of black hole complexity*, *JHEP* **08** (2025) 056, arXiv:2502.17179 [hep-th].

[78] M. A. Nielsen, *A geometric approach to quantum circuit lower bounds*, *Quant. Inf. Comput.* **6** (2006) 213–262, arXiv:quant-ph/0502070.

[79] D. Patramanis and W. Sybesma, *Emergence of Krylov complexity through quantum walks: An exploration of the quantum origins of complexity*, arXiv:2602.04949 [hep-th].

[80] U. H. Danielsson, G. Dibitetto, and S. Giri, *Black holes as bubbles of AdS*, *JHEP* **10** (2017) 171, arXiv:1705.10172 [hep-th].

[81] C. Bambi *et al.*, *Black hole mimickers: from theory to observation,* 5, 2025. arXiv:2505.09014 [gr-qc].

[82] P. O. Mazur and E. Mottola, *Gravitational Condensate Stars: An Alternative to Black Holes, Universe* **9** (2023) 88, arXiv:gr-qc/0109035.

[83] M. Visser and D. L. Wiltshire, *Stable gravastars: An Alternative to black holes?, Class. Quant. Grav.* **21** (2004) 1135–1152, arXiv:gr-qc/0310107.

[84] W. Israel, *Singular hypersurfaces and thin shells in general relativity, Nuovo Cim. B* **44S10** (1966) 1. [Erratum: Nuovo Cim.B 48, 463 (1967)].

[85] K. Lanczos, *Flächenhafte Verteilung der Materie in der Einsteinschen Gravitationstheorie, Annalen Phys.* **379** (1924) 518–540.

[86] N. Sen, *Über die Grenzbedingungen des Schwerefeldes an Unstetigkeitsflächen, Annalen Phys.* **378** (1924) 365–396.

[87] P. Kraus and S. D. Mathur, *Nature abhors a horizon, Int. J. Mod. Phys. D* **24** (2015) 1543003, arXiv:1505.05078 [hep-th].

[88] U. Danielsson, V. Mohan, and L. Thorlacius, *Black shell thermodynamics, JHEP* **09** (2025) 167, arXiv:2506.02117 [hep-th].

[89] V. Mohan and L. Thorlacius, *Spacetime from Operator Algebras,* arXiv:2606.10924 [hep-th].

[90] R. Haag, *Local quantum physics: Fields, particles, algebras.* 1992.

[91] M. Takesaki, *Tomita's Theory of Modular Hilbert Algebras and its Applications.* Lecture Notes in Mathematics. Springer-Verlag, 1970.

[92] S. A. W. Leutheusser and H. Liu, *Emergent Times in Holographic Duality, Phys. Rev. D* **108** (2023) 086020, arXiv:2112.12156 [hep-th].

[93] S. Leutheusser and H. Liu, *Causal connectability between quantum systems and the black hole interior in holographic duality, Phys. Rev. D* **108** (2023) 086019, arXiv:2110.05497 [hep-th].

[94] S. Leutheusser and H. Liu, *Subregion-subalgebra duality: Emergence of space and time in holography, Phys. Rev. D* **111** (2025) 066021, arXiv:2212.13266 [hep-th].

[95] E. Witten, *Gravity and the crossed product, JHEP* **10** (2022) 008, arXiv:2112.12828 [hep-th].

[96] H. Araki and E. J. Woods, *Representations of the canonical commutation relations describing a nonrelativistic infinite free bose gas, Journal of Mathematical Physics* **4** (05, 1963) 637–662.

[97] J. Dereziński, *Introduction to Representations of the Canonical Commutation and Anticommutation Relations*, pp. 63–143. Springer Berlin Heidelberg. `http://dx.doi.org/10.1007/3-540-32579-4_3`.

[98] K. Furuya, N. Lashkari, M. Moosa, and S. Ouseph, *Information loss, mixing and emergent type III$_1$ factors, JHEP* **08** (2023) 111, arXiv:2305.16028 [hep-th].

[99] H. J. Borchers, *The CPT theorem in two-dimensional theories of local observables, Commun. Math. Phys.* **143** (1992) 315–332.

[100] H. W. Wiesbrock, *Half sided modular inclusions of von Neumann algebras, Commun. Math. Phys.* **157** (1993) 83–92. [Erratum: Commun.Math.Phys. 184, 683–685 (1997)].

[101] H. J. Borchers and J. Yngvason, *Modular groups of quantum fields in thermal states, J. Math. Phys.* **40** (1999) 601–624, arXiv:math-ph/9805013.

[102] H. J. Borchers, *Half-sided modular inclusion and the construction of the poincaré group, Communications in Mathematical Physics* **179** (Sep, 1996) 703–723.

[103] V. Chandrasekaran, G. Penington, and E. Witten, *Large N algebras and generalized entropy, JHEP* **04** (2023) 009, arXiv:2209.10454 [hep-th].

[104] J. Kudler-Flam, S. Leutheusser, and G. Satishchandran, *Generalized black hole entropy is von Neumann entropy, Phys. Rev. D* **111** (2025) 025013, arXiv:2309.15897 [hep-th].

[105] M. Janssen and J. Renn, *How Einstein Found His Field Equations: Sources and Interpretation.* Classic Texts in the Sciences. Birkhäuser, Cham, Switzerland, 1st ed., 2022. XV, 357 pages.

[106] A. Connes, *Geometry from the spectral point of view, Letters in Mathematical Physics* **34** (Jul, 1995) 203–238.

[107] S. Banerjee, J. Erdmenger, and J. Karl, *Nonlocality induces isometry and factorisation in holography, Phys. Rev. D* **112** (2025) L021902, arXiv:2411.09616 [hep-th].

[108] C. Akers, N. Engelhardt, D. Harlow, G. Penington, and S. Vardhan, *The black hole interior from non-isometric codes and complexity, JHEP* **06** (2024) 155, arXiv:2207.06536 [hep-th].

[109] C. Krishnan and V. Mohan, *State-independent black hole interiors from the crossed product, JHEP* **05** (2024) 278, arXiv:2310.05912 [hep-th].

[110] V. Balasubramanian, R. N. Das, J. Erdmenger, J. Karl, and H. Verlinde, *Complexity and the Hilbert space dimension of 3D gravity,* arXiv:2602.02645 [hep-th].

[111] P. Saad, *Late Time Correlation Functions, Baby Universes, and ETH in JT Gravity,* arXiv:1910.10311 [hep-th].

[112] A. Blommaert, T. G. Mertens, and H. Verschelde, *Eigenbranes in Jackiw-Teitelboim gravity, JHEP* **02** (2021) 168, arXiv:1911.11603 [hep-th].

[113] A. Blommaert, J. Kruthoff, and S. Yao, *The power of Lorentzian wormholes, JHEP* **10** (2023) 005, arXiv:2302.01360 [hep-th].

[114] V. Balasubramanian, A. Lawrence, J. M. Magan, and M. Sasieta, *Microscopic Origin of the Entropy of Black Holes in General Relativity, Phys. Rev. X* **14** (2024) 011024, arXiv:2212.02447 [hep-th].

Paper I

Black hole singularities from holographic complexity

Vyshnav Mohan

JHEP **07** (2025) 275

Published for SISSA by Springer

Received: April 23, 2025
Revised: June 2, 2025
Accepted: June 28, 2025
Published: July 29, 2025

Black hole singularities from holographic complexity

Vyshnav Mohan

Science Institute, University of Iceland,
Dunhaga 3, 107 Reykjavík, Iceland
Institutionen för fysik och astronomi, Uppsala Universitet
Box 803, SE-751 08 Uppsala, Sweden

E-mail: vyshnav.vijay.mohan@gmail.com

Abstract: Using a second law of complexity, we prove a black hole singularity theorem. By introducing the notion of trapped extremal surfaces, we show that their existence implies null geodesic incompleteness inside globally hyperbolic black holes. We also demonstrate that the vanishing of the growth rate of the volume of extremal surfaces provides a sharp diagnostic of the black hole singularity. In static, uncharged, spherically symmetric spacetimes, this corresponds to the growth rate of spacelike extremal surfaces going to zero at the singularity. In charged or rotating spacetimes, such as the Reissner-Nordström and Kerr black holes, we identify novel timelike extremal surfaces that exhibit the same behavior at the timelike singularity.

Keywords: Black Holes, Spacetime Singularities, AdS-CFT Correspondence

ArXiv ePrint: 2504.10194

Contents

1 Introduction **1**

2 Growth of extremal surfaces **3**

3 Geodesic incompleteness from second law **6**

4 To Cauchy horizons and beyond **8**
4.1 Reissner-Nordström black hole 8
4.2 Kerr black hole 11

5 Incompleteness in Rindler wedge **12**

6 Discussion **14**

1 Introduction

Penrose proved that a globally hyperbolic, inextendible spacetime manifold M is null geodesically incomplete if it contains a trapped surface [1]. A surface is future-trapped if the future-directed null geodesics orthogonal to the surface converge. The proof crucially assumes the null energy condition, but there exist states in relativistic quantum field theories that violate this condition [2]. Wall [3] showed that the energy condition can be given up in favour of the generalized second law, which states that the generalized entropy always increases. The generalized entropy of a codimension-two surface is defined as the following sum

$$S_{\text{gen}} = \frac{A}{4G_N\hbar} + S_{\text{out}}\,, \tag{1.1}$$

where A is the area of the surface and S_{out} is the entanglement entropy of the quantum fields in the exterior of the surface. The generalized second law reflects the thermal properties of the black hole. Since no counterexamples to the generalized second law are known, Wall's proof puts the singularity theorem on a firmer footing. Significant advancements in the last decade have further refined the singularity theorem, resulting in wider applicability (see [4] and references therein).

The study of quantum complexity has also led us to another version of the second law of black hole thermodynamics. The *Second Law of Complexity* (SLC) states that if the complexity of a black hole is below its saturation value — which is of the exponential order in the Bekenstein-Hawking entropy — it will always increase [5, 6]. The complexity of black holes can be holographically realized through the "Complexity=Volume" (CV) prescription, where complexity is defined as the volume of boundary-anchored extremal co-dimension one surface passing through the interior of the black hole [7, 8]. Therefore, it is natural to ask whether we can use the CV prescription in conjunction with the second law of complexity to arrive at a singularity theorem. In this paper, we show that the answer is affirmative.

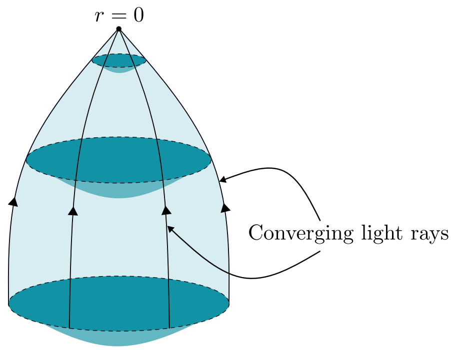

Figure 1. Extremal surfaces anchored to an infalling null sheet.

We begin by proposing a generalization of the second law of complexity: the volume of extremal surfaces anchored to a causal horizon increases as the anchor points are pushed to the future (see section 3 for more details). While we do not provide a proof, we take this statement as an assumption, supported by various physically relevant examples. The second law of complexity provides a powerful *bulk* condition that can be used to establish a singularity theorem. The following heuristic picture explains the interplay between singularities and SLC. Consider a sheet of future-directed null rays in the interior of a black hole. Let us look at extremal volume surfaces confined to the region between these null rays. The volume of these surfaces decreases as we move it toward the singularity, as shown below:

We refer to these extremal surfaces as trapped extremal surfaces. If the null rays were infinitely extendable, they would form a causal horizon, and the SLC would then force the volume of extremal surfaces to increase. However, focusing the light rays prevents this, leading to geodesic incompleteness in the black hole interior.

An interesting consequence of this picture is the observation that there is no 'space' for the extremal surfaces to grow at the singularity. As a result, the vanishing growth rate of the volume serves as a robust probe for diagnosing the existence of the singularity. In the case of a static uncharged spherically symmetric black hole, this translates to the statement that the volume of spacelike extremal surfaces vanishes at the singularity. In section 4, we show that the growth rate of timelike extremal surfaces, not their spacelike counterparts, goes to zero at the singularity in Reissner-Nordström and Kerr black holes.

The remainder of the paper is organized as follows. In section 2, we study the volume growth of extremal surfaces anchored to null surfaces. We introduce the notion of trapped extremal surfaces and prove a singularity theorem in section 3. In section 4, we examine the growth of extremal surfaces in Reissner-Nordström and Kerr black holes, identifying novel timelike extremal surfaces whose growth rate vanishes at the singularities. In section 5, we make the important observation that SLC implies null geodesic incompleteness, which does not always correspond to the presence of a singularity. We explore this distinction by studying complexity growth in AdS-Rindler, where incompleteness arises from the coordinate chart's failure to cover the entire Poincaré patch.

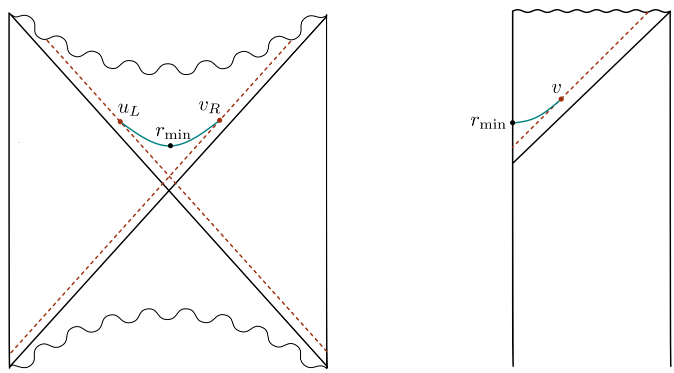

Figure 2. Extremal volume surfaces anchored to null surfaces are shown, with anchor surfaces indicated by red dashed lines. We have displayed the extremal curves in the Penrose diagrams of an eternal (left) and a single-sided black hole (right). In both cases, the location of the null surfaces and the anchoring point can be conveniently specified by using Eddington-Finkelstein coordinates u, v. The turning point of the surface is located at $r = 0$.

2 Growth of extremal surfaces

In this section, we calculate the growth rate of extremal surfaces anchored to null surfaces inside a black hole (see figure 2). In the standard treatment, the extremal surfaces are anchored to a constant radial surface in the asymptotic region (see [9] for a review). Our discussion here differs from the conventional approach in our choice of boundary conditions. In an eternal black hole, we anchor the extremal surface onto two symmetric null surfaces in the interior of the black hole. In the case of a single-sided black hole, we instead use the bridge-to-nowhere prescription [10] where the extremal surface ends at $r = 0$. Since the anchor surface falls into the black hole, the growth rate of the extremal surfaces differs from the standard behavior, as discussed below.

Consider an uncharged $(d+1)$-dimensional static eternal black hole with the metric

$$\mathrm{d}s^2 = -f(r)\mathrm{d}t^2 + \frac{\mathrm{d}r^2}{f(r)} + r^2\mathrm{d}\Omega_{d-1}^2\,, \tag{2.1}$$

where $f(r)$ is the blackening factor. The black hole spacetime is allowed to asymptote to AdS, dS, or flat space. The event horizon is located at $r = r_h$. The Eddington-Finkelstein coordinates u and v are defined as follows

$$v = t + r^*, \quad u = t - r^*, \qquad \text{where } \frac{\mathrm{d}r^*}{\mathrm{d}r} = \frac{1}{f(r)}\,. \tag{2.2}$$

We then specify the location of the null surfaces by choosing their corresponding Eddington-Finkelstein coordinates to be a constant, which we will denote by u_0.

The volume of a spherically symmetric codimension-one surface anchored onto these null surfaces is given by

$$\mathcal{V} = \Omega_{d-1}\int \mathrm{d}\lambda\; r^{d-1}\sqrt{-f(r)\dot{v}^2 + 2\dot{v}\dot{r}}\,. \tag{2.3}$$

Here, we have used λ to parametrizes the surface as $(v(\lambda), r(\lambda))$. We have also denoted the volume of a $(d-1)$-dimensional unit sphere by Ω_{d-1}. We anchor the surface at symmetric points by choosing the coordinates of their endpoints to be $u_L = v_R = v$ (see figure 2). Furthermore, we will use r_v to denote the value of the r coordinate at the anchor points.

The extremal volume surfaces are then obtained by extremizing the volume functional. Since the volume integral is reparametrization invariant, we choose λ by imposing the following condition,

$$r^{d-1}\sqrt{-f\dot{v}^2 + 2\dot{v}\dot{r}} = 1\,, \tag{2.4}$$

and this gives us the equations of motion

$$\begin{aligned} p &= r^{2(d-1)}(f(r)\dot{v} - \dot{r})\,, \\ r^{2(d-1)}\dot{r}^2 &= f(r) + r^{-2(d-1)}p^2\,. \end{aligned} \tag{2.5}$$

Here, p is a conserved quantity along the extremal surface. The location of the turning point r_{min} can be obtained by setting $\dot{r}$ to zero in the above expression

$$r_{\text{min}}^{2d-2} f(r_{\text{min}}) + p^2 = 0\,. \tag{2.6}$$

We choose λ to increase from left to right in the Penrose diagram. Evaluating the equations of motion at the turning point, we find that p is negative.

Performing a change of coordinates, we can recast the second equation in (2.5) as a particle scattering off a Newtonian potential $V_{\text{eff}} = -r^{2d-2}f(r)$ [9, 11]:

$$\dot{\tilde{r}}^2 + V_{\text{eff}} = p^2, \qquad \text{where} \quad \frac{\mathrm{d}\tilde{r}}{\mathrm{d}r} = r^{2d-2}\,. \tag{2.7}$$

Here, p^2 plays the role of the total energy of the particle. The scattering picture is handy in characterizing the extremal surfaces since we do not have explicit closed-form expressions. The effective potential has a maximum at some $r = r_a$, which we refer to as the *accumulation surface*. The region around this surface plays a crucial role in the usual holographic volume complexity computations [7–9, 11].

Now, let us read off the properties of the extremal curves using the effective potential. Consider the case in which the anchor point is near the bifurcation surface of the black hole, i.e., r_v is close to r_h. The associated extremal surface is represented by curve 1 in the left panel of figure 3. In the scattering picture, the surface corresponds to a particle scattering off the right side of the potential (see curve 1 in the right panel of figure 3). The particle starts at $r = r_v$, reaches a turning point located at $r_a < r_{\text{min}} < r_v$, and then returns to the anchor surface.

As we move the anchor point along the null surface, v increases, and r_v decreases. The energy of the particle p^2 increases and the turning point approaches the top of the potential. When $r_v = r_a$, the extremal surface becomes a constant-r surface. In the scattering picture, this corresponds to a particle sitting at the top of the effective potential.

For any larger value of v, p^2 decreases. The extremal surfaces beyond this point correspond to a particle scattering off the left side of the effective potential (see curve 2 in figure 3). This ensures that $\dot{r}$ in equation (2.5) takes only real values.

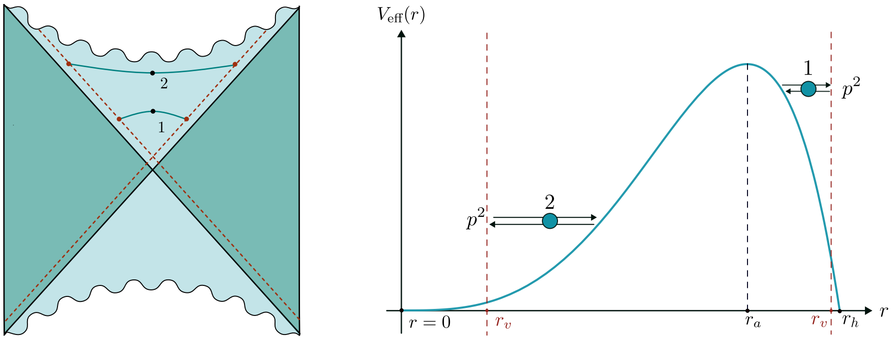

Figure 3. *(Left)* Two extremal surfaces in the interior of a static spherically symmetric uncharged black hole. *(Right)* The corresponding trajectories in the scattering picture. The red dashed lines are the locations of the anchor surface.

Now, let us compute the volume of the corresponding surfaces. Since λ increases from left to right in the Penrose diagram, we can use (2.4) to rewrite the volume integral (2.3) as follows:

$$\mathcal{V} = 2\Omega_{d-1} \int_{\lambda(r=r_{\text{min}})}^{\lambda(r=r_v)} \mathrm{d}\lambda = 2\Omega_{d-1} \int_{r_{\text{min}}}^{r_v} \frac{\mathrm{d}r}{\dot{r}} \,. \tag{2.8}$$

We have used the symmetry about the $t = 0$ surface to simplify the expression. Using the equations of motion, we get

$$\mathcal{V} = \pm 2\Omega_{d-1} \int_{r_{\text{min}}}^{r_v} \mathrm{d}r \frac{r^{2(d-1)}}{\sqrt{f(r) r^{2(d-1)} + p^2}} \,. \tag{2.9}$$

The choice of sign is determined by the sign of $\dot{r}$. When $r_{\text{min}} \geq r_a$, $\dot{r}$ is positive while it is negative for the extremal surfaces with $r_{\text{min}} < r_a$. This reverses the limits of integration. In the scattering picture, this corresponds to choosing the opposite orientation of the particle.

Using (2.5), we can express v as another r integral:

$$v - r^*_{\text{min}} = \int_{r_{\text{min}}}^{r_v} \mathrm{d}r \left[\frac{p}{f(r)\sqrt{f(r) r^{2(d-1)} + p^2}} + \frac{1}{f(r)} \right] \,. \tag{2.10}$$

Here r^*_{min} is the location of the turning point in the tortoise coordinate. Since r_{min} is related to p through (2.6), v depends only on p. Therefore, the anchoring point v fixes a value of p, which in turn fixes the location of the turning point.

Now, let us calculate the growth rate of these surfaces. When $r_{\text{min}} \geq r_a$, we can use (2.9) and (2.10) to arrive at the following expression [9]

$$\frac{\mathcal{V}}{2\Omega_{d-1}} = \int_{r_{\text{min}}}^{r_v} \mathrm{d}r \left[\frac{\sqrt{f(r) r^{2(d-1)} + p^2}}{f(r)} + \frac{p}{f(r)} \right] - p \left(v - r^*_{\text{min}} \right) \,. \tag{2.11}$$

Taking a derivative of the above expression w.r.t. v, we find that

$$\frac{1}{2\Omega_{d-1}}\frac{\mathrm{d}\mathcal{V}}{\mathrm{d}v} = \frac{\mathrm{d}r_v}{\mathrm{d}v}\left[\frac{\sqrt{f(r_v)r_v^{2(d-1)}+p^2}}{f(r_v)} + \frac{p}{f(r_v)}\right] - p\,. \tag{2.12}$$

We have used (2.10) to simplify the expression. Using $r_v^* = (v - u_0)/2$, we get

$$\frac{\mathrm{d}\mathcal{V}}{\mathrm{d}v} = \Omega_{d-1}\left(-p + \sqrt{f(r_v)r_v^{2(d-1)}+p^2}\right)\,. \tag{2.13}$$

Since p is negative, the extremal surfaces grow with v. This growth, however, ends when the turning point reaches the accumulation surface. When $r_{\min} < r_a$, we can follow the same steps, and find that

$$\frac{\mathrm{d}\mathcal{V}}{\mathrm{d}v} = \Omega_{d-1}\left(p - \sqrt{f(r_v)r_v^{2(d-1)}+p^2}\right)\,. \tag{2.14}$$

The growth rate is now negative, and the volume decreases when v increases.

When the anchor point reaches the singularity, the growth rate becomes zero. This is because the corresponding extremal surface is just the $r = 0$ surface and p vanishes on it. Since the growth rate vanishes only at the $r = 0$ surface, we can use it as an effective diagnostic of the black hole singularity. An important consequence of this observation is that once the anchor point passes the accumulation surface, extremal surfaces are inevitably 'doomed' to fall into the singularity where their volume growth goes to zero. The accumulation surface, therefore, acts as a *trapping* surface. We will use this crucial fact to prove a singularity theorem in the next section.

3 Geodesic incompleteness from second law

The location of the anchor surfaces in the previous section can be generalized using the causal structure of spacetime. Consider some point p on the spacetime manifold M. We define its chronological future $I^+(p)$ as the set of all points in M that can be reached by future-directed timelike curves passing through p. Then, by definition, the boundary of $I^+(p)$, which we will denote by $\partial I^+(p)$, is an achronal boundary [12]. Moreover, $N \equiv \partial I^+(p)$ is generated by null geodesics emanating from p (see Theorem 8.1.2 in [13]). The extremal surfaces we studied in the previous section can be understood as being anchored to N for some choice of p. In the case of a static black hole, we chose p to be a point lying on the $t = 0$ surface.

Now let us define a notion of a *causal horizon*. Consider a future-infinite timelike worldline W. We define a future-causal horizon H_{fut} as the boundary of the past of the worldline, that is, $H_{\text{fut}} = \partial I^-(W)$ [14]. It is important to emphasize that W is future-infinite; that is, the proper time along the worldline runs all the way to infinity. This distinguishes H_{fut} from the future boundary of the domain of dependence of arbitrary subregions. We can then quickly verify that this definition of causal horizons includes black hole event horizons as well as observer-dependent horizons, such as Rindler and cosmological horizons.

Using the definition of a causal horizon, we rephrase the second law in [5, 6] as follows:

> **Second Law of Complexity** (SLC). *The volume of extremal surfaces anchored to a causal horizon H_{fut} always increases as we move the anchor point along the surface.*

It is important to note that we do not have a proof of SLC. Explicit computations of holographic complexity in various cases, for example, in static black holes [9], Rindler wedges, rotating black holes [15], even non-static black holes [16, 17] all point towards the validity of SLC.[1] We will not attempt to prove SLC here. Instead, we assume its validity.

The second law, as stated here, is coarse-grained in that we have ignored quantum corrections to it. It is known that there are corrections non-perturbative in the exponential of the Bekenstein-Hawking entropy, which will cause the saturation of the volume [11, 19, 20]. We ignore these corrections for now and revisit them in section 6.

Now, let us define a future *trapped extremal surface* as an extremal surface anchored to N with the property that its volume decreases as the anchor point is moved into the future. We see that the extremal surfaces in the previous section with $r_{\min} < r_a$ are trapped extremal surfaces. An important point to note here is that the existence of these surfaces does not violate SLC, as the anchoring surfaces are not causal horizons. Also, by definition, trapped extremal surfaces are compact.

In this section, we restrict ourselves to globally hyperbolic spacetimes, where (a) there are no closed timelike curves, and (b) for any two points p and q, $J^+(p) \cap J^-(q)$ is compact, where $J^{\pm}(p)$ is the causal future/past of p.

The statement of the SLC turns out to be extremely powerful because it provides a *bulk* condition on the growth rate of volumes anchored to causal horizons. An immediate implication of the SLC is that if there are trapped extremal surfaces somewhere in the spacetime, then they *cannot* be anchored to a causal horizon. Now, let us use this fact to arrive at a singularity theorem.

Theorem 1. *Consider a globally hyperbolic spacetime M with a trapped extremal surface T. Then, the spacetime is null geodesically incomplete.*

Proof. Let us assume the trapped extremal surface T is anchored to a null surface $N = \partial I^+(p)$, for some point $p \in M$. We will suppose for a contradiction that the affine parameter of every null geodesic generating N can be extended infinitely into the future. This would then imply that N is a causal horizon. From SLC, the volume of the trapped surface would always increase, contradicting the defining property of a trapped extremal surface. Therefore, the affine parameter of the null geodesics on N must terminate at a finite value.

Now, we can complete the proof using the original Penrose theorem [1] (see [3, 12] for more details). Suppose M were null geodesically complete. Then the null geodesic generators of N could be extended to the future beyond N. An important point to note is that the affine parameter *on* $N = \partial I^+(p)$ is bounded, and any extension of the null generators to the future would lie inside $I^+(p)$, not on its boundary (see Proposition 4.5.14 and section 8.2 of [12] for a related discussion). Null geodesic completeness of M implies that the endpoints of the null geodesic generators of N lie within the spacetime and therefore remain part of N, ensuring that N is closed.

[1] Readers familiar with holographic complexity computations might notice that the SLC used here differs from standard definition, as the extremal surface is anchored to the horizon rather than to a cutoff surface in the asymptotic region. However, we can quickly convince ourselves that the growth of these surfaces comes from the turning point, which lies well inside the horizon, and that both formulations are classically equivalent [9] (see also [8, 11, 18] for related discussions).

We now argue that N is compact. Since the affine parameters are bounded, we can rescale them to lie within the range $[0,1]$. Then N can be topologically written as $T \times [0,1]$, which is a product of a compact space and a closed interval, making N compact.

This conclusion contradicts the assumption that the spacetime is globally hyperbolic. To see this, consider a connected, non-compact Cauchy slice Σ. We can always find a smooth timelike vector field t^μ whose integral curves intersect Σ exactly once. Because $N \equiv \partial I^+(p)$ is achronal, these integral curves intersect N at most once as well. This allows us to define a one-to-one map between Σ and N using the integral curves of t^μ. However, this leads to a contradiction since the global hyperbolicity of the spacetime prohibits the evolution of a non-compact slice Σ into a compact surface N. Therefore, the assumption that M is null geodesically complete, which was used to argue that N is compact, is incompatible with the other assumptions. □

Before we conclude the discussion, a few comments are in order:

- Our theorem follows the same structure as other singularity theorems [21]. Specifically, we impose a 'causality condition' by assuming global hyperbolicity of the spacetime, which helps rule out important edge cases (see, e.g., [22]). The second law of complexity replaces the usual 'energy condition,' while trapped extremal surfaces provide the 'initial condition.'

- In the standard CV prescription, complexity is assigned to the volume of a surface that lies outside the accumulation surface. No such prescription exists for trapped extremal surfaces located inside the accumulation surface. While it may be possible to define a notion of complexity for these trapped surfaces, the proof does not rely on such a definition. The SLC is carefully phrased to depend only on the volume of extremal surfaces anchored to causal horizons. As a result, we avoid the need to interpret trapped extremal surfaces in terms of complexity and do not rely on any non-standard notions of holographic complexity.

4 To Cauchy horizons and beyond

In section 2, we studied the growth of extremal surfaces in static, uncharged black holes. In this section, we will extend this discussion to the case of a charged black hole. Since the metric of these black holes can also be brought to the static form in (2.1), similar computations are expected to hold. However, the presence of a Cauchy horizon in the interior brings in new surprises.

4.1 Reissner-Nordström black hole

Consider a Reissner-Nordström (RN) black hole in asymptotically flat spacetime. We will work in $3+1$-dimensions. The black hole has the metric (2.1), with the following blackening factor

$$f(r) = \left(1 - \frac{r_+}{r}\right)\left(1 - \frac{r_-}{r}\right), \tag{4.1}$$

where $r_\pm$ are the location of the horizons with $r_+ > r_-$. The inner horizon is a Cauchy horizon and signals the breakdown of global hyperbolicity [12]. The original Penrose theorem

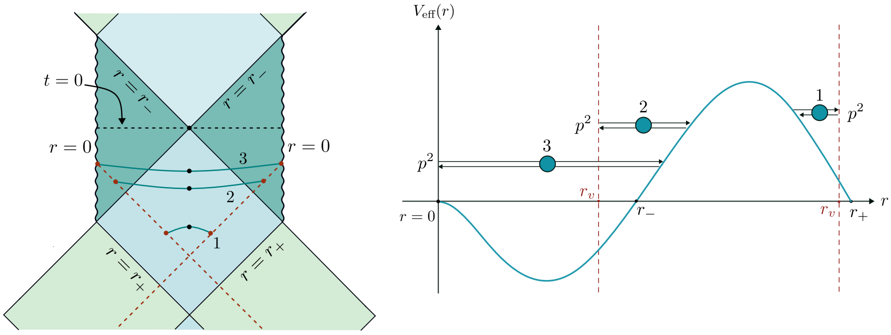

Figure 4. *(Left)* Spacelike extremal surfaces in a Reissner-Nordström black hole. *(Right)* The corresponding trajectories in the scattering picture. The anchor surface of curve 3 is located at the singularity.

and its entropic reformulations do not apply to such black holes because of this breakdown of global hyperbolicity.

Now let us study the growth rate of *spacelike* extremal volume surfaces. As in the previous section, we will look at spherically symmetric extremal volume surfaces anchored onto two symmetric null surfaces in the interior of the black hole. The equations of motion for these surfaces are once again given by (2.5). The extremal volumes in the interior of the Reissner-Nordström (RN) black hole were studied in [23], and we have illustrated a few of these surfaces in figure 4.

In the scattering picture, these surfaces can be thought of as particles scattering off the effective potential $V_{\rm eff}$ (see right panel of figure 4). As we move the anchor point towards the singularity, the volume of extremal surfaces initially increases but begins to decrease once the anchor point crosses the accumulation surface. The volume growth rates are given by (2.13) and (2.14). The crucial difference from the uncharged case is that p never goes to zero, even when the anchoring point has reached the singularity.

To see this, consider (2.13) where the growth rate can be seen to be proportional to p. From the first equation in (2.5), we observe that p vanishes if and only if $f(r)=0$ or $t=$ constant along the extremal surface. Since the condition $f(r)=0$ is never satisfied, the only possibility is to consider null anchoring surfaces that reach the singularity at the $t=0$ slice (depicted by the horizontal dotted line in the Penrose diagram in figure 4). For any other general anchoring surface, the growth rate remains nonzero. Therefore, the fate of the trapped extremal surfaces is not as doomed as in the previous case, as their volumes never shrink to zero when the anchor point reaches the singularity. This is because the null anchoring surfaces go off to timelike $r=0$ slices in two *different* coordinate patches. This suggests that the vanishing of the volume of extremal surfaces ceases to be a suitable probe of the singularity.

However, we can consider an alternate computation that fixes this problem. We do not anchor both the endpoints of the extremal surface to the null surfaces. Instead, we will anchor only the 'right' endpoint and let the 'left' one terminate at its turning point on the

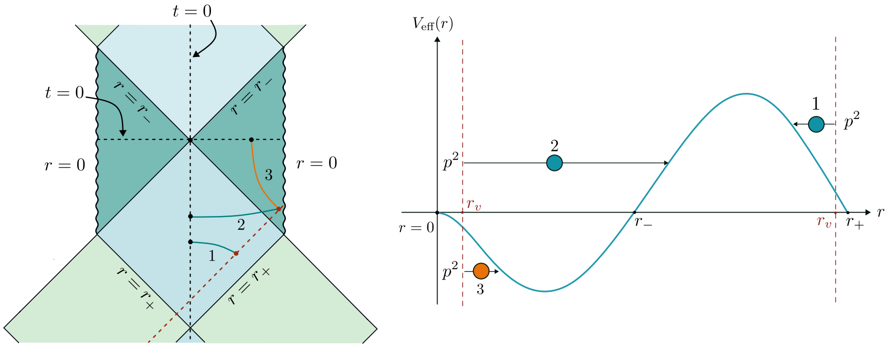

Figure 5. The teal curves correspond to spacelike extremal surfaces, while the orange curve is timelike. The red dashed lines once again correspond to the locations of the anchor surface.

$t = 0$ line. Now, let us repeat the extremal surface computation. When $r_- < r_v < r_a$, we obtain precisely half of the spacelike extremal surfaces (see curve 1 in figure 5). As discussed earlier, the growth rate of the extremal surfaces is always positive.

When the anchor point crosses the inner horizon, we find new behaviour. There are now two possible choices for the extremal surfaces. We have the usual spacelike surface (curve 2 in figure 5). Additionally, we get a timelike surface that satisfies the same boundary conditions (curve 3 in figure 5). The orientation of the scattering trajectory in figure 5 is chosen to ensure that $\dot{r}$ remains real. The lack of a unique extremal surface is a consequence of the breakdown of global hyperbolicity of the spacetime. The growth rate of these timelike surfaces can be computed using the techniques in section 2. This time, we choose the parameter along the surface as follows:

$$r^{d-1}\sqrt{-f\dot{v}^2 + 2\dot{v}\dot{r}} = -1\,, \tag{4.2}$$

where the negative sign on the right-hand side comes from the fact that we are working with timelike surfaces. Denoting the conserved quantity along the surface by p, we arrive at the following equations of motion

$$\begin{aligned} p &= r^{2(d-1)}(f(r)\dot{v} - \dot{r})\,, \\ r^{2(d-1)}\dot{r}^2 &= -f(r) + r^{-2(d-1)}p^2\,. \end{aligned} \tag{4.3}$$

Note that the equations of motion can also be obtained from (2.5) by the simple substitution $p \to ip$ and $\lambda \to i\lambda$. Choosing λ to increase in the downward direction in the Penrose diagram, we find that $p \geq 0$.

We can once again rewrite the equation involving the r coordinate as a particle scattering of an effective potential $\tilde{V}_{\text{eff}}$. The new effective potential turns out to be the negative of the spacelike effective potential V_{eff}:

$$\tilde{V}_{\text{eff}}(r) = -V_{\text{eff}}(r) = r^{2d-2}f(r)\,. \tag{4.4}$$

As in the case of spacelike surfaces, there is an accumulation surface whose location corresponds to the maximum of $\tilde{V}_{\text{eff}}$, which is the same as the minimum of V_{eff}. We will denote the location of this surface by $r = \hat{r}_a$. The orientation of the particle in the scattering picture depends on its turning point w.r.t. to the new accumulation surface. When $r_{\text{min}} \geq \hat{r}_a$, the volume of these timelike extremal surfaces is given by

$$\mathcal{V}_{\text{timelike}} = i\Omega_{d-1} \int_{r_{\text{min}}}^{r_v} \mathrm{d}r \frac{r^{2(d-1)}}{\sqrt{-f(r) r^{2(d-1)} + p^2}} \,. \tag{4.5}$$

The volume is imaginary, which follows from our choice of metric signature. The limits of integration reverse when $r_{\text{min}} < \hat{r}_a$. The growth rate can then be found to be:

$$\frac{\mathrm{d}\mathcal{V}_{\text{timelike}}}{\mathrm{d}v} = \begin{cases} \frac{i\Omega_{d-1}}{2} \left(p - \sqrt{p^2 - f(r_v) r_v^{2(d-1)}} \right) & r_{\text{min}} \geq \hat{r}_a \\ \frac{i\Omega_{d-1}}{2} \left(-p + \sqrt{p^2 - f(r_v) r_v^{2(d-1)}} \right) & r_{\text{min}} < \hat{r}_a \end{cases} . \tag{4.6}$$

As in the spacelike case, the growth rate changes its sign when the anchor point crosses the accumulation surface. This prompts us to call the surfaces with $r_{\text{min}} < \hat{r}_a$ *timelike trapped extremal surfaces*.

More importantly, we observe that p vanishes when $r_v = 0$. In this case, the extremal surface simplifies and becomes the constant $r = 0$ slice, and the right-hand side of the first equation of motion (4.3) vanishes identically. Consequently, the growth rate of the extremal surface drops to zero. Since the singularity is the only region where the growth rate vanishes, this behavior can be used as a robust signature of the black hole singularity.

While it is perhaps not surprising that timelike extremal surfaces are sensitive to timelike singularities, their dual interpretation remains unclear. In particular, the meaning of the volume of a timelike extremal surface in the boundary theory is not immediately evident. Nonetheless, it is tempting to speculate that this may hint at a notion of "timelike complexity" in the dual description. Interestingly, timelike entanglement entropy has been proposed as a method for computing what is referred to as pseudo-entropy in the boundary theory [24–27]. It is natural to expect a corresponding dictionary to exist in the case of complexity. We leave this for future work.

4.2 Kerr black hole

The vanishing of the growth rate of timelike extremal surfaces at the black hole singularity is not limited to spherically symmetric black holes. We can see this by studying a $3+1$-dimensional Kerr black hole of mass M and angular momentum aM. The metric in Boyer-Lindquist coordinates is given by

$$\mathrm{d}s^2 = -\frac{\Delta}{\rho^2} \left(\mathrm{d}t - a \sin^2\theta \mathrm{d}\phi \right)^2 + \frac{\sin^2\theta}{\rho^2} \left[\left(r^2 + a^2 \right) \mathrm{d}\phi - a \mathrm{d}t \right]^2 + \frac{\rho^2}{\Delta} \mathrm{d}r^2 + \rho^2 \mathrm{d}\theta^2 \,, \tag{4.7}$$

where

$$\Delta = r^2 - 2GMr + a^2 \quad \text{and} \quad \rho^2 = r^2 + a^2 \cos^2\theta \,. \tag{4.8}$$

The black hole horizons are located at $r_\pm$. The ring singularity sits at $r = 0$ and $\theta = \pi/2$. We can also define an Eddington-Finkelstein coordinate $v = t + r^*$, where

$$\mathrm{d}r^* = \frac{r^2 + a^2}{\Delta}\mathrm{d}r\,. \tag{4.9}$$

As in the RN case, we consider extremal surfaces anchored at a null surface inside the black hole. However, we now focus on axially symmetric configurations, as the black hole is rotating. We anchor the 'right' endpoint of the extremal surfaces at the null surface. The other endpoint is chosen to lie at its turning point. The spacetime is not globally hyperbolic, and as a result, when the anchor point crosses the inner horizon, there are new timelike extremal surfaces. In particular, as the anchor point approaches the singularity, the timelike extremal surfaces approach the singularity. Let us see how this works out.

Consider a general axisymmetric hypersurface in the interior of the black hole. The r coordinate can be parametrized by $r(t, \theta)$ and the line element of this three-manifold can be computed by substituting $\mathrm{d}r = r_{,t}\mathrm{d}t + r_{,\theta}\mathrm{d}\theta$ into to the metric (4.7). Once we have the metric, we can compute the volume by integrating over the variables t, θ, and ϕ. The full expression is given in [23], although we will not need it explicitly here since we are only focusing on surfaces near the ring singularity.

We therefore restrict ourselves to the case where r is just a function of θ. We will also assume that the surface is t-independent. In this case, the three-metric computation simplifies significantly, and we obtain [15, 28]

$$\mathrm{d}\mathcal{V} = \sqrt{\rho^2\left(|\Delta| - r_{,\theta}^2\right)}\sin\theta dt \wedge d \wedge d\theta \wedge d\phi\,. \tag{4.10}$$

The extremal hypersurfaces are given by extremizing this integral over the volume element. If $r =$ constant, the Euler-Lagrange equation is given by the simple expression

$$\frac{\mathrm{d}}{\mathrm{d}r}\left(\rho^2\Delta\right) = 0\,. \tag{4.11}$$

We can see that this is trivially satisfied by the ring singularity at $r = 0$ and $\theta = \pi/2$. Therefore, the singularity is an extremal volume surface. Moreover, it is a *timelike* extremal surface.

Now, let us compute the growth rate of the timelike surfaces as they approach the singularity. Since $\mathrm{d}v = \mathrm{d}t$ on a constant r slice, we can use the volume element (4.10) to obtain

$$\frac{\mathrm{d}\mathcal{V}}{\mathrm{d}v} = \int \sqrt{\rho^2\Delta}\sin\theta\ \mathrm{d}\theta \wedge \mathrm{d}\phi\,. \tag{4.12}$$

At the singularity, the integrand vanishes, and the growth of timelike extremal surfaces goes to zero. This suggests that the growth rate of timelike or spacelike extremal surfaces can serve as a useful probe of black hole singularities in various cases.

5 Incompleteness in Rindler wedge

Incompleteness of null geodesics does not necessarily imply the presence of a singularity where the geodesics terminate [12]. In this section, we explore the alternative possibility by studying complexity growth in AdS-Rindler wedges. In global coordinates, AdS_3 has the metric

$$\mathrm{d}s^2 = \frac{1}{\cos^2\rho}\left(-\mathrm{d}\tau^2 + \mathrm{d}\rho^2 + \sin^2\rho\mathrm{d}\theta^2\right)\,. \tag{5.1}$$

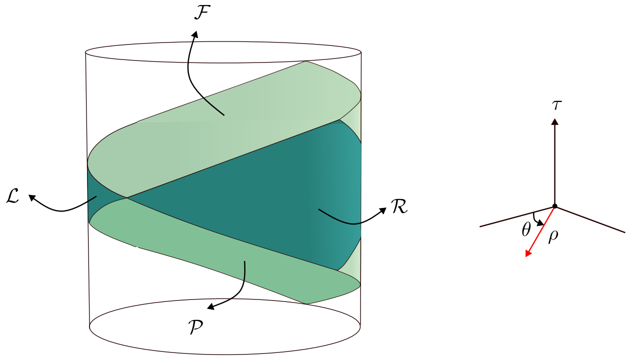

Figure 6. The Poincaré patch of AdS_3. The global coordinates cover the entire cylinder. The Poincaré coordinates cover only the solid region shown in the figure, which can be further divided into four Rindler wedges.

We have set the AdS length scale to one for convenience. Using the coordinate transformations,

$$\begin{aligned} t &= \frac{\sin\tau}{\cos\tau + \sin\rho\cos\theta}\,, \\ x &= \frac{\sin\theta\sin\rho}{\cos\tau + \sin\rho\cos\theta}\,, \\ z &= \frac{\cos\rho}{\cos\tau + \sin\rho\cos\theta}\,, \end{aligned} \tag{5.2}$$

we can rewrite the metric in the Poincaré coordinates as follows:

$$\mathrm{d}s^2 = \frac{\mathrm{d}z^2 - \mathrm{d}x^+\mathrm{d}x^-}{z^2}\,, \qquad \text{where } x^\pm = t \pm x\,. \tag{5.3}$$

The region $z > 0$ and $x^\pm \in (-\infty, \infty)$ defines the Poincaré patch of the spacetime. We can divide the patch into four Rindler regions depending on the signs of (x^+, x^-). We label these regions $\mathcal{R}, \mathcal{L}, \mathcal{F}$, and $\mathcal{P}$ when the signs are (+, -), (-, +), (+, +), and (-, -) respectively (see figure 6). The relevance of the boundary of these wedges in the context of AdS/CFT correspondence can be found in [29].

It turns out that we can also cover these Rindler regions using a set of BTZ coordinates (t, r, ϕ) given by

$$e^{2t} = \frac{x^+}{x^-}, \quad e^{2\phi} = z^2 - x^+x^-, \quad r^2 = \frac{z^2 - x^+x^-}{z^2}\,. \tag{5.4}$$

The metric in these coordinates takes the form

$$\mathrm{d}s^2 = -\left(r^2 - 1\right)\mathrm{d}t^2 - \frac{\mathrm{d}r^2}{(r^2-1)} + r^2\mathrm{d}\phi\,. \tag{5.5}$$

The crucial difference between the BTZ metric and the AdS-Rindler metric in BTZ coordinates (5.5) is that ϕ is non-compact in the latter case.

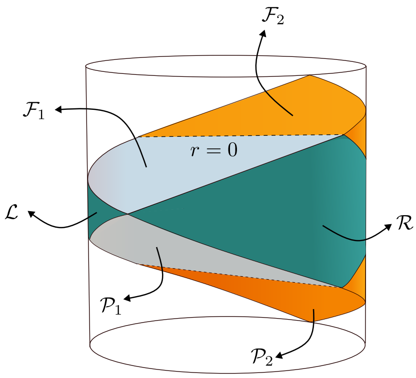

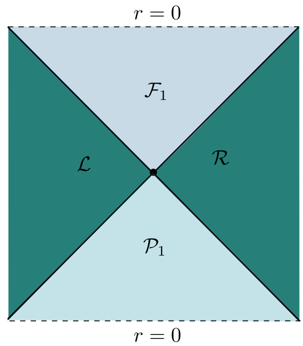

Figure 7. *(Left)* The patch $\mathcal{F}$ is divided into two regions, $\mathcal{F}_1$ and $\mathcal{F}_2$. The BTZ coordinates cover only $\mathcal{F}_1$. *(Right)* The mapping of various Rindler regions to the corresponding BTZ "black hole.".

The AdS-Rindler horizon is at $r = 1$. The Rindler regions $\mathcal{R}, \mathcal{L}$ are mapped to the left and right exterior wedges of the BTZ "black hole." In contrast, the Rindler regions $\mathcal{F}, \mathcal{P}$ are mapped to the future and past interiors, respectively. Now, let us look at the growth of extremal surfaces in this coordinate system. We will study surfaces that are symmetric in the ϕ coordinate. Since this direction is non-compact, we will regularize the volume by choosing appropriate constant-ϕ cutoff surfaces. The metric (5.5) has the same form as (2.1). This allows us to port the uncharged static black hole computations. A trapped extremal surface exists in the interior of the "black hole," our singularity theorem tells us that null geodesics are incomplete.

The theorem is signaling the existence of the $r = 0$ surface. Clearly, this surface is not a singularity in the full AdS spacetime. Nevertheless, it appears problematic from the perspective of the BTZ coordinate system. To understand the significance of the $r = 0$ surface, we must look at the relationship between the Poincaré coordinates and the BTZ coordinates.

It turns out that the BTZ coordinates do not cover the entire Rindler region $\mathcal{F}$ [29]. The BTZ coordinates cover only a part of $\mathcal{F}$, which we will denote by $\mathcal{F}_1$ (see figure 7).

In the region $\mathcal{F}_2$, we must use a different set of coordinates (the coordinate transformations can be found in [29]). The surface $r = 0$ corresponds to the boundary between $\mathcal{F}_1$ and $\mathcal{F}_2$. Therefore, the geodesic incompleteness stemming from SLC indicates the inability of the coordinate patch to cover the entirety of the Poincaré patch.

We will end this discussion with an important note. The inability to conclusively identify the terminus of null geodesics as a singularity is a general feature of all singularity theorems, not merely a limitation of our own.

6 Discussion

Our proof of geodesic incompleteness is structurally similar to that of Wall [3]. However, it is important to highlight the differences. The generalized entropy defined in (1.1) consists of a classical area term and a quantum entanglement entropy term. The inclusion of both terms is essential for obtaining a second law [30].

In contrast, holographic complexity involves the computation of a classical volume. Quantum corrections become important only when the complexity is of exponential order in the Bekenstein-Hawking entropy. This is explicitly evident in 2d models of quantum gravity [19, 31]. The absence of a quantum term significantly simplifies the computations. It is well known in the literature that the entanglement entropy term complicates the comparison of arbitrary shape deformations of generalized entropy (see [4] for more details). Our volume calculations sidestep this technical challenge by remaining purely classical.

The growth rate of extremal surfaces has been very useful in signaling the existence of a singularity inside the black hole. A natural question is: what does this object mean in a quantum theory, for instance, in the language of operator growth [32]? Since we are computing the volume of a *subregion* inside the black hole, a natural guess would be to compute the complexity of a subsystem. This notion of subsystem complexity should be distinguished from existing ideas in the literature, such as the one in [33], where the volume enclosed by the Ryu-Takayanagi (RT) surface is used to define a notion of subregion complexity in the boundary theory. In contrast, the bulk subregion considered here lies within the black hole interior. It is therefore natural to expect that the associated subregion complexity computes the complexity of boundary operators that are dual to interior degrees of freedom. These operators are inherently non-local in the boundary theory and can, for example, be constructed using the Papadodimas-Raju proposal [34–36].

If one can make this notion of subregion complexity more precise, we can use these ideas to diagnose the existence of singularities in their holographic duals. Recent developments in the study of operator algebras suggest that the emergence of a Killing horizon in the bulk can be attributed to a particular notion of chaos in the boundary theory [37, 38]. Complexity might provide a natural framework for understanding the emergence of black hole singularities and the interior (see, e.g., [39, 40]). Operator complexity, for example, has been very useful in describing aspects of the exterior geometry of the black hole [41–44]. Therefore, it is natural to expect complexity to teach us something about the emergence of the black hole interior.

An important takeaway from our calculations and that of Wall [3] is that the black hole singularity is deeply tied to the thermodynamic irreversibility of the second law of thermodynamics. It will be interesting to see if we can use an appropriate notion of thermodynamic irreversibility to directly motivate a boundary diagnostic of black hole singularities.

In this paper, we have ignored quantum corrections to the volume calculation. It is known that non-perturbative effects play an important role in the computation of complexity [11, 19]. These corrections are expected to appear at the semiclassical level as bulk 'wormholes' and are believed to account for the finiteness of the black hole Hilbert space [20]. Including such effects would modify the growth rate calculations and may offer a path toward resolving the singularity.

Acknowledgments

I would like to thank Friðrik Freyr Gautason, Watse Sybesma, and Lárus Thorlacius for useful discussions. This work was supported in part by the Icelandic Research Fund under grant 228952-053 and by a doctoral grant from The University of Iceland Science Park.

Data Availability Statement. This article has no associated data or the data will not be deposited.

Code Availability Statement. This article has no associated code or the code will not be deposited.

References

[1] R. Penrose, *Gravitational collapse and space-time singularities*, *Phys. Rev. Lett.* **14** (1965) 57 [INSPIRE].

[2] H. Epstein, V. Glaser and A. Jaffe, *Nonpositivity of energy density in Quantized field theories*, *Nuovo Cim.* **36** (1965) 1016 [INSPIRE].

[3] A.C. Wall, *The Generalized Second Law implies a Quantum Singularity Theorem*, *Class. Quant. Grav.* **30** (2013) 165003 [*Erratum ibid.* **30** (2013) 199501] [arXiv:1010.5513] [INSPIRE].

[4] R. Bousso, *Robust Singularity Theorem*, *Phys. Rev. Lett.* **135** (2025) 011501 [arXiv:2501.17910] [INSPIRE].

[5] A.R. Brown, L. Susskind and Y. Zhao, *Quantum Complexity and Negative Curvature*, *Phys. Rev. D* **95** (2017) 045010 [arXiv:1608.02612] [INSPIRE].

[6] A.R. Brown and L. Susskind, *Second law of quantum complexity*, *Phys. Rev. D* **97** (2018) 086015 [arXiv:1701.01107] [INSPIRE].

[7] L. Susskind, *Computational Complexity and Black Hole Horizons*, *Fortsch. Phys.* **64** (2016) 24 [arXiv:1403.5695] [INSPIRE].

[8] D. Stanford and L. Susskind, *Complexity and Shock Wave Geometries*, *Phys. Rev. D* **90** (2014) 126007 [arXiv:1406.2678] [INSPIRE].

[9] D. Carmi et al., *On the Time Dependence of Holographic Complexity*, *JHEP* **11** (2017) 188 [arXiv:1709.10184] [INSPIRE].

[10] L. Susskind and Y. Zhao, *Switchbacks and the Bridge to Nowhere*, arXiv:1408.2823 [INSPIRE].

[11] F.F. Gautason, V. Mohan and L. Thorlacius, *Late-Time Saturation of Black Hole Complexity*, arXiv:2502.17179 [INSPIRE].

[12] S.W. Hawking and G.F.R. Ellis, *The Large Scale Structure of Space-Time*, Cambridge University Press (2023) [DOI:10.1017/9781009253161] [INSPIRE].

[13] R.M. Wald, *General Relativity*, Chicago Univ. Pr., Chicago, USA (1984) [DOI:10.7208/chicago/9780226870373.001.0001] [INSPIRE].

[14] T. Jacobson and R. Parentani, *Horizon entropy*, *Found. Phys.* **33** (2003) 323 [gr-qc/0302099] [INSPIRE].

[15] J. Couch, S. Eccles, T. Jacobson and P. Nguyen, *Holographic Complexity and Volume*, *JHEP* **11** (2018) 044 [arXiv:1807.02186] [INSPIRE].

[16] S. Chapman, H. Marrochio and R.C. Myers, *Holographic complexity in Vaidya spacetimes. Part I*, *JHEP* **06** (2018) 046 [arXiv:1804.07410] [INSPIRE].

[17] S. Chapman, H. Marrochio and R.C. Myers, *Holographic complexity in Vaidya spacetimes. Part II*, *JHEP* **06** (2018) 114 [arXiv:1805.07262] [INSPIRE].

[18] L. Schneiderbauer, W. Sybesma and L. Thorlacius, *Holographic Complexity: Stretching the Horizon of an Evaporating Black Hole*, *JHEP* **03** (2020) 069 [arXiv:1911.06800] [INSPIRE].

[19] L.V. Iliesiu, M. Mezei and G. Sárosi, *The volume of the black hole interior at late times*, *JHEP* **07** (2022) 073 [arXiv:2107.06286] [INSPIRE].

[20] V. Balasubramanian, A. Lawrence, J.M. Magan and M. Sasieta, *Microscopic Origin of the Entropy of Black Holes in General Relativity*, *Phys. Rev. X* **14** (2024) 011024 [arXiv:2212.02447] [INSPIRE].

[21] J.M.M. Senovilla, *Singularity Theorems and Their Consequences*, *Gen. Rel. Grav.* **30** (1998) 701 [arXiv:1801.04912] [INSPIRE].

[22] A. Borde, *Open and closed universes, initial singularities and inflation*, *Phys. Rev. D* **50** (1994) 3692 [gr-qc/9403049] [INSPIRE].

[23] M.J. Duncan, *Maximally slicing a black hole with minimal distortion*, *Phys. Rev. D* **31** (1985) 1267.

[24] K. Doi et al., *Pseudoentropy in dS/CFT and Timelike Entanglement Entropy*, *Phys. Rev. Lett.* **130** (2023) 031601 [arXiv:2210.09457] [INSPIRE].

[25] K. Narayan, *de Sitter space, extremal surfaces, and time entanglement*, *Phys. Rev. D* **107** (2023) 126004 [arXiv:2210.12963] [INSPIRE].

[26] K. Doi et al., *Timelike entanglement entropy*, *JHEP* **05** (2023) 052 [arXiv:2302.11695] [INSPIRE].

[27] K. Narayan and H.K. Saini, *Notes on time entanglement and pseudo-entropy*, *Eur. Phys. J. C* **84** (2024) 499 [arXiv:2303.01307] [INSPIRE].

[28] X.Y. Chew and Y.C. Ong, *Interior volume of Kerr-AdS black holes*, *Phys. Rev. D* **102** (2020) 064055 [arXiv:2005.01312] [INSPIRE].

[29] S.A.W. Leutheusser and H. Liu, *Emergent Times in Holographic Duality*, *Phys. Rev. D* **108** (2023) 086020 [arXiv:2112.12156] [INSPIRE].

[30] J.D. Bekenstein, *Black holes and the second law*, *Lett. Nuovo Cim.* **4** (1972) 737 [INSPIRE].

[31] Z. Yang, *The Quantum Gravity Dynamics of Near Extremal Black Holes*, *JHEP* **05** (2019) 205 [arXiv:1809.08647] [INSPIRE].

[32] D.E. Parker et al., *A Universal Operator Growth Hypothesis*, *Phys. Rev. X* **9** (2019) 041017 [arXiv:1812.08657] [INSPIRE].

[33] M. Alishahiha, *Holographic Complexity*, *Phys. Rev. D* **92** (2015) 126009 [arXiv:1509.06614] [INSPIRE].

[34] K. Papadodimas and S. Raju, *An Infalling Observer in AdS/CFT*, *JHEP* **10** (2013) 212 [arXiv:1211.6767] [INSPIRE].

[35] K. Papadodimas and S. Raju, *Black Hole Interior in the Holographic Correspondence and the Information Paradox*, *Phys. Rev. Lett.* **112** (2014) 051301 [arXiv:1310.6334] [INSPIRE].

[36] K. Papadodimas and S. Raju, *State-Dependent Bulk-Boundary Maps and Black Hole Complementarity*, *Phys. Rev. D* **89** (2014) 086010 [arXiv:1310.6335] [INSPIRE].

[37] E. Gesteau and H. Liu, *Toward stringy horizons*, arXiv:2408.12642 [INSPIRE].

[38] S. Ouseph et al., *Local Poincaré algebra from quantum chaos*, *JHEP* **01** (2024) 112 [arXiv:2310.13736] [INSPIRE].

[39] D. Areán, H.-S. Jeong, J.F. Pedraza and L.-C. Qu, *Kasner interiors from analytic hairy black holes*, *JHEP* **11** (2024) 138 [arXiv:2407.18430] [INSPIRE].

[40] E. Cáceres, Á.J. Murcia, A.K. Patra and J.F. Pedraza, *Kasner eons with matter: holographic excursions to the black hole singularity*, *JHEP* **12** (2024) 077 [arXiv:2408.14535] [INSPIRE].

[41] Z.-Y. Fan, *Momentum-Krylov complexity correspondence*, arXiv:2411.04492 [INSPIRE].

[42] P. Caputa et al., *Spread Complexity Rate as Proper Momentum*, arXiv:2410.23334 [INSPIRE].

[43] M. Dodelson, *Black holes from chaos*, arXiv:2501.06170 [INSPIRE].

[44] H.-S. Jeong, A. Kundu and J.F. Pedraza, *Brickwall one-loop determinant: spectral statistics & Krylov complexity*, *JHEP* **05** (2025) 154 [arXiv:2412.12301] [INSPIRE].

Paper II

Late-time saturation of black hole complexity

Friðrik Freyr Gautason, Vyshnav Mohan, and Lárus Thorlacius

JHEP **08** (2025) 056

Published for SISSA by Springer
Received: *March 20, 2025*
Accepted: *July 7, 2025*
Published: *August 7, 2025*

Late-time saturation of black hole complexity

Friðrik Freyr Gautason[a,b] **Vyshnav Mohan**[a,c] **and Lárus Thorlacius**[a,c]

[a] *Science Institute, University of Iceland, Dunhaga 3, 107 Reykjavík, Iceland*
[b] *STAG Research centre & Mathematical Sciences, University of Southampton, Highfield, Southampton SO17 1BJ, U.K.*
[c] *Institutionen för fysik och astronomi, Uppsala Universitet, Box 803, SE-751 08 Uppsala, Sweden*

E-mail: ffg1m24@soton.ac.uk, vym1@hi.is, lth@hi.is

Abstract: The holographic complexity of a static spherically symmetric black hole, defined as the volume of an extremal surface, grows linearly with time at late times in general relativity. The growth comes from a region at a constant transverse area inside the black hole and continues forever in the classical theory. In this region the volume complexity of any spherically symmetric black hole in $d + 1$ spacetime dimensions reduces to a geodesic length in an effective two-dimensional JT-gravity theory. The length in JT-gravity has been argued to saturate at very late times via non-perturbative corrections obtained from a random matrix description of the gravity theory. The same argument, applied to our effective JT-gravity description of the volume complexity, leads to complexity saturation at times of exponential order in the Bekenstein-Hawking entropy of a $d + 1$-dimensional black hole. Along the way, we explore a simple toy model for complexity growth, based on a discretisation of Nielsen complexity geometry, that can be analytically shown to exhibit the expected late-time complexity saturation.

Keywords: Black Holes, 2D Gravity, Nonperturbative Effects

ArXiv ePrint: 2502.17179

Contents

1 Introduction **1**

2 A toy model for complexity **3**
2.1 Random walk on a hypercube 4

3 Growth of extremal volume surfaces **7**

4 Complexity = length **8**

5 Emergent JT gravity description **13**
5.1 A late-time JT limit 13
5.2 Emergent JT action 16

6 Saturation of black hole complexity **18**
6.1 Length of geodesics in JT gravity 19
6.2 Late time behavior of black hole complexity 20

7 Discussion **22**

A Examples from asymptotically AdS, dS, and flat spacetime **23**
A.1 (AdS-)Schwarschild black hole 23
A.2 de Sitter-Schwarzschild black hole 25
A.3 Reissner-Nordström black hole 26

1 Introduction

In this paper, we consider the very late time behaviour of the holographic complexity of black holes in $d+1 \geq 2$ spacetime dimensions. Our starting point is the well-known Complexity=Volume (CV) prescription [1, 2] for a static spherically symmetric black hole, where the complexity is defined to be proportional to the extremal volume of spacelike slices that pass through the black hole interior and are anchored at fixed area spherical surfaces outside the black hole.

According to the principle of black hole complementarity [3], a black hole appears to distant observers as a quantum system with a finite number of degrees of freedom that account for the Bekenstein-Hawking entropy of the black hole. The associated quantum dynamics, which must be sufficiently chaotic to scramble quantum information on a relatively short timescale, then provides a holographic dual representation of the spacetime geometry and matter inside the black hole. In particular, the holographic complexity is a geometric feature of the bulk gravity that corresponds to quantum computational complexity in a quantum circuit description of the black hole dynamics (see [4] for a review).

The quantum computational complexity of a chaotic system exhibits universal features that are independent of the exact details of the system. In particular, complexity grows linearly for an extended time for any macroscopic system, following an initial period of scrambling. The growth rate is proportional to the number of degrees of freedom of the system. Moreover, complexity saturates at very late times of the order of exponential of the entropy [5–10]. This ramp-plateau structure is expected to be a universal behaviour of all finite-dimensional chaotic systems including black holes. The volume of extremal surfaces, however, grows forever and never saturates and it is not *a priori* clear that a semiclassical prescription can reproduce the very late time plateau. We will explore this question and show that complexity, defined through the CV prescription, saturates at the expected time scales in any static, spherically symmetric black hole in any number of dimensions.

Our main argument for the saturation of holographic black hole complexity follows from the following observations. Susskind and Stanford [2] noted that the volume of extremal surfaces can be expressed as a geodesic length in an auxiliary two-dimensional metric. Additionally, at late times, the growth of the extremal volume comes almost exclusively from a region inside the black hole where the transverse area remains constant. We refer to the limiting constant area slice at infinite time as the *accumulation surface*. In the spacetime region near the accumulation surface, the auxiliary two-dimensional metric is negatively curved, and since the accumulation surface sits at a constant radial coordinate, it will have a fixed negative curvature in this region. Consequently, we can rephrase the late-time growth of the extremal volume as the growth of geodesic length in a Jackiw-Teitelboim (JT) gravity theory [11, 12] with an AdS_2 length scale derived from the higher-dimensional theory.

The length of geodesics in classical JT gravity was considered in [13] and found to grow linearly for perpetuity at the expected rate. Subsequently, a quantum representation of geodesic length was defined and studied in [14–17] and it was shown that the *quantum* length in fact saturates at very late times. We argue that one can use the quantum description of geodesic length in JT-gravity to arrive at a non-perturbative description of the complexity of a $d+1$-dimensional black hole at late times. This is because quantum corrections to the classical volume are exponentially suppressed by the area of the transverse $(d-1)$-sphere in Planck units. Since the transverse area is macroscopic for the entire extremal volume surface, it would seem that quantum corrections do not play a role at all. However, the strong suppression is eventually compensated by the growing span of the Einstein-Rosen bridge and quantum corrections cannot be neglected at sufficiently late times. The crucial point is that the dominant contribution to the volume increase, that comes from the region near the accumulation surface, is captured by the emergent JT description. On the other hand, the contribution to the extremal volume from regions away from the accumulation surface does not grow with time and furthermore the transverse area is even larger in those regions, leading to even stronger suppression of quantum corrections. Translating the JT-gravity results back to higher dimensions, we find that complexity saturates at times of the order $e^{O(S)}$, where S is the entropy of the higher-dimensional black hole (refer to table 1 below for explicit expressions). Such a time scale is expected from general arguments [18].

The rest of the paper is organized as follows. To provide a simple, intuitive picture of the saturation of quantum computational complexity, we begin in section 2 by considering a toy model that can be viewed as a discretisation of Nielsen complexity geometry [19] as a high-dimensional hypercube. The evolution of the quantum state is modelled by a random walk on the hypercube, where the walker starts from an arbitrarily chosen origin and can advance to a nearest neighbor at each time step. The average graph distance of the walker from the origin will then exhibit the expected behaviour of complexity. After a long period of linear growth, the distance saturates as the walker reaches the "bulk" of the hypercube, where the total distance from the origin is equally likely to increase or decrease with the next step. Section 3 briefly reviews the Complexity=Volume prescription. In section 4, we reduce the volume calculation to a geodesic length calculation in an effective two-dimensional metric, following [2] and in section 5, we show how the emergent two-dimensional metric on the relevant part of the extremal slice reduces to that of JT-gravity at late times. In section 6, we use JT-gravity results to obtain the time scales at which the complexity saturates. We close with a brief discussion in section 7 and some explicit examples are worked out in appendix A.

2 A toy model for complexity

Before embarking on explorations in holographic complexity, which composes the bulk of this paper, we discuss some general features of quantum computational complexity by studying a simplified toy model. Recall that circuit complexity of an operator is a measure of how many 'simple' operations are required to build that target operator from a given reference operator. As such, complexity depends on the precise definition of the 'simple' operations (usually called gate set), the reference, and the tolerance by which we allow the constructed operator to deviate from the target under consideration. Our interest will be in the growth of complexity with time under Hamiltonian evolution of some initial state and in particular its late time behaviour. It turns out, that different detailed definitions of complexity lead to broadly speaking the same behaviour on long time scales. In particular, complexity is expected to grow linearly for a long time, at a rate proportional to the number of degrees of freedom that participate in the quantum dynamics, and then eventually saturate.

Relative complexity of two operators defines a distance on the set of all unitary operators acting on the Hilbert space, which inspired Nielsen to define complexity geometry [19–21] which involves a choice of a metric on the group manifold of all unitary transformations. Complexity is then defined to be the shortest geodesic distance between two points on the manifold as measured by the complexity metric. Once again, different choices of metric will assign different values to the complexity but a broad class of metrics is expected to lead to the generic behaviour of the complexity discussed above.

In [22] Lin introduced a simplified notion of complexity which involves choosing a large but finite subgroup G of the unitary group that has a generating set S. Such a finite group has a natural graph structure called a Cayley graph, where each element $g \in G$ is assigned a vertex and for every $g \in G$ and $s \in S$ there is a (directed) edge between the vertices g and gs. If the generating set S is closed under inversion the graph is undirected. Relative complexity between two group elements is the shortest graph distance between them, i.e. the minimal number of edges that connect the two corresponding vertices in the Cayley graph. Replacing the continuous Nielsen geometry by a discrete Cayley graph can be visualized as picking a particularly large tolerance ϵ where we are not so concerned with constructing precisely the target operator but are content with reaching its approximate neighbourhood (as measured by the inner product).

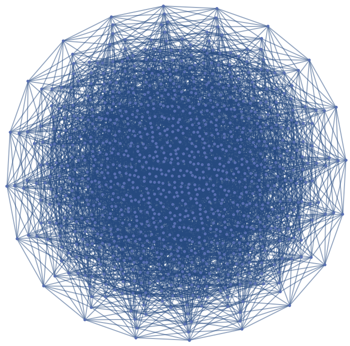

Figure 1. Graph representation of a ten-dimensional cube.

2.1 Random walk on a hypercube

A particularly simple choice of a finite group is $\mathbb{Z}_2^D$ with the generating set

$$S = \{(1,0,0,\cdots),(0,1,0,\cdots),\cdots\}\,. \tag{2.1}$$

The resulting Cayley graph is a high-dimension hypercube where each corner of the cube labels an operator and each edge connected to a given corner represents one of D simple operations in this model. We will model the time evolution by a random walk on the hypercube starting from some reference vertex. We are interested in studying the graph distance between the current location of the walker and its initial position as a proxy for the complexity growth. This is a classic problem that has been studied for instance in [23], which we follow. The position of the walker can be parametrized by a D-dimensional vector where each entry takes the values 0 or 1. For simplicity, we take the reference state and the start point of the random walk to be at the origin $\mathbf{x} = \mathbf{0}$. The random walk we consider is such that the walker takes one step to one of its nearest neighbours or stays put with equal probability $P = 1/(D+1)$. This means that at each time step the position vector $\mathbf{x}$ either stays unchanged or one of its entries is switched from 0 to 1 or vice versa. The graph distance is given by $|\mathbf{x}| = x_1 + x_2 + x_3 + \cdots$.

As explained in [23], in the continuum version of the random walk, each entry in the position vector independently satisfies

$$P[x_i = 1] = \frac{1}{2}\left(1 - \mathrm{e}^{-2\tau/D}\right), \tag{2.2}$$

where τ is the time variable that counts the time steps. This can be understood as follows; for large D the variable x_i can be thought of as counting the times that entry has been changed modulo 2. So it counts the occurrences of the random jump to that entry. Since each occurrence is rare and is independent of the previous ones it follows a Poisson distribution with the expectation $\lambda = \tau/(D+1) \approx \tau/D$. The probability of k occurrences is $\lambda^k \mathrm{e}^{-\lambda}/k!$ and the probability for our variable x_i to change an odd number of times is given by the sum

$$P[x_i = 1] = \sum_{k=0}^{\infty} \frac{\lambda^{2k+1}}{(2k+1)!}\mathrm{e}^{-\lambda} = \mathrm{e}^{-\lambda}\sinh\lambda\,, \tag{2.3}$$

which agrees with (2.2).

The result (2.2) shows that on long time scales the uniform distribution is reached $P[x_i = 1] = 1/2$. That means we are equally likely to find the random walker on any vertex of the cube. In other words the walker has completely forgotten its initial location. For the uniform distribution it is simple to compute the expected distance to the origin and all higher moments. These are defined as

$$\langle x^d \rangle = \frac{1}{2^D} \sum_{x=1}^{D} \binom{D}{x} x^d \,, \tag{2.4}$$

where we use the graph distance (here denoted by simply x) to perform the expectation value. The moments can be computed using the exponential generating function,

$$G_D(y) \equiv \sum_{d=0}^{\infty} \langle x^d \rangle \frac{y^d}{d!} = \frac{1}{2^D} \sum_{x=1}^{D} \binom{D}{x} (\mathrm{e}^y)^x = \left(\frac{1+\mathrm{e}^y}{2} \right)^D \,, \tag{2.5}$$

by taking y-derivatives and setting y to zero at the end. In this way we compute

$$\langle 1 \rangle = 1 \,, \quad \langle x \rangle = \frac{D}{2} \,, \quad \langle x^2 \rangle = \frac{D(D+1)}{4} \,, \quad \langle x^3 \rangle = \frac{D^2(D+3)}{8} \,, \quad \cdots \tag{2.6}$$

and the standard deviation is $\Delta \equiv \sqrt{\langle x^2 \rangle - \langle x \rangle^2} = \sqrt{D}/2$.

Let us now return to the time-dependent problem. Using the result (2.2), we can compute the expected distance as a function of time

$$C(\tau) \equiv \langle x(\tau) \rangle = \frac{D}{2} \left(1 - \mathrm{e}^{-2\tau/D} \right) , \tag{2.7}$$

which saturates at late times to the expected distance $D/2$. This saturation can be estimated to happen when $\langle x(\tau) \rangle$ is one standard deviation from the mean, i.e. when

$$\langle x(\tau_{\text{sat}}) \rangle = \frac{D}{2} - \frac{\sqrt{D}}{2} \,, \tag{2.8}$$

or

$$\tau_{\text{sat}} = \frac{1}{4} D \log D \,. \tag{2.9}$$

After the saturation time is reached, the random walker explores the cube according to the uniform distribution. Randomly it will come back to its original starting position with probability 2^{-D}. The expected time between visiting the same point twice is therefore $\tau_P \sim 2^D$. This serves as the Poncáre recurrence time in our model.

In order to make a connection to holographic complexity, we will take the dimensionality of our hypercube to be of exponential order in the black hole entropy $D = \mathrm{e}^{\alpha S}$ where α is a constant. Since it is mainly the exponential dependence on S that is important, we set $\alpha = 1$ to keep the notation simple. Notice that the function $C(\tau)$ in (2.7) grows linearly at early times,

$$C(\tau) = \tau + \mathcal{O}(\tau^2) \,, \tag{2.10}$$

just like the volume of the Einstein-Rosen bridge does. However, as discussed at the end of section 3, the growth rate of the volume complexity of a black hole is proportional to

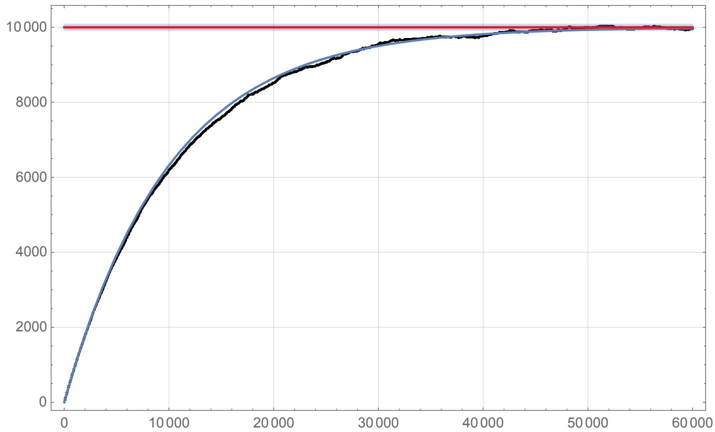

Figure 2. The black curve shows the distance of a simulated random walker on a $D = 20000$ dimensional cube from its starting point — the origin. In blue we show the expected distance (2.7). We also display the saturation value at $D/2$ and shade in the standard deviation.

the black hole entropy S in dimensionless Rindler-like time units. Indeed the choice of the time coordinate has been somewhat arbitrary so far, where each time step represents a step of the random walk. To match with black hole complexity we choose $t = \tau/S$ as our dimensionless time coordinate.[1] Then

$$C(t) \equiv \frac{\mathrm{e}^S}{2}\left(1 - \mathrm{e}^{-2tS\mathrm{e}^{-S}}\right). \tag{2.11}$$

The two important time-scales in these variables are the saturation time and Poincaré recurrence time, given by

$$t_{\mathrm{sat}} = \frac{1}{4}\mathrm{e}^S, \qquad t_P \sim S\, 2^{\mathrm{e}^S}. \tag{2.12}$$

In figure 2 we display a sample simulation of a random walk and show that it follows the expected distance (2.7) quite closely.

Note that the random walker has reached approximately half the maximal graph distance from the origin on the hypercube at the saturation time. From then on the graph distance is equally likely to increase or decrease in a given step. We expect similar behaviour in a more realistic description of quantum complexity, i.e. that saturation occurs well before the complexity reaches its maximal possible value and that complexity equilibrium can be explored by studying a uniform distribution on the Hilbert space. Decreasing complexity has been linked to opaqueness of a black hole horizon [5] and in our simple model such a complexity 'firewall' occurs with probability one-half after the complexity has saturated. This matches recent results in JT gravity [16, 24], where the probability of a firewall is also found to be one-half at late times.

[1] For notational simplicity, we have set another dimensionless constant to one in our definition of the Rindler time.

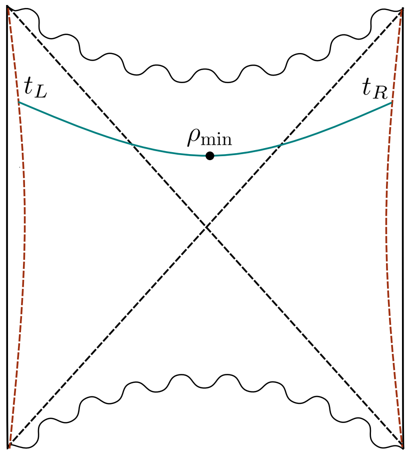

Figure 3. Penrose diagram of an eternal AdS-Schwarzschild black hole in $(d+1)$ dimensions with a spacelike extremal volume surface anchored to fixed area cutoff surfaces at boundary times $t_{R,L}$. The turning point, $\rho = \rho_{\min}$, is in the black hole interior.

3 Growth of extremal volume surfaces

Let us briefly review the Complexity=Volume proposal [1, 2]. Consider a static, spherically symmetric, black hole solution in $d+1$ dimensions, whose metric is given by

$$ds^2 = -f(\rho)\mathrm{d}t^2 + \frac{\mathrm{d}\rho^2}{f(\rho)} + \rho^2 \mathrm{d}\Omega^2_{d-1}\,, \tag{3.1}$$

where $\mathrm{d}\Omega^2_{d-1}$ is the line element of a $d-1$-dimensional unit sphere. The event horizon is located at the outermost radius $\rho = \rho_h$ at which $f(\rho_h) = 0$. Now consider a spherically symmetric codimension-1 surface anchored to a cutoff surface in the asymptotic region (shown in figure 3 for a two-sided AdS-Schwarzschild black hole). We will consider the symmetric case where the surface is anchored at boundary times $t_R = t_L \equiv \tau$. The volume of the surface can be expressed as the following integral,

$$\mathcal{V} = \Omega_{d-1} \int \mathrm{d}\lambda\, \rho^{d-1} \sqrt{-f(\rho)\dot{t}^2 + \dot{\rho}^2/f(\rho)}\,, \tag{3.2}$$

where Ω_{d-1} is the volume of the $d-1$-dimensional unit sphere and $\{t(\lambda), \rho(\lambda)\}$ parametrises the longitudinal coordinates of the surface. The derivatives in (3.2) are with respect to λ. Up to constant multiplicative factors, the holographic volume complexity of the black hole at boundary time τ is obtained by extremizing the volume functional in (3.2) [2],

$$C_V(\tau) = \frac{\mathcal{V}_{\text{ext}}(\tau)}{G_{d+1} L_0}\,. \tag{3.3}$$

Here, L_0 is a characteristic length scale of the black hole and G_{d+1} is Newton's constant in $d+1$ dimensions. In the case of an static black hole in AdS, we choose L_0 to be the AdS curvature scale L while for a Schwarzschild or Reissner-Nordström black hole in asymptotically flat spacetime we would instead use the radial coordinate at the event horizon.

The extremal surface has a turning point at $\rho = \rho_{\min}$ in the interior of the black hole. A straightforward calculation yields the following expression for the growth rate of the complexity (see e.g. [25] and section 4 below),

$$\frac{\mathrm{d}C_V}{\mathrm{d}\tau} = \frac{2\Omega_{d-1}}{G_{d+1}L_0}\sqrt{-f(\rho_{\min})}\rho_{\min}^{d-1}\,. \tag{3.4}$$

At late times, the extremal volume surfaces approach a constant radius slice in the interior of the black hole. We will refer to this limiting surface as the *accumulation surface*. The radial location of the accumulation surface, which we will denote by ρ_a, is given by [2, 25, 26],

$$\frac{\mathrm{d}}{\mathrm{d}\rho}\left(f(\rho)\rho^{2d-2}\right)\Big|_{\rho=\rho_a} = 0\,. \tag{3.5}$$

This gives us a constant late-time growth rate [2, 25],

$$\frac{\mathrm{d}C_V}{\mathrm{d}\tau} = \frac{2\Omega_{d-1}}{G_{d+1}L_0}\sqrt{-f(\rho_a)}\rho_a^{d-1}\,, \tag{3.6}$$

and in classical gravity this growth persists forever. Furthermore, if the characteristic length scale L_0 in the definition of C_V in equation (3.3) is chosen so as to be consistent with the more refined Complexity=Action proposal [27], then the late-time rate of growth of the holographic complexity (in units of Rindler time) of a generic spherically symmetric static black hole is found to be proportional to the number of degrees of freedom carried by the black hole [28],

$$\frac{1}{T}\frac{\mathrm{d}C_V}{\mathrm{d}\tau} \propto S\,, \tag{3.7}$$

where S and T are the black hole entropy and temperature.

4 Complexity = length

The volume problem of the previous section reduces in a natural way to finding an extremal length in an auxiliary two-dimensional spacetime. This way of phrasing the problem, which was already noticed in [2], will be particularly useful when discussing the saturation of complexity. To see this, we perform a spherical reduction of the $d+1$-dimensional metric to two dimensions,

$$\mathrm{d}s_{d+1}^2 = \Phi^{-2}g_{\alpha\beta}\mathrm{d}x^\alpha\mathrm{d}x^\beta + \Phi^{\frac{2}{d-1}}\ell_p^2\mathrm{d}\Omega_{d-1}^2\,, \tag{4.1}$$

where ℓ_p is the Planck length of the higher-dimensional theory, rescaled by a power of Ω_{d-1} to simplify some formulas below,

$$\ell_p^{d-1} \equiv \frac{G_{d+1}}{\Omega_{d-1}}\,. \tag{4.2}$$

The dynamical variables of the reduced theory, i.e. the two-dimensional metric $g_{\alpha\beta}$ and the dilaton field Φ, are assumed to only depend on the two-dimensional coordinates x^α. In (4.1) we have chosen a Weyl frame for the two-dimensional metric so that the volume measured in the $d+1$-dimensional metric is equivalent to a geodesic length measured in the 2-dimensional metric. Indeed, by expressing the black hole background in (3.1) in terms of the two-dimensional variables,

$$-f(\rho)\,\mathrm{d}t^2+\frac{\mathrm{d}\rho^2}{f(\rho)}=\Phi^{-2}g_{\alpha\beta}\mathrm{d}x^\alpha\,\mathrm{d}x^\beta\,,\qquad\qquad \rho^{d-1}=\Phi\,\ell_p^{d-1}\,,\tag{4.3}$$

and inserting into the volume integral (3.2) we obtain

$$\mathcal{V}=\ell_p^{d-1}\Omega_{d-1}\,\ell\,,\tag{4.4}$$

where ℓ is the geodesic length computed using the two-dimensional metric,

$$\ell\equiv\int\mathrm{d}\lambda\sqrt{g_{\alpha\beta}\dot{x}^\alpha\dot{x}^\beta}\,.\tag{4.5}$$

The computation of the holographic volume complexity thus reduces to finding an extremal length in the two-dimensional geometry specified by (4.1),

$$C_V=\frac{\mathcal{V}_{\text{ext}}}{G_{d+1}L_0}=\frac{\ell_{\text{ext}}}{L_0}\,,\tag{4.6}$$

and in this Weyl frame there is no explicit dependence on the dilaton field.

To proceed further, we identify two-dimensional coordinate time with its higher-dimensional counterpart and adopt a static ansatz for the two-dimensional metric and dilaton field,

$$g_{\alpha\beta}\mathrm{d}x^\alpha\mathrm{d}x^\beta=-\xi(r)\,\mathrm{d}t^2+\frac{\mathrm{d}r^2}{\xi(r)}\,,\qquad\qquad \Phi=\Phi(r)\,.\tag{4.7}$$

A static black hole metric of the form (3.1) translates into,

$$\xi(r)=\left(\frac{\rho(r)}{\ell_p}\right)^{2(d-1)}f\big(\rho(r)\big)\,,\qquad \Phi(r)=\left(\frac{\rho(r)}{\ell_p}\right)^{d-1}\,,\tag{4.8}$$

where

$$\frac{\mathrm{d}\rho}{\mathrm{d}r}=\left(\frac{\rho}{\ell_p}\right)^{-2(d-1)}\,.\tag{4.9}$$

We can now follow a standard route to obtain the proper length of a spacelike geodesic (see [25] for the corresponding computation in $d+1$ dimensions before dimensional reduction). The first step is to switch to infalling Eddington-Finkelstein coordinates,

$$\mathrm{d}s^2=-\xi(r)\mathrm{d}v^2+2\mathrm{d}r\mathrm{d}v\qquad\text{where}\qquad \mathrm{d}v=\mathrm{d}t+\frac{1}{\xi(r)}\mathrm{d}r\,,\tag{4.10}$$

and parametrize the spacelike geodesic $x^\mu(\lambda)$ so as to have unit tangent vector everywhere,

$$u^\mu=\dot{x}^\mu\,,\qquad u\cdot u=1\,.\tag{4.11}$$

Since ∂_v is a Killing vector we have a conserved quantity,

$$p\equiv-u_v=\xi(r)\,\dot{v}-\dot{r}\,,\tag{4.12}$$

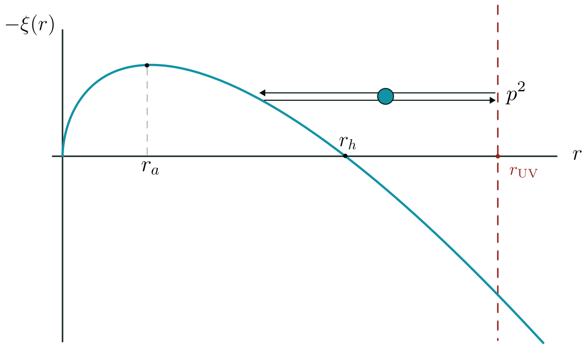

Figure 4. One-dimensional effective potential $V_{\text{eff}} = -\xi(r)$ for an AdS-Schwarzschild black hole.

which can be combined with the tangent vector normalization in (4.11) to obtain

$$\dot{r}^2 - \xi(r) = p^2 \,, \tag{4.13}$$

where the dot denotes a derivative with respect to λ.

At this point it is useful to introduce a simple classical mechanics analogy where equation (4.13) expresses energy conservation for a massive particle moving in one dimension with the affine parameter λ playing the role of time and $r(\lambda)$ the particle location. The effective potential is given by $V_{\text{eff}} = -\xi(r)$ and p^2 is the total energy. Figure 4 shows the effective potential obtained by applying the spherical reduction (4.1) to a higher-dimensional eternal AdS-Schwarzschild black hole (see appendix A for explicit formulas). The effective potential vanishes at the event horizon and has a smooth maximum at $r = r_a$ inside the black hole region. As we will see below, the behaviour of extremal volume surfaces at late boundary times in the original higher-dimensional theory is controlled by the effective potential near its maximum. In particular, $r = r_a$ is the radial location of the accumulation surface.

These features are not unique to AdS-Schwarzschild black holes. In fact, every spherically symmetric static black hole solution in $d \geq 2$ that we have considered gives rise to an effective potential that vanishes at the event horizon and has a positive maximum inside the black hole. Several examples are worked out in appendix A, including AdS-Schwarzschild, Schwarzschild, dS-Schwarzschild, and Reissner-Nordström black holes. In the charged black hole case, the accumulation surface is located in the region between the outer and inner horizons.

Our auxiliary two-dimensional spacetime inherits the Penrose diagram in figure 3 (with the relabelling $\rho_{\text{min}} \to r_{\text{min}}$). We are interested in spacelike geodesics that extend between timelike anchor curves in the left and right quadrants. In the classical mechanics analogy, such a geodesic corresponds to a particle with total energy in the range $0 < p^2 < -\xi(r_a)$ that travels inwards from $r = r_{\text{UV}}$ until it comes to a turning point inside the black hole at $r = r_{\text{min}} > r_a$, where $p^2 = -\xi(r_{\text{min}})$, and then returns to $r = r_{\text{UV}}$. At the turning point we have $u^r = \dot{r} = 0$ but $u^v = \dot{v} \neq 0$ and it follows that the return journey of the particle corresponds to continuing the spacelike geodesic through the black hole interior to emerge on the opposite side of the Penrose diagram.[2] The proper length of the spacelike geodesic is given by the total time it takes the particle to make the return trip from r_{UV} to the turning point and back again, which in turn depends on the particle energy p^2. As the energy approaches the maximum of the effective potential, the particle spends more and more time moving very slowly near its turning point, and in the limit $p^2 \to -\xi(r_a)$ the geodesic length diverges. A particle with energy $p^2 > -\xi(r_a)$ corresponds to a spacelike geodesic that runs into the singularity at $r = 0$ and does not connect the two asymptotic regions.

Using equation (4.13) the geodesic length can be expressed as a radial integral,

$$\ell = \int \mathrm{d}\lambda = 2\int_{r_{\min}}^{r_{\mathrm{UV}}} \frac{\mathrm{d}r}{\sqrt{p^2+\xi(r))}}\,. \tag{4.14}$$

The factor of two reflects the fact that the return leg of the particle trajectory takes the same amount of time as the infall. Placing the anchor curves at a finite radial distance regulates the otherwise divergent integral. The precise value of r_{UV} is not important as we are usually only interested in the derivative of the geodesic length with respect to the boundary time τ. The integral in (4.14) depends on the boundary time via the conserved charge p and also through $r_{\min}$, the location of the turning point, which enters both in the integrand and as the lower limit of integration. The integrand diverges as $r \to r_{\min}$, and so some intermediate steps are in order before taking the τ derivative. The infalling Eddington-Finkelstein time interval along the geodesic, from the turning point to where it intersects the anchor curve, can be written as another radial integral,

$$v_{\mathrm{UV}} - v_{\min} = \int_{r_{\min}}^{r_{\mathrm{UV}}} \mathrm{d}r\, \frac{1}{\xi(r)}\left(1 + \frac{p}{\sqrt{p^2+\xi(r)}}\right)\,, \tag{4.15}$$

where we have used equations (4.12), (4.13) and parametrised the geodesic left-to-right in figure 3 so that $p < 0$. This expression can be combined with (4.14) to obtain

$$\ell + 2\,p\,(v_{\mathrm{UV}} - v_{\min}) = 2\int_{r_{\min}}^{r_{\mathrm{UV}}} \mathrm{d}r\,\frac{1}{\xi(r)}\left(\sqrt{p^2+\xi(r)} + p\right)\,. \tag{4.16}$$

Here the integrand is well defined as $r \to r_{\min}$ and, since we have $p < 0$, the integrand is also well behaved across the horizon at $r = r_h$. Differentiating the terms in (4.16) with respect to τ results in

$$\frac{\mathrm{d}\ell}{\mathrm{d}\tau} + 2p\left(\frac{\mathrm{d}v_{\mathrm{UV}}}{\mathrm{d}\tau} - \frac{\mathrm{d}v_{\min}}{\mathrm{d}\tau}\right) = -\frac{2p}{\xi(r_{\min})}\frac{\mathrm{d}r_{\min}}{\mathrm{d}\tau}\,, \tag{4.17}$$

where we have used (4.15) to cancel the terms that involve a factor of $\frac{\mathrm{d}p}{\mathrm{d}\tau}$. The Eddington-Finkelstein time v is related to Schwarzschild time τ through $v = \tau + r^*$, where $r^* = \int \mathrm{d}r/\xi(r)$, and since the radial position of the anchor curve $r = r_{\mathrm{UV}}$ is independent of τ, it follows that

$$\frac{\mathrm{d}v_{\mathrm{UV}}}{\mathrm{d}\tau} = 1\,. \tag{4.18}$$

[2] The sign of the conserved charge p in (4.12) determines whether the geodesic is parametrised left-to-right or right-to-left in figure 3.

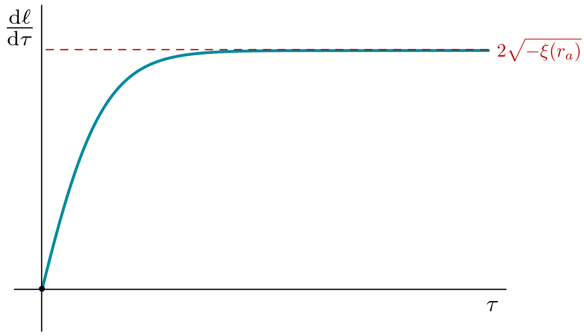

Figure 5. Rate of growth of the proper length of a spacelike geodesic anchored symmetrically in the two asymptotic regions as a function of the boundary anchor time τ. The growth rate increases from zero at $\tau = 0$ until it saturates as the energy of the corresponding classical particle approaches the critical point of the effective potential.

Furthermore, for the geodesics that we consider, the interior Schwarzschild time at the turning point is $\tau_{\min} = 0$ for all τ and we obtain

$$\frac{dv_{\min}}{d\tau} = \frac{dr^*_{\min}}{d\tau} = \frac{1}{\xi(r_{\min})}\frac{dr_{\min}}{d\tau}. \tag{4.19}$$

Inserting (4.18) and (4.19) into (4.17) immediately leads to the following rather compact expression for the rate of growth of the geodesic length,

$$\frac{d\ell}{d\tau} = -2p(\tau), \tag{4.20}$$

in agreement with [25]. The τ dependence of p, which is implicitly determined via (4.14) and (4.15), can only be solved for numerically in general but key features (sketched in figure 5) are easily inferred from the classical mechanics analogy. First of all, at $\tau = 0$ the spacelike geodesic is a straight horizontal line that intersects the horizon at the bifurcation point in the Penrose diagram in figure 3. The corresponding classical particle turns around at $r_{\min} = r_h$ and from the effective potential in figure 4 we read off $p(0) = 0$. Then, as τ is increased from zero, the turning point moves into the black hole interior and the particle energy p^2 is a monotonically growing function of τ. At late boundary times, the energy approaches the local maximum of the effective potential at $r = r_a$. This leads to a constant growth rate for the geodesic length,

$$\frac{d\ell}{d\tau} \to 2\sqrt{-\xi(r_a)}, \tag{4.21}$$

which in turn translates into equation (3.4) for the late-time rate of growth of the volume complexity in the original higher-dimensional variables.

In this section, we have shown how to map the holographic volume complexity of a spherically symmetric black hole in any number of spacetime dimensions onto the problem of determining the proper length of spacelike geodesics in a two-dimensional geometry. In

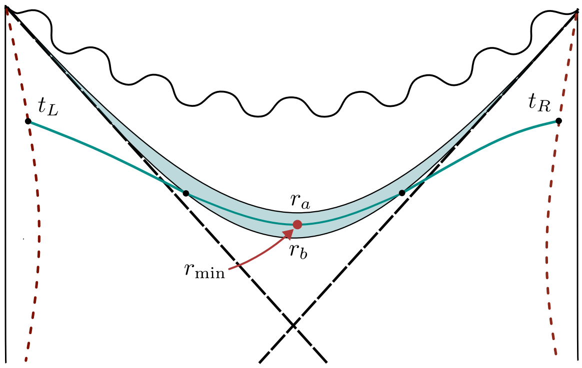

Figure 6. The region shaded in blue is bounded by the accumulation surface $r = r_a$ and another constant radial surface defined by $r = r_b > r_a$ in the interior of the black hole. The parts of the spacelike geodesic that lie outside this region have constant length at late boundary anchor times.

the following section, we will see how the two-dimensional problem simplifies at late times to the calculation of geodesic length in JT gravity, which has been extensively studied in the literature (see e.g. [13–17]).

5 Emergent JT gravity description

In the previous section, we re-expressed holographic volume complexity in terms of the proper length of spacelike geodesics in a two-dimensional dimensional auxiliary spacetime. In this section, we begin with a simple but important observation about the length of these geodesics.

5.1 A late-time JT limit

Consider a fixed radial curve defined by $r = r_b$, with $r_a < r_b < r_h$, in the region of the auxiliary spacetime that corresponds to the interior of the black hole, as in figure 6. At sufficiently late times, our boundary-anchored spacelike geodesic crosses this curve, i.e. $r_a < r_{\rm min} < r_b$. We can then write the length (4.14) of the spacelike geodesic as a sum of two terms coming from 'inside' and 'outside' the $r = r_b$ curve,

$$\begin{aligned}\ell &= 2\int_{r_{\rm min}}^{r_b} \frac{\mathrm{d}r}{\sqrt{\xi - \xi(r_{\rm min})}} + 2\int_{r_b}^{r_{\rm UV}} \frac{\mathrm{d}r}{\sqrt{\xi - \xi(r_{\rm min})}} \\ &\equiv \tilde{\ell} + 2\int_{r_b}^{r_{\rm UV}} \frac{\mathrm{d}r}{\sqrt{\xi - \xi(r_{\rm min})}}\,,\end{aligned} \tag{5.1}$$

where we have defined $\tilde{\ell}$ as the length of the section of the geodesic that is inside $r = r_b$. Taking a derivative with respect to τ, we get

$$\frac{\mathrm{d}\left(\ell - \tilde{\ell}\right)}{\mathrm{d}\tau} = \frac{\mathrm{d}\xi(r_{\rm min})}{\mathrm{d}\tau} \int_{r_b}^{r_{\rm UV}} \frac{\mathrm{d}r}{(\xi - \xi(r_{\rm min}))^{3/2}} \tag{5.2}$$

At late times, the turning point approaches the constant radial location of the accumulation surface so that $\frac{\mathrm{d}\xi(r_{\min})}{\mathrm{d}\tau} \to 0$. Since $r_b > r_a$, the integral in (5.2) remains finite in the limit and this implies that the right hand side vanishes as $r_{\min} \to r_a$. Integrating at late time thus gives

$$\ell(\tau) \approx \tilde{\ell}(\tau) + \ell_0 \,, \tag{5.3}$$

where ℓ_0 is a time independent constant. In other words, the late-time growth of the geodesic length comes from the region near the accumulation surface (shaded in blue in figure 6). This approximation becomes better and better as time passes.

A second observation is that the auxiliary two-dimensional spacetime has negative curvature at the accumulation surface,

$$R\,|_{r=r_a} = -\xi''(r_a) < 0 \,. \tag{5.4}$$

This is immediately apparent from the shape of the effective potential in figure 4. Since we are interested only in the late-time growth rate of the geodesic length, we can restrict our attention to the region near the accumulation surface. Introducing a new radial coordinate η, defined by

$$r = r_a + \eta \,, \tag{5.5}$$

with $\eta \ll r_a$, and expanding in powers of η leads to

$$\xi(r) = \xi(r_a) + \xi'(r_a)\eta + \frac{\xi''(r_a)}{2}\eta^2 + O(\eta^3) \,. \tag{5.6}$$

Since r_a is a critical point ξ, the linear term in the η expansion vanishes. Truncating the expression at the quadratic order, and plugging it back into the metric, leads to

$$\mathrm{d}s^2 = -\left(\xi(r_a) + \frac{\xi''(r_a)}{2}\eta^2\right)\mathrm{d}t^2 + \frac{\mathrm{d}\eta^2}{\left(\xi(r_a) + \frac{\xi''(r_a)}{2}\eta^2\right)} \,. \tag{5.7}$$

The accumulation surface lies inside the horizon and hence $\xi(r_a) < 0$. Therefore, we can identify (5.7) with an AdS_2 black hole metric,

$$\mathrm{d}s^2 = -\left(\frac{\eta^2}{L_2^2} - \mu\right)\mathrm{d}t^2 + \frac{\mathrm{d}\eta^2}{\left(\frac{\eta^2}{L_2^2} - \mu\right)} \,, \tag{5.8}$$

where L_2 is an *emergent* AdS_2 length scale and μ a mass parameter,

$$L_2^2 = \frac{2}{\xi''(r_a)}, \qquad \mu = -\xi(r_a) \,. \tag{5.9}$$

The horizon of this emergent black hole is located at $\eta_h = \sqrt{\mu}L_2$ and its temperature is given by

$$T_2 = \frac{\eta_h}{2\pi L_2^2} \equiv \frac{1}{\beta_2} \,. \tag{5.10}$$

If the $r = r_b$ curve in figure 6 is placed near the accumulation surface, i.e.

$$r_b - r_a \ll r_a \,, \tag{5.11}$$

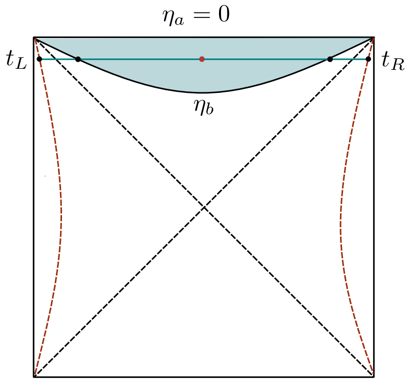

Figure 7. Penrose diagram for the AdS_2 black hole (5.7). The length of the geodesic inside the region enclosed by the $\eta = \eta_b$ and $\eta = 0$ curves (shaded in blue) is denoted by $\tilde{\ell}_{\rm JT}$ in the main text, while the length of the full geodesic anchored to a constant η surface in the asymptotic AdS_2 region is denoted by $\ell_{\rm JT}$.

then the AdS_2 black hole metric (5.8) is valid over the entire spacetime region where the late-time complexity growth takes place.[3]

The Penrose diagram for the AdS_2 black hole is shown in figure 7. The shaded region, between the $\eta = 0$ and $\eta = \eta_b \equiv r_b - r_a$ curves, corresponds to the similarly shaded region in figure 6. The condition (5.11) ensures that the curve $\eta = \eta_b$ lies well inside the horizon of the AdS_2 black hole. We are interested in spacelike geodesics that are symmetrically anchored in the asymptotic AdS_2 region at boundary times $t_L = t_R = \tau$. Such geodesics are straight horizontal curves of constant global time in the AdS_2 Penrose diagram [13] and at sufficiently late boundary times they will intersect the shaded region in figure 7.

The analysis of spacelike geodesics in section 4, including the classical mechanics analogy, can be applied to the emergent AdS_2 metric (5.8). The resulting effective potential takes a particularly simple form,

$$V_{\rm eff}(\eta) = \mu - \frac{\eta^2}{L_2^2}\,, \tag{5.12}$$

with L_2 and μ defined in (5.9). This corresponds to zooming in on the critical point of the effective potential at $r = r_a$ in figure 4 and expanding to quadratic order in $\eta = r - r_a$. At late boundary times, our spacelike geodesics can be divided into a part that passes through the shaded region inside the curve $\eta = \eta_b$ in figure 7 and external parts that attach onto the anchor

[3]The fact that we find an emergent AdS_2 geometry when expanding around the accumulation surface is perhaps not surprising. Any two-dimensional metric with a timelike Killing symmetry can be brought to the form (4.7) and an expansion to quadratic order always leads to a spacetime metric with constant curvature. What is important about the expansion around the accumulation surface is that it leads to a spacetime metric with constant *negative* curvature and that the late-time growth of the volume complexity exclusively comes from the region where this expansion is valid.

curves in the asymptotic AdS_2 regions. Accordingly, the geodesic length consists of two terms,

$$\ell_{\mathrm{JT}}(\tau) = \tilde{\ell}_{\mathrm{JT}}(\tau) + \ell^0_{\mathrm{JT}}\,, \tag{5.13}$$

where the JT subscript indicates that this is in fact the length of a boundary anchored spacelike geodesic in an emergent two-dimensional Jackiw-Teitelboim dilaton gravity theory that we will elaborate on below.

The same line of reasoning that led to (5.3) implies that the outside length ℓ^0_{JT} approaches a time independent constant at late times. Since the emergent AdS_2 metric only applies near the accumulation surface, and the location of the AdS_2 anchor curve differs from the original anchor curve, the full geodesic length at a given late boundary time will differ between (5.3) and (5.13). However, if r_b (or equivalently η_b) is chosen so that the shaded region in figure 6 is well described by the emergent AdS_2 metric, then the *time dependent* part of the geodesic length is the same in both descriptions at late times,

$$\tilde{\ell}(\tau) = \tilde{\ell}_{\mathrm{JT}}(\tau)\,. \tag{5.14}$$

It follows that the late-time volume complexity can be expressed as

$$C_V(\tau) \approx C_0 + \frac{\ell_{\mathrm{JT}}(\tau)}{L_0}\,, \tag{5.15}$$

where C_0 is a time independent constant. The problem of determining the late-time growth of volume complexity of a spherically symmetric black hole in any number of spacetime dimensions thus maps onto the problem of determining the late-time growth of geodesic length in a two-dimensional geometry of constant negative curvature, i.e. two-dimensional locally anti-de Sitter spacetime. This rather general result is one of the main conclusions of this paper. The characteristic length scale in (5.9) of the JT gravity theory in question is inherited from the higher-dimensional, static, spherically symmetric, black hole solution that we start with (see appendix A for some examples). In the following subsection we show how the action of two-dimensional JT gravity arises from spherical reduction in this context.

5.2 Emergent JT action

Applying the spherical reduction ansatz (4.1) to $d+1$-dimensional Einstein gravity yields a two-dimensional dilaton-gravity theory,

$$S = \frac{1}{16\pi}\int \mathrm{d}^2x\sqrt{-g}\left(\Phi R - \frac{d}{d-1}\frac{(\nabla\Phi)^2}{\Phi} + W(\Phi)\right), \tag{5.16}$$

that has been analysed extensively in the past by numerous authors (see e.g. [29] for a review). The form of the dilaton potential $W(\Phi)$ depends on details of the higher-dimensional theory, such as the value of the $d+1$-dimensional cosmological constant for instance. The equations of motion that follow from (5.16) can be expressed as

$$\begin{aligned}
0 &= \nabla_\mu(\Phi^{\frac{d}{d-1}}\nabla_\nu\Phi) - \frac{1}{2}g_{\mu\nu}\nabla\cdot(\Phi^{\frac{d}{d-1}}\nabla\Phi)\,,\\
0 &= \nabla^2\Phi - W(\Phi)\,,\\
0 &= R + \frac{d}{(d-1)}\left(2\frac{\nabla^2\Phi}{\Phi} - \frac{(\nabla\Phi)^2}{\Phi^2}\right) + W'(\Phi)\,.
\end{aligned} \tag{5.17}$$

The first equation can be interpreted as Killing's equation for

$$K^\mu = \Phi^{\frac{d}{d-1}} \epsilon^{\mu\nu} \nabla_\nu \Phi \,, \tag{5.18}$$

and the value of the dilaton is preserved along the Killing vector $\mathcal{L}_K \Phi = 0$ [30]. Our starting point is some static black hole solution of the higher-dimensional theory, which suggests we take K^μ to be timelike. A two-dimensional metric with a time-like Killing vector can always be put into the form of (4.7) with a time-independent dilaton field.

Plugging the ansatz (4.7) into the equations of motion (5.17), we obtain simple ODEs that can be explicitly solved for arbitrary dilaton potential [29],

$$\begin{aligned} \partial_r \Phi &= e^{-Q_0} \Phi^{-\frac{d}{d-1}} \,, \\ \xi(\Phi) &= e^{Q_0} \Phi^{\frac{d}{d-1}} w(\Phi) \,, \end{aligned} \tag{5.19}$$

where the function $w(\Phi)$ is an integral involving the dilaton potential

$$w(\Phi) = w_0 + \int^\Phi d\tilde{\Phi} \; W(\tilde{\Phi}) \; \tilde{\Phi}^{\frac{d}{d-1}} e^{Q_0} \,, \tag{5.20}$$

and Q_0, w_0 are constants of integration whose values are determined by the higher-dimensional black hole solution via (4.8).

The accumulation surface inside the higher-dimensional black hole corresponds to a spacelike curve of constant dilaton field $\Phi = \Phi_a \equiv \Phi(r_a)$ in the two-dimensional spacetime of the dilaton gravity theory. In order to zoom in on the spacetime region near the accumulation surface, we want to expand the dilaton field around Φ_a while also keeping track of the background value of $\nabla^\mu \Phi$. Operationally, this can be achieved by introducing an auxiliary field, which, when evaluated on-shell, reproduces the original action (5.16) and its associated equations of motion. Concretely, we introduce a new vector field λ_μ through the action

$$S = \frac{1}{16\pi} \int \mathrm{d}^2 x \sqrt{-g} \left(\Phi R + W(\Phi) + \frac{d}{(d-1)} (\lambda^2 \Phi - 2\lambda^\mu \nabla_\mu \Phi) \right) . \tag{5.21}$$

Varying this action with respect to Φ and λ_μ, we get the following equations of motion,

$$R + W'(\Phi) + \frac{d}{(d-1)} (\lambda^2 + 2\nabla_\mu \lambda^\mu) = 0 \,, \tag{5.22}$$

$$\lambda^\mu - \frac{\nabla^\mu \Phi}{\Phi} = 0 \,. \tag{5.23}$$

Substituting (5.23) in (5.21) and (5.22), we get back the original action (5.16) and its dilaton field equation in (5.17). Therefore, the theories described by (5.21) and (5.16) are classically equivalent.

Now let us expand the fields Φ and λ_μ around some constant values,

$$\Phi = \Phi_0 + \phi \,, \qquad \lambda_\mu = \Lambda_\mu + \tilde{\lambda}_\mu \,, \tag{5.24}$$

and evaluate the action (5.21) to *linear* order in the fluctuations, dropping total derivatives, to obtain

$$\begin{aligned} S \simeq{}& \frac{1}{16\pi} \int \mathrm{d}^2 x \sqrt{-g} \left(\Phi_0 R + W(\Phi_0) + \frac{d}{(d-1)} \Lambda^2 \Phi_0 \right) \\ &+ \frac{1}{16\pi} \int \mathrm{d}^2 x \sqrt{-g} \left((R + W'(\Phi_0)) \phi + \frac{d}{(d-1)} (\Lambda^2 \phi + 2\Phi_0 \Lambda_\mu \tilde{\lambda}^\mu) \right) . \end{aligned} \tag{5.25}$$

For a static solution, the only non-vanishing component of the field λ^μ is given by

$$\lambda^r = \frac{\partial^r \Phi}{\Phi} = e^{-Q_0} \Phi^{\frac{-2d+1}{d-1}} \xi(\Phi) \equiv \mathrm{U}(\Phi)\,, \tag{5.26}$$

where we have used equations (5.23) and (5.19). Inserting the expansions (5.24) on both sides, we obtain

$$\Lambda^r + \tilde{\lambda}^r = \mathrm{U}(\Phi_0) + U'(\Phi_0)\phi\,, \tag{5.27}$$

which allows us to identify

$$\Lambda^r = \mathrm{U}(\Phi_0) \quad \text{and} \quad \tilde{\lambda}^r = U'(\Phi_0)\phi\,. \tag{5.28}$$

Similarly, we find that the background vector with the index lowered is given by

$$\Lambda_r = e^{-Q_0} \Phi_0^{\frac{-2d+1}{d-1}}\,. \tag{5.29}$$

Substituting these expressions into the action in (5.25) leads to

$$\begin{aligned} S = &\frac{1}{16\pi} \int \mathrm{d}^2 x \sqrt{-g} \left(\Phi_0 R + \frac{d}{(d-1)} \Lambda^2 \Phi_0 + W(\Phi_0) \right) \\ &+ \frac{1}{16\pi} \int \mathrm{d}^2 x \sqrt{-g} \left(R + W'(\Phi_0) + \frac{d}{d-1} (\Lambda^2 + 2\Lambda_r U'(\Phi_0)\Phi_0) \right) \phi + O(\phi^2)\,. \end{aligned} \tag{5.30}$$

Finally, if the background Φ_0 is chosen to have the value of the dilaton at the accumulation surface, $\Phi_0 = \Phi_a$, the second and third term in the first line of (5.30) cancel each other out, and the action reduces to a simple form,

$$S = \frac{\Phi_a}{16\pi} \int \mathrm{d}^2 x \sqrt{-g} R + \frac{1}{16\pi} \int \mathrm{d}^2 x \sqrt{-g} \left(R + \frac{2}{L_2^2} \right) \phi + O(\phi^2)\,. \tag{5.31}$$

As expected, the action (5.31) governing the dynamics near the accumulation surface, takes the form of JT gravity [11, 12] with the same AdS_2 length scale L_2 that we encountered in the JT black hole metric in (5.8). The coefficient in front of the topological term in (5.31) is given by the area of the transverse $d-1$-sphere at the accumulation surface inside the higher-dimensional black hole rather than its horizon area but the two areas only differ by an order-one multiplicative constant that depends on the higher-dimensional black hole under consideration.

6 Saturation of black hole complexity

In section 5, we saw how the calculation of the classical volume of extremal surfaces at late times in various static black hole solutions reduces to calculating a geodesic length in an emergent two-dimensional JT gravity theory. With this equivalence in hand, we can take advantage of an existing quantum mechanical description of JT gravity to arrive at a non-perturbative definition of complexity for static spherically symmetric black holes in any number of spacetime dimensions. Building on earlier work relating the partition function of JT gravity to matrix integrals [31, 32], a quantum mechanical definition of geodesic length in JT gravity was given in [14] and demonstrated to saturate on extremely long time scales. If we adopt the same quantum definition of geodesic length in our emergent JT gravity description of black hole complexity in higher-dimensional gravity, then it immediately follows that holographic volume complexity saturates on extremely long time scales in the higher-dimensional case as well. In our setup, the parameters of the JT gravity theory are inherited from the higher-dimensional black hole under consideration, and thus the two-dimensional results of [14] can be adapted to predict the time-scale on which the higher-dimensional black hole complexity saturates. In the remainder of this section, we summarise the results of [13, 14] that are relevant to the present paper and then translate those results into saturation time-scales for higher-dimensional black hole complexity via the emergent JT description.

6.1 Length of geodesics in JT gravity

In a two-dimensional theory, there is only one spatial dimension. The volume complexity of a JT black hole is therefore given by the length of a spacelike geodesic (divided by a fixed characteristic length scale), with the spacelike geodesic anchored to timelike boundary curves in the asymptotic AdS_2 regions on either side of the two-dimensional Penrose diagram in figure 7. This problem was considered in [13], where the geodesic length was found to grow linearly with the boundary anchor time, giving the expected growth rate for JT black hole complexity,

$$\frac{\mathrm{d}C_V}{\mathrm{d}\tau} \propto S\,T\,. \tag{6.1}$$

Here S and T are the Bekenstein-Hawking entropy and temperature of the $3+1$-dimensional near-extremal Reissner-Nordström black hole, whose near-horizon region is described by the effective JT gravity theory in [13]. At the classical level, this linear growth of complexity continues forever, which is in line with extremal volume calculations in higher-dimensional gravity theories, but in contrast with the expected saturation of quantum complexity at very late times. However, since JT gravity is more amenable to quantisation than its higher-dimensional cousins, one can envisage a quantum representation of geodesic length as in [14]. We will not repeat their detailed arguments here but simply state some of the main results.

The starting point is the action (5.31) for two-dimensional JT gravity (supplemented by the usual boundary terms). Following [33, 34], we impose boundary conditions,

$$\mathrm{d}s^2 = \frac{L_2^2}{\epsilon}\mathrm{d}u^2\,, \quad \phi = \frac{\phi_b}{\epsilon}\,, \tag{6.2}$$

where u is the boundary time. Here ϕ_b has the dimensions of length and characterises the scale of time reparametrisation symmetry breaking. The boundary has a fixed proper length $\frac{\beta\phi_b}{\epsilon}$, where β is the inverse temperature of the black hole.

The length of spacelike geodesics anchored onto the asymptotic boundaries can be *non-perturbativley* defined in JT gravity using its matrix model description [14, 15], via

$$\langle \ell(\tau)\rangle = \int_0^\infty \mathrm{d}E_1\mathrm{d}E_2\,\langle \rho\left(E_1\right)\rho\left(E_2\right)\rangle\, e^{-\frac{\beta}{2}(E_1+E_2)}e^{-i\tau(E_1-E_2)}\mathcal{M}_\Delta\left(E_1,E_2\right)\,, \tag{6.3}$$

where $\rho(E)$ is the density of states. The quantity $\mathcal{M}_\Delta(E_1, E_2)$ is related to the matrix elements of a boundary operator $\mathcal{O}_\Delta$,

$$\mathcal{M}_\Delta(E_1, E_2) = -\lim_{\Delta\to 0} \frac{\partial}{\partial\Delta} \left|\langle E_1|\mathcal{O}_\Delta|E_2\rangle\right|^2 , \tag{6.4}$$

where Δ is the scaling dimension of $\mathcal{O}_\Delta$. Heuristically, this amounts to defining the quantum mechanical length in terms of a two-point correlation function of scaling operators in the boundary dual theory, that are inserted at the boundary anchor time of the geodesic. The classical geodesic length is then reproduced in a semi-classical limit where the correlation function can be evaluated in a geodesic approximation.

Now we can use the fact that JT gravity is dual to a matrix model [31], and that the two-point function of the density of states has a universal form when $E_1 \to E_2$ [32, 35],

$$\langle \rho(E)\rho(E')\rangle = \rho_0(E)\rho_0(E') - \frac{\sin^2\left(\pi\rho_0(\bar{E})\,(E-E')\right)}{\left(\pi\,(E-E')\right)^2} + \rho_0(\bar{E})\delta\left(E-E'\right) , \tag{6.5}$$

where we have defined $2\bar{E} = E + E'$. Here $\rho_0 = \mathrm{e}^{\frac{\Phi_a}{4}} \sinh(2\pi\sqrt{E})$ is the disk contribution to the density of states, with Φ_a the parameter multiplying the topological term in the JT gravity action in (5.31). The second term in the above expression is non-perturbative in $e^{\frac{\Phi_a}{4}}$, and it is usually referred to as the *sine kernel* in the matrix model literature. Plugging in the explicit expressions of $\rho_0(E)$ and $\mathcal{M}_\Delta(E_1, E_2)$, one can evaluate the integral to obtain [14],

$$\langle \ell(\tau)\rangle \approx \begin{cases} C_1\tau + \dots & \tau \ll e^{\frac{\Phi_a}{4}}\phi_b \\ C_0 - \dots & \tau \gg e^{\frac{\Phi_a}{4}}\phi_b \end{cases} \tag{6.6}$$

where

$$\begin{aligned} C_0 &= \frac{e^{\frac{\Phi_a}{4}}\phi_b}{6\pi^2}\left[e^{6\pi^2\phi_b/\beta}\left(1+\frac{16\pi^2\phi_b}{\beta}\right) - e^{-2\pi^2\phi_b/\beta}\right], \\ C_1 &= 2e^{-2\pi^2\phi_b/\beta}\sqrt{\frac{\phi_b}{\pi\beta/2}} + \frac{\mathrm{erf}\left(\sqrt{\frac{2\pi^2\phi_b}{\beta}}\right)}{\pi}\left(1+\frac{4\pi^2\phi_b}{\beta}\right). \end{aligned} \tag{6.7}$$

The linear growth at early times can be traced back to the leading disconnected piece in (6.5), but at very late times, this contribution is cancelled by another contribution that comes from the sine kernel, resulting in the saturation of the length.

6.2 Late time behavior of black hole complexity

The length calculations in [14] were performed in units where ϕ_b is set to 1. To obtain the late-time behaviour of holographic complexity in our formalism, it is necessary to obtain an explicit expression for ϕ_b. Expanding the dilaton solution (5.19) around its value at the accumulation surface, we find that

$$\phi = \frac{(d-1)}{(2d-1)}\frac{\Phi_a\eta}{r_a}. \tag{6.8}$$

The boundary conditions in JT gravity are usually specified in the Poincaré coordinate z, defined via the relation

$$\frac{L_2^2}{z^2} = \frac{\eta^2-\eta_h^2}{L_2^2}. \tag{6.9}$$

	AdS-Schwarzschild	Schwarzschild	Near-Extremal RN
Saturation Time (τ_S)	$\exp\left(2^{\left(\frac{1-d}{d}\right)}S+\cdots\right)\frac{L^2}{\rho_h}$	$\exp\left(\left(\frac{d}{2d-2}\right)^{\frac{d-1}{d-2}}S+\cdots\right)\rho_h$	$\exp\left(S+\cdots\right)\rho_+$
Saturation Value ($\mathcal{C}_0$)	$\exp\left(2^{\left(\frac{1-d}{d}\right)}S+\cdots\right)$	$\exp\left(\left(\frac{d}{2d-2}\right)^{\frac{d-1}{d-2}}S+\cdots\right)$	$\frac{\delta\rho}{\rho_+}\exp\left(S+\cdots\right)$

Table 1. The table lists the saturation time τ_s and the saturation value $\mathcal{C}_0$ for the volume complexity of various $d+1$-dimensional black holes. Here S is the Bekenstein-Hawking entropy of the black hole. The dots correspond to logarithmically subleading terms.

Choosing the cutoff surface to be at $z=\epsilon$, we can use (6.2) to determine the boundary value of the dilaton as follows

$$\phi_b = \frac{(d-1)}{(2d-1)}\frac{\Phi_a L_2^2}{r_a}\,. \tag{6.10}$$

Now we can use (5.15) and (6.6) to obtain the late-time behaviour of holographic complexity

$$C_V(\tau) \approx \frac{\ell_0}{L_0} + \begin{cases} \mathcal{C}_1\tau + \dots & \tau \ll \tau_S \\ \mathcal{C}_0 - \dots & \tau \gg \tau_S \end{cases}. \tag{6.11}$$

The saturation time τ_S can be calculated using (6.10) and we find that

$$\tau_S = e^{\frac{\Phi_a}{4}}\phi_b = \frac{(d-1)}{(2d-1)}\left(\frac{\Phi_a L_2^2}{r_a}\right)e^{\frac{\Phi_a}{4}}\,. \tag{6.12}$$

Finally, we can work out τ_S and $\mathcal{C}_{0,1}$ for different black hole solutions by using the explicit expressions in appendix A (see table 1). To reproduce the classical growth rates in appendix A, we have rescaled the boundary time τ.

For all static spherically symmetric black holes, we find that the complexity saturates at times of exponential order in S, the Bekenstein-Hawking entropy of the higher-dimensional black hole, that is,

$$\tau_S = e^{O(S)}\tau_0\,, \tag{6.13}$$

where τ_0 is some characteristic timescale associated to the black hole. This is precisely the expected behaviour of operator complexity in a chaotic system [18].

The coefficient of S in the exponent of (6.13) depends on the higher-dimensional black hole and its spacetime dimensions (see table 1). Indeed, the relevant higher-dimensional area is that of the transverse two-sphere at the accumulation surface, which is smaller than the horizon area of the black hole by an order-one numerical coefficient that depends on the black hole solution in question. In the case of a near-extremal Reissner-Nordström (RN) black hole, this coefficientis in fact equal to one and complexity saturates at times of the order e^S. As a simple consistency check, we note that the same timescale is obtained if we instead use the usual effective JT gravity description in the near-horizon region of a near-extremal RN black hole to compute τ_S directly.

7 Discussion

In this paper we have shown that the linear growth of volume complexity for any static spherically symmetric black hole at late times can be understood as the linear growth of a geodesic length in an effective AdS_2 geometry. This is true for black holes in dimensions $d \geq 2$ and follows from a dimensional reduction of the extremal volume problem to two dimensions along with a judicious choice of a Weyl frame which transforms it to the calculation of a geodesic.

Since the black hole Hilbert space is expected to be finite dimensional, any quantity (like complexity) that evolves for a long time should eventually saturate. The fact that volume complexity of black holes does not saturate in classical gravity suggests that some quantum gravity effects should take over and lead to the expected saturation. As was discussed in section 6 above, the matrix model description of JT gravity provides an appealing resolution of this issue for the complexity of two-dimensional JT black holes, and by extension for generic spherically symmetric black holes via the universal nature of complexity growth observed in the present paper. Whether such an effect can be modelled directly in higher-dimensional quantum gravity, e.g. via some non-perturbative corrections to the gravitational path integral, remains an open question (see for example [16, 36–39]).

It is intriguing that, even without a detailed understanding of the saturation mechanism in higher-dimensional gravity, we can still make progress by utilising the impressive recent progress for JT gravity. Indeed, we have argued in the case of complexity saturation, that the results for JT gravity can be directly translated to other higher dimensional black holes. The computation of non-perturbative corrections in JT gravity involves the inclusion of certain fixed energy boundary conditions, which can be reinterpreted as a worldsheet boundary ending on a D-brane [31, 32, 40]. We can similarly speculate that D-branes reprise their role in the saturation of higher dimensional holographic complexity. The existence of such non-perturbative structures in the black hole spacetime would alter its interior, as expected by the breakdown of bulk reconstruction of interior operators at the saturation of the complexity bound [41, 42].

We note that the saturation of holographic complexity argued for, both in this paper and in the earlier papers on JT gravity, represents an interesting breakdown of semi-classical gravity through infrared effects. Usually, violations of semi-classical gravity are associated with short distance physics and strong spacetime curvature, but in this problem the accumulation surface, where the bulk of the complexity growth takes place, remains well separated from the black hole singularity and the deviation from (semi-)classical physics is instead due to the enormous volume of the extremal surface at very late times. Another example of the breakdown of semiclassical gravity computations due to infrared effects is seen in the evaporation of a large near-extremal charged black hole [43, 44]. In this case, the corrections that invalidate semi-classical calculations at extremely low temperatures come from Schwarzian modes in the emergent JT gravity description of the near-horizon geometry, i.e. from a region which lies far from the singularity of the black hole.

Acknowledgments

We are grateful to Chethan Krishnan and Watse Sybesma for useful discussions. Research supported in part by the Icelandic Research Fund under grant 228952-053. VM is supported by a doctoral grant from The University of Iceland Science Park. We would also like to thank the Isaac Newton Institute for Mathematical Sciences, Cambridge, for support and hospitality during the programme Black holes: bridges between number theory and holographic quantum information, where work on this project was undertaken. This work was supported by EPSRC grant EP/R014604/1.

A Examples from asymptotically AdS, dS, and flat spacetime

Our general argument in the main text, that the evaluation of holographic volume complexity at late times reduces to a calculation of geodesic length in a two-dimensional JT-gravity theory, applies to all static spherically symmetric black holes in $d+1$-dimensional Einstein gravity, for any $d \geq 2$. In particular, it does not rely on the presence or absence of a cosmological constant in the higher-dimensional spacetime, and it also goes through for charged Reissner-Nordström black holes. In this appendix we work out specific examples in more detail.

A.1 (AdS-)Schwarschild black hole

Consider the line element of an eternal AdS black hole in $d+1$-dimensions,

$$\mathrm{d}s^2 = -f(\rho)\mathrm{d}t^2 + \frac{\mathrm{d}\rho^2}{f(\rho)} + \rho^2 \mathrm{d}\Omega_{d-1}^2 \,, \qquad f(\rho) = 1 + \frac{\rho^2}{L^2} - \frac{16\pi M \ell_p^{d-1}}{(d-1)\rho^{d-2}} \,, \tag{A.1}$$

where we have absorbed Newton's constant into the definition of ℓ_p as in (4.2). The horizon of the black hole ρ_h is related to the black hole mass through the relation

$$\frac{16\pi M \ell_p^{d-1}}{d-1} = \rho_h^{d-2} \left(\frac{\rho_h^2}{L^2} + 1 \right) . \tag{A.2}$$

Here L is the $d+1$-dimensional AdS length scale. The entropy and the temperature of the black hole are given by

$$S = \frac{1}{4} \left(\frac{\rho_h}{\ell_p} \right)^{d-1} , \quad T = \frac{1}{4\pi} \frac{\partial f}{\partial \rho}\bigg|_{\rho=\rho_h} = \frac{1}{4\pi \rho_h} \left(\frac{d}{L^2} \rho_h^2 + (d-2) \right) . \tag{A.3}$$

To obtain the explicit form of the corresponding dilaton potential in (5.16) we start from the Einstein-Hilbert action,

$$I = \frac{1}{16\pi G_{d+1}} \int \mathrm{d}^{d+1}x \sqrt{-g^{(d+1)}} \left(R^{(d+1)} + \frac{d(d-1)}{L^2} \right) . \tag{A.4}$$

Performing a spherical reduction in the Weyl frame defined by (4.1), we end up with a two-dimensional dilaton gravity theory of the form (5.16) with

$$W(\Phi) = \frac{d(d-1)}{L^2} \Phi^{-1} + \frac{(d-1)(d-2)}{\ell_p^2} \Phi^{\frac{(1+d)}{(1-d)}} . \tag{A.5}$$

The two-dimensional metric in (4.8), corresponding to a $d+1$-dimensional AdS-Schwarzschild black hole, takes a simple form when expressed in terms of the dilaton,

$$\xi(r) = \Phi^2 + \frac{\ell_p^2}{L^2} \Phi^{\frac{2d}{(d-1)}} - \frac{16\pi M \ell_p}{(d-1)} \Phi^{\frac{d}{(d-1)}} , \tag{A.6}$$

and the dilaton profile is given by

$$\Phi(r) = \left(\frac{\rho(r)}{\ell_p}\right)^{(d-1)} = \left((2d-1)\frac{r}{\ell_p}\right)^{\frac{(d-1)}{(2d-1)}}, \tag{A.7}$$

where we have integrated (4.9) to obtain the relation between r and ρ.

Holographic complexity of the higher-dimensional AdS-Schwarzschild black hole reduces to a geodesic length in this two-dimensional metric. As explained in section 4, the geodesic computation can be rephrased as a particle scattering off an effective potential $V_{\text{eff}}(r) = -\xi(r)$. Plotting the explicit expression, the potential has a local maximum inside the black hole which corresponds to the radial location of the accumulation surface (see figure 4). At the maximum of the potential, the two-dimensional curvature scalar is negative, $R = -\xi''(r_a) = V''_{\text{eff}}(r_a) < 0$, and it follows that near the accumulation surface the two-dimensional metric reduces to that of a locally AdS_2 spacetime with an emergent AdS_2 length scale that can be obtained from a straightforward analysis of (A.6). To obtain closed-form expressions, we will work in two limits of the metric:

Large AdS black hole ($\rho_h \gg L$). In this limit, the accumulation surface sits at

$$r_a = \frac{1}{(2d-1)}\left(\frac{\rho_a}{\ell_p}\right)^{2d-1}\ell_p\,, \quad \text{with} \quad \rho_a \simeq 2^{-1/d}\rho_h\,. \tag{A.8}$$

Here ρ_a and ρ_h are the radial locations of the accumulation surface and the black hole horizon, respectively, in the higher dimensional black hole coordinates. The late-time rate of growth of the complexity, given by (4.21), reduces to

$$\frac{\mathrm{d}C_V}{\mathrm{d}\tau} \simeq \frac{16\pi M}{(d-1)} \propto ST\,. \tag{A.9}$$

Expanding the two-dimensional metric as in section 5.1, we obtain an AdS_2 black hole with a characteristic length scale L_2 and mass parameter μ, with

$$L_2 = \sqrt{\frac{2}{\xi''(r_a)}} \simeq \frac{1}{d}\left(\frac{\rho_a}{\ell_P}\right)^{d-1} L \qquad \text{and} \qquad \mu \simeq \left(\frac{\ell_p}{L}\right)^2\left(\frac{\rho_a}{\ell_p}\right)^{2d}. \tag{A.10}$$

Up to a d dependent constant, the emergent AdS_2 length scale is given by the Weyl transformation of the higher-dimensional AdS length scale.

Small AdS black hole ($\rho_h \ll L$). In this limit, the higher dimensional black hole reduces to an asymptotically flat Schwarzschild black hole and the accumulation surface is located at

$$r_a = \frac{1}{(2d-1)}\left(\frac{d}{2(d-1)}\right)^{\frac{2d-1}{d-2}}\left(\frac{\rho_h}{\ell_p}\right)^{2d-1}\ell_p\,. \tag{A.11}$$

As before, the volume complexity is proportional to the length of a geodesic in an emergent two-dimensional theory. This time around, since the AdS length L is effectively infinite in the small black hole limit, the characteristic length scale L_0 of the higher-dimensional problem is given by the Schwarzschild radius ρ_h, and equation (4.6) becomes

$$C_V = \frac{\ell}{\rho_h}\,. \tag{A.12}$$

The late-time growth rate turns out to be

$$\frac{\mathrm{d}C_V}{\mathrm{d}\tau} \simeq \sqrt{\frac{d-2}{d}} \left(\frac{d}{2(d-1)}\right)^{\frac{(d-1)}{(d-2)}} \frac{\rho_h^{d-2}}{\ell_P^{d-1}} \propto ST\,. \tag{A.13}$$

With these conventions, the growth rate of the volume complexity (in Rindler units) is once again proportional to the number of degrees of freedom of the black hole.

As in section 5.1, we expand the two-dimensional metric near the accumulation surface. This leads to an AdS_2 black hole metric with an emergent length scale given by

$$L_2 = \frac{2}{d}\sqrt{\frac{d-1}{d-2}} \left(\frac{\rho_h}{\ell_p}\right)^d \ell_p\,, \tag{A.14}$$

which is again equal to the Weyl transform of the characteristic higher dimensional length scale, up to a d dependent constant.

A.2 de Sitter-Schwarzschild black hole

Now consider the $d+1$-dimensional Schwarzschild-de Sitter (SdS) spacetime, whose metric is given by

$$\mathrm{d}s^2 = -f(\rho)\mathrm{d}t^2 + \frac{\mathrm{d}\rho^2}{f(\rho)} + \rho^2 \mathrm{d}\Omega_{d-1}^2\,, \qquad f(\rho) = 1 - \frac{\rho^2}{L^2} - \frac{2\mu}{\rho^{d-2}}\,. \tag{A.15}$$

We choose the mass parameter μ to lie between 0 and μ_N, where

$$\mu_N = \frac{L^{d-2}}{d}\left(\frac{d-2}{d}\right)^{\frac{d-2}{2}}\,, \tag{A.16}$$

corresponds to the Nariai limit. For a mass parameter in this range, there is a black hole horizon at $\rho = \rho_h$, and a cosmological horizon at $\rho = \rho_c > \rho_h$ [45, 46]. The SdS metric (A.15) is a solution of the equations of motion of d+1-dimensional Einstein gravity with positive cosmological constant,

$$I = \frac{1}{16\pi G_{d+1}} \int \mathrm{d}^{d+1}x \sqrt{-g^{(d+1)}} \left[R^{(d+1)} - \frac{d(d-1)}{L^2}\right]\,. \tag{A.17}$$

A spherical reduction using the ansatz (4.1), leads to a two-dimensional theory of the form (5.16) with the dilaton potential

$$W(\Phi) = -\frac{d(d-1)}{L^2}\Phi^{-1} + \frac{(d-1)(d-2)}{\ell_p^2}\Phi^{\frac{1+d}{1-d}}\,. \tag{A.18}$$

The $d+1$-dimensional de Sitter length provides a reference length scale for the volume complexity,

$$C_V = \frac{\ell}{L}\,. \tag{A.19}$$

The geodesic length ℓ is calculated using the following two-dimensional metric,

$$\xi = \Phi^2 - \frac{\ell_p^2}{L^2}\Phi^{\frac{2d}{d-1}} - \frac{2\mu}{\ell_p^{d-2}}\Phi^{\frac{d}{d-1}}\,, \qquad \Phi^{\frac{2d-1}{d-1}} = \frac{(2d-1)r}{\ell_p}\,, \tag{A.20}$$

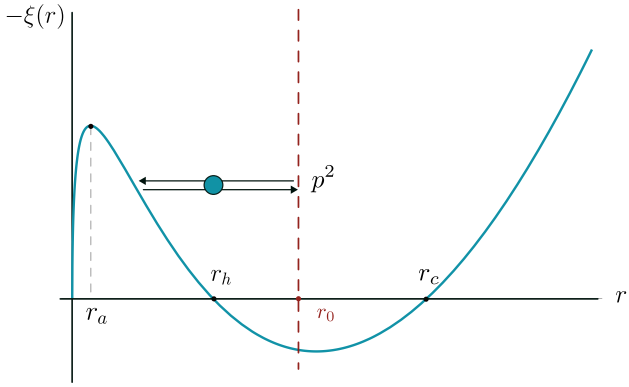

Figure 8. Effective potential for spacelike geodesics in SdS spacetime. Here, $r = r_{h,c}$ corresponds to the location of the black hole and cosmological horizons. The geodesic is symmetrically anchored to cutoff surfaces at $r = r_0$ in the static patches on either side of the two-sided black hole.

where the dilaton profile given by (A.7). Since our goal is to understand the complexity of the black hole, we will consider extremal volume surfaces that pass through the interior of the black hole and are symmetrically anchored at cutoff surfaces in static patches on either side.[4] The effective potential for the corresponding classical particle has a maximum inside the black hole region, as shown in figure 8. The turning point of the geodesic approaches this maximum at late times and in the neighbourhood of the critical point one again finds an AdS_2 black hole metric with an emergent AdS_2 length scale that descends from the higher-dimensional black hole. Since closed-form expressions are unavailable, we do not present the emergent AdS_2 length scale here.

A.3 Reissner-Nordström black hole

The Reissner-Nordström (RN) black hole in $(d+1)$-dimensions has the metric

$$\mathrm{d}s^2 = -f(\rho)\mathrm{d}t^2 + \frac{\mathrm{d}\rho^2}{f(\rho)} + \rho^2\mathrm{d}\Omega_{d-1}^2\,, \qquad f(\rho) = 1 - \frac{16\pi M\ell_p^{d-1}}{(d-1)\rho^{d-2}} + \frac{Q^2\ell_p^{2(d-2)}}{\rho^{2(d-2)}}\,. \tag{A.21}$$

We denote the location of the outer and inner black hole horizons by $\rho = \rho_\pm$, with $\rho_+ > \rho_-$. The metric is a solution to the equations of motion of Einstein-Maxwell theory

$$I = \frac{1}{16\pi G_{d+1}}\int \mathrm{d}^{d+1}x\sqrt{-g^{(d+1)}}\left[R^{(d+1)} - F_{\mu\nu}F^{\mu\nu}\right]\,, \tag{A.22}$$

where we have absorbed the coupling constant $1/4g^2$ into the definition of the electromagnetic field strength. Spherical reduction using (4.1) yields a two-dimensional dilaton gravity theory coupled to a two-dimensional Maxwell field,

$$S_{\text{bulk}} = \frac{1}{16\pi}\int \mathrm{d}^2x\sqrt{-g}\left(\Phi R - \frac{d}{d-1}\frac{(\nabla\Phi)^2}{\Phi} + \frac{(d-1)(d-2)}{\ell_p^2}\Phi^{\frac{1+d}{1-d}} - \Phi^3F^2\right)\,. \tag{A.23}$$

[4] Holographic complexity associated with the cosmological horizon was studied in [47].

To bring the action to the form (5.16), we proceed as in [13] and integrate out the electromagnetic field strength. We find that

$$\nabla_\alpha \left(\Phi^3 F^{\alpha\beta}\right) = 0 \qquad \Longrightarrow \qquad F_{\alpha\beta} = \frac{Q}{\ell_p}\sqrt{\frac{(d-1)(d-2)}{2}}\Phi^{-3}\epsilon_{\alpha\beta}\,, \tag{A.24}$$

where $\epsilon_{\alpha\beta}$ is the 2d Levi-Civita tensor. We have chosen the constants in the above solution so that the solutions of the resulting 2d theory match the dimensional reduction of (A.21). After introducing an appropriate boundary term, following [13], we substitute the on-shell expression for $F_{\alpha\beta}$ to obtain (5.16) with the following dilaton potential

$$W(\Phi) = \frac{(d-1)(d-2)}{\ell_p^2}\Phi^{\frac{1+d}{1-d}} - \frac{Q^2(d-1)(d-2)}{\ell_p^2}\Phi^{-3}. \tag{A.25}$$

Once again, the holographic volume complexity can be expressed in terms of a two-dimensional geodesic length,

$$C_V(\tau) = \frac{\ell(\tau)}{\rho_+}\,, \tag{A.26}$$

where we have chosen the radial location of the outer horizon ρ_+ as the reference length scale. The turning points of the geodesics approach an accumulation surface located between the two horizons, where the corresponding classical particle effective potential reaches a maximum (see figure 9). As in the previous cases, the late-time complexity growth comes from an emergent AdS_2 spacetime near the accumulation surface and can be expressed in terms of geodesic length in a two-dimensional JT gravity theory. This is true for any Reissner-Nordström black hole. In particular, it does not require the black hole to be near extremal. It is, however, interesting to consider the near-extremal limit, on the one hand because it leads to a closed-form expression for the late-time complexity growth, and on the other hand because the effective low-energy gravitational dynamics in the near-horizon region of near-extremal RN black hole is well known to be governed by a two-dimensional JT gravity theory [13, 48, 49]. It is natural to ask whether our JT-gravity prescription for computing volume complexity, when applied to a near-extremal RN black hole, differs from the standard near-horizon JT-gravity theory.

To proceed, let us choose $d = 3$, and work in the near-extremal limit where

$$\rho_+ - \rho_- \equiv \delta\rho \ll \rho_+\,. \tag{A.27}$$

The accumulation surface is determined by the critical point of the effective potential,

$$r_a \simeq \frac{\rho_+^5}{5\ell_p^4} - \left(\frac{\rho_+^4}{\ell_p^4}\right)\frac{\delta\rho}{2}\,. \tag{A.28}$$

Expanding the two-dimensional theory near the accumulation surface as in section 5, we obtain an AdS_2 metric with an emergent length scale,

$$L_2 \simeq \frac{\rho_+^3}{\ell_p^2}, \tag{A.29}$$

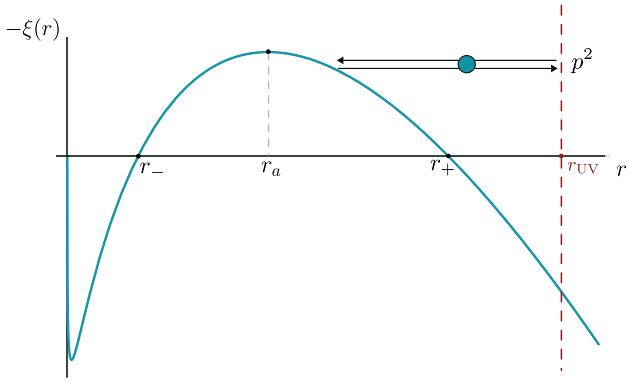

Figure 9. Effective potential for spacelike geodesics in Reissner-Nordström spacetime. Here, $r = r_\pm$ corresponds to the two black hole horizons and the geodesics are symmetrically anchored to cutoff surfaces in asymptotic regions on opposite sides of the black hole in a Penrose diagram.

and the late-time growth rate of complexity is given by

$$\frac{\mathrm{d}C_V}{\mathrm{d}\tau} \simeq \frac{\delta\rho}{\ell_p^2}\,. \tag{A.30}$$

Using

$$T = \frac{\delta\rho}{4\pi\rho_+^2} \quad \text{and} \quad S = \frac{\pi\rho_+^2}{G_4}\,, \tag{A.31}$$

we once again find the growth rate to be proportional to the number of degrees of freedom of the black hole

$$\frac{\mathrm{d}C_V}{\mathrm{d}\tau} \propto ST\,. \tag{A.32}$$

In the near-extremal limit, the location of the accumulation surface in the higher dimensional black hole coordinates is $\rho_a \simeq \rho_+ - \frac{\delta\rho}{2}$. This falls inside the near-horizon region governed by 'standard' JT-gravity theory and, by comparing the Weyl frames and emergent length scales of the two JT gravity theories, one finds that they are indeed equivalent in this limit.

Data Availability Statement. This article has no associated data or the data will not be deposited.

Code Availability Statement. This article has no associated code or the code will not be deposited.

References

[1] L. Susskind, *Computational Complexity and Black Hole Horizons*, *Fortsch. Phys.* **64** (2016) 24 [arXiv:1403.5695] [INSPIRE].

[2] D. Stanford and L. Susskind, *Complexity and Shock Wave Geometries*, *Phys. Rev. D* **90** (2014) 126007 [arXiv:1406.2678] [INSPIRE].

[3] L. Susskind, L. Thorlacius and J. Uglum, *The stretched horizon and black hole complementarity*, *Phys. Rev. D* **48** (1993) 3743 [hep-th/9306069] [INSPIRE].

[4] L. Susskind, *Three Lectures on Complexity and Black Holes*, Springer Cham (2018) [DOI:10.1007/978-3-030-45109-7] [arXiv:1810.11563] [INSPIRE].

[5] L. Susskind, *The Typical-State Paradox: Diagnosing Horizons with Complexity*, *Fortsch. Phys.* **64** (2016) 84 [arXiv:1507.02287] [INSPIRE].

[6] A.R. Brown, L. Susskind and Y. Zhao, *Quantum Complexity and Negative Curvature*, *Phys. Rev. D* **95** (2017) 045010 [arXiv:1608.02612] [INSPIRE].

[7] V. Balasubramanian, M. Decross, A. Kar and O. Parrikar, *Quantum Complexity of Time Evolution with Chaotic Hamiltonians*, *JHEP* **01** (2020) 134 [arXiv:1905.05765] [INSPIRE].

[8] L. Susskind, *Black Holes at Exp-time*, arXiv:2006.01280 [INSPIRE].

[9] V. Balasubramanian et al., *Complexity growth in integrable and chaotic models*, *JHEP* **07** (2021) 011 [arXiv:2101.02209] [INSPIRE].

[10] J. Haferkamp et al., *Linear growth of quantum circuit complexity*, *Nature Phys.* **18** (2022) 528 [arXiv:2106.05305] [INSPIRE].

[11] R. Jackiw, *Lower Dimensional Gravity*, *Nucl. Phys. B* **252** (1985) 343 [INSPIRE].

[12] C. Teitelboim, *Gravitation and Hamiltonian Structure in Two Space-Time Dimensions*, *Phys. Lett. B* **126** (1983) 41 [INSPIRE].

[13] A.R. Brown et al., *Complexity of Jackiw-Teitelboim gravity*, *Phys. Rev. D* **99** (2019) 046016 [arXiv:1810.08741] [INSPIRE].

[14] L.V. Iliesiu, M. Mezei and G. Sárosi, *The volume of the black hole interior at late times*, *JHEP* **07** (2022) 073 [arXiv:2107.06286] [INSPIRE].

[15] M. Alishahiha, S. Banerjee and J. Kames-King, *Complexity via replica trick*, *JHEP* **08** (2022) 181 [arXiv:2205.01150] [INSPIRE].

[16] L.V. Iliesiu et al., *On the non-perturbative bulk Hilbert space of JT gravity*, *JHEP* **10** (2024) 220 [arXiv:2403.08696] [INSPIRE].

[17] D. Stanford and Z. Yang, *Firewalls from wormholes*, arXiv:2208.01625 [INSPIRE].

[18] J.L.F. Barbón, E. Rabinovici, R. Shir and R. Sinha, *On The Evolution Of Operator Complexity Beyond Scrambling*, *JHEP* **10** (2019) 264 [arXiv:1907.05393] [INSPIRE].

[19] M.A. Nielsen, *A geometric approach to quantum circuit lower bounds*, *Quant. Inf. Comput.* **6** (2006) 213 [quant-ph/0502070] [INSPIRE].

[20] M.A. Nielsen, M.R. Dowling, M. Gu and A.C. Doherty, *Quantum Computation as Geometry*, *Science* **311** (2006) 1133 [quant-ph/0603161] [INSPIRE].

[21] M.R. Dowling and M.A. Nielsen, *The geometry of quantum computation*, *Quant. Inf. Comput.* **8** (2008) 0861 [quant-ph/0701004] [INSPIRE].

[22] H.W. Lin, *Cayley graphs and complexity geometry*, *JHEP* **02** (2019) 063 [arXiv:1808.06620] [INSPIRE].

[23] P. Diaconis, R.L. Graham and J.A. Morrison, *Asymptotic analysis of a random walk on a hypercube with many dimensions*, *Random Struct. Algorithm.* **1** (1990) 51.

[24] A. Blommaert, C.-H. Chen and Y. Nomura, *Firewalls at exponentially late times*, *JHEP* **10** (2024) 131 [arXiv:2403.07049] [INSPIRE].

[25] D. Carmi et al., *On the Time Dependence of Holographic Complexity*, *JHEP* **11** (2017) 188 [arXiv:1709.10184] [INSPIRE].

[26] S. Fischetti and D. Marolf, *Complex Entangling Surfaces for AdS and Lifshitz Black Holes?*, *Class. Quant. Grav.* **31** (2014) 214005 [arXiv:1407.2900] [INSPIRE].

[27] A.R. Brown et al., *Holographic Complexity Equals Bulk Action?*, *Phys. Rev. Lett.* **116** (2016) 191301 [arXiv:1509.07876] [INSPIRE].

[28] A.R. Brown et al., *Complexity, action, and black holes*, *Phys. Rev. D* **93** (2016) 086006 [arXiv:1512.04993] [INSPIRE].

[29] D. Grumiller and R. McNees, *Thermodynamics of black holes in two (and higher) dimensions*, *JHEP* **04** (2007) 074 [hep-th/0703230] [INSPIRE].

[30] T. Banks and M. O'Loughlin, *Two-dimensional quantum gravity in Minkowski space*, *Nucl. Phys. B* **362** (1991) 649 [INSPIRE].

[31] P. Saad, S.H. Shenker and D. Stanford, *JT gravity as a matrix integral*, arXiv:1903.11115 [INSPIRE].

[32] P. Saad, *Late Time Correlation Functions, Baby Universes, and ETH in JT Gravity*, arXiv:1910.10311 [INSPIRE].

[33] J. Maldacena, D. Stanford and Z. Yang, *Conformal symmetry and its breaking in two dimensional Nearly Anti-de-Sitter space*, *PTEP* **2016** (2016) 12C104 [arXiv:1606.01857] [INSPIRE].

[34] N. Banerjee, T. Mandal, A. Rudra and M. Saha, *Equivalence of JT gravity and near-extremal black hole dynamics in higher derivative theory*, *JHEP* **01** (2022) 124 [arXiv:2110.04272] [INSPIRE].

[35] M. Mehta, *Random Matrices*, Elsevier/Academic Press (2004) [ISBN: 9780120884094].

[36] V. Balasubramanian, A. Lawrence, J.M. Magan and M. Sasieta, *Microscopic Origin of the Entropy of Black Holes in General Relativity*, *Phys. Rev. X* **14** (2024) 011024 [arXiv:2212.02447] [INSPIRE].

[37] V. Balasubramanian et al., *Factorization of the Hilbert space of eternal black holes in general relativity*, *JHEP* **01** (2025) 046 [arXiv:2410.00091] [INSPIRE].

[38] J. Boruch, L.V. Iliesiu, G. Lin and C. Yan, *How the Hilbert space of two-sided black holes factorises*, *JHEP* **06** (2025) 092 [arXiv:2406.04396] [INSPIRE].

[39] H. Geng and Y. Jiang, *Microscopic origin of the entropy of single-sided black holes*, *JHEP* **04** (2025) 133 [arXiv:2409.12219] [INSPIRE].

[40] A. Blommaert, T.G. Mertens and H. Verschelde, *Eigenbranes in Jackiw-Teitelboim gravity*, *JHEP* **02** (2021) 168 [arXiv:1911.11603] [INSPIRE].

[41] C. Akers et al., *The black hole interior from non-isometric codes and complexity*, *JHEP* **06** (2024) 155 [arXiv:2207.06536] [INSPIRE].

[42] C. Krishnan and V. Mohan, *State-independent black hole interiors from the crossed product*, *JHEP* **05** (2024) 278 [arXiv:2310.05912] [INSPIRE].

[43] A.R. Brown, L.V. Iliesiu, G. Penington and M. Usatyuk, *The evaporation of charged black holes*, arXiv:2411.03447 [INSPIRE].

[44] V. Mohan and L. Thorlacius, *Non-Perturbative Corrections to Charged Black Hole Evaporation*, *JHEP* **04** (2025) 069 [arXiv:2411.13454] [INSPIRE].

[45] V. Balasubramanian, J. de Boer and D. Minic, *Mass, entropy and holography in asymptotically de Sitter spaces*, *Phys. Rev. D* **65** (2002) 123508 [hep-th/0110108] [INSPIRE].

[46] A.M. Ghezelbash and R.B. Mann, *Action, mass and entropy of Schwarzschild-de Sitter black holes and the de Sitter / CFT correspondence*, *JHEP* **01** (2002) 005 [hep-th/0111217] [INSPIRE].

[47] S.E. Aguilar-Gutierrez, S. Baiguera and N. Zenoni, *Holographic complexity of the extended Schwarzschild-de Sitter space*, *JHEP* **05** (2024) 201 [arXiv:2402.01357] [INSPIRE].

[48] J. Navarro-Salas and P. Navarro, *AdS_2/CFT_1 correspondence and near extremal black hole entropy*, *Nucl. Phys. B* **579** (2000) 250 [hep-th/9910076] [INSPIRE].

[49] P. Nayak et al., *On the Dynamics of Near-Extremal Black Holes*, *JHEP* **09** (2018) 048 [arXiv:1802.09547] [INSPIRE].

Paper III

Black shell thermodynamics

Ulf Danielsson, Vyshnav Mohan, and Lárus Thorlacius

JHEP **09** (2025) 167

Published for SISSA by Springer

Received: *July 3, 2025*
Accepted: *August 18, 2025*
Published: *September 19, 2025*

Black shell thermodynamics

Ulf Danielsson,[a] **Vyshnav Mohan**[a,b] **and Lárus Thorlacius**[a,b]

[a] *Institutionen för fysik och astronomi, Uppsala Universitet, Box 803, SE-751 08 Uppsala, Sweden*
[b] *Science Institute, University of Iceland, Dunhaga 3, 107 Reykjavík, Iceland*

E-mail: ulf.danielsson@physics.uu.se, vyshnav.vijay.mohan@gmail.com, lth@hi.is

Abstract: Black shells have been proposed as black hole mimickers, i.e. horizonless ultra-compact objects that replace black holes. In this paper, we assume the existence of black shells and consider their thermodynamic properties, but remain agnostic about their wider role in gravitational physics. An ambient negative cosmological constant is introduced in order to have a well-defined canonical ensemble, leading to a rich phase structure. In particular, the Hawking-Page transition between thermal AdS vacuum and large AdS black holes is split in two, with an intermediate black shell phase, which may play a role in gauge/gravity duality at finite volume. Similarly, for non-vanishing electric charge below a critical value, a black shell phase separates two black hole phases at low and high temperatures. Above the critical charge, there are no phase transitions and large AdS black holes always have the lowest free energy.

Keywords: Black Holes, Black Holes in String Theory, Classical Theories of Gravity

ArXiv ePrint: 2506.02117

Contents

1 **Introduction** 1

2 **Black shells in asymptotically AdS$_{3+1}$ spacetime** 3

3 **Electrically charged black shells** 8

4 **Interpreting the results** 12

1 Introduction

Various ultra-compact horizonless objects, collectively referred to as black hole mimickers, have been proposed as alternatives to black holes. The main motivation is theoretical, to sidestep thorny issues connected with curvature singularities and event horizons in classical and semiclassical gravity. The study of black hole mimickers is also driven by astrophysical observations, to identify potential signatures that can distinguish non-singular compact objects from true black holes. See [1] for a recent status report of the field.

In the present paper, we focus on so-called black shells, which are a particular form of black hole mimickers motivated by string theory [2]. The main assumption of the black shell proposal is that the vacuum is unstable against the formation of a bubble of AdS spacetime, contained within a dynamical shell formed by string theory 0-branes dissolved in a 2-brane. Open strings ending on the branes, carry a large number of degrees of freedom with entropy comparable to that of a black hole of the same mass.

The area of a static black shell is determined by the Israel-Lanczos junction conditions [3, 4], supplemented by the condition that the matter on the shell, separating the exterior geometry from the interior empty AdS spacetime, should have the equation of state of massless radiation [2]. For a Schwarzschild exterior, the shell is located at the so-called Buchdahl radius, 9/8 times the Schwarzschild radius. The matching procedure is easily adapted to static black shells with electric charge and a Reissner-Nordström exterior [2], while spinning black shells have been considered in [5].

If black shells are to succeed as black hole mimickers, replacing black holes in Nature, then they have to be the natural endpoint of gravitational collapse rather than black holes. In this case, when matter is on the verge of collapse into a black hole, a bubble of the true vacuum nucleates and the collapsing matter is converted into a black shell with an area that exceeds that of the would-be event horizon. *A priori*, such a nucleation, which is non-local and involves quantum tunneling on a macroscopic scale, may seem unlikely but the enormous available phase space associated with the large number of degrees of freedom of the black shell makes it more plausible. A similar argument for fuzzball formation is discussed in [6].

Without the right dynamical ingredients, such a black shell is unstable and either expands, which would spell disaster for the universe, or collapses into a black hole. As shown in [7, 8], it is possible to stabilize the shell against small radial perturbations by introducing a mechanism

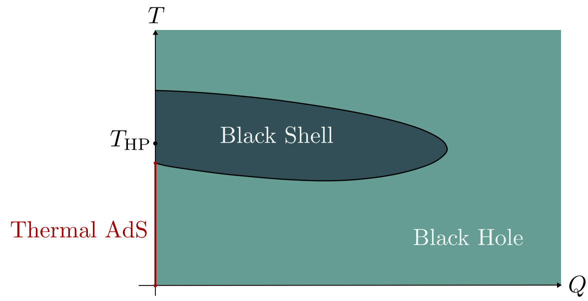

Figure 1. The plot indicates the configuration with the lowest free energy for any given values of temperature and charge. The red line segment along $Q = 0$ corresponds to the thermal AdS solution. $T_{\rm HP}$ denotes the Hawking-Page transition temperature.

that transfers energy between the tension of the 2-brane the radiation carried by the brane. A detailed string-theoretic derivation of such a mechanism is still lacking but see [5] for suggestive speculations.

In the following, we consider the thermodynamics of black shells in the canonical ensemble at fixed temperature and compare to black hole thermodynamics. As long as our goal is restricted to equilibrium thermodynamics, we do not need to address the issue of dynamical black shell formation in gravitational collapse, nor argue for or against black shells replacing black holes. In thermal equilibrium, the existence of black shell configurations, independent of any hypothetical stabilization mechanism, is sufficient in order to compare to black holes.

We work in Euclidean signature throughout and embed the system into an external AdS-spacetime in order to have a well-defined canonical ensemble. A small negative cosmological constant can be viewed as a regulator if the system of interest is a black shell in asymptotically flat spacetime. Alternatively, an asymptotically AdS black shell is a candidate gravitational dual to a thermal state in a strongly coupled boundary theory.

Our results are summarized in figure 1. We find a rich structure, with phase transitions between black holes, black shells and the thermal vacuum in the canonical ensemble. In section 2, we obtain the free energy of an electrically neutral black shell. We find that the well-known Hawking-Page phase transition between thermal AdS spacetime and AdS-Schwarzschild black holes [9] is split in two. There is a phase transition from thermal AdS spacetime to a phase dominated by black shells at a temperature of order the AdS scale but below the Hawking-Page temperature. Then there is a second phase transition from the black-shell phase to a more conventional black-hole phase at a temperature somewhat higher than the Hawking-Page temperature.

The situation is more involved when we allow the black shells to carry electric charge. Under gauge/gravity duality, this amounts to turning on a conserved global U(1) charge in the boundary gauge theory. At fixed non-vanishing charge, below a certain critical value, there are phase transitions from black holes to black shells, and back again to black holes, as the temperature is increased. Above the critical charge, however, black holes dominate the ensemble at all temperatures.

The remainder of the paper is organized as follows. We begin in section 2 with a brief review of the original black shell construction of [2]. We then obtain a closed form expression for the free energy of an electrically neutral black shell that can be compared to the free energy of an AdS-Schwarzschild black hole. In section 3 we repeat the matching procedure for black shells with non-vanishing electric charge and numerically evaluate the resulting free energy as a function of charge and temperature in the canonical ensemble. In section 4 we conclude with a brief discussion of our results and their possible relevance to the suggested role of black shells as black hole mimickers.

2 Black shells in asymptotically AdS_{3+1} spacetime

We begin with a brief review of the black shell construction of [2] with the added twist of a small negative cosmological constant outside the shell in order to have a finite free energy in the canonical ensemble. In this case, the spacetime is asymptotically AdS rather than asymptotically flat as in [2].

Consider a spherically symmetric shell of radius r_0 in 3+1 spacetime dimensions. Inside the shell, the spacetime is taken to be AdS with a characteristic length scale ℓ, while outside the shell, it is described by an AdS-Schwarzschild geometry with mass M and AdS length scale $L \gg \ell$. The metric is then given by:

$$\begin{aligned} \mathrm{d}s_-^2 &= -\left(\frac{r^2}{\ell^2}+1\right)\mathrm{d}t_-^2 + \frac{\mathrm{d}r^2}{\left(\frac{r^2}{\ell^2}+1\right)} + r^2\mathrm{d}\Omega_2^2 \qquad && \text{if } r < r_0 \\ \mathrm{d}s_+^2 &= -\left(\frac{r^2}{L^2}+1-\frac{2M}{r}\right)\mathrm{d}t_+^2 + \frac{\mathrm{d}r^2}{\left(\frac{r^2}{L^2}+1-\frac{2M}{r}\right)} + r^2\mathrm{d}\Omega_2^2 \qquad && \text{if } r > r_0 \end{aligned} \tag{2.1}$$

We work in units where Newton's constant G_N is set to 1 and denote the time coordinates outside and inside the shell by t_+ and t_-, respectively. We use the area of the two-transverse sphere to label the radial position, via $A = 4\pi r^2$, both outside and inside the shell. The solution with Minkowski space inside the shell, along with its thermodynamics, was studied in [10].

The parameters of the metric are constrained by the usual junction conditions [3, 4, 11]:

- The induced metric is continuous across the shell

$$h_{ij}^+ = h_{ij}^- \,. \tag{2.2}$$

- The discontinuity in the extrinsic curvature is related to the stress-energy tensor on the shell:

$$K_{ij}^+ - K_{ij}^- = -8\pi\left(S_{ij} - \frac{1}{2}h_{ij}h^{kl}S_{kl}\right) . \tag{2.3}$$

Using the definition of the induced metric,

$$h_{ij} = g_{kl}\frac{\partial X^k}{\partial\sigma^i}\frac{\partial X^l}{\partial\sigma^j} \,, \tag{2.4}$$

and identifying the time coordinate σ^0 on the shell with the exterior AdS-Schwarzschild time t_+, the first junction condition relates the time coordinates across the shell,

$$\frac{\mathrm{d}t_-}{\mathrm{d}t_+} = \sqrt{\frac{\frac{r_0^2}{L^2} + 1 - \frac{2M}{r_0}}{\frac{r_0^2}{\ell^2} + 1}} \,. \tag{2.5}$$

To proceed further, we take the stress-energy tensor on the shell to be that of a perfect fluid at rest,

$$S_{ij} = (\rho + p) u_i u_j + p h_{ij} \,, \tag{2.6}$$

where ρ and p are, respectively, the energy density and pressure of the fluid, and the components of the fluid 3-velocity,

$$u^{t_+} = \frac{1}{\sqrt{\frac{r_0^2}{L^2} + 1 - \frac{2M}{r_0}}} \,, \qquad u^\phi = u^\theta = 0 \,, \tag{2.7}$$

satisfy $u \cdot u = -1$. This gives us

$$S_{tt} = \rho \left(\frac{r_0^2}{L^2} + 1 - \frac{2m}{r_0} \right) , \quad S_{\theta\theta} = p\, r_0^2 \,, \quad S_{\phi\phi} = p\, r_0^2 \sin^2\theta \,, \quad h^{kl} S_{kl} = -\rho + 2p \,. \tag{2.8}$$

The second junction condition (2.3) relates the shell pressure and energy density. For a metric of the form

$$\mathrm{d}s^2 = N^2(r)\mathrm{d}r^2 + h_{ij}\mathrm{d}x^i\mathrm{d}x^j \,, \tag{2.9}$$

the extrinsic curvature K_{ij} of a constant r surface is given by $\frac{1}{2N}\frac{\partial h_{ij}}{\partial r}$. This gives us

$$K^+_{tt} = -\left(\frac{m}{r_0^2} + \frac{r_0}{L^2} \right) \sqrt{\frac{r_0^2}{L^2} + 1 - \frac{2m}{r_0}} \,, \qquad K^+_{\theta\theta} = r_0 \sqrt{\frac{r_0^2}{L^2} + 1 - \frac{2m}{r_0}} \,, \tag{2.10}$$

$$K^-_{tt} = -\frac{r_0}{\ell^2} \left(\frac{\frac{r_0^2}{L^2} + 1 - \frac{2m}{r_0}}{\sqrt{\frac{r_0^2}{\ell^2} + 1}} \right) , \qquad K^-_{\theta\theta} = r_0 \sqrt{\frac{r_0^2}{\ell^2} + 1} \,. \tag{2.11}$$

We now plug these expressions into the junction condition (2.3), and solve for the energy density and pressure,

$$\rho = \frac{1}{4\pi r_0} \left(\sqrt{\frac{r_0^2}{\ell^2} + 1} - \sqrt{\frac{r_0^2}{L^2} + 1 - \frac{2M}{r_0}} \right) , \tag{2.12}$$

$$p = \frac{1}{8\pi r_0} \left(\frac{\frac{2r_0^2}{L^2} + 1 - \frac{M}{r_0}}{\sqrt{\frac{r_0^2}{L^2} + 1 - \frac{2M}{r_0}}} - \frac{1 + \frac{2r_0^2}{\ell^2}}{\sqrt{\frac{r_0^2}{\ell^2} + 1}} \right) . \tag{2.13}$$

Formula (2.12) for the energy density can be rearranged as follows,

$$4\pi r_0^2 \rho - r_0 \left(\sqrt{\frac{r_0^2}{\ell^2} + 1} - \sqrt{1 + \frac{r_0^2}{L^2}} \right) = r_0 \left(\sqrt{\frac{r_0^2}{L^2} + 1} - \sqrt{\frac{r_0^2}{L^2} + 1 - \frac{2M}{r_0}} \right) . \tag{2.14}$$

The terms on the left hand side can be interpreted as the energy of the shell and a negative energy of the AdS bubble inside the shell. These contributions add up to the total energy of the AdS-Schwarzschild geometry (with respect to empty AdS spacetime) on the right,

$$E = r_0 \left(\sqrt{\frac{r_0^2}{L^2} + 1} - \sqrt{\frac{r_0^2}{L^2} + 1 - \frac{2M}{r_0}} \right) . \tag{2.15}$$

The total energy of the shell configuration includes gravitational self-interaction and satisfies the relation,

$$M = E\sqrt{\frac{r_0^2}{L^2} + 1} - \frac{E^2}{2r_0} , \tag{2.16}$$

from which it is easily checked that $0 < E < M$ for any $M > 0$.

The energy density of a black shell of energy E and radius r_0 is then

$$\rho_b \equiv \frac{E}{4\pi r_0^2} = \frac{1}{4\pi r_0} \left(\sqrt{\frac{r_0^2}{L^2} + 1} - \sqrt{\frac{r_0^2}{L^2} + 1 - \frac{2M}{r_0}} \right) . \tag{2.17}$$

For a dynamical shell of radius r, the surface energy density $\rho_b(r)$ combines with a surface pressure $p_b(r)$ in a shell stress-energy tensor of the form (2.6). The relation

$$p_b = -\rho_b - \frac{r}{2} \frac{d\rho_b}{dr} \bigg|_{r=r_0} \tag{2.18}$$

follows from the conservation of the stress-energy tensor on the shell. Substituting the expression (2.17) for ρ_b then leads to the following expression for the surface pressure,

$$p_b = \frac{1}{8\pi r_0} \left(\frac{\frac{2r_0^2}{L^2} + 1 - \frac{M}{r_0}}{\sqrt{\frac{r_0^2}{L^2} + 1 - \frac{2M}{r_0}}} - \frac{1 + \frac{2r_0^2}{L^2}}{\sqrt{1 + \frac{r_0^2}{L^2}}} \right) . \tag{2.19}$$

Furthermore, if we take the equation of state on the shell to be that of radiation,

$$\rho_b = 2p_b \, , \tag{2.20}$$

then we find that the radius of the shell is given by the simple expression

$$M = \frac{4r_0}{9} \left(\frac{1 + \frac{3r_0^2}{2L^2}}{1 + \frac{r_0^2}{L^2}} \right) \tag{2.21}$$

When $L \gg r_0$, we reproduce the Buchdahl radius in [2]. When $L \ll r$, we find that $r_0 = \frac{3}{2}M$.

We note that the radiation equation of state in (2.20) is not derived from first principles, but it is motivated by string theory, by viewing the shell as a collection of D0-particles dissolved in a spherical D2-brane, with a gas of massless open strings ending on the D-branes [2]. Having dynamical matter on the shell is crucial to its stability against small perturbations and also provides a mechanism for exchanging energy with a thermal environment.

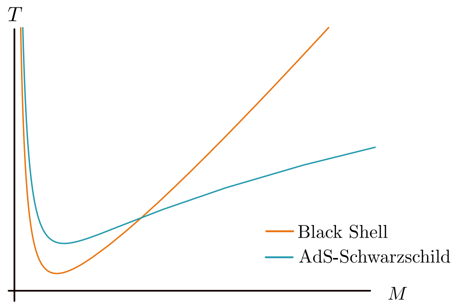

Figure 2. The temperature of black holes and black shells versus their mass.

We are interested in the thermodynamics of these black shell configurations. Let us start by calculating the temperature of the system. The gas of open strings on the shell is not in free fall and accordingly it will equilibrate at the local Unruh temperature [2, 12]. If a is the proper acceleration of an observer sitting at a constant r_0 surface, the corresponding local Unruh temperature is given by

$$T_U = \frac{a}{2\pi} = \frac{1}{2\pi r_0^2} \frac{M + \frac{r_0^3}{L^2}}{\sqrt{\frac{r_0^2}{L^2} + 1 - \frac{2M}{r_0}}} \,. \tag{2.22}$$

Stripping off the redshift factor, we obtain the following shell temperature

$$T_S = \frac{1}{2\pi r_0^2} \left(M + \frac{r_0^3}{L^2} \right) , \tag{2.23}$$

shown in figure 2, where we have included the Hawking temperature of an AdS-Schwarzschild black hole of the same mass, for comparison. We note that in both cases there is a minimum temperature, of order the AdS length scale, that separates two branches, i.e. small and large black objects. Small black holes and small black shells have negative specific heat while their large counterparts have positive specific heat and can therefore be thermodynamically stable. In remainder of this section, we investigate the question of thermodynamic stability by evaluating and comparing the free energy of black holes and black holes at fixed temperature.

The entropy can be obtained via the thermodynamic relation

$$\frac{\mathrm{d}S}{\mathrm{d}M} = \frac{1}{T} \,. \tag{2.24}$$

For an AdS-Schwarzschild black hole we have

$$T_{\mathrm{BH}} = \frac{1}{4\pi r_h} \left(1 + \frac{3r_h^2}{L^2} \right) , \qquad M_{\mathrm{BH}} = \frac{r_h}{2} \left(\frac{r_h^2}{L^2} + 1 \right) , \tag{2.25}$$

which gives expected result,

$$S_{\mathrm{BH}} = \int_0^{r_h} \mathrm{d}r \, \frac{1}{T_{\mathrm{BH}}} \frac{\mathrm{d}M_{\mathrm{BH}}}{\mathrm{d}r} = \pi r_h^2 \,. \tag{2.26}$$

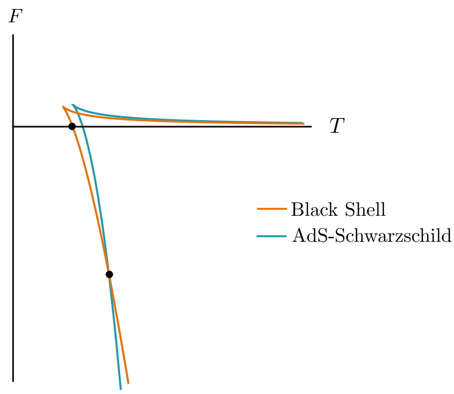

Figure 3. Free energies of black holes and black shells as functions of temperature. Thermal AdS spacetime has zero free energy and therefore corresponds to the horizontal axis. The two first order phase transitions are marked by black dots.

For a black shell, we instead use (2.21) and (2.23) for the mass and temperature, respectively, and obtain

$$S = \frac{2}{3}\pi L^2 \left(3\log\left(L^2 + r_0^2\right) - 2\log\left(L^3 + \frac{3Lr_0^2}{4}\right)\right). \tag{2.27}$$

When $L \gg r$, the leading contribution to the entropy is the standard area term

$$S \simeq \pi r_0^2 + O\left(\frac{r_0^4}{L^2}\right). \tag{2.28}$$

In [2], the large entropy of a string-theoretic black shell configuration is attributed to brane/anti-brane pairs supporting a gas of massless open strings but, so far, a detailed enumeration of black shell microstates is lacking.

The black shell free energy is then given by the following expression,

$$\begin{aligned} F &= M - T_S S\,, \\ &= \frac{2r\left(2L^2 + 3r_0^2\right)}{9\left(L^2 + r_0^2\right)} - \frac{15L^2r_0^2 + 4L^4 + 9r_0^4}{27r^3 + 27L^2r_0}\left[3\log\left(L^2 + r_0^2\right) - 2\log\left(L^3 + \frac{3Lr_0^2}{4}\right)\right]. \end{aligned} \tag{2.29}$$

In figure 3, we plot the free energy as a function of temperature, and for comparison, we also include the free energy of an AdS-Schwarzschild black hole, which is given by

$$F_{\mathrm{BH}} = \frac{r_h}{4}\left(1 - \frac{r_h^2}{L^2}\right). \tag{2.30}$$

The plot reveals interesting phase structure. In the absence of black shells the canonical ensemble is dominated by thermal AdS spacetime (with $F = 0$) at low temperature and undergoes the well-known Hawking-Page transition to a phase dominated by large black holes at a temperature of order the AdS length scale. If the black shell solutions considered here are indeed allowed configurations in the thermal ensamble then the Hawking-Page transition to black holes is preempted by a first-order transition to a black-shell phase at a temperature below the Hawking-Page temperature (but still of order the AdS scale). The system then has another first-order phase transition to a large black hole phase at a temperature higher than the usual Hawking-Page temperature. The two phase transitions are indicated by black dots in figure 3.

The existence of black shells has immediate implications for holographic duality at finite volume in that there is a range of temperatures for which the gravitational dual description of a thermal state is given by a black shell rather than a black hole. This curious fact merits further study but it does not appear to require any major revision of existing results. This is because most applications of gauge/gravity duality to strongly coupled quantum critical systems involve taking a planar limit on the gravitational side of the duality, for which planar AdS black holes still dominate the ensemble.

3 Electrically charged black shells

It is straightforward to generalize our considerations to black shells carrying electric charge. As in the previous section, we will denote the radius of the shell by r_0. Inside the shell, the spacetime is AdS with a length scale ℓ, while outside the shell, we have an AdS-RN black hole with AdS length scale $L \gg \ell$. This gives us the metric:

$$\begin{aligned} \mathrm{d}s_-^2 &= -\left(\frac{r^2}{\ell^2}+1\right)\mathrm{d}t_-^2 + \frac{\mathrm{d}r^2}{\left(\frac{r^2}{\ell^2}+1\right)} + r^2\mathrm{d}\Omega_2^2 && \text{when } r < r_0 \\ \mathrm{d}s_+^2 &= -f(r)\mathrm{d}t_+^2 + \frac{\mathrm{d}r^2}{f(r)} + r^2\mathrm{d}\Omega_2^2 && \text{when } r < r_0 \end{aligned} \tag{3.1}$$

where

$$f(r) = \frac{r^2}{L^2} + 1 - \frac{2M}{r} + \frac{Q^2}{r^2}\,. \tag{3.2}$$

Using the junction conditions (2.2) and (2.3), we find that

$$\rho = \frac{1}{4\pi r_0}\left(\sqrt{\frac{r_0^2}{\ell^2}+1} - \sqrt{\frac{r_0^2}{L^2}+1-\frac{2M}{r_0}+\frac{Q^2}{r^2}}\right), \tag{3.3}$$

and

$$p = \frac{1}{8\pi r_0}\left(\frac{\frac{2r_0^2}{L^2}+1-\frac{M}{r_0}}{\sqrt{\frac{r_0^2}{L^2}+1-\frac{2M}{r_0}+\frac{Q^2}{r^2}}} - \frac{1+\frac{2r_0^2}{\ell^2}}{\sqrt{\frac{r_0^2}{\ell^2}+1}}\right). \tag{3.4}$$

Once again, we can rewrite the junction condition involving ρ as in (2.14). This gives us the following expression for the total energy,

$$E = r_0\sqrt{1+\frac{r_0^2}{L^2}} - r_0\sqrt{\frac{r_0^2}{L^2}+1-\frac{2M}{r_0}+\frac{Q^2}{r^2}} \equiv 4\pi r_0^2\rho_b\,. \tag{3.5}$$

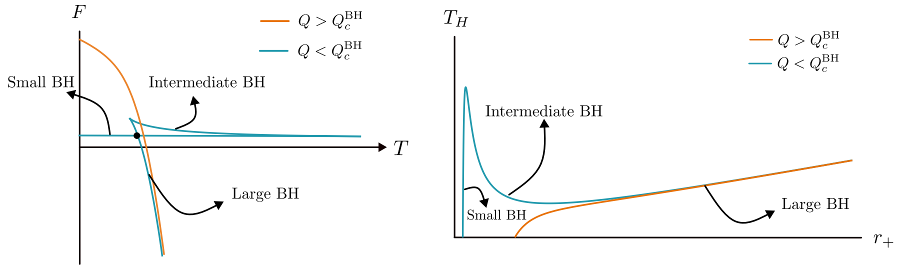

Figure 4. *(Left)* Free energy of a charged black hole as a function of temperature for two different values of the charge. *(Right)* Temperature of the black hole as a function of the event horizon radius for the same charge values. In both plots, three branches of black holes are visible below the critical charge $Q < Q_c^{\mathrm{BH}}$.

Using the conservation equation (2.18), we find that the pressure on the shell is given by

$$p_b = \frac{1}{8\pi r_0}\left(\frac{\frac{2r_0^2}{L^2}+1-\frac{M}{r_0}}{\sqrt{\frac{r_0^2}{L^2}+1-\frac{2M}{r_0}+\frac{Q^2}{r^2}}} - \frac{1+\frac{2r_0^2}{L^2}}{\sqrt{1+\frac{r_0^2}{L^2}}}\right). \tag{3.6}$$

As before, we impose a radiation equation of state $\rho_b = 2p_b$ on the shell. Then the shell radius is related to the mass M via the relation

$$M = \frac{1}{9}\frac{(3r_0^2+2L^2)}{(r_0^2+L^2)}\left(r_0 + \sqrt{r_0^2 + \frac{3Q^2}{L^2}\left(r_0^2+L^2\right)}\right) + \frac{Q^2}{3r_0}, \tag{3.7}$$

giving a family of charged black shell solutions that reduce to the uncharged case, considered above, in the $Q \to 0$ limit.

Before computing the free energy of the black shell, it is instructive to study the black hole case first. Working in the fixed charge ensemble, we find that

$$F_{\mathrm{BH}} = -\frac{r_+^3}{4L^2} + \frac{3Q^2}{4r_+} + \frac{r_+}{4}, \qquad T_{\mathrm{BH}} = \frac{1}{4\pi r_+}\left(\frac{3r_+^2}{L^2} - \frac{Q^2}{r_+^2} + 1\right). \tag{3.8}$$

Let us first examine the behaviour of the black hole temperature T_{BH}. Figure 4 plots the temperature as a function of r_+ for two different charge values. The blue curve corresponds to a charge below a critical value, denoted by Q_c^{BH}. For a range of temperatures, a line of constant T will intersect the plot at three different values of r_+. These branches correspond to small, intermediate, and large black holes. For black hole charge above the critical value, $Q > Q_c^{\mathrm{BH}}$, only a single branch remains. For $Q \gg Q_c^{\mathrm{BH}}$, this branch corresponds to the large black hole solutions.

Next, let us look at the free energy of the black hole as a function of temperature. When $Q < Q_c^{\mathrm{BH}}$, we find classic swallowtail behaviour. Each segment of the swallowtail corresponds to the branches we identified in the temperature plot (see figure 4). Only small black holes exist at low temperature. As we increase T, we find a range of temperatures where all three

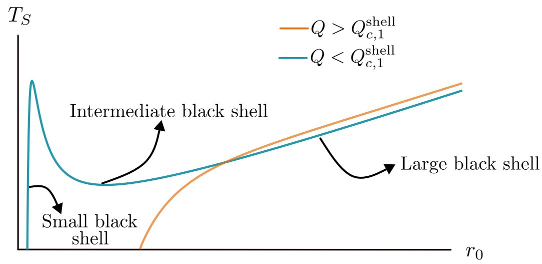

Figure 5. Temperature of a black shell as function of its radius. When $Q < Q_{c,1}^{\text{shell}}$, three branches appear, corresponding to small, intermediate, and large black shells. When $Q > Q_{c,1}^{\text{shell}}$, the branches disappear.

black hole branches coexist. Inside this range there is a critical temperature where a first-order phase transition (indicated by a black dot in figure 4) occurs from the low-temperature small black hole phase to a high-temperature large black hole phase. When $Q > Q_c^{\text{BH}}$, there is no phase transition as there is only a single branch.

The value of the critical charge Q_c^{BH} is easily determined by requiring that the local maximum and local minimum of T_{BH} merge at a single value of r_+, giving

$$Q_c^{\text{BH}} = \frac{L}{6}\,. \tag{3.9}$$

Now, we turn our attention to the charged black shell configuration and compute its temperature and free energy. The proper acceleration in the rest frame of the shell surface at $r = r_0$ gives the shell temperature,

$$T_S = \frac{1}{2\pi r_0^2}\left(M + \frac{r_0^3}{L^2} - \frac{Q^2}{r_0}\right)\,. \tag{3.10}$$

As in the black hole case, there is a critical value of the charge, $Q = Q_{c,1}^{\text{shell}}$, below which there are three branches which we refer to as small, intermediate, and large black shells (see figure 5). Above the critical charge, $Q > Q_{c,1}^{\text{shell}}$, there is only a single branch. We find that $Q_{c,1}^{\text{shell}}$ is always larger than the corresponding black hole critical charge, Q_c^{BH}.

Since we work in a fixed charge ensemble, the first law, $\mathrm{d}M = T\mathrm{d}S + \mu \mathrm{d}Q$, reduces to (2.24). This allows us to find S as a function of r_0. We can also compute the free energy using the relation $F = M - TS$. Unfortunately, closed-form expressions are not available for these quantities, but they are easily evaluated numerically. In figure 6 we plot the resulting free energy as a function of the shell temperature for various values of the charge. In each case, the free energy of a black hole with the same charge is included for comparison.

Let us analyze these plots in some detail. First of all, in the limit of zero temperature, black holes and black shells have the same free energy and can therefore coexist. This holds for any non-vanishing value of the charge. The zero temperature limit corresponds to the extremal limit of the charged black hole. By comparing free energies at finite temperature, we uncover a rich phase structure that depends on the value of the electric charge carried by the compact object.

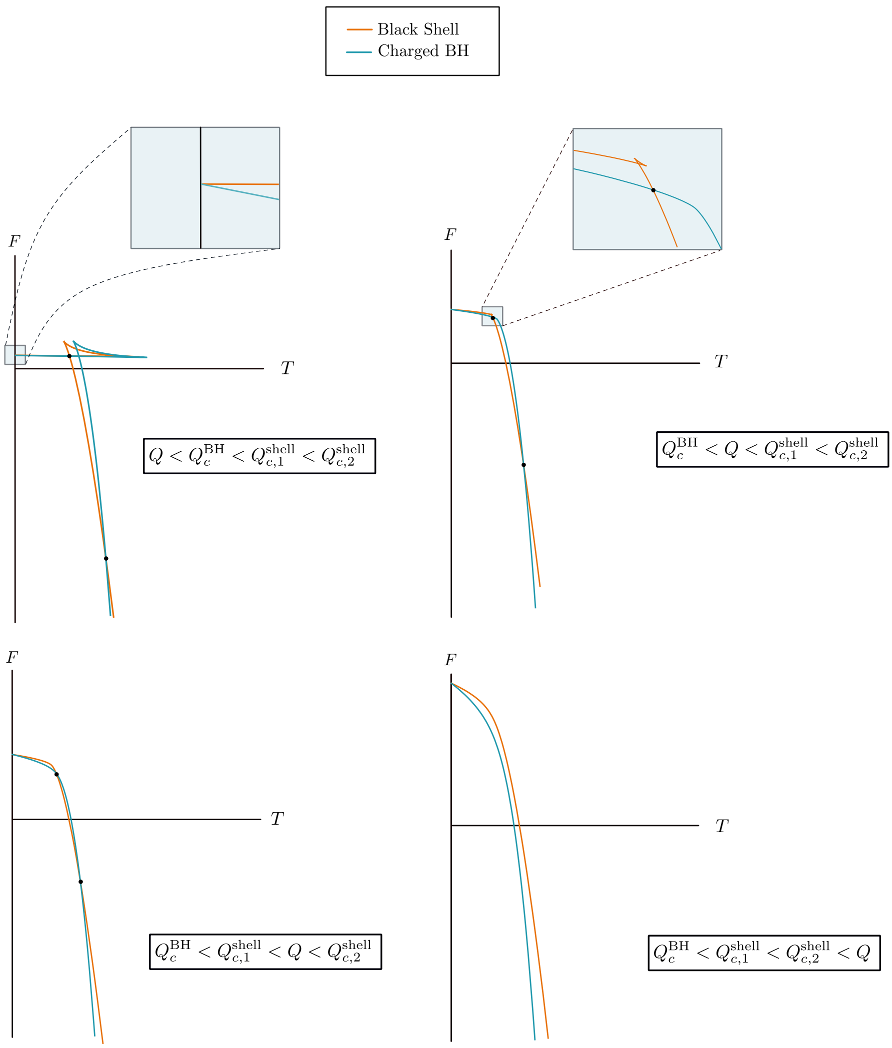

Figure 6. Comparison of free energies of black shells and black holes at various charges. First-order phase transitions are indicated by black dots.

At small charge, $Q < Q_c^{\mathrm{BH}} < Q_{c,1}^{\mathrm{shell}}$, the free energies of black shells and black holes both display swallowtail behaviour, where each segment corresponds to the small, intermediate or large branch of black shells and black holes, respectively. At low temperature, the black hole free energy is lower than that of black shells, making small black holes thermodynamically favored in this temperature regime. As we increase the temperature we reach a critical point where the system undergoes a first order phase transition to a phase dominated by large black shells. This phase persists until we reach a second critical temperature, where there is another first order phase transition to a large black hole phase. For all temperatures above this point, large black holes dominate with the lowest free energy.

Next, let us consider a low-to-intermediate charge case, where $Q_c^{\mathrm{BH}} < Q < Q_{c,1}^{\mathrm{shell}}$. We observe the same phase transition structure as in the previous case. The only difference is that the black hole free energy no longer exhibits swallowtail behaviour.

Finally, we consider the case where the charge is above both critical values, $Q_c^{\mathrm{BH}} < Q_{c,1}^{\mathrm{shell}} < Q$ and the swallowtail structure in the black shell free energy plot has also disappeared. In this regime, a new scale emerges, which we denote by $Q_{c,2}^{\mathrm{shell}}$. For $Q_c^{\mathrm{BH}} < Q_c^{\mathrm{shell}} < Q < Q_{c,2}^{\mathrm{shell}}$, the same phase transition structure persists. However, when $Q > Q_{c,2}^{\mathrm{shell}}$, the phase transitions disappear and black holes always have the lowest free energy. The only temperature at which black holes and black shells can co-exist in this regime is at the extremal limit of the black hole.

4 Interpreting the results

Black shells have been proposed as black hole mimickers that replace black holes. An important motivation is to provide a resolution to the black hole information paradox. For that to work, black shells have to be overwhelmingly favored over black holes as the endpoint of gravitational collapse of matter.[1] We do not address this crucial dynamical question here, but our results on the equilibrium thermodynamics of black shells versus black holes can be viewed as indirect evidence for black shells being favored in a certain range of parameters.

For the purposes of this paper, we have assumed the possible coexistence of black shells and black holes, and investigated thermodynamical transitions between the two types of objects. We have uncovered a rather rich structure in the phase diagram. For instance, as illustrated in figure 1, we find that the Hawking-Page transition between the thermal AdS vacuum and neutral AdS-Schwarzschild black holes is split across a black shell phase. For non-vanishing charge, below a certain critical value, the phase transition between small and large black holes is similarly split, revealing an intermediate black shell phase.

If we want to say something about the information paradox, the most interesting black holes are those with negative specific heat, which evaporate in the absence of a heat bath and potentially lead to a paradox. In figure 7 we highlight in purple the region where black holes have negative specific heat. In the same diagram, we also indicate in yellow the values of M and Q for which the entropy of a black shell is higher than for the corresponding black hole. According to the black shell proposal any black hole that threatens to form in this region, would instead transit into a black shell of the same mass due to its higher entropy. We observe that all AdS-Schwarzschild black holes with negative specific heat are inside the

[1]Strictly speaking, the issue of information loss persists as a formal theoretical problem as long as the probability to form a true black hole in gravitational collapse is non-vanishing.

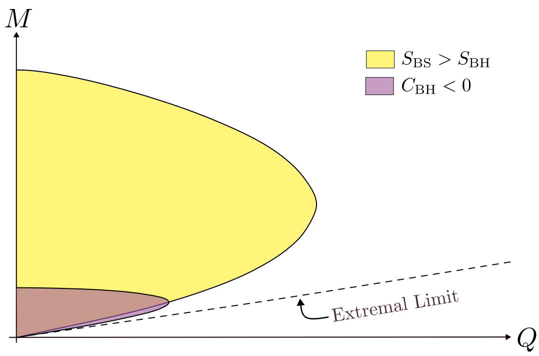

Figure 7. The region shaded in yellow corresponds to the values of M and Q for which the black shell entropy is greater than the black hole entropy at a given mass. The purple region indicates where black holes have negative specific heat C_{BH}.

yellow region The same is true for most charged black holes with negative specific heat as well. Still, there is a narrow strip of purple outside of the yellow region in figure 7, that contains charged black holes with a negative specific heat where the black hole entropy is higher than the one of a black shell. However, in view of the weak gravity conjecture, such charged black holes are expected to discharge themselves through emission of particles with more charge than mass. This brings the system into the yellow region in figure 7, where, according to the black shell proposal, the black hole can safely nucleate into a non-singular black shell before continuing to evaporate.

Our results on black shell thermodynamics thus appear to be consistent with the black shell proposal of [2] but they do not offer any direct insight into the key dynamical questions concerning the production and stability of black shells. Gaining a better theoretical handle on quantum tunneling into high-entropy final states is an important goal, with implications for a wide range of theoretical problems, and not limited to the area of black hole mimickers.

More specific to black shells, is the issue of their stability against small radial perturbations. While the considerations in [7, 8] are suggestive, a top-down derivation from string theory of a mechanism to support their stability would settle the matter. Subject to this caveat, black shells appear to be valid solutions of string theory and as such they feature in any thermodynamic ensembles involving gravity. Regardless of whether they can serve as black hole mimickers, we find our results on black shell thermodynamics intriguing.

Acknowledgments

We would like to thank Diego Hidalgo for useful discussions. This work was supported in part by the Icelandic Research Fund under grant 228952-053. VM is supported by a doctoral grant from The University of Iceland Science Park. Support from Kungliga Vetenskapssamhället i Uppsala and Kungliga Fysiografiska sällskapet i Lund is also acknowledged.

Data Availability Statement. This article has no associated data or the data will not be deposited.

Code Availability Statement. This article has no associated code or the code will not be deposited.

References

[1] C. Bambi et al., *Black hole mimickers: from theory to observation*, arXiv:2505.09014 [INSPIRE].

[2] U.H. Danielsson, G. Dibitetto and S. Giri, *Black holes as bubbles of AdS*, *JHEP* **10** (2017) 171 [arXiv:1705.10172] [INSPIRE].

[3] K. Lanczos, *Flächenhafte Verteilung der Materie in der Einsteinschen Gravitationstheorie*, *Annalen Phys.* **379** (1924) 518 [INSPIRE].

[4] W. Israel, *Singular hypersurfaces and thin shells in general relativity*, *Nuovo Cim. B* **44S10** (1966) 1 [*Erratum ibid.* **48** (1967) 463] [INSPIRE].

[5] U. Danielsson and S. Giri, *Reexamining the stability of rotating horizonless black shells mimicking Kerr black holes*, *Phys. Rev. D* **104** (2021) 124086 [arXiv:2110.10542] [INSPIRE].

[6] S.D. Mathur and M. Mehta, *The Fuzzball Paradigm*, arXiv:2412.09495 [INSPIRE].

[7] U. Danielsson, L. Lehner and F. Pretorius, *Dynamics and observational signatures of shell-like black hole mimickers*, *Phys. Rev. D* **104** (2021) 124011 [arXiv:2109.09814] [INSPIRE].

[8] S. Giri, U. Danielsson, L. Lehner and F. Pretorius, *Exploring black hole mimickers: Electromagnetic and gravitational signatures of AdS black shells*, *Phys. Rev. D* **111** (2025) 024007 [arXiv:2405.08062] [INSPIRE].

[9] S.W. Hawking and D.N. Page, *Thermodynamics of Black Holes in anti-De Sitter Space*, *Commun. Math. Phys.* **87** (1983) 577 [INSPIRE].

[10] O. Henriksson et al., *Higgs phases at non-zero density from holography*, *JHEP* **08** (2023) 186 [arXiv:2212.07364] [INSPIRE].

[11] N. Sen, *Über die Grenzbedingungen des Schwerefeldes an Unstetigkeitsflächen*, *Annalen Phys.* **378** (1924) 365 [INSPIRE].

[12] M. Saravani, N. Afshordi and R.B. Mann, *Empty black holes, firewalls, and the origin of Bekenstein-Hawking entropy*, *Int. J. Mod. Phys. D* **23** (2015) 1443007 [arXiv:1212.4176] [INSPIRE].

Paper IV

Spacetime from Operator Algebras

Vyshnav Mohan, and Lárus Thorlacius

arXiv:2606.10924 [hep-th]

Spacetime from Operator Algebras

Vyshnav Mohan and Lárus Thorlacius

Science Institute, University of Iceland
Dunhaga 3, 107 Reykjavík, Iceland.

vyshnav.vijay.mohan@gmail.com, lth@hi.is

Abstract

Under suitable assumptions, geometric objects such as the spacetime metric and curvature tensor can be reconstructed from the algebra of operators of quantized matter fields in the limit of vanishing Newton's constant. In this framework, the full non-linear Einstein equations can be expressed in the language of operator algebras, extending Jacobson's derivation without invoking the area law for Bekenstein-Hawking entropy. These assumptions can then be used as a criterion for determining whether the semiclassical limit of a given quantum theory admits an emergent gravitational description. Going in the other direction, the discrete spectrum of a holographic theory at finite N can be modelled by adding non-perturbative corrections to semiclassical operator algebras. The type III von Neumann algebra that arises in the vanishing Newton's constant limit can be enlarged by adjoining its modular Hamiltonian. A random matrix theory completion of this enlarged algebra, followed by ensemble averaging, results in a type I von Neumann algebra whose minimal projectors approximate those of the underlying microstates. In the case of an eternal black hole, the dimension of the type I algebra equals the Bekenstein-Hawking entropy with universal logarithmic corrections. The complexity of probe operators in the boundary theory provides a diagnostic of the validity of the corresponding bulk semiclassical effective field theory.

Contents

1 Introduction **2**

2 Emergence of Gravity in the Semiclassical Limit **6**

2.1 Construction of a Length Function 7

2.2 Curvature from Local Flows 9

2.3 Einstein's Equations from Locally Stationary States 14

3 Type I Algebras from Random Matrix Theory Corrections **17**

3.1 Microstates from a Boundary Dual 18

3.2 Crossed Product and the Construction of a type I_d Algebra 20

3.3 Complexity as a Probe of the Emergent Geometry 29

4 Discussion **31**

A Basic Definitions and von Neumann Algebras **32**

B Construction of the Poincaré Algebra **35**

1 Introduction

A profound realization of the past few decades is that gravity may be an emergent phenomenon arising from non-gravitational degrees of freedom [1–5] (see [6] for a more comprehensive list of references). From this perspective, the technical difficulties associated with the canonical quantization of gravity can be avoided. The AdS/CFT correspondence [7–9] provides a concrete realization of this idea, in which a theory of gravity emerges in the semiclassical limit of a non-gravitational quantum field theory. This naturally raises a fundamental question: what is the appropriate language for understanding the emergence of gravity?

An important clue comes from the reconstruction theorem of Connes [10, 11]. Let M be a compact, oriented Riemannian spin manifold. Connes' reconstruction theorem states that such a manifold can be recovered from the commutative spectral triple

$$(C^\infty(M), \mathcal{H}, \mathcal{D}) , \tag{1.1}$$

where $C^\infty(M)$ is the algebra of smooth complex-valued functions on M, $\mathcal{H} = L^2(M,S)$ is the Hilbert space of square-integrable sections of the spinor bundle $S \to M$, and $\mathcal{D}$ is the self-adjoint Dirac operator associated with the Levi-Civita connection. The algebra $C^\infty(M)$ acts on $\mathcal{H}$ by pointwise multiplication, and under suitable regularity conditions [10], the spectrum of the algebra recovers the underlying topological space, while the metric is reconstructed via Connes' distance formula. This reformulation of geometry follows a standard mathematical strategy where one replaces a complicated geometric object with the vector space of functions defined on it, and then uses linear algebra to study its properties (see [12] for further examples). In physics, this idea of reconstructing the geometry from its spectral properties is often referred to as the problem of "hearing the shape of a drum" [13].

When the goal is to understand the emergence of gravity from an underlying quantum theory, a natural extension of Connes' strategy is to study the algebra of operators acting on the Hilbert space of the theory itself. One would then like spacetime geometry and gravitational dynamics to emerge from this algebraic structure in an appropriate semiclassical limit. An indication that this is the correct framework comes from the $G_N \to 0$ limit of AdS/CFT, which corresponds to sending both g_s and α'/L^2_{AdS} to zero. When a holographic dual exists, the corresponding boundary limit is given by $N, \lambda \to \infty$, where λ is the 't Hooft coupling. In this regime, the bulk theory reduces to free fields propagating on a fixed background geometry. Remarkably, geometric structures such as Killing horizons can already be seen to emerge purely from the operator algebra of the quantized matter fields [14–16], bolstering the intuition that operator algebras provide an appropriate framework for understanding the emergence of spacetime geometry.

In Section 2, we extend these results by showing that the operator algebra of the quantized matter fields encodes *all* the local geometric information of the spacetime, not just that of the Killing horizons. In particular, we consider the $G_N \to 0$ limit, where the bulk description consists of free fields on some $D = d+1$-dimensional fixed curved manifold. For simplicity, we restrict the matter sector to a free massive scalar field. Such a description naturally arise in large N holographic theories, for example in the bulk dual of $\mathcal{N} = 4$ super Yang-Mills theory [14, 15, 17]. Then, we show that the geometric data of the spacetime, such as the metric and curvature tensors, can be systematically extracted from the triple

$$(\mathcal{A}, \mathcal{H}, |\omega\rangle) , \tag{1.2}$$

where $\mathcal{A}$ is the operator algebra of the quantized scalar field, $\mathcal{H}$ is the Hilbert space on which these operators act, and $|\omega\rangle$ is some preferred 'vacuum' vector in this Hilbert space, provided the following conditions are satisfied:

(1) $|\omega\rangle$ satisfies the Hadamard condition.

(2) The algebra $\mathcal{A}$ contains a family of subalgebras $\mathcal{W}_j$ which satisfy certain conditions that we will specify in Section 2. We refer to these as *local Rindler algebras*.

(3) The correlation functions of quantized scalar field in $|\omega\rangle$ has a well-defined large mass limit.

Precise definitions are given in Section 2, but it is useful to briefly consider the physical content of these assumptions. Taken together, the two conditions (1)-(2) provide an operator algebraic realization of the equivalence principle, while condition (3) implements a semiclassical limit. The equivalence principle is not merely the statement that locally flat coordinates exist, since *any* Lorentzian manifold admits such coordinate patches by definition. Rather, the crucial requirement is that one can pass to a local inertial frame in which non-gravitational physics reduces to special relativity up to tidal corrections. The Hadamard condition ensures that the short-distance behaviour of the scalar two-point function is universally governed by the flat space singularity structure. Local Rindler algebras are obtained by restricting the scalar field to Rindler wedges within local patches of the manifold. We then require that each such algebra can be approximated by an exact Rindler algebra. In Section 2, we show that this assumption can be used to identify the approximate local Poincaré generators of the spacetime. In this sense, the matter fields "see" a flat spacetime in the neighbourhood of every point.

Although we arrive at the conditions (1)-(3) by working with a scalar field living on a pre-existing geometry, the crucial point is that the conditions themselves are purely algebraic and do not require geometric input. This opens the door to the inverse problem. Given an abstract algebraic triple $(\mathcal{A}, \mathcal{H}, |\omega\rangle)$ arising as an appropriate semiclassical limit of some quantum theory, one can ask directly whether the conditions (1)-(3) are satisfied in the operator algebra, without assuming any background geometry. If they are, a spacetime geometry can be systematically reconstructed from the algebraic data alone.

It remains unclear, however, whether the emergent geometry satisfies Einstein's field equations. In Section 2, we show that upon including perturbative G_N corrections around the $G_N \to 0$ limit, additional assumptions guarantee the validity of the Einstein equations. In particular, we show that if, for every local Rindler wedge algebra $\mathcal{W}_j$, there exists a state ω_j, which we refer to as a *locally stationary state*, then the emergent geometry satisfies the full nonlinear Einstein equations sourced by the matter fields. There is a simple way to understand this condition. Jacobson showed how the Einstein equations can be derived from a local equilibrium condition imposed on the local Rindler horizons of the theory [1]. In the operator-algebraic approach, the existence of locally stationary states ω_j plays the role of this local equilibrium. There is, however, a crucial difference between Jacobson's argument and our result. Jacobson's derivation relies on the Bekenstein-Hawking entropy formula. In our approach this input is replaced by the existence of locally stationary states and their semiclassical coherent excitations, providing a novel perspective on the quantum origins of the Einstein equations.

To summarize, the emergence of gravity can be reformulated in terms of an operator algebra, and associated Hilbert space, satisfying conditions (1)-(3), together with the existence of the locally stationary states ω_j. This characterization is independent of the spacetime dimension and applies to spacetimes with arbitrary asymptotics.

In most cases, however, the full quantum theory of gravity is not known, and a more useful question is whether one can instead work within the semiclassical theory and incorporate non-perturbative quantum gravity effects to model features of the full theory.[1] In Section 3, we show that operator algebras provide a natural setting to incorporate these effects. To make concrete statements, we use holography. In particular, we study an eternal AdS black hole dual to a thermofield double state. The $G_N \to 0$ limit corresponds to the $N, \lambda \to \infty$ limit of the boundary theory. In this large N limit, only single-trace operators survive, and the algebra of bulk scalar fields is dual to the algebra generated by these operators. It turns out that the algebra associated with a single boundary CFT is a type III von Neumann algebra [14, 15, 18]. This algebra is pathological in the sense that it admits neither density matrices nor a trace.

Including $1/N^2$ perturbative corrections around the $N \to \infty$ limit modifies the algebra to a type II_∞ algebra [17], allowing one to define a trace and density matrices. However, it still does not contain pure states. To access, for example, the microstates of the theory and count them, we need pure states. These states are only available in an algebra of type I. Unfortunately, there is no canonical way to obtain a type I algebra from a type III or type II algebra. This is not surprising, since there is no a priori reason for the semiclassical limit of a theory to encode information about the full quantum Hilbert space.

In Section 3.2, we show that there is nevertheless a natural way to obtain an *approximate* type I algebra starting from the type II_∞ algebra. A convenient way to systematically incorporate non-perturbative quantum gravity corrections is to treat the large N perturbative quantum gravity limit as an effective random matrix theory (RMT) [19, 20]. Operationally, this amounts to replacing the density of states in the spectral decomposition of the elements of the type II_∞

[1] In this paper, we use the term *semiclassical theory* to refer to the perturbative quantum gravity regime, in which we study the $G_N \to 0$ limit, together with perturbative G_N corrections around it, but without non-perturbative effects in G_N.

algebra by the RMT density of states. We show that the resulting algebra can be ensemble averaged to produce a type I algebra acting on a finite-dimensional Hilbert space. In the case of an eternal black hole, the dimension of this Hilbert space is given by the exponential of the Bekenstein-Hawking entropy together with the universal logarithmic correction in the black hole area.

There are different ways to motivate this RMT construction, beyond the fact that it produces the desired algebraic structure. In the large N limit, information about the discreteness of the energy spectrum is lost, and this discreteness is crucial for isolating individual microstates. The RMT construction introduces level repulsion, effectively emulating the spectral discreteness.

The RMT description makes the chaotic nature of black holes manifest. This point makes it clear that the RMT construction is not intrinsically tied to gravity. The idea of using random matrix theory to describe universal spectral properties of complex quantum systems goes back to Wigner [21] and an emergent random matrix description in the semiclassical limit has been used in systems such as a gas of hard spheres in a box to understand thermalization and chaos [22, 23]. From this perspective, the averaging and randomness in our construction provides a physically motivated approximation scheme for semiclassical theories, which is not specific to gravity.

The finite-dimensional Hilbert space on which the type I algebra acts has recently been obtained in the literature from bulk wormhole contributions, using Euclidean path integral methods to construct approximate microstates [24–26]. Here, we sidestep the need for Euclidean path integrals, and instead proceed in close parallel with the algebraic computation of the generalized entropy of a black hole in [27].

The paper is organized as follows. In Section 2, we show how the metric and curvature tensors can be extracted from operator algebras. In Section 3, we construct an approximate type I algebra starting from the type II algebra obtained by adjoining the modular Hamiltonian to the large N type III algebra.

2 Emergence of Gravity in the Semiclassical Limit

In this section, we work in the $G_N \to 0$ limit, where the theory reduces to free fields propagating on a fixed background. A key observation in [14, 15] is that in this strict $G_N \to 0$ limit, one already sees the emergence of Killing horizons from the algebra of the quantized scalar field. Below, we push this picture further and explain how local geometric objects, including the spacetime metric and curvature tensor, emerge in this limit.

2.1 Construction of a Length Function

Consider a minimally coupled non-interacting massive scalar field Φ of mass m living on a $D = d + 1$-dimensional curved spacetime M. Let $\mathcal{A}$ be the algebra of operators built out of the scalar field $\{\Phi(x)\}$ evaluated at points $x \in \mathcal{M}$, where $\Phi(x)$ is understood as an operator-valued distribution.[2] These operators act on a Fock space $\mathcal{H}$. Let $|\omega\rangle$ be a vector in this Hilbert space. Motivated by the reconstruction program of Connes [11], we will work with the triple $(\mathcal{A}, \mathcal{H}, |\omega\rangle)$ and show that this encodes *all* the local information about the underlying geometry.

However, as we will see in the following, to get the geometry from these algebraic objects, one also needs to impose additional constraints on $|\omega\rangle$ and the operators in the algebra. In particular, we will assume that $|\omega\rangle$ satisfies the Hadamard condition. This requirement is very physical, as it is an operator algebraic realisation of the equivalence principle. Additionally, it can be shown that if we want the time derivative of the quantized fields to have finite fluctuations, then $|\omega\rangle$ must be Hadamard [28]. Moreover, a theorem of Wald and Kay states that whenever the background spacetime admits a Killing vector, one can always construct a Hadamard state on its maximal extension [29].

In addition to this, we will also assume that the mass of the scalar field is known. In certain spacetimes, all the generators of the symmetries can be constructed from the operator algebraic data (see Appendix B for an example). In such cases, one can obtain the mass of the scalar field from the action of these generators on the scalar field through the standard relations. When the mass cannot be determined from the operator algebra, we simply assume that it is known.

With these algebraic inputs in hand, we now extract the relevant geometrical structures. The algebra $\mathcal{A}$ is spanned by a family of operators $\mathcal{O}_i$ obtained by evaluating the quantized scalar field at some point $x_i \in M$. We will treat i as a continuous index and set aside its geometric origin. In this way, we regard each spacetime point as being associated with an operator in the algebra.

Once we have a notion of spacetime points in terms of these operators, we can introduce a notion of distance between them. Using the two-point functions $\langle\omega|\mathcal{O}_i\mathcal{O}_j|\omega\rangle$, we define a length function by taking two limits. First, we take the large mass limit, and generically find that

$$\langle\omega|\mathcal{O}_i\mathcal{O}_j|\omega\rangle_0 \sim e^{-m\ell(i,j)} \times m^k \,, \tag{2.1}$$

where k is some constant. The subscript on the left-hand side indicates that we are keeping only the leading order term in the large mass limit. Here ℓ is a distance function, which can

[2]The technically precise objects are the smeared operators $\Phi(f) = \int \mathrm{d}^D x\sqrt{-g}\, \Phi(x)f(x)$, for $f \in C_0^\infty(\mathcal{M})$. Here, we work with pointwise $\Phi(x)$ and revert to smeared operators only where precision is required.

then be extracted by taking the second limit:

$$\ell(i,j) = -\lim_{m\to 0}\left(\frac{1}{\langle\omega|\mathcal{O}_i\mathcal{O}_j|\omega\rangle_0}\frac{\partial}{\partial m}\langle\omega|\mathcal{O}_i\mathcal{O}_j|\omega\rangle_0\right)_{\text{reg.}}, \tag{2.2}$$

We regularize the above expression by removing the $1/m$ divergent term before taking the limit. Now let us briefly explain the origin of (2.2). The scalar field obeys the wave equation on the curved spacetime. The large mass limit corresponds to the geometrical optics limit in which the wave equation reduces to the geodesic equation (see Appendix A of [30] for an explicit computation). Consequently, the two-point function is dominated by the contribution of a particle propagating along the geodesic connecting the insertion points, allowing us to extract the distance between them.[3]

If one were to start with some arbitrary triple $(\mathcal{A}, \mathcal{H}, |\omega\rangle)$, the length function ℓ can be used to diagnose whether the emergent structure associated with the operator algebra admits a genuine geometric interpretation. In particular, we expect the length function to satisfy the following properties

$$\ell(i,j) = \ell(j,i)\,, \qquad \ell(i,i) = 0\,. \tag{2.3}$$

In the case where $|\omega\rangle$ is a cyclic and separating vector with a geometric modular flow associated to it (see Appendix A for definitions), we have more stringent constraints on the emergent geometry. Note that geometric modular flows are present when the action of the modular Hamiltonian $\hat{H}$ corresponds to a symmetry of the spacetime [32, 33]. Let us define

$$\mathcal{O}_j = e^{-i\hat{H}s_1}\mathcal{O}_i e^{i\hat{H}s_1}\,, \qquad \mathcal{O}_k = e^{-i\hat{H}s_2}\mathcal{O}_i e^{i\hat{H}s_2} \qquad \text{with } 0 \le s_2 \le s_1\,, \tag{2.4}$$

so that the corresponding spacetime points $x_{i,j,k}$ associated with the operator insertions are timelike separated. The emergent length function is then required to satisfy the reverse triangle inequality:

$$|\ell(i,j)| \ge \; |\ell(i,k)| + |\ell(k,j)|\,. \tag{2.5}$$

This provides an additional constraint on the length functions associated to the operator algebras supported on a pseudo-Riemannian geometry. Also, if we keep i, j fixed and search for all possible $\mathcal{O}_k$ that saturate the above inequality, then we can find the operators inserted along the timelike geodesic connecting x_i and x_j. Therefore, the availability of a length function can be used to extract various important geometrical objects (see [34] for more details).

[3] There is an important caveat here. When two points are sufficiently far apart, there need not exist a real valued geodesic connecting them. In such cases, the two-point function instead encodes the lengths of complex geodesics connecting the two points [31]. This issue does not arise here, as we are only concerned with local geometric properties extracted from the coincidence limit of the distance function.

Now, let us work out a few examples.

Example 1 : Scalar field in Flat Space

The Wightman function of a free scalar field in $d+1$ Minkowski space can be explicitly solved for,

$$\langle\omega|\mathcal{O}_i\mathcal{O}_j|\omega\rangle = \frac{(2\pi)^{-\frac{d+1}{2}}}{\ell^{d-1}}\,(m\ell)^{\frac{d-1}{2}}\,K_{\frac{d-1}{2}}\,(m\ell)\ , \tag{2.6}$$

where K_ν is the modified Bessel function and ℓ is the flat-space geodesic distance. In the large mass limit, we have

$$\langle\omega|\mathcal{O}_i\mathcal{O}_j|\omega\rangle_0 \sim \frac{(2\pi)^{-\frac{d}{2}}}{2\ell^{d-1}}(m\ell)^{\frac{d-2}{2}}e^{-m\ell} \tag{2.7}$$

Plugging this expression into (2.2), we can see that our definition reproduces the Minkowski length function.

Example 2 : Scalar field in AdS$_{d+1}$

The Wightman function in the Euclidean space is given by [35]:

$$\langle\omega|\mathcal{O}_i\mathcal{O}_j|\omega\rangle = 2^{\Delta}C_\Delta\xi^{\Delta}F\left(\frac{\Delta}{2},\frac{\Delta}{2}+\frac{1}{2};\Delta-\frac{d}{2}+1;\xi^2\right). \tag{2.8}$$

where

$$\xi = \frac{1}{\cosh\ell}\,,\qquad C_\Delta = \frac{\Gamma(\Delta)\Gamma\left(\Delta-\frac{d}{2}-\frac{1}{2}\right)}{(4\pi)^{(d+1)/2}\Gamma(2\Delta-d+1)}\,, \\ m^2 = \Delta\,(\Delta-d) \tag{2.9}$$

Note that the characteristic AdS length scale is set to one. Taking the large mass limit by using an asymptotic expansion of the Hypergeometric function [36, 37], followed by Stirling's approximation, we obtain

$$\langle\omega|\mathcal{O}_i\mathcal{O}_j|\omega\rangle_0 \sim m^{\frac{d-4}{2}}e^{-m\ell}\,, \tag{2.10}$$

where we have dropped an m independent overall constant. Therefore, (2.2) once again gives us the correct length function.

2.2 Curvature from Local Flows

In order to specify a metric-compatible (pseudo-) Riemannian geometry, one needs to have access to the metric and its derivatives at all points on the manifold. Once we have identified

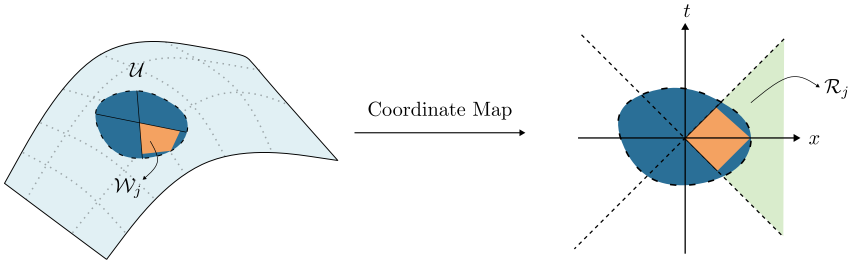

Figure 1. Consider a locally flat patch $\mathcal{U}$ on the manifold. In this patch, we can identify local Rindler horizons that partition the patch into multiple partial Rindler wedges. We denote the algebra of operators restricted to a causal diamond in one such partial wedge by $\mathcal{W}_j$. On the right, we have the map of the patch to a globally flat spacetime. The partial Rindler wedge has a global extension in this Minkowski space. The algebra of operators of a massive scalar field on the full Rindler wedge is denoted by $\mathcal{R}_j$.

the length function on the manifold, it is straightforward to construct the metric tensor. First, let us introduce a quantity σ, often referred to as Synge's world function [38],

$$\sigma(i,j) = \frac{\ell^2}{2}\,, \tag{2.11}$$

with $\ell(i,j)$ defined in (2.2). On a pseudo-Riemannian manifold the metric tensor can be obtained from the world function via

$$\lim_{x\to x'} \frac{\partial^2}{\partial x^\mu \partial x'^\nu}\sigma(x,x') = g_{\mu\nu}\,, \tag{2.12}$$

where x and x' are two points on the manifold [39]. Here, however, our "points" are merely labels $i, j, \ldots$ indexing operators, with no a priori geometric meaning attached to them. Therefore, we can neither take derivatives nor coincident limits. To sidestep this difficulty, we use the equivalence principle. For every point $\mathcal{P}$ on the manifold, one can find a sufficiently small neighbourhood $\mathcal{U}$ in which a flat chart exists. Within this locally flat patch, we consider a family of Rindler wedges whose bifurcation surfaces all pass through the point $\mathcal{P}$. We denote by $\mathcal{W}_j$ the algebra of operators supported on these wedges. We will choose $\mathcal{W}_j$ to be supported in a causal diamond inside the Rindler wedge to make the algebra well-defined (see the left panel of Figure 1). We then require these subalgebras to satisfy the following condition:

- For each $\mathcal{W}_j$, there exists a pair

$$(\mathcal{R}_j, \omega_{\text{Mink}})\,, \tag{2.13}$$

where $\mathcal{R}_j$ is the operator algebra of a massive scalar field on an *entire* $(d+1)$-dimensional Rindler spacetime, such that the correlation functions of operators in $\mathcal{W}_j$ in $|\omega\rangle$ are well approximated by the vacuum expectation values of local operators in $\mathcal{R}_j$. In this sense, every operator in $\mathcal{W}_j$ can be approximated by a local operator in $\mathcal{R}_j$.

We will refer to the subalgebras $\mathcal{W}_j$ as *local Rindler algebras*. There is a natural geometrical way to understand each $\mathcal{W}_j$ and its corresponding Rindler algebra $\mathcal{R}_j$ (see Figure 1). The locally flat patch $\mathcal{U}$ can be divided into various Rindler wedges, and each $\mathcal{W}_j$ corresponds to the algebra of operators living in these wedges. The flat coordinates we introduce on $\mathcal{U}$ admit a global Minkowski extension, and the Rindler wedges in $\mathcal{U}$ can similarly be extended to full Rindler spacetimes using the same coordinate chart. The algebras $\mathcal{R}_j$ are then precisely the algebras of operators on these extended Rindler spacetimes. Note that, by construction, $\mathcal{R}_j$ is a much larger set than $\mathcal{W}_j$.

If one has access to algebras of operators in multiple Rindler wedges of a globally flat Minkowski spacetime, then the entire Poincaré algebra of the spacetime can be reconstructed purely from the operator algebras [40, 41]. We briefly outline the steps here but an explicit example is worked out in Appendix B. By the Bisognano–Wichmann theorem [42, 43], one can associate a modular operator Δ_j to each wedge algebra, and these operators generate boosts that preserve the respective wedges. The boost generators of the local Poincaré algebra are then given by these modular operators. For each wedge, one can further construct subalgebras with an inclusion structure, which leads to half-sided modular translations. These can, in turn, be used to construct local translation generators. Combining the boost operators associated with different wedges with these translation generators, one can reconstruct rotations and, ultimately, the full Poincaré group.

This construction allows us to use the $\mathcal{R}_j$ algebras to construct the Poincaré algebra associated to the global Minkowski extension of the patch $\mathcal{U}$. Since we assume the operators in $\mathcal{W}_j$ to be approximately equal to local operators in $\mathcal{R}_j$, these emergent generators act as approximate symmetry generators on $\mathcal{W}_j$. Therefore, the assumption of local Rindler algebras implies that matter effectively "sees" flat space locally, thereby realizing the equivalence principle via operator algebras.

But most importantly, the emergence of these approximate symmetry generators allows us to identify approximate Killing flows in the local patch $\mathcal{U}$ purely in the language of operator algebras. Using these flows, we can then define derivatives and a coincident limit. As an example, consider the boost generated by one of the modular operators Δ_j, and let ξ^μ denote the corresponding approximate Killing vector field.

Now consider an operator $a_{\text{Rind}} \in \mathcal{R}_j$. Its modular evolution is given by

$$a_{\text{Rind}}(s) = \Delta_j^{is}\, a_{\text{Rind}}\, \Delta_j^{-is}\,. \tag{2.14}$$

Since $a_{\text{Rind}}(s)$ is the image under the modular flow of an *exact* Rindler spacetime, the evolution corresponds to a geometric flow along the vector field ξ^μ, and hence defines a one-parameter family of operators associated with points along this flow. The existence of a map from the operators in $\mathcal{W}_j$ to local operators in $\mathcal{R}_j$ and vice versa automatically induces a one-parameter family of operators $\mathcal{O}(s)$ for every $\mathcal{O} \in \mathcal{W}_j$. The important point to note here is that $\mathcal{O}(s)$ for every value of s is a local operator in $\mathcal{W}_j$.

Therefore, the existence of a map to a true Rindler algebra allows us to associate a pointwise flow within $\mathcal{W}_j$. The continuous parameter s labeling this flow then enables us to define derivatives and, in particular, a coincident limit. Consider the following two-point function

$$\langle\omega|\mathcal{O}_i(s_1)\mathcal{O}_i(s_2)|\omega\rangle \equiv G(i_{s_1}, i_{s_2})\,. \tag{2.15}$$

Then by following the procedure in Section 2.1, we can compute $\sigma(i_{s_1}, i_{s_2})$. Since $s_{1,2}$ are continuous parameters, we find that

$$\lim_{s_1,s_2\to 0} \frac{\partial^2}{\partial s_1 \partial s_2}\sigma(i_{s_1}, i_{s_2}) = g_{\mu\nu}\xi^\mu\xi^\nu\,. \tag{2.16}$$

Therefore, we obtain the contraction of the metric with respect to one of the approximate Killing vectors of the locally flat patch. Repeating the same computation for the other local flows gives the contractions of the metric with respect to the remaining approximate Killing vectors. Since this can be done for *all* the approximate symmetries of the local patch, we have sufficient information to determine all components of the metric tensor.

Now, let us compute curvature tensors from the operator algebra. The idea is to use the fact that curvature tensors appear in the subleading terms of the coincidence limit of the Wightman function [44]. To see this, let us consider the two-point function

$$\langle\omega|\mathcal{O}_i\mathcal{O}_i(s)|\omega\rangle \equiv G(i, i_s)\,, \tag{2.17}$$

where the operator $\mathcal{O}_i(s)$ is the family of operators corresponding to an operator insertion on the curve generated by the action of a local Rindler boost. We can see that taking $s \to 0$ then gives us the coincidence limit of the two-point function.

In this limit, the two-point functions have the following universal Hadamard form [44],

$$\langle\omega|\mathcal{O}_i\mathcal{O}_j|\omega\rangle = \frac{i\alpha}{2}\left(\frac{U\,(i,j)}{\left[\sigma\,(i,j)+i\epsilon\right]^{D/2-1}} + V\,(i,j)\ln\left[\sigma\,(i,j)+i\epsilon\right] + W\,(i,j)\right), \tag{2.18}$$

where α is a constant that depends only on the dimensions of the spacetime. Note that the logarithmically divergent piece in (2.18) shows up only in even spacetime dimensions. Now let us replace $\mathcal{O}_j$ with the operator evolved by the local Rindler boost for some modular time s, as in (2.17).

In the $s \to 0$ limit, the coefficient U goes to 1 and the leading behaviour approaches the propagator of a massless scalar field in Minkowski space:

$$G(i, i_s) = \frac{i\alpha}{2} \frac{1}{[\sigma(i, i_s) + i\epsilon]^{D/2-1}} . \tag{2.19}$$

In particular, the number of spacetime dimensions D appears in the leading term.

Now let us look at the subleading behaviour of the two-point function. It turns out that we can expand the function U in powers of σ [44],

$$U(i, j) = \Delta_V^{1/2} + O(\sigma) , \tag{2.20}$$

where Δ_V is the van Vleck-Morette determinant, and this quantity in turn has the following expansion [39],

$$\Delta_V \approx 1 + \frac{1}{6} R_{\mu\nu} \sigma^\mu \sigma^\nu , \qquad \text{where} \quad \sigma^\mu \approx s\xi^\mu . \tag{2.21}$$

Therefore, we can extract the Ricci tensor from the two-point functions as follows,

$$\lim_{s \to 0} \frac{\partial^2}{\partial s^2} \frac{12\sigma^{D/2-1}}{i\alpha} G(i, i_s) = R_{\mu\nu} \xi^\mu \xi^\nu . \tag{2.22}$$

There is a simple reason why the Ricci tensor can be extracted from the two-point functions of the theory. The van Vleck-Morette determinant arises from the one-loop correction to the semiclassical approximation of the propagator, which contains information about the focusing/defocusing of geodesics. This, in turn, means it contains information about the Ricci tensor through the Raychaudhuri equation [45].

Let us recap our results, so far. Under the conditions (1)-(3), the metric and curvature tensors at every point on the manifold can be extracted entirely from algebraic data. The derivation assumed the existence of an underlying geometry, in particular, a local Rindler horizon structure. Yet the conditions (1)-(3) themselves are formulated purely in the language of operator algebras and their associated Hilbert spaces. The absence of any geometrical input in these conditions means that they can be read equally as criteria for the *emergence of spacetime*. One may begin with an abstract triple $(\mathcal{A}, \mathcal{H}, |\omega\rangle)$ carrying no *a priori* geometric interpretation and ask whether conditions (1)-(3) are satisfied. If they are, a spacetime geometry can be systematically constructed from the algebraic data.

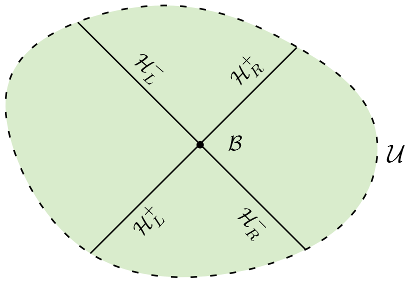

Figure 2. Consider a Rindler horizon in a locally flat patch $\mathcal{U}$ on the manifold. We can divide the horizon into four null hyperplanes as shown in the figure. The bifurcation surface is denoted by $\mathcal{B}$.

2.3 Einstein's Equations from Locally Stationary States

In the previous subsection, we identified the conditions under which a spacetime geometry emerges from the operator algebra and Hilbert space of a quantized massive scalar field. The resulting geometry need not satisfy Einstein's field equations. As we are in the strict $G_N \to 0$ limit, there is, however, a simple check for the validity of Einstein's equations. In this limit, they reduce to the vacuum equations

$$R_{\mu\nu} = \frac{2\Lambda}{D-2} g_{\mu\nu} \,. \tag{2.23}$$

Using the expressions for the emergent metric (2.16) and Ricci tensor (2.22), the contraction of Einstein's equations with the approximate Killing vectors of a locally flat patch can be written as

$$\lim_{s\to 0} \frac{\partial^2}{\partial s^2} \frac{24\sigma^{D/2-1}}{i\alpha} G(i, i_s) = \left(\frac{2\Lambda}{D-2}\right) \lim_{s_1,s_2\to 0} \frac{\partial^2}{\partial s_1 \partial s_2} \sigma(i_{s_1}, i_{s_2}) \,. \tag{2.24}$$

Choosing different approximate Killing vectors results in a set of equations that, when satisfied simultaneously, guarantee the validity of the vacuum Einstein equations.

We have arrived at an operator-algebraic diagnostic for Einstein's field equations, but why should they emerge in the first place? We now show that an additional operator-algebraic condition is sufficient to derive them, provided we include perturbative G_N corrections around the $G_N \to 0$ limit so that the scalar field back-reacts on the geometry (see [46–48] for more details on this limit).

A major breakthrough in understanding the origin of Einstein's field equations came in the seminal work of Jacobson [1]. We can always find a small neighbourhood of a spacetime point $\mathcal{P}$ where a locally flat chart exists and consider an accelerating observer in this patch.

In any such local Rindler frame, Einstein's equations can be derived from a local equilibrium condition via the Clausius relation [1],

$$\delta Q = T\mathrm{d}S\,, \tag{2.25}$$

where δQ is the heat flux across the local Rindler horizon, T is the corresponding Unruh temperature, and $\mathrm{d}S$ is the change in the horizon entropy. Jacobson's argument clarifies the emergent nature of gravity: gravity is a theory of local Rindler horizons and their associated thermodynamics (see also [49]).

Our goal, is to identify an operator-algebraic analogue of Jacobson's Clausius relation (2.25). We start with the Weyl algebra $\mathcal{W}$ generated by bounded operators $W(f) = e^{i\Phi(f)}$, where $f \in C_0^\infty(\mathcal{M})$. Now consider a locally flat patch $\mathcal{U}$ in the emergent geometry. As in the previous section, we find a local Rindler horizon in this patch composed of two null hypersurfaces $\mathcal{H}^\pm$ and a bifurcation surface $\mathcal{B}$. Each hypersurface decomposes as the union of a left and right hyperplane as $\mathcal{H}^\pm = \mathcal{H}_L^\pm \cup \mathcal{H}_R^\pm$ (see Figure 2). Consider the von Neumann algebra $\mathcal{M}_\mathcal{R}$ associated to the right Rindler wedge of this local patch [50]. Let $\mathcal{N}_R \subset \mathcal{M}_R$ be the von Neumann algebra of operators restricted to $\mathcal{H}_R^-$.

Consider a state ω_0 on $\mathcal{W}$ (see Appendix A for the definition of a state). We now assume that ω_0 is a quasifree[4] Hadamard state stationary under the affine dilations along $\mathcal{H}_R^-$. We refer to such states as *locally stationary states*.

The restriction of the state ω_0 to the horizon algebra $\mathcal{N}_R$, which we denote by $\omega_0|_{\mathcal{N}_R}$, satisfies the Kubo-Martin-Schwinger (KMS) condition at an inverse temperature β:

$$\omega_0|_{\mathcal{N}_R}\left(a_1\alpha_{t+i\beta}[a_2]\right) = \omega_0|_{\mathcal{N}_R}\left(\alpha_t[a_2]a_1\right), \qquad a_{1,2} \in \mathcal{N}_R \text{ and } t \in \mathbb{R}\,, \tag{2.26}$$

where $\alpha_t[a]$ is the flow of $a \in \mathcal{N}_R$ under affine dilations along $\mathcal{H}_R^-$ [52]. The inverse temperature β is given by $\frac{2\pi}{\kappa}$, where κ is the surface gravity of $\mathcal{H}_R^-$. Now consider the Gelfand–Naimark–Segal (GNS) representation of $(\mathcal{N}_R, \omega_0|_{\mathcal{N}_R})$. We denote the vector associated to $\omega_0|_{\mathcal{N}_R}$ by $|\Omega_0\rangle$. The KMS condition implies that the GNS vector $|\Omega_0\rangle$ is separating for $\mathcal{N}_R$, so that Tomita-Takesaki theory applies and the modular operator Δ_{Ω_0} is well-defined. By the Bisognano-Wichmann theorem as extended to Killing horizons [50, 52], Δ_{Ω_0} acts as affine dilations along $\mathcal{H}_R^-$. Finally, let ω_ϕ be a coherent excitation of ω_0. In the GNS Hilbert space, this state is represented by $|\Omega_\phi\rangle = e^{i\Phi(\phi)}|\Omega_0\rangle$, where ϕ is a smooth solution of the Klein-Gordon equation with support only on $\mathcal{H}_R^-$.

We now include perturbative G_N corrections around the $G_N \to 0$ limit. In this perturbative quantum gravity regime, observables are not fully diffeomorphism invariant, but are instead

[4] A quasifree, or Gaussian, state is one in which all odd n-point functions vanish, while the even n-point functions are completely determined by Wick contractions (see [29, 51] for further details).

invariant under the symmetries of the fixed background geometry. In our case, we require observables to be invariant under the flow generated by Δ_{Ω_0}. To construct such observables, one must appropriately "dress" the operators with the charges associated with this flow (see [46, 47] for details). We will not review this construction here, but note that the resulting algebra is a crossed product algebra (see Section 3.2 for definitions), and is of type II. This allows us to define density matrices, traces, and entropy for states in the algebra.

In this crossed product algebra, we can then define a state $|\hat{\Omega}_\phi\rangle$ corresponding to the coherent excitation $|\Omega_\phi\rangle$ as follows:

$$|\hat{\Omega}_\phi\rangle = \int_{\mathbb{R}} \mathrm{d}x \; f(x) \, |\Omega_\Phi\rangle \otimes |x\rangle \,, \tag{2.27}$$

where $f(x) \in L^2(\mathbb{R})$ and $|x\rangle$ denotes the generalized position basis of $L^2(\mathbb{R})$. We make this state *semiclassical* by choosing the function $f(x)$ to vary 'slowly' in x. Then it follows that

$$S^{\text{rel}}\left(\omega_0 \| \omega_\phi\right) = \left\langle \frac{A}{4G_{\text{N}}} \right\rangle_{\hat{\Omega}_\phi} - \frac{A}{4G_{\text{N}}} + S_{\text{vN}}\left(\omega_\phi|_{\mathcal{H}_{\text{R}}^-}\right) - S_{\text{vN}}\left(\omega_0|_{\mathcal{H}_{\text{R}}^-}\right) \,, \tag{2.28}$$

where A is the 'background area' of the bifurcation surface [46]. The quantity on the left-hand side is the relative entropy between the two states. The von Neumann entropy on the right-hand side corresponds to the entanglement entropy of the states restricted to the past of the bifurcation surface. A version of this equality was originally used in proving the generalized second law for causal horizons [48] (see [47] for the derivation of this expression in the case of operators restricted to a causal diamond).

There are two important technical points that we would like to emphasize before proceeding. First, the relative entropy on the left-hand side of (2.28) is well defined, whereas the individual terms appearing on the right-hand side are not separately well defined in the $G_N \to 0$ limit. The claim, however, is that the particular combination of these terms remains well defined even in the $G_N \to 0$ limit [53]. Second, our definition for the expectation value of the area operator in (2.28) differs from [46]. There, it includes the background area A, along with a perturbative correction from the inclusion of the charge associated with Δ_{Ω_0}, as well as contributions from the matter flux through the horizon. However, since the perturbative charge correction drops out of the computation of the relative entropy, we omit this term in the definition of the expectation value of the area for brevity.

Now let us look at the left-hand side of (2.28). For coherent excitations, the relative entropy is given by

$$S^{\text{rel}}\left(\omega_0 \| \omega_\phi\right) = i \frac{d}{dt}\bigg|_{t=0} \left\langle \Omega_\phi \mid \Delta_{\Omega_0}^{it} \Omega_\phi \right\rangle . \tag{2.29}$$

In [54] it was shown that this expression can be rewritten as

$$S^{\text{rel}}\left(\omega_0\|\omega_\phi\right) = -2\pi \int_{\mathcal{H}_R^-} U \left\langle : T_{\mu\nu} : \right\rangle k^\mu k^\nu \mathrm{d}U \mathrm{dvol}_{\mathcal{S}}\,, \tag{2.30}$$

where k^μ is the tangent vector to the horizon, $\langle : T_{\mu\nu} : \rangle$ is the expectation value of the stress energy tensor of the quantum field in the state ω_ϕ and U corresponds to the null coordinate along the horizon. The energy flux through the Rindler horizon is then given by [50, 54]

$$\delta Q = \frac{S^{\text{rel}}\left(\omega_0\|\omega_\phi\right)}{\beta}\,. \tag{2.31}$$

In order to determine the right-hand side of (2.28), we observe that for coherent excitations of the Minkowski vacuum, the entanglement entropy remains unchanged [55, 56]. Therefore the difference in the von Neumann entropy of the states drops out, and we are left with

$$S^{\text{rel}}\left(\omega_0\|\omega_\phi\right) = \frac{\delta A}{4\pi G_N}\,. \tag{2.32}$$

Using (2.31) and (2.32), we obtain Jacobson's Clausius relation (2.25).

We complete the derivation of Einstein's equation by noting that

$$\frac{\delta A}{4\pi G_N} = \frac{1}{4G_N}\int_{\mathcal{H}_R^-} \theta \mathrm{d}U \mathrm{dvol}_{\mathcal{S}}\,, \tag{2.33}$$

where θ is the expansion parameter of the null congruence that forms the local Rindler horizon. This gives us

$$\frac{1}{4G_N}\int_{\mathcal{H}_R^-} \theta \mathrm{d}U \mathrm{dvol}_{\mathcal{S}} = -2\pi \int_{\mathcal{H}_R^-} U \left\langle : T_{\mu\nu} : \right\rangle k^\mu k^\nu \mathrm{d}U \mathrm{dvol}_{\mathcal{S}}\,. \tag{2.34}$$

Imposing conservation of the stress energy tensor and using the Raychaudhuri equation, we arrive at the Einstein's equation in standard form [1],

$$R_{\mu\nu} - \frac{1}{2}R g_{\mu\nu} + \Lambda g_{\mu\nu} = 8\pi G_N \left\langle : T_{\mu\nu} : \right\rangle\,. \tag{2.35}$$

3 Type I Algebras from Random Matrix Theory Corrections

In the previous section, we worked in the $G_N \to 0$ limit and incorporated perturbative corrections in G_N round this limit. When we instead turn on a small but finite G_N, non perturbative quantum gravity corrections become important. In this section, we show how these corrections can be systematically incorporated by using holography.

3.1 Microstates from a Boundary Dual

In recent years, there have been several constructions of microstates of non-supersymmetric black holes [19, 20, 24–26]. In this subsection, we briefly review the considerations of [19, 20], where non-perturbative corrections, obtained via random matrix theory, are used to arrive at a finite-dimensional Hilbert space of black hole microstates.

Consider a pair of CFTs in the thermofield double (TFD) state dual to an eternal AdS black hole,

$$|\mathrm{TFD}\rangle = \frac{1}{\sqrt{Z(\beta)}} \sum_n e^{-\frac{\beta}{2}E_n} |E_n\rangle_L |E_n\rangle_R \,, \tag{3.1}$$

where $|E_n\rangle_{L,R}$ are the energy eigenstates of the left and the right CFT, and the partition function is given by

$$Z(\beta) = \sum_n e^{-\beta E_n} \,. \tag{3.2}$$

We can construct an infinite family of time-shifted TFD states by acting on the TFD state only with the right CFT Hamiltonian,

$$|\mathrm{TFD}(t)\rangle = e^{-iH_R t}\,|\mathrm{TFD}\rangle = \frac{1}{\sqrt{Z(\beta)}} \sum_n e^{-\frac{\beta}{2}E_n} e^{-itE_n} |E_n\rangle_L |E_n\rangle_R \,. \tag{3.3}$$

These states are closely related to the thin-shell states studied in [25, 26], where instead of acting with the right boundary Hamiltonian, one inserts a heavy operator. Time-evolved TFD states were also used in the state-dependent reconstruction of interior operators of an eternal black hole in [57]. Now consider the Hilbert space spanned by a discrete set of n time-shifted TFD states,

$$\mathcal{H}_n = \mathrm{span}\{|\mathrm{TFD}(t_j)\rangle : t_j = jt_1 \text{ and } j = 1, \ldots n\} \,, \tag{3.4}$$

for a fixed time-step t_1 taken sufficiently large (a few times the inverse temperature β) such that all $|t_i - t_j|$ are well-separated [20]. To determine the dimension of this Hilbert space, we study the Gram matrix,

$$G_{ij} = \langle \mathrm{TFD}(t_i) | \mathrm{TFD}(t_j) \rangle \;. \tag{3.5}$$

The dimension of $\mathcal{H}_n$ is then given by

$$d_n = n - \ker(G) \,, \tag{3.6}$$

where $\ker(G)$ is the dimension of the kernel of the Gram matrix. In the $N \to \infty$ limit of the boundary CFT, $G_{ij} = \delta_{ij}$ [19]. As a result, $d_n = n$, and the dimension diverges in the limit $n \to \infty$.

At finite N, however, the overlaps receive non-perturbative corrections and in principle one needs control over the boundary theory at finite N to describe the physics. As it turns out, finite N effects can be modelled within the $N \to \infty$ limit itself by treating the large N theory as a random matrix theory (RMT) [19, 20]. We implement this approximation in two steps. We first assume that in the $N \to \infty$ limit, the CFT admits a continuous density of states $\rho_0(E)$. Operationally, this amounts to making the following replacement:

$$\sum_n \rightarrow \int \mathrm{d}E \, \rho_0(E) \,, \qquad \text{and} \qquad |E_n\rangle \rightarrow |E\rangle \,. \tag{3.7}$$

The density of states can be computed from the partition function through an inverse Laplace transform,

$$\rho_0(E) = \lim_{N\to\infty} \frac{1}{2\pi i} \int_{\gamma - i\infty}^{\gamma + i\infty} \mathrm{d}\beta \, e^{\beta E} Z(\beta) \,. \tag{3.8}$$

We then substitute the density of states $\rho_0(E)$ with the density of states $\rho(E)$ of a random matrix theory, satisfying $\overline{\rho(E)} = \rho_0(E)$. For now, we choose the higher point functions of the RMT to follow a Poisson distribution [20],

$$\overline{\rho(E)\rho\left(E'\right)} = \rho_0(E)\rho_0\left(E'\right) + \rho_0(E)\delta\left(E - E'\right) \,. \tag{3.9}$$

We refer to the inclusion of RMT corrections via this procedure as an *RMT completion* of the theory. An important consequence of the completion is the modification of the overlap of the time-shifted TFD states. Consider

$$|G_{ij}|^2 = |\langle \mathrm{TFD}(t_i)|\mathrm{TFD}(t_j)\rangle|^2 = \frac{1}{Z(\beta)^2} \sum_{n,m} e^{-\beta(E_n + E_m)} e^{-i(t_j - t_i)(E_m - E_n)} \,. \tag{3.10}$$

The expression on the right-hand side is called the spectral form factor (SFF). Making the replacement (3.7) and averaging, we get

$$\overline{|G_{ij}|^2} = \frac{|Z(\beta - i(t_i - t_j))|^2}{Z(\beta)^2} + \frac{Z(2\beta)}{Z(\beta)^2} \,. \tag{3.11}$$

The first disconnected piece decays for large $(t_i - t_j)$ and produces the 'dip' in the SFF. The second term is constant and gives rise to the 'plateau' in the SFF (see [58, 59] for more details). The second term can be evaluated in a saddle point approximation, using

$$Z(\beta) = e^{-\beta M + S_{\mathrm{BH}}} \,, \tag{3.12}$$

where M is the mass of the black hole. This gives us

$$\left.\overline{|G_{ij}|^2}\right|_c = e^{-S_{\mathrm{BH}}} = e^{-O(N^2)} \,. \tag{3.13}$$

The rank of G can be computed from the connected component of these overlaps using resolvent techniques and one finds that the dimension of the RMT-completed Hilbert space $\overline{\mathcal{H}_n}$ saturates at $d_n = \min(n, e^{S_{\rm BH}})$ [19, 25, 60]. Now define

$$\mathcal{H}_{\rm BH} = \lim_{n\to\infty} \overline{\mathcal{H}_n}\,. \tag{3.14}$$

The dimension of $\mathcal{H}_{\rm BH}$ is then given by $d = e^{S_{\rm BH}}$. Therefore, RMT completion results in a finite-dimensional Hilbert space carrying precisely the Bekenstein-Hawking entropy.

We have arrived at a finite-dimensional Hilbert space by including RMT corrections. In the $N \to \infty$ limit, information about the discreteness of the CFT energy spectrum is lost, since level spacings are suppressed as $e^{-O(N^2)}$. One is therefore forced to work with a smooth density of states $\rho_0(E)$, and it is this 'information loss' that leads to the orthogonality of the time-shifted TFD states.[5] At any finite N, however, the spectrum is discrete, and the spectral form factor necessarily stops decaying and saturates [58, 59]. One role of the RMT completion is to restore the discreteness of the spectrum at finite N.

One can alternatively motivate the introduction of an RMT description in the boundary theory by appealing to *chaos* and *thermalization*. From the bulk perspective, this is quite natural, since black holes are known to be maximally chaotic systems in the sense of fast scrambling of quantum information [58, 62–65]. On the CFT side, the use of RMT dynamics has gained prominence in recent years [66–72]. The emergence of an RMT description in the semiclassical limit need not be tied specifically to gravity or black holes. Rather, RMT provides a general framework for modeling chaotic dynamics in quantum systems. A classic example is a gas of hard spheres in a box, which is an integrable quantum system but nevertheless exhibits emergent RMT behaviour in the semiclassical limit [22, 23]. From this perspective, the discussion in this and the following sub-sections extends to a broader class of chaotic systems.

With $\mathcal{H}_{\rm BH}$ in hand, we turn to the algebra $\mathcal{B}(\mathcal{H}_{\rm BH})$ of bounded operators acting on it. The finite dimensionality of $\mathcal{H}_{\rm BH}$ strongly suggests this algebra is of type I, as argued in [19], via the discreteness of the spectrum. In the next subsection, we make this more explicit by constructing the minimal projectors required for a type I algebra.

3.2 Crossed Product and the Construction of a type I_d Algebra

The microstates of the previous section were generated by acting with H_R on the TFD state, so a natural next step is to enlarge the large N operator algebra by adjoining H_R to it. In the large N limit of $\mathcal{N} = 4$ supersymmetric Yang-Mills theory, the relevant starting point is the

[5] The continuum spectrum is also at the root of Maldacena's large N information problem [61].

algebra of single-trace operators and adjoining H_R to it is made precise by the crossed product construction [17].

Consider the boundary CFTs in the previous section and pick an energy eigenstate $|E_0\rangle$ with energy $E_0 = O(N^2)$. Then a microcanonical version of the TFD state, centered around $|E_0\rangle$, can be defined as follows [27],

$$|\widetilde{\mathrm{TFD}}\rangle = e^{-S_{\mathrm{BH}}/2} \sum_i e^{-\beta(E_i - E_0)/2} f\left(E_i - E_0\right) |E_i\rangle_L \, |E_i\rangle_R \,. \tag{3.15}$$

Here, f is a smooth, square-integrable function that can be chosen to be a Gaussian function with standard deviation $\sigma = O(N^0)$ without loss of generality. We denote by $\mathcal{A}_{0,R}$ the algebra of single-trace operators in the right CFT. Working above the Hawking-Page temperature, this algebra becomes type III$_1$ in the $N \to \infty$ limit [14, 15, 18]. We then consider the renormalized right CFT Hamiltonian,

$$h_R = H_R - E_0 \,. \tag{3.16}$$

The action of h_R on the microcanonical TFD state produces fluctuations that are $O(N^0)$ [27]. If one were using the standard canonical TFD state, the fluctuations of the right CFT Hamiltonian would diverge in the large N limit. Therefore, working with the microcanonical TFD state is advantageous as we can directly add h_R to the single-trace algebra even in the strict $N \to \infty$ limit. We can *formally* decompose the right Hamiltonian as follows

$$h_R = \hat{h} + X \,, \qquad \text{with } X = h_L \equiv H_L - E_0 \,, \tag{3.17}$$

where H_L is the Hamiltonian of the left CFT and the operator $\hat{h} = H_R - H_L$ is the modular Hamiltonian of the TFD state (rescaled by a factor of $1/\beta$). The extended Hilbert space takes the form $\mathcal{H} \cong \mathcal{H}_{\mathrm{TFD}} \otimes L^2(\mathbb{R})$, where $\mathcal{H}_{\mathrm{TFD}}$ is the GNS Hilbert space generated by the action of single-trace operators on the TFD state. The appearance of this tensor product structure follows from the fact that the renormalized left Hamiltonian h_L commutes with all operators in the right CFT. Consequently, its action furnishes an independent tensor factor. The algebra acting on the extended Hilbert space is known in the literature as the crossed product algebra,

$$\mathcal{A}_R = \mathcal{A}_{0,R} \rtimes \mathbb{R}_h \,. \tag{3.18}$$

It is generated by elements of the form $a \otimes 1$ with $a \in \mathcal{A}_{0,R}$, together with unitary operators of the form $e^{i\hat{h}s} \otimes e^{iXs}$. As a result, a general element of the algebra can be written as

$$\hat{a} = \int_{-\infty}^{\infty} \mathrm{d}s \; a(s) e^{is(\hat{h}+X)} \,, \qquad a(s) \in \mathcal{A}_{0,R} \,, \tag{3.19}$$

and a general state in the extended Hilbert space $\mathcal{H}$ has the form

$$|\hat{\Phi}\rangle = \int_{-\infty}^{\infty} \mathrm{d}x \; g(x) |\Phi\rangle |x\rangle \,, \qquad |\Phi\rangle \in \mathcal{H}_{\mathrm{TFD}} \,. \tag{3.20}$$

Here $g(x) \in L^2(\mathbb{R})$ is a normalizable function and $|x\rangle$ are states on which the operator X acts as a position operator. The microcanonical TFD state is then identified with

$$|\hat{\Psi}\rangle = \int_{-\infty}^{\infty} \mathrm{d}x \; f(x)|\Psi\rangle|x\rangle \,, \tag{3.21}$$

where $|\Psi\rangle$ is some element of the single-trace Hilbert space $\mathcal{H}_{\mathrm{TFD}}$.

The crucial point here is that the resulting enlarged algebra is a type II_∞ factor, and as a result, we can define density matrices and a trace on it. In particular, for *any* $|\hat{\Phi}\rangle \in \mathcal{H}$, we can define a density matrix $\rho_{\hat{\Phi}} \in \mathcal{A}_R$ that satisfies the property [17, 27]:

$$\mathrm{tr}\,[\rho_\Phi \hat{a}] = e^c \langle\hat{\Phi}|\hat{a}|\hat{\Phi}\rangle \,, \quad \forall \hat{a} \in \mathcal{A}_R \,. \tag{3.22}$$

Note that this trace is defined only up to a multiplicative constant. Using this trace, we can then define a von Neumann entropy,

$$S_{\mathrm{vN}}(\rho_{\hat{\Phi}}) = -\langle\hat{\Phi}|\log \rho_{\hat{\Phi}}|\hat{\Phi}\rangle + c \,. \tag{3.23}$$

Factors of type I_d and type II_∞ have a standard form, which we will quickly review here (see [73] for more details). Let us first look at a type I_d factor acting on a d-dimensional Hilbert space $\mathcal{H}$. By definition, a type I algebra has a non-zero minimal projector P. We can also construct a family of pairwise orthogonal projectors $\{P_i\}$, which are equivalent to P, satisfying the identity $\sum_i P_i = 1$. Consider the Hilbert space $\mathcal{H}'$ spanned by vectors $|P_i\rangle$ associated to the projectors. Then the algebra can be mapped to the tensor product $\mathcal{B}(\mathcal{H}') \otimes 1_{P\mathcal{H}}$ by a unitary conjugation [73]. Note that the Hilbert space $\mathcal{H}'$ has dimension d. One can think of this decomposition in the following way. In a type I algebra, all minimal projectors are equivalent to each other. So the algebra splits into the product of $\mathcal{B}(\mathcal{H}')$ and a c-number multiple of the identity operator acting in the subspace obtained by acting with *some* minimal projector $1_{P\mathcal{H}}$.

Now consider a type II_∞ algebra $\mathcal{A}$ and let P be a non-zero projector. Since the algebra is type II, the projector P will not be minimal but we can still find a set of projectors $\{P_i\}$ equivalent to P that resolve the identity operator in the algebra. We identify the Hilbert space $\mathcal{H}'$ with the span of the projectors $\{P_i\}$. The type II_∞ algebra is then isomorphic to $\mathcal{B}(\mathcal{H}') \otimes P\mathcal{A}P$. The difference between a type I_d and a type II_∞ algebra is twofold. First of all, the Hilbert space $\mathcal{H}'$ is finite-dimensional in the case of a type I_d algebra, while it is infinite-dimensional in the case of the type II algebra. Moreover, $P\mathcal{A}P$ reduces to a multiple of the identity operator in the case of a type I algebra since we have minimal projectors.

It turns out that RMT completion provides a natural construction of a type I_d algebra starting from the type II_∞ crossed product algebra. As explained in the previous subsection, the elements of the large N enlarged algebra $\mathcal{A}_R$ can be expressed as an integral over the density of states $\rho_0(E)$,

$$\hat{a} = \int \mathrm{d}s\ a(s) e^{i h_R s} = \int \mathrm{d}s \int \mathrm{d}E\ a(s) e^{i(E-E_0)s} P_E\,, \tag{3.24}$$

where P_E is the projector of the right boundary Hamiltonian onto a sector of energy E,

$$P_E = \rho_0(E)|E\rangle\langle E|\,. \tag{3.25}$$

We have dropped the subscript R on the bras and kets for brevity. Note that P_E is a projector onto a single energy eigenvalue and can be formally rewritten as $\delta(H_R - E)$. Since this is an unbounded operator, it is not an element of $\mathcal{A}_R$. We can, however, construct a projector that is an element of $\mathcal{A}_R$ as follows:

$$P_{E_i,\Delta E} = \int \mathrm{d}E \rho_0(E) \chi_{E_i,\Delta E}(E)\ |E\rangle\langle E|\,, \tag{3.26}$$

where χ is the characteristic function,

$$\chi_{E_i,\Delta E}(E) = \begin{cases} 1\,, & E \in [E_i - \Delta E, E_i + \Delta E]\,, \\ 0\,, & E \notin [E_i - \Delta E, E_i + \Delta E]\,. \end{cases} \tag{3.27}$$

The operator $P_{E_i,\Delta E}$ is a spectral projection of H_R onto a non-zero measure subset of the spectrum, namely the interval $[E_i - \Delta E, E_i + \Delta E]$. By the spectral theorem, all such projections are bounded operators. Since $\mathcal{A}_R$ is a von Neumann algebra, it is closed in the weak operator topology, and therefore contains all such bounded spectral projections of its operators. It follows that $P_{E_i,\Delta E} \in \mathcal{A}_R$. We can see that the projector $P_{E_i,\Delta E}$ is not a minimal projector as we can always define another projector $P_{E_i,\Delta E'}$ with a spread in the energy $\Delta E' < \Delta E$. This absence of a minimal projector is what we expect from a type II_∞ algebra.

Now build a family of projectors $\{P_{E_i,\Delta E}\}$ by fixing

$$\Delta E = \frac{1}{2\rho_0(E_0)}\,, \tag{3.28}$$

and choosing a sequence of evenly spaced E_i (with $E = E_0$ included in the sequence) separated by $2\Delta E$, so that $\sum_i P_{E_i,\Delta E} = 1$. The resulting projectors are pairwise orthogonal. The Hilbert space $\mathcal{H}'$ is then constructed by acting with these projectors on the TFD state,

$$\mathcal{H}' = \left\{ \sum_{j\in\mathbb{Z}} \alpha_j P_{E_j,\Delta E} |\hat{\Psi}\rangle \ \Big|\ \forall \alpha_j \in \mathbb{C} \text{ and } E_j = E_0 + 2j\Delta E \text{ satisfying } E_j \geq 0 \right\}\,. \tag{3.29}$$

Here $|\hat{\Psi}\rangle$ is the state corresponding to the microcanonical TFD state in the crossed product algebra (3.21).

The construction of such a family of non-zero projectors allows us to rewrite the enlarged algebra $\mathcal{A}_{\mathcal{R}}$ in its standard form:

$$\mathcal{A}_R \cong \mathcal{B}(\mathcal{H}') \otimes P\mathcal{A}_R P \,, \tag{3.30}$$

where we have chosen $P = P_{E_0,\Delta E}$. Now, we can RMT complete this description by replacing $\rho_0(E)$ with the density of states $\rho(E)$ of a random matrix theory with $\overline{\rho(E)} = \rho_0(E)$.[6] Below, we will argue that

$$\mathcal{B}(\overline{\mathcal{H}'}) \otimes \overline{P\mathcal{A}_R P} = \mathcal{B}(\mathcal{H}_{\rm BH}) \otimes 1_{\overline{P\mathcal{H}}} \,, \tag{3.31}$$

up to small corrections suppressed by powers of $\exp\left(-S_{\rm BH}\right)$. Here $\mathcal{H}_{\rm BH}$ is the RMT completed finite-dimensional Hilbert space defined in (3.14). Therefore, the RMT completed cross product algebra, after an ensemble averaging, reduces to a type I_d algebra!

The result in (3.31) is obtained as follows: First, we have to show that the second tensor factors agree on both sides of the equation, that is, $\overline{P\mathcal{A}_R P} = \mathbb{C}\overline{P}$. Before RMT completion we have

$$P\hat{a}P = \left(\int \mathrm{d}E \rho_0(E)\chi_{E_0,\Delta E}(E)\ |E\rangle\langle E|\right) \hat{a} \left(\int \mathrm{d}E' \rho_0(E')\chi_{E_0,\Delta E}(E')\ |E'\rangle\langle E'|\right) \,, \tag{3.32}$$

where $\hat{a} \in \mathcal{A}_R$. By using the general form of $\hat{a}$ (3.24), we find that

$$P\hat{a}P = \int \mathrm{d}s \int \mathrm{d}E\mathrm{d}E' \rho_0(E)\rho_0(E')\chi_{E_0,\Delta E}(E)\chi_{E_0,\Delta E}(E') e^{i(E'-E_0)s} \left\langle E|a(s)|E'\right\rangle |E\rangle\langle E'|. \tag{3.33}$$

This expression can then be RMT completed by replacing the density of states. Taking an ensemble average of the resulting expression, we get

$$\overline{P\hat{a}P} = \int \mathrm{d}s \int \mathrm{d}E\mathrm{d}E'\ \overline{\rho(E)\rho(E')}\ \chi_{E_0,\Delta E}(E)\chi_{E_0,\Delta E}(E') e^{i(E'-E_0)s} \left\langle E|a(s)|E'\right\rangle |E\rangle\langle E'|. \tag{3.34}$$

The presence of the characteristic functions restricts the energy values that contribute to the integral to a narrow range centered on E_0. This means we have to go beyond the Poisson approximation in (3.9) to evaluate the integral and instead we work with a Gaussian Unitary Ensemble (GUE),

$$\overline{\rho(E)\rho\left(E'\right)} = \rho_0(E)\rho_0\left(E'\right) + \rho_0(E)\delta\left(E - E'\right) - \frac{\sin^2\left(\pi\rho_0(E_{\rm avg})\left(E - E'\right)\right)}{\pi^2\left(E - E'\right)^2} \,, \tag{3.35}$$

where $E_{\rm avg} = (E + E')/2$ is the average energy. The third term on the right hand side is referred to as the *sine-kernel* and encodes the level repulsion of the RMT. This term is present in all

[6] See also [74], where the inclusion of a Poisson distribution in the context of operator algebras and third quantization was discussed.

Gaussian ensembles in the $E \to E'$ limit [75], so the choice of a Gaussian unitary ensemble is not restrictive.

Before we continue with the computation of (3.34), let us examine the sine kernel contribution to the averaged two-point function (3.35). In particular, let us look at the case where $E_{\text{avg}} \gg |E - E'|$. This limit corresponds to $E_0 \gg \Delta E$, so it is precisely the range of energies that contribute to the integral (3.34). In this case, we can approximate the sine-kernel with a Gaussian function as follows:

$$\overline{\rho(E)\rho\left(E'\right)} = \rho_0(E_{\text{avg}})^2 \left[1 - \exp\left(-\frac{\pi^2 \rho_0(E_{\text{avg}})^2 \left(E - E'\right)^2}{3}\right)\right] + \rho_0(E)\delta\left(E - E'\right). \quad (3.36)$$

The Gaussian approximation to the sine kernel is obtained by matching (3.35) and (3.36) up to second order in a Taylor expansion in the parameter $\rho_0(E_{\text{avg}})\left(E - E'\right)$. Gaussian approximations to sinc-type functions are widely used in optics and signal processing to enable analytic treatment of diffraction and phase-matching problems [76]. In our case, this approximation allows us to obtain closed-form expressions for integrals.

It is now easy to see how RMT corrections introduce level repulsion in the large N theory. Let us ignore the delta function term in (3.36) for the moment. When the energy difference is larger than $\rho_0(E_{\text{avg}})^{-1}$, the Gaussian term can be dropped, and the averaged two-point function of the density of states is equal to the product of the density of states. Thus, for large energy separations, the spectrum behaves as if it were uncorrelated. In contrast, when the energy difference drops below $\rho_0(E_{\text{avg}})^{-1}$, the averaged two-point function becomes parametrically suppressed.

Now let us return to the computation of the integral in equation (3.34). Plugging in the averaged two-point function, we get

$$\begin{aligned}\overline{P\hat{a}P} = \int \mathrm{d}s \int \mathrm{d}E \mathrm{d}E' \; \rho_0(E_{\text{avg}})^2 &\left[1 - \exp\left(-\frac{\pi^2 \rho_0(E_{\text{avg}})^2 \left(E - E'\right)^2}{3}\right)\right] \\ &\chi_{E_0,\Delta E}(E)\chi_{E_0,\Delta E}(E')e^{i(E'-E_0)s} \left\langle E|a(s)|E'\right\rangle \; |E\rangle\langle E'| \\ &+ O(\rho_0(E_0)^{-1}) \, .\end{aligned} \quad (3.37)$$

The $O(\rho_0(E_0)^{-1})$ correction term in the above expression comes from the delta function term in (3.36) and is exponentially suppressed in the Bekenstein-Hawking entropy of the black hole, as will be clear from equation (3.53) below. This 'contact' term in the density of states is also responsible for the exponentially suppressed plateau term in the spectral form factor.

It is convenient to change the integration variables from (E, E') to (E_{avg}, ω), where we define $\omega = E - E'$. We now adopt a standard assumption from the RMT literature. Since $E_0 \gg \Delta E$, we assume that the matrix elements and the states depend only on the average energy $E_{\rm avg}$. This diagonal approximation gives us

$$\overline{P\hat{a}P} \simeq \int \mathrm{d}s \int_{E_0-\Delta E}^{E_0+\Delta E} \mathrm{d}E_{\rm avg}\ \rho_0(E_{\rm avg})^2 e^{i(E_{\rm avg}-E_0)s}\ \langle E_{\rm avg}|a(s)|E_{\rm avg}\rangle \\ \int_{-2\widetilde{\Delta E}}^{2\widetilde{\Delta E}} \mathrm{d}\omega \left[1-\exp\left(-\frac{\pi^2\rho_0(E_{\rm avg})^2\omega^2}{3}\right)\right] |E_{\rm avg}\rangle\langle E_{\rm avg}|\,, \tag{3.38}$$

where we have introduced a new quantity $\widetilde{\Delta E} = \Delta E - |E_{\rm avg} - E_0|$ to express the above equation compactly. Evaluating the ω integral in closed form yields

$$\overline{P\hat{a}P} = \int \mathrm{d}s \int_{E_0-\Delta E}^{E_0+\Delta E} \mathrm{d}E_{\rm avg}\ \rho_0(E_{\rm avg})^2 e^{i(E_{\rm avg}-E_0)s}\ \langle E_{\rm avg}|a(s)|E_{\rm avg}\rangle \\ \left(4\widetilde{\Delta E} - \frac{\sqrt{\frac{3}{\pi}}\mathrm{erf}\left(\frac{2\pi\widetilde{\Delta E}\rho_0(E_{\rm avg})}{\sqrt{3}}\right)}{\rho_0(E_{\rm avg})}\right) |E_{\rm avg}\rangle\langle E_{\rm avg}|\,. \tag{3.39}$$

The functions $\rho_0(E_{\rm avg})$ and $\langle E_{\rm avg}|a(s)|E_{\rm avg}\rangle$ vary slowly over the narrow integration range, so we approximate them by their values at E_0 and pull them out of the $E_{\rm avg}$ integral to obtain

$$\overline{P\hat{a}P} \approx \left(\Delta E^2 \int \mathrm{d}s\ \rho_0(E_0)\,\langle E_0|a(s)|E_0\rangle\right) \rho_0(E_0)|E_0\rangle\langle E_0|\,. \tag{3.40}$$

The same steps lead to the expression $\overline{P} \approx \rho_0(E_0)|E_0\rangle\langle E_0|$ for the avaraged projector and therefore, we have $\overline{P\mathcal{A}_R P} \simeq \mathbb{C}\overline{P}$, as advertised.

We have shown that P acts as a minimal projector after RMT completion, but our final result followed from approximating an integral by its value at a point in its domain of integration. This suggests that another projector onto an even narrower energy window,

$$Q = \int \mathrm{d}E\rho(E)\chi_{E_0,\Delta E'}(E)\ |E\rangle\langle E|\,, \quad \text{with } \Delta E' < \Delta E \tag{3.41}$$

will also give us $\overline{Q\mathcal{A}_R Q} \approx \mathbb{C}\overline{Q}$. Clearly $Q < P$, making P a non-minimal projector, but when we RMT complete and average over the projectors, the situation is different. Let us first assume that $\Delta E' \lesssim \Delta E$, i.e. the new energy range is only a little bit narrower than before. In this case, we can go through the same computations to find that

$$\overline{Q\hat{a}Q} \approx \overline{P\hat{a}P} \implies \overline{Q} \approx \overline{P}\,. \tag{3.42}$$

When $\Delta E' \ll \Delta E$, however, the behaviour changes in an interesting way. In this case, contributions from the two terms inside the square bracket in (3.38) cancel against each other, leading to a parametric suppression in the final result,

$$\overline{Q\hat{a}Q} \sim \left(\frac{\Delta E'}{\Delta E}\right)^2 \overline{P\hat{a}P}\,. \tag{3.43}$$

Therefore, we arrive at the statement

$$\forall Q < P\,, \qquad \text{either} \quad \overline{Q} \approx \overline{P} \quad \text{or} \quad \overline{Q} \approx 0\,. \tag{3.44}$$

In this sense, $\overline{P}$ behaves as a minimal projector, as any subprojection $\overline{Q}$ gives negligible matrix elements or is approximately equal to $\overline{P}$. This is a direct consequence of the level repulsion in RMT. When the energy separation is below the characteristic scale of level repulsion in the theory, the energy levels are effectively discrete.

Now we return to (3.31) and show that first tensor factors also match, i.e. $\mathcal{B}(\overline{\mathcal{H}'}) = \mathcal{B}(\mathcal{H}_{\rm BH})$. We can construct a projector from the discrete Fourier transform of elements of $\mathcal{B}(\mathcal{H}_{\rm BH})$ as follows:

$$\widetilde{P}_{E_i} = 2\pi \sum_{j=1}^{k} e^{-iE_i t_j}\, e^{iH_R t_j}\,, \qquad t_j = j t_1\,. \tag{3.45}$$

The energy resolution of $\widetilde{P}_{E_i}$ is of order $1/(kt_1)$. Since $\mathcal{H}_{\rm BH}$ is finite dimensional, with dimension $e^{S_{\rm BH}}$, and $t_1 = O(\beta)$, this resolution matches that of the minimal projectors $P_{E_i,\Delta E}$ (we will show this in (3.53)). Therefore, the projectors $P_{E_i,\Delta E}$ can be reconstructed from operators in $\mathcal{B}(\mathcal{H}_{\rm BH})$. This establishes that $\mathcal{B}(\overline{\mathcal{H}'}) \subset \mathcal{B}(\mathcal{H}_{\rm BH})$. Now let us look at the reverse inclusion. The right Hamiltonian can be approximated as

$$h_R \approx \sum_i (E_i - E_0)\; P_{E_i,\Delta E}\,. \tag{3.46}$$

When we RMT complete the Hilbert spaces, we introduce an effective level spacing of ΔE through level repulsion, and as a result, (3.46) becomes an excellent approximation. This gives us $\mathcal{B}(\overline{\mathcal{H}'}) \subset \mathcal{B}(\mathcal{H}_{\rm BH})$. Therefore, we have $\mathcal{B}(\overline{\mathcal{H}'}) = \mathcal{B}(\mathcal{H}_{\rm BH})$, concluding the proof of (3.31).

Now let us revisit the computation of the dimensionality of the RMT-completed Hilbert space $\mathcal{H}_{\rm BH}$ outlined in Section 3.1. Our goal is to reformulate this calculation in the language of operator algebras. We start with the microcanonical TFD state $|\hat{\Psi}\rangle$ defined in equation (3.21). We denote the density matrix associated to this state by $\rho_{\hat{\Psi}}$. Then for every operator $\hat{a}$ in the crossed product algebra, the trace of the operator in the state $|\hat{\Psi}\rangle$ is given by (3.22). Since we are dealing with a type II_∞ algebra, the trace is non-unique with the ambiguity encoded in the constant c in (3.22). In our case, however, there is a natural way to fix this constant. The key point is that the trace on the crossed product algebra induces a trace on the factor $\mathcal{B}(\mathcal{H}')$, which in turn defines an inner product on $\mathcal{H}'$. We can therefore fix the normalization by imposing the condition that the trace of the "minimal" projector P in the microcanonical TFD state is unity,[7]

$$\mathrm{tr}[\rho_{\hat{\Psi}} P] = 1\,. \tag{3.47}$$

[7]The ambiguity in the definition of the trace arises because the decomposition of a type II_∞ algebra into

Using the definition (3.21) of the state $|\hat{\Psi}\rangle$, we have

$$\mathrm{tr}[\rho_{\hat{\Psi}} P] = e^c \int_{-\infty}^{\infty} \mathrm{d}x \; (f(x))^2 \langle x|\langle\Psi|P|\Psi\rangle|x\rangle \, . \tag{3.48}$$

We now express the projector P in terms of its Fourier representation,

$$P = \int \mathrm{d}s \; b(s) e^{is(X+\hat{h}+E_0)} \, , \tag{3.49}$$

where $b(s)$ are the Fourier coefficients that implement the finite energy range of the characteristic function $\chi_{E_0,\Delta E}$. Substituting this into the trace gives

$$\mathrm{tr}[\rho_{\hat{\Psi}} P] = e^c \int_{-\infty}^{\infty} \mathrm{d}x \int \mathrm{d}s \; b(s)(f(x))^2 \; \langle\Psi|e^{is(x+\hat{h}+E_0)}|\Psi\rangle \, . \tag{3.50}$$

Since $\hat{h}|\Psi\rangle = 0$, the matrix element simplifies, and we obtain

$$\mathrm{tr}[\rho_{\hat{\Psi}} P] = e^c \int_{-\infty}^{\infty} \mathrm{d}x \; (f(x))^2 \int \mathrm{d}s \; b(s) e^{is(x+E_0)} = e^c \int_{-\infty}^{\infty} \mathrm{d}x \; (f(x))^2 \chi_{E_0,\Delta E}(x+E_0) \, . \tag{3.51}$$

Here the integral over s is the Fourier transform of $b(s)$, which reduces to the characteristic function χ. Since $f(x)$ is slowly varying on the scale of ΔE, we can pull it out of the integral and evaluate it at the center. We then obtain the normalization condition

$$\rho_0(E_0) \simeq e^c (f(0))^2 \, . \tag{3.52}$$

The normalization of the density of states can also be read off from (3.15), giving

$$\rho_0(E_0) \simeq e^{S_{\mathrm{BH}}} (f(0))^2 \, . \tag{3.53}$$

Comparing these expressions, we find

$$c \simeq S_{\mathrm{BH}} \, . \tag{3.54}$$

As in the previous subsection, we define time-shifted thermofield states by evolving with the right Hamiltonian,

$$|\hat{\Psi}(t)\rangle \equiv e^{i\hat{h}t} e^{iXt} |\hat{\Psi}\rangle \, . \tag{3.55}$$

We can associate density matrices $\rho_{\hat{\Psi}(t)}$ to these states. Using the definition (3.22) together with the cyclicity of the trace, we find that

$$\rho_{\hat{\Psi}(t)} = e^{i\hat{h}t} e^{iXt} \rho_{\hat{\Psi}} e^{-i\hat{h}t} e^{-iXt} \, . \tag{3.56}$$

the standard form (3.30) is not unique (see Section 3.6 of [77]). In general, one may choose any non-minimal projector P to obtain such a decomposition and then impose the condition (3.47) to fix the trace, leading to multiple possible choices for the constant c. However, the RMT completion produces a minimal projector, which in turn provides a canonical choice for c.

Now consider the quantity

$$\mathrm{tr}\left[\rho_{\hat{\Psi}(t_1)}\rho_{\hat{\Psi}(t_2)}\right] , \tag{3.57}$$

which equals the square of the overlap in equation (3.10). From the definition of the trace, we find that

$$\mathrm{tr}\left[\rho_{\hat{\Psi}(t_1)}\rho_{\hat{\Psi}(t_2)}\right] = e^{c}\langle\hat{\Psi}|e^{-ih_R t_1}\rho_{\hat{\Psi}}e^{ih_R t_1}|\hat{\Psi}\rangle\,. \tag{3.58}$$

Expanding the right Hamiltonian in terms of the density of states, we get

$$e^{-ih_R t_1}\rho_{\hat{\Psi}}e^{ih_R t_1} = \int \mathrm{d}E\mathrm{d}E'\ \rho_0(E)\rho_0(E')\ e^{i(t_2-t_1)(E-E')}\langle E|\rho_{\hat{\Psi}}|E'\rangle\ |E\rangle\langle E'|\,. \tag{3.59}$$

Now, let us take an average of this quantity in the RMT completion. We can use the Poisson distribution (3.9) to get the connected component

$$\left.\overline{\mathrm{tr}\left[\rho_{\hat{\Psi}(t_1)}\rho_{\hat{\Psi}(t_2)}\right]}\right|_c = e^{c}\langle\hat{\Psi}|\rho_{\hat{\Psi}}|\hat{\Psi}\rangle\,. \tag{3.60}$$

Then by the definition of the von Neumann entropy (3.23), we have

$$\left.\overline{\mathrm{tr}\left[\rho_{\hat{\Psi}(t_1)}\rho_{\hat{\Psi}(t_2)}\right]}\right|_c = e^{-S_{\mathrm{vN}}(\rho_{\hat{\Psi}})}\,. \tag{3.61}$$

The von Neumann entropy can be shown to be equal to [17, 27]

$$S_{\mathrm{vN}}(\rho_{\hat{\Psi}}) = c - \langle\hat{\Psi}|\log|f\left(h_R\right)|^2|\hat{\Psi}\rangle = S_{\mathrm{BH}} + S_{\log}\,, \tag{3.62}$$

where we have used (3.54) to fix the value of c in the final step. The second term $S_{\log}$ is the "fluctuation entropy," which captures the universal logarithmic corrections to the black hole entropy [78]. The dimensionality of the Hilbert space $\overline{H_{\mathrm{BH}}}$ is given by $d = e^{S_{\mathrm{BH}}+S_{\log}}$.

Holographic duality allows us to carry out a similar construction in the bulk. In the case of an eternal black hole, the right algebra corresponds to the algebra of a massive scalar field on the right wedge of the spacetime. Instead of the thermofield state, we have the Hartle-Hawking state. The modular Hamiltonian generates boosts inside the wedge. The analogue of the right CFT Hamiltonian will be played by the right ADM Hamiltonian. Going through all the steps above, we would arrive at a type I_d algebra in the bulk.

3.3 Complexity as a Probe of the Emergent Geometry

Once the microstates of the theory have been constructed, it is natural to ask when the low-energy semiclassical description breaks down. In the language of time-shifted TFD states, this corresponds to where the non-perturbative RMT corrections to the density of states dominate. We note from (3.11) that the overlap of the time-shifted TFD states is the spectral form factor,

$$\overline{|\langle \mathrm{TFD}(t_1)|\mathrm{TFD}(t_2)\rangle|^2} = \mathrm{SFF}(|t_1 - t_2|, \beta)\,. \tag{3.63}$$

The spectral form factor of RMT has a distinct behaviour [58]. Plotted as a function of time, there is an initial dip, followed by a ramp and plateau. During the dip, the SFF decays for a long time, and only when $t \sim e^{O(S_{\mathrm{BH}})}$ do the ramp and plateau become visible. The late-time ramp and the plateau are a result of the sine-kernel and the Dirac delta terms dominating the averaged two-point function of the density of states (3.35). At this exponential timescale the semiclassical description breaks down.[8]

A natural way to reframe these observations is through the notion of complexity. In particular, consider Krylov complexity [79], which assigns a "size" to an operator under Hamiltonian evolution. In chaotic systems, operator complexity exhibits a generic pattern, growing linearly with time for a long period, and saturating at times of exponential order in the system's entropy [80]. The ramp and plateau in the SFF are responsible for this saturation of complexity (see [81] for details). From this perspective, the semiclassical description breaks down if we probe the black hole spacetime with an operator whose complexity is of exponential order in the Bekenstein-Hawking entropy. See [82–84] for related discussions. This idea can be made very explicit by using the Complexity=Volume (CV) prescription [85, 86], where bulk complexity is defined as the volume of a spacelike extremal codimension-one surface passing through the interior of the black hole. In two-dimensional spacetimes, there are bulk wormhole corrections to the semiclassical volume computations when the boundary anchoring time of the surface reaches $e^{O(S_{\mathrm{BH}})}$ [81], and this leads to the saturation of complexity. Similar behaviour is found in higher dimensions [25, 87]. This breakdown of the semiclassical picture has important consequences. The region where the semiclassical volume calculation fails is precisely the region where certain *trapped extremal surfaces* appear [88]. These surfaces lead to null geodesic incompleteness in the interior and signal the presence of the black hole singularity. The corrections responsible for the saturation of holographic complexity must therefore also modify the volume computation that gives rise to these pathological surfaces, hinting at a possible resolution of black hole singularities.

A puzzling feature of the geometry probed by an operator is that it appears to be highly *observable dependent*. At first glance, this may seem troubling but it lies at the heart of the principle of black hole complementarity [89]. When a quantum black hole is probed with

[8] As emphasized in the Introduction, the semiclassical description is here taken to include perturbative quantum gravity corrections but non-perturbative corrections are neglected. It is important to distinguish this from the small but non-zero G_N limit of the full theory, where non-perturbative corrections are exponentially suppressed but nevertheless always present.

a "simple operator", the resulting spacetime looks like the classical geometry. There is an event horizon, and an infalling observer experiences a smooth infall. However, when the black hole is probed with a "complex operator", the semiclassical limit breaks down. One may encounter a wormhole or a baby universe emission. The crucial point is that these different observable-dependent descriptions are complementary — each measurement probes a different operational regime.

4 Discussion

Operator algebras are useful for the study of quantum gravity and the emergence of spacetime as these techniques eliminate the need for (Euclidean) path integrals and their saddle-point approximations, and do not rely on formulating the theory in terms of a Lagrangian. In this framework, Hilbert spaces emerge as representations of operator algebras. This perspective is particularly useful, since treating Hilbert spaces as fundamental objects leads to conceptual puzzles such as the factorisation problem (see, for example, [90, 91]).

A remarkable feature of general relativity is that gravity is encoded in the curvature of spacetime through the equivalence principle and Einstein's field equations. Our analysis in Section 2 shows that both the equivalence principle and the field equations follow from the existence of multiple local Rindler algebras and locally stationary states, along with a well-defined large-mass limit for the matter field correlation functions. This provides a characterization of gravity purely in terms of operator algebras, which are the natural building blocks of quantum mechanics. The reformulation of geometry carries philosophical implications, as gravity is no longer viewed as fundamental but instead emerges from the operator algebras of *matter fields*. An important further step is to extend our analysis to more realistic matter fields of the kind present in our universe and to understand how the constructions in this paper generalize to that setting.

We would like to emphasize that, in Section 2, we have not assumed the existence of a boundary dual. In particular, the existence of a smooth d-dimensional spacetime in the boundary theory would significantly simplify the reconstruction of the bulk metric and curvature tensors, since boundary points could then be used to localize bulk points as in, for example, [92]. One could then directly use the smooth differentiable structure of the boundary to extract the metric and curvature tensors [93]. Our approach deliberately avoids making this assumption.

In Section 3, we showed how a type I algebra can be obtained from a type III algebra by a random matrix theory completion of the crossed product algebra. There is mounting evidence for randomness and the necessity of averaging in operator-algebraic descriptions of quantum gravity, see e.g. [94–96]. The RMT construction restores the discreteness of the spectrum that is lost in the large N limit and naturally leads to chaos and thermalization. Once these effects are incorporated, the completed algebra also captures non-perturbative contributions from bulk wormholes. An important aspect of our RMT implementation is that it does not call for a modification of the standard AdS/CFT correspondence, which has passed numerous precision tests. We use the effective RMT description to capture the large N semiclassical limit of the theory, which is a standard strategy for understanding generic chaotic systems and is not restricted to gravity.

Acknowledgments

We would like to thank Rahul Poddar for useful discussions. VM is supported by a doctoral grant from the University of Iceland Science Park.

A Basic Definitions and von Neumann Algebras

In this appendix, we provide a brief review of some key definitions and properties of von Neumann algebras. We recommend [73, 97] for a more comprehensive treatment.

Consider a Hilbert space $\mathcal{H}$. We will denote the algebra of all bounded local operators acting on this Hilbert space by $\mathcal{B}(\mathcal{H})$. A $*$-*subalgebra* is a subalgebra of $\mathcal{B}(\mathcal{H})$ that is closed under scalar multiplication, operator multiplication, operator addition, and adjoints. It also contains the identity element. The commutant algebra $\mathcal{M}'$ is the set of all operators in $\mathcal{B}(\mathcal{H})$ that commute with every element of a subalgebra $\mathcal{M}$. A *von Neumann algebra* $\mathcal{M}$ is a subalgebra of $\mathcal{B}(\mathcal{H})$ that is equal to its own double commutant, that is, $\mathcal{M} = \mathcal{M}''$. A von Neumann algebra $\mathcal{M}$ is a *factor* if the center $\mathcal{Z} \equiv \mathcal{M} \cap \mathcal{M}'$ is composed of scalar multiples of the identity operator.

A function ω from an algebra $\mathcal{M}$ to the complex numbers is called a *state* if it is

1. linear : $\omega(\alpha a + \beta b) = \alpha\omega(a) + \beta\omega(b)$, for all $a, b \in \mathcal{M}$.
2. positive : $\omega(a^* a) \geq 0, \ \forall a \in \mathcal{M}$.
3. normalized : $\omega(1) = 1$.

An orthogonal projector P, or simply a *projector*, is an element of a von Neumann algebra $\mathcal{M}$ with the properties $P = P^2 = P^*$, where P^* is the adjoint operator. A pairwise orthogonal set of projectors $\{P_i\}$ satisfies $P_i P_j = \delta_{ij} P_j$ for all i, j.

Two projectors P and Q are equivalent if and only if there exists an operator $V \in \mathcal{M}$ with $VV^* = P$ and $V^*V = Q$. We denote this relation by $P \sim Q$. We write $P > Q$ if the projectors P and Q are not equivalent and $P\mathcal{H} \supset Q\mathcal{H}$. We then refer to Q as a proper subprojector of P.

A projector P is finite if every non-zero proper subprojector $Q < P$ is inequivalent to P. A non-zero projector is *minimal* if $P\mathcal{M}P = \mathbb{C}P$. Using this definition, we can classify von Neumann algebras into the following categories

1. **Type I** : contains a non-zero minimal projector P.
2. **Type II** : contains non-zero finite projectors, but no non-zero minimal projectors.
3. **Type III** : contains no non-zero finite projectors.

We call a vector $|\omega\rangle \in \mathcal{H}$ *cyclic* if the set of $a|\omega\rangle$, for all $a \in \mathcal{M}$, is dense in $\mathcal{H}$. The vector is *separating* if $a|\omega\rangle = 0$ iff $a = 0$. If $|\omega\rangle$ is cyclic and separating, then Tomita-Takesaki theory guarantees the existence of two operators Δ and J [98]. The first operator Δ is called the *modular operator* while the second operator is called *modular conjugation*.

The modular operator generates modular flows in the von Neumann algebra:

$$\Delta^{it}\mathcal{M}\Delta^{-it} = \mathcal{M}\,, \qquad \forall t \in \mathbb{R}\,. \tag{A.1}$$

The modular Hamiltonian $\hat{h}$ is related to the modular operator through the relation

$$\Delta = e^{-\hat{h}}\,. \tag{A.2}$$

The modular conjugation takes elements of the algebra to its commutant:

$$J\mathcal{M}J = \mathcal{M}'\,. \tag{A.3}$$

The notion of half-sided modular inclusions was introduced by Wiesbrock [99]. Consider a subalgebra $\mathcal{N} \subset \mathcal{M}$ for a von Neumann algebra $\mathcal{M}$ with a common cyclic separating vector $|\omega\rangle$. Let us also assume that the subalgebra is preserved under the modular flow of $\mathcal{M}$:

$$\Delta^{it}_{\mathcal{M}}\mathcal{N}\Delta^{-it}_{\mathcal{M}} \subset \mathcal{N} \quad \forall\, t \leq 0. \tag{A.4}$$

Half-sided modular inclusions are generated by a one-parameter family of operators given by

$$U(s) = e^{-iGs}\,, \tag{A.5}$$

where

$$2\pi G = \hat{h}_{\mathcal{M}} - \hat{h}_{\mathcal{N}} \geq 0\,. \tag{A.6}$$

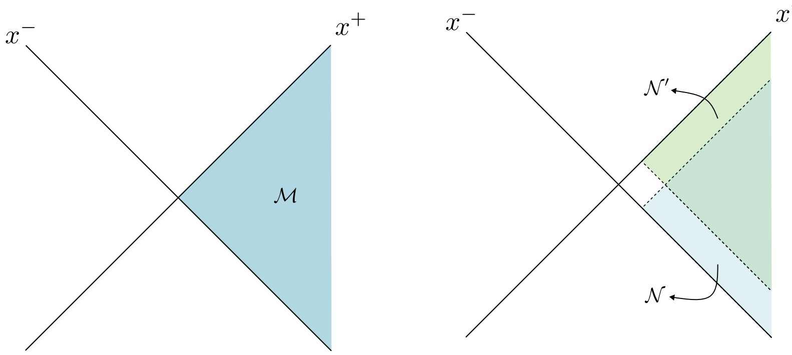

Figure 3. The figure on the left shows the entire right wedge algebra $\mathcal{M}$. On the right are two subalgebras $\mathcal{N}, \mathcal{N}'$ obtained by shifting the right wedge along the null directions.

Here $\hat{h}_{\mathcal{M},\mathcal{N}}$ are the modular Hamiltonians of the two algebras. Now we will study an example to see how the boosts, along with the half-sided modular translations $U(s)$, can be used to obtain the generators of the spacetime.

Consider a $1+1$-dimensional Minkowski spacetime written in null coordinates $x^{\pm}$. Let us take a massive scalar field whose support is restricted to the right Rindler wedge defined by $x^+ \geq 0$ and $x^- \leq 0$, and denote the corresponding algebra of operators by $\mathcal{M}$. Now introduce a shifted wedge algebra $\mathcal{N}$, consisting of operators supported in the region $x^+ \geq 0$ and $x^- \leq -1$ (see Figure 3). One can then show that the modular Hamiltonian associated with $\mathcal{M}$ generates the Rindler boost K in the right wedge, while the half-sided modular translations associated with the inclusion $\mathcal{N} \subset \mathcal{M}$ are given by [14]

$$U_+(s) = e^{-isP^+}\,, \tag{A.7}$$

where P^+ is the generator of translations along x^+.

If we choose another subalgebra $\mathcal{N}'$ composed of operators with support in the region $x^+ \geq 1$ and $x^- \leq 0$ (see Figure 3), then we will end up with another half-sided modular translation

$$U_-(s) = e^{-isP^-}\,. \tag{A.8}$$

The generators $\{K, P^{\pm}\}$ close to form the two-dimensional Poincaré algebra. In Appendix B, we demonstrate that the operator algebraic construction of the Poincaré algebra generalizes to higher dimensions.

B Construction of the Poincaré Algebra

Let us show how the Poincaré generators of a globally flat spacetime can be constructed from operators restricted to multiple Rindler wedges. Consider a massive scalar field living on a $d+1$-dimensional spacetime. We will use the Cartesian coordinates $(t, x_1, x_2, ...)$ to label the points on the spacetime.

Now let us look at the operators restricted to a Rindler wedge $\mathcal{R}_i = \{x_i > |t|\}$. As reviewed in Appendix A, we can construct the generators of the null translations $t \pm x_i$ using the half-sided modular translations $U_\pm(s)$. This then gives us

$$e^{-isX_0} = U_+(s/2)U_-(s/2)\,, \qquad e^{-isX_i} = U_+(s/2)U_-(-s/2)\,, \tag{B.1}$$

where X_0 generates time translations, while X_i generates translations along the spatial direction. By repeating this construction with a different wedge algebra $\mathcal{R}_j$, we can similarly obtain a generator along another spatial direction. In this way, we build a set of translation generators, denoted by $\{X_j\}$. From this set, we can select d mutually orthogonal spatial generators by imposing the condition

$$\lim_{s_1, s_2 \to 0} \frac{\partial^2}{\partial s_1 \partial s_2} \sigma_{jk}(i_{s_1}, i_{s_2}) = \delta_{jk}\,, \tag{B.2}$$

where $\sigma_{jk}(i_{s_1}, i_{s_2})$ is the Synge world function extracted from the correlator

$$\langle\omega| \left(e^{is_1 X_j} \mathcal{O}_i e^{-is_1 X_j}\right) \left(e^{is_2 X_k} \mathcal{O}_i e^{-is_2 X_k}\right) |\omega\rangle \equiv G_{jk}(i_{s_1}, i_{s_2})\,. \tag{B.3}$$

Here $\mathcal{O}_i$ is an operator that lies in both $\mathcal{W}_j$ and $\mathcal{W}_k$. We have used (2.12) to arrive at the orthogonality condition (B.2).

Next, let us denote by K_j the boost operator associated with the wedges of each of these d spatial translations. Together, the boosts K_j, the mutually orthogonal spatial translations X_j, and the time translation generator X_0 furnish the boosts and translations of the local Poincaré algebra. Using the commutation relations

$$[K_j, K_k] = -i\epsilon_{jkl} J_l, , \tag{B.4}$$

we can then obtain the rotation generators J_k, thereby recovering the full Poincaré algebra.

References

[1] T. Jacobson, *Thermodynamics of space-time: The Einstein equation of state*, *Phys. Rev. Lett.* **75** (1995) 1260 [gr-qc/9504004].

[2] T. Padmanabhan, *Thermodynamical Aspects of Gravity: New insights*, *Rept. Prog. Phys.* **73** (2010) 046901 [0911.5004].

[3] E.P. Verlinde, *On the Origin of Gravity and the Laws of Newton*, *JHEP* **04** (2011) 029 [1001.0785].

[4] M. Van Raamsdonk, *Building up spacetime with quantum entanglement*, *Gen. Rel. Grav.* **42** (2010) 2323 [1005.3035].

[5] J. Maldacena and L. Susskind, *Cool horizons for entangled black holes*, *Fortsch. Phys.* **61** (2013) 781 [1306.0533].

[6] R. Bousso, X. Dong, N. Engelhardt, T. Faulkner, T. Hartman, S.H. Shenker et al., *Snowmass White Paper: Quantum Aspects of Black Holes and the Emergence of Spacetime*, 2201.03096.

[7] J.M. Maldacena, *The Large N limit of superconformal field theories and supergravity*, *Adv. Theor. Math. Phys.* **2** (1998) 231 [hep-th/9711200].

[8] E. Witten, *Anti-de Sitter space and holography*, *Adv. Theor. Math. Phys.* **2** (1998) 253 [hep-th/9802150].

[9] S.S. Gubser, I.R. Klebanov and A.M. Polyakov, *Gauge theory correlators from noncritical string theory*, *Phys. Lett. B* **428** (1998) 105 [hep-th/9802109].

[10] A. Connes, *Noncommutative Geometry*, Academic Press, San Diego, CA (1994).

[11] A. Connes, *Geometry from the spectral point of view*, *Letters in Mathematical Physics* **34** (1995) 203.

[12] D.A. Vogan, Jr., *Review of "lectures on the orbit method" by A. A. Kirillov*, *Bulletin of the American Mathematical Society* **42** (2005) 535.

[13] M. Kac, *Can one hear the shape of a drum?*, *The American Mathematical Monthly* **73** (1966) 1.

[14] S.A.W. Leutheusser and H. Liu, *Emergent Times in Holographic Duality*, *Phys. Rev. D* **108** (2023) 086020 [2112.12156].

[15] S. Leutheusser and H. Liu, *Causal connectability between quantum systems and the black hole interior in holographic duality*, *Phys. Rev. D* **108** (2023) 086019 [2110.05497].

[16] S. Ouseph, K. Furuya, N. Lashkari, K.L. Leung and M. Moosa, *Local Poincaré algebra from quantum chaos*, *JHEP* **01** (2024) 112 [2310.13736].

[17] E. Witten, *Gravity and the crossed product*, *JHEP* **10** (2022) 008 [2112.12828].

[18] K. Furuya, N. Lashkari, M. Moosa and S. Ouseph, *Information loss, mixing and emergent type III_1 factors*, *JHEP* **08** (2023) 111 [2305.16028].

[19] S. Banerjee, J. Erdmenger and J. Karl, *Nonlocality induces isometry and factorisation in holography*, *Phys. Rev. D* **112** (2025) L021902 [2411.09616].

[20] J.M. Magan and Q. Wu, *Two types of quantum chaos: testing the limits of the Bohigas-Giannoni-Schmit conjecture*, 2411.08186.

[21] E.P. Wigner, *On the statistical distribution of the widths and spacings of nuclear resonance levels*, *Mathematical Proceedings of the Cambridge Philosophical Society* **47** (1951) 790.

[22] M. Srednicki, *Chaos and Quantum Thermalization*, *Phys. Rev. E* **50** (1994) [cond-mat/9403051].

[23] C. Krishnan and V. Mohan, *Hints of gravitational ergodicity: Berry's ensemble and the universality of the semi-classical Page curve*, *JHEP* **05** (2021) 126 [2102.07703].

[24] V. Balasubramanian, A. Lawrence, J.M. Magan and M. Sasieta, *Microscopic Origin of the Entropy of Astrophysical Black Holes*, *Phys. Rev. Lett.* **132** (2024) 141501 [2212.08623].

[25] V. Balasubramanian, A. Lawrence, J.M. Magan and M. Sasieta, *Microscopic Origin of the Entropy of Black Holes in General Relativity*, *Phys. Rev. X* **14** (2024) 011024 [2212.02447].

[26] A. Climent, R. Emparan, J.M. Magan, M. Sasieta and A. Vilar López, *Universal construction of black hole microstates*, *Phys. Rev. D* **109** (2024) 086024 [2401.08775].

[27] V. Chandrasekaran, G. Penington and E. Witten, *Large N algebras and generalized entropy*, *JHEP* **04** (2023) 009 [2209.10454].

[28] C.J. Fewster and R. Verch, *The Necessity of the Hadamard Condition*, *Class. Quant. Grav.* **30** (2013) 235027 [1307.5242].

[29] B.S. Kay and R.M. Wald, *Theorems on the Uniqueness and Thermal Properties of Stationary, Nonsingular, Quasifree States on Space-Times with a Bifurcate Killing Horizon*, *Phys. Rept.* **207** (1991) 49.

[30] D. Berenstein, Z. Li and J. Simon, *ISCOs in AdS/CFT*, *Class. Quant. Grav.* **38** (2021) 045009 [2009.04500].

[31] L. Fidkowski, V. Hubeny, M. Kleban and S. Shenker, *The Black hole singularity in AdS / CFT*, *JHEP* **02** (2004) 014 [hep-th/0306170].

[32] D. Buchholz and S.J. Summers, *An algebraic characterization of vacuum states in minkowski space*, *Communications in Mathematical Physics* **155** (1993) 449.

[33] D. Buchholz, O. Dreyer, M. Florig and S.J. Summers, *Geometric modular action and space-time symmetry groups*, *Rev. Math. Phys.* **12** (2000) 475 [math-ph/9805026].

[34] Y.A. Rylov, *Geometry without topology as a new conception of geometry*, *International Journal of Mathematics and Mathematical Sciences* **30** (2002) 733.

[35] E. D'Hoker and D.Z. Freedman, *General scalar exchange in AdS(d+1)*, *Nucl. Phys. B* **550** (1999) 261 [hep-th/9811257].

[36] R.B. Paris, *Asymptotics of the Gauss hypergeometric function with large parameters, I*, *J. Class. Anal.* **2** (2013) 183.

[37] R.B. Paris, *Asymptotics of the Gauss hypergeometric function with large parameters, II*, *J. Class. Anal.* **3** (2013) 1.

[38] J.L. Synge, *Relativity: The General Theory*, Series in Physics, North-Holland Publishing Company, Amsterdam (1960).

[39] B.S. DeWitt and R.W. Brehme, *Radiation damping in a gravitational field*, *Annals Phys.* **9** (1960) 220.

[40] H.J. Borchers, *Half-sided modular inclusion and the construction of the poincaré group*, *Communications in Mathematical Physics* **179** (1996) 703.

[41] R. Brunetti, D. Guido and R. Longo, *Modular structure and duality in conformal quantum field theory*, *Commun. Math. Phys.* **156** (1993) 201 [funct-an/9302008].

[42] J.J. Bisognano and E.H. Wichmann, *On the Duality Condition for a Hermitian Scalar Field*, *J. Math. Phys.* **16** (1975) 985.

[43] J.J. Bisognano and E.H. Wichmann, *On the Duality Condition for Quantum Fields*, *J. Math. Phys.* **17** (1976) 303.

[44] Y. Decanini and A. Folacci, *Hadamard renormalization of the stress-energy tensor for a quantized scalar field in a general spacetime of arbitrary dimension*, *Phys. Rev. D* **78** (2008) 044025 [gr-qc/0512118].

[45] M. Visser, *van Vleck determinants: Geodesic focusing and defocusing in Lorentzian space-times*, *Phys. Rev. D* **47** (1993) 2395 [hep-th/9303020].

[46] J. Kudler-Flam, S. Leutheusser and G. Satishchandran, *Generalized black hole entropy is von Neumann entropy*, *Phys. Rev. D* **111** (2025) 025013 [2309.15897].

[47] K. Jensen, J. Sorce and A.J. Speranza, *Generalized entropy for general subregions in quantum gravity*, *JHEP* **12** (2023) 020 [2306.01837].

[48] A.C. Wall, *A proof of the generalized second law for rapidly changing fields and arbitrary horizon slices*, *Phys. Rev. D* **85** (2012) 104049 [1105.3445].

[49] T. Padmanabhan, *Gravity: The inside story*, *Gen. Rel. Grav.* **40** (2008) 2031.

[50] P. Dorau and A. Much, *From Quantum Relative Entropy to the Semiclassical Einstein Equations*, *Phys. Rev. Lett.* **136** (2026) 091602 [2510.24491].

[51] I. Khavkine and V. Moretti, *Algebraic QFT in Curved Spacetime and quasifree Hadamard states: an introduction*, in *Advances in Algebraic Quantum Field Theory*, R. Brunetti, C. Dappiaggi, K. Fredenhagen and J. Yngvason, eds., pp. 191–251 (2014), DOI [1412.5945].

[52] S.J. Summers and R. Verch, *Modular inclusion, the Hawking temperature and quantum field theory in curved space-time*, *Lett. Math. Phys.* **37** (1996) 145.

[53] L. Susskind and J. Uglum, *Black hole entropy in canonical quantum gravity and superstring theory*, *Phys. Rev. D* **50** (1994) 2700 [hep-th/9401070].

[54] F. Kurpicz, N. Pinamonti and R. Verch, *Temperature and entropy–area relation of quantum matter near spherically symmetric outer trapping horizons*, *Lett. Math. Phys.* **111** (2021) 110 [2102.11547].

[55] T.M. Fiola, J. Preskill, A. Strominger and S.P. Trivedi, *Black hole thermodynamics and information loss in two-dimensions*, *Phys. Rev. D* **50** (1994) 3987 [hep-th/9403137].

[56] E. Benedict and S.-Y. Pi, *Entanglement entropy of nontrivial states*, *Annals Phys.* **245** (1996) 209 [hep-th/9505121].

[57] K. Papadodimas and S. Raju, *Local Operators in the Eternal Black Hole*, *Phys. Rev. Lett.* **115** (2015) 211601 [1502.06692].

[58] J.S. Cotler, G. Gur-Ari, M. Hanada, J. Polchinski, P. Saad, S.H. Shenker et al., *Black Holes and Random Matrices*, *JHEP* **05** (2017) 118 [1611.04650].

[59] P. Saad, *Late Time Correlation Functions, Baby Universes, and ETH in JT Gravity*, 1910.10311.

[60] G. Penington, S.H. Shenker, D. Stanford and Z. Yang, *Replica wormholes and the black hole interior*, *JHEP* **03** (2022) 205 [1911.11977].

[61] J.M. Maldacena, *Eternal black holes in anti-de Sitter*, *JHEP* **04** (2003) 021 [hep-th/0106112].

[62] Y. Sekino and L. Susskind, *Fast Scramblers*, *JHEP* **10** (2008) 065 [0808.2096].

[63] S.H. Shenker and D. Stanford, *Black holes and the butterfly effect*, *JHEP* **03** (2014) 067 [1306.0622].

[64] J. Maldacena, S.H. Shenker and D. Stanford, *A bound on chaos*, *JHEP* **08** (2016) 106 [1503.01409].

[65] D.A. Lowe and L. Thorlacius, *Post AdS/CFT*, *JHEP* **12** (2024) 033 [2407.06860].

[66] S. Collier, A. Maloney, H. Maxfield and I. Tsiares, *Universal dynamics of heavy operators in* CFT_2, *JHEP* **07** (2020) 074 [1912.00222].

[67] J. Cotler and K. Jensen, AdS_3 *gravity and random CFT*, *JHEP* **04** (2021) 033 [2006.08648].

[68] A. Belin and J. de Boer, *Random statistics of OPE coefficients and Euclidean wormholes*, *Class. Quant. Grav.* **38** (2021) 164001 [2006.05499].

[69] F.M. Haehl, C. Marteau, W. Reeves and M. Rozali, *Symmetries and spectral statistics in chaotic conformal field theories*, *JHEP* **07** (2023) 196 [2302.14482].

[70] G. Di Ubaldo and E. Perlmutter, AdS_3/RMT_2 *duality*, *JHEP* **12** (2023) 179 [2307.03707].

[71] S. Collier, L. Eberhardt, B. Muehlmann and V.A. Rodriguez, *The Virasoro minimal string*, *SciPost Phys.* **16** (2024) 057 [2309.10846].

[72] D.L. Jafferis, L. Rozenberg and G. Wong, *3d Gravity as a random ensemble*, 2407.02649.

[73] J. Sorce, *Notes on the type classification of von Neumann algebras*, *Rev. Math. Phys.* **36** (2024) 2430002 [2302.01958].

[74] Y. Chen, M. Junge and N. Lashkari, *Operator Algebras and Third Quantization*, 2509.02293.

[75] M.L. Mehta, *Random Matrices*, vol. 142 of *Pure and Applied Mathematics*, Elsevier/Academic Press, Amsterdam, 3rd ed. (2004).

[76] B. Baghdasaryan, F. Steinlechner and S. Fritzsche, *Maximizing the validity of the Gaussian approximation for the biphoton state from parametric down-conversion*, *Phys. Rev. A* **106** (2022) 063714 [2210.02340].

[77] E. Witten, *Why does quantum field theory in curved spacetime make sense? And what happens to the algebra of observables in the thermodynamic limit?*, (2022), DOI [2112.11614].

[78] S. Das, P. Majumdar and R.K. Bhaduri, *General logarithmic corrections to black hole entropy*, *Class. Quant. Grav.* **19** (2002) 2355 [hep-th/0111001].

[79] D.E. Parker, X. Cao, A. Avdoshkin, T. Scaffidi and E. Altman, *A Universal Operator Growth Hypothesis*, *Phys. Rev. X* **9** (2019) 041017 [1812.08657].

[80] J.L.F. Barbón, E. Rabinovici, R. Shir and R. Sinha, *On The Evolution Of Operator Complexity Beyond Scrambling*, *JHEP* **10** (2019) 264 [1907.05393].

[81] L.V. Iliesiu, M. Mezei and G. Sárosi, *The volume of the black hole interior at late times*, *JHEP* **07** (2022) 073 [2107.06286].

[82] C. Akers, N. Engelhardt, D. Harlow, G. Penington and S. Vardhan, *The black hole interior from non-isometric codes and complexity*, *JHEP* **06** (2024) 155 [2207.06536].

[83] C. Krishnan and V. Mohan, *State-independent black hole interiors from the crossed product*, *JHEP* **05** (2024) 278 [2310.05912].

[84] V. Balasubramanian, R.N. Das, J. Erdmenger, J. Karl and H. Verlinde, *Complexity and the Hilbert space dimension of 3D gravity*, 2602.02645.

[85] L. Susskind, *Computational Complexity and Black Hole Horizons*, *Fortsch. Phys.* **64** (2016) 24 [1403.5695].

[86] D. Stanford and L. Susskind, *Complexity and Shock Wave Geometries*, *Phys. Rev. D* **90** (2014) 126007 [1406.2678].

[87] F.F. Gautason, V. Mohan and L. Thorlacius, *Late-time saturation of black hole complexity*, *JHEP* **08** (2025) 056 [2502.17179].

[88] V. Mohan, *Black hole singularities from holographic complexity*, *JHEP* **07** (2025) 275 [2504.10194].

[89] L. Susskind, L. Thorlacius and J. Uglum, *The Stretched horizon and black hole complementarity*, *Phys. Rev. D* **48** (1993) 3743 [hep-th/9306069].

[90] D. Harlow and D. Jafferis, *The Factorization Problem in Jackiw-Teitelboim Gravity*, *JHEP* **02** (2020) 177 [1804.01081].

[91] J. Boruch, L.V. Iliesiu, G. Lin and C. Yan, *How the Hilbert space of two-sided black holes factorises*, *JHEP* **06** (2025) 092 [2406.04396].

[92] N. Engelhardt and G.T. Horowitz, *Towards a Reconstruction of General Bulk Metrics*, *Class. Quant. Grav.* **34** (2017) 015004 [1605.01070].

[93] X. Jiang, P. Wang, H. Wu and H. Yang, *How Einstein's equations emerge from CFT2*, *Phys. Rev. D* **112** (2025) 8 [2410.19711].

[94] H. Liu, *Towards a holographic description of closed universes*, 2509.14327.

[95] H. Liu, *"Filtering" CFTs at large N: Euclidean Wormholes, Closed Universes, and Black Hole Interiors*, 2512.13807.

[96] J. Kudler-Flam and E. Witten, *Emergent Mixed States for Baby Universes and Black Holes*, 2510.06376.

[97] R. Haag, *Local Quantum Physics: Fields, Particles, Algebras*, Texts and Monographs in Physics, Springer-Verlag, Berlin, Heidelberg, 2nd ed. (1992).

[98] M. Takesaki, *Tomita's Theory of Modular Hilbert Algebras and its Applications*, Lecture Notes in Mathematics, Springer-Verlag (1970), 10.1007/bfb0065832.

[99] H.W. Wiesbrock, *Half sided modular inclusions of von Neumann algebras*, *Commun. Math. Phys.* **157** (1993) 83.